

UNIVERSITA' DEGLI STUDI DI MILANO
PhD School of Industrial Chemistry - XXXV Cycle
Department of Chemistry



UNIVERSITÀ DEGLI STUDI DI MILANO

**Towards Sustainable Catalysis: Design of Earth-Abundant Metal
Complexes for Waste Valorization**

**PhD Thesis of
Panza Nicola
R12761**

TUTOR: Prof. Alessandro Caselli

CO-TUTOR: Dr. Fausto Cargnoni

COORDINATOR: Prof. Dominique Roberto

Academic year 2021-2022

*Se il matto persistesse
nella sua follia, andrebbe incontro alla saggezza.* William Blake

*Cessando di essere
pazzo, diventò stupido.* Marcel Proust

PREFACE

The story behind this thesis, behind my doctorate journey, has a common thread: **sustainability**. This word is referred to something that satisfies the requisites of the current global population, without compromising the needs of future generations. As we are (unfortunately) probably all conscious, today we are facing a truly harsh global socio-environmental-economic situation. The environmental problems arisen after industrial development in the last century has brought humanity to the edge of extinction, more than everyone has ever even thought. Institutions are trying to dictate the guidelines to limit and overcome these issues, especially in terms of contain the rising of global temperature to a maximum limit of 1.5 degrees that would lead to catastrophic consequences for human beings. I want to stress out the fact that sustainability is a human related problem, rather than a problem of Earth, meaning that if we do not change our way of living, we are going to be the only ones that will suffer the effects of our behavior.

The major threat to the environment and life is the uncontrolled increase of carbon dioxide emission in the atmosphere. Today almost 40 GTons are released each year, leading to a series of consequences like global warming and climate change that will affect, with a ripple effect, different aspects of our health. The levels of carbon dioxide in the atmosphere reached almost 400 ppm, that uncontextualized might sound like a small quantity, but we have to remember that very little increase in ppm levels in the atmosphere (from 350 to 400) led to an increase of global temperature of more than a degree. Moreover, levels of 5 to 10% of carbon dioxide are completely incompatible with human life, causing a global extinction.

The interesting aspect of carbon dioxide is that the molecule is so thermodynamically stable that it is actually the “pit” of every single process that we perform on Earth. Everything that we burn, transforms in carbon dioxide, the more stable expression of carbon. We should not only limit our vision to combustion, since every other process, by the fact that we live in an oxidizing atmosphere, ends up generating carbon dioxide. So ultimately, revisiting the Bible passage in Genesis “*Memento, homo, quia pulvis es, et in pulverem reverteris*”, that says that we were dust, and we will become dust

again, from a more scientifically precise view we should consider us as becoming a gas, *carbon dioxide*.

As the natural process of death and decomposition is unavoidable, the problem arising from carbon dioxide uncontrolled emission should probably not be accounted to an inexplicable increase in mortality (even if this might become a secondary effect, more than the cause) but specifically to the industrial development that we faced starting from the XIX century.

Industrial revolution completely changed society, from an economic and social point of view. Nevertheless, the effects of the uncontrolled development of industries are only clear today, almost 150 years later. Talking about my generation, we grew up thinking about pollution as a relatively far problem, usually more related to developing countries. The reality is by far different, with the western world that keeps pointing the finger to undeveloped parts of the world, as major responsible of the incredible pollution of Earth. This might be true in the sense of lack of regulations in certain areas of the planet today, but we do not have to forget that the situation that we are facing today is responsibility only of the more industrialized western countries, which faced an exponential growth of industrial production (also delocalizing the factories in developing countries) not adequately accompanied by a growth of awareness in pollution treatment and reduction.

As incredible as it may sounds, scientists are today struggling like never before to find processes for the sequestration and recovery of carbon dioxide from the atmosphere, while species that we usually overlook as inferior, *plants*, are able to subtract carbon dioxide from the air and transform it into fuel (sugars), using solar light as power source. The overall efficiency of the process is ridiculously low, but the large number of plants populating our planet, united with the use of infinite source of power as solar light, makes this *photosynthetic* process a real "jewel" of nature.

Of course, we cannot think to solve our current situation by planting an infinite number of plants, and the efforts made by the scientific community to find a real solution are completely justified. In my vision we should take nature as an example, by exploiting different renewable energy sources to power processes in which carbon dioxide is transformed in more complex molecules.

There is indeed a rush in carbon dioxide chemistry, thanks to the fact that we are going to reach **carbon neutrality** within 2050, that is building a solid knowledge for the transformation of this “inert” molecule in something useful such as energy, fuel, solvents, polymers, chemicals of the more disparate kind.

In this view, thanks to my background in homogeneous catalysis, I spent most of my doctorate in finding sustainable ways to transform carbon dioxide in chemicals, more specifically into cyclic carbonates and carbamates. Of course, this is just a drop in the ocean, as relevance on the dimension of the problem we are facing globally, but still we need to think more and more at processes in which carbon dioxide is exploited as carbon source, to make it part of an artificial carbon cycle. This concept of **circularity** is fundamental also in the education of new generations, which will need more awareness about the consequences of every choice we make and how our life impacts on the planet.

Catalysis is firmly one of the pillars of sustainability and circularity, allowing the development of processes and chemical transformation that would require an enormous amount of energy or time to be done. The largest part of catalysis is related to metals and therefore we must consider some critical aspects in the choice of which metal to use as catalyst.

There are today very few metals that are not considered as **endangered elements**, due to the uncontrolled extraction and use of any sort of metal in the last centuries for manufacturing and catalytic application. Moreover, we have to consider to environmental footprint that some toxic heavy metals might have when used as catalysts, with the ultimate goal of finding more sustainable substitutes that are abundant and non-toxic. Lastly, we also have to consider the social aspect related to metals extraction, with the aim at limiting the use of metals coming from warzone countries, and the child exploitation.

One of the most abundant, non-toxic metal on Earth's crust is **iron**. There has been an exponential increase in publishing related to the use of iron in catalysis, since it has been selected as the most promising candidate to replace noble and heavy metals. As by myself, I started working with iron catalysis during my bachelor and I kept studying new applications even during my doctorate, clearly having in mind its potential as sustainable metal.

After successfully exploiting its activity in alcohol oxidation, I also successfully employed different iron-based catalysts for the reaction of carbon dioxide with heterocycles.

The use of intricate ligands in catalysis is usually due to their stabilization on the metal center, to tailor its activity. This is of course true for many transformations but in the case of the valorization of carbon dioxide, the use of complicated ligands might impact on the overall sustainability of the catalytic process. For this reason, during my period of doctorate I also focused on the research of simple active form of iron catalysts.

Ultimately, I merged my experiences and knowledge of sustainability and catalysis in a project regarding the **chemical recycling** of waste plastics. This is an aspect that probably would not need an introduction or explanation, since we all know the problems related to the uncontrolled spillover of plastic materials in the environment.

What I can add is the fact that, as true for carbon dioxide, we should change our vision towards plastics from a material to repudiate into valuable feedstock. The possibility to use a waste product to produce valuable chemicals is incredible, as we are overcoming different issues at one single time.

Regarding the recycling of **PET waste** (i.e., plastic bottles), the market is growing incredibly fast, as more and more recycled PET is used in the manufacture of different goods. The mechanical recycling applied today will be compensated in the future by chemical recycling in a virtuous synergy, for the sustainable production of plastics, with the fundamental vision of **Reducing, Reusing and Recycling**.

I had the pleasure and the opportunity, during my PhD, to exit my comfort zone of the academic laboratory: I was able to explore the different aspects of innovation, from the laboratory idea to the realization of the industrial application, the market needs, and the aspect related to project developing and fundings.

I hope I gave you a sufficient introductory look at the vision behind my PhD, my idea of sustainability and the journey that I experienced during the last 3 years of research in my group. I will for sure pursue my ambitions in the future, firmly having in mind the values that built my chemical background, whatever awaits me.

1	CATALYTIC OXIDATION OF ALCOHOLS WITH PYCLEN IRON(III) COMPLEXES	19
1.1	INTRODUCTION:	19
1.2	RESULTS AND DISCUSSION	26
1.2.1	Synthesis of the iron complexes:.....	26
1.2.2	Iron-catalyzed alcohol oxidations:.....	30
1.2.3	Reaction scope:.....	35
1.2.4	Discussion on the proposed reaction mechanism:.....	40
1.2.5	Complex 8:	43
1.2.6	Complex 9:	44
1.2.7	Complex 10:	47
1.2.8	Raman spectroscopy:	50
1.2.9	Complex 5b and 8:	51
1.2.10	Complex 6c and 9:	53
1.2.11	Complex 7 and 10:	54
1.3	CONCLUSIONS:	56
2	CYCLOADDITION OF CO ₂ TO EPOXIDES WITH PYCLEN METAL COMPLEXES AS CATALYSTS	57
2.1	INTRODUCTION:	57
2.2	RESULTS AND DISCUSSION:	65
2.2.1	Preparation of the zinc complexes:	65
2.2.2	Optimization of the reaction:	68
2.2.3	Scope of the reaction:	73
2.2.4	Catalyst recovery and recycle:.....	76
2.2.5	Preparation of iron complex:.....	77
2.2.6	Optimization of the reaction:	79
2.2.7	Scope of the reaction:	80
2.2.8	Scale up:.....	82
2.3	CONCLUSIONS:	82

3	AMMONIUM METALLATES FOR CYCLIC CARBONATES SYNTHESIS FROM EPOXIDES AND CO ₂ :	83
3.1	INTRODUCTION:	83
3.1.1	Chlorometallates for hydrosilylation / hydrogermylation:	83
3.1.2	Chloroferrate in the polymerization of epoxides:	85
3.1.3	Iron containing ionic liquids for alternative catalysis:	85
3.1.4	Iodocuprate(I) compound for coupling reactions:	87
3.1.5	Controlling the selectivity in aldehyde functionalization by iron catalysts:	89
3.1.6	Finding the best candidate:	90
3.2	RESULTS AND DISCUSSION:	91
3.2.1	Synthesis of tetrabutylammonium tetrahalogenoferrate salts:	91
3.2.2	Evaluation of the catalytic activity of ammonium ferrates in cyclic carbonate formation:	92
3.2.3	Effect of the reaction temperature:	94
3.2.4	Effect of the CO ₂ pressure:	96
3.2.5	Scope of the reaction:	97
3.2.6	Scale up of the reaction and recycling of the catalyst:	99
3.2.7	Density Functional Theory (DFT) investigation:	99
3.2.8	Synthesis of tetrabutylammonium tetrahalogenozincate salts:	102
3.2.9	Evaluation of the catalytic activity of ammonium zincates in cyclic carbonate formation:	103
3.2.10	Effect of temperature and CO ₂ pressure:	105
3.2.11	Effect of the catalyst loading and final optimization:	106
3.2.12	Reaction scope:	108
3.3	CONCLUSIONS:	110
4	SYNTHESIS OF OXAZOLIDINONES FROM AZIRIDINES AND CO ₂ CATALYZED BY AMMONIUM FERRATES:	111
4.1	INTRODUCTION:	111
4.2	RESULTS AND DISCUSSION:	116
4.2.1	Synthesis of aziridines:	116
4.2.2	Initial optimization of the reaction conditions:	116

4.2.3	Solvent screening:	118
4.2.4	Optimization of the reaction:	119
4.2.5	Kinetic study:	120
4.2.6	Reaction scope:.....	123
4.2.7	Scale up experiments:	123
4.2.8	Mechanistic investigation:.....	124
4.3	CONCLUSIONS:	126
5	CHEMICAL RECYCLING OF POLYETHYLENE TEREPHTHALATE (PET):.....	127
5.1	INTRODUCTION:	127
5.1.1	The era of plastics:.....	127
5.1.2	Development of polyesters: ^[200]	129
5.1.3	Synthesis of polyethylene terephthalate:	130
5.1.4	Plastics waste life cycle:.....	134
5.1.5	Life cycle of PET:	135
5.1.6	The situation in Italy:	137
5.1.7	Chemical recycling of PET:.....	138
5.1.8	Aerobic oxidation:	139
5.1.9	Hydrolysis:	140
5.1.10	Alcoholysis:	141
5.1.11	Glycolysis:	142
5.1.12	Aminolysis:.....	143
5.1.13	Industrial application of chemical recycling of PET:	144
5.1.14	Our approach:.....	145
5.2	RESULTS AND DISCUSSION:	145
5.2.1	Glycolysis:	145
5.2.2	Methanolysis:	149
5.2.3	Ammonolysis:	150
5.3	CONCLUSIONS:	151
6	EXPERIMENTAL SECTION	153
6.1	General experimental details:	153

6.2	Synthesis of ligands:	154
6.3	Synthesis of iron complexes:	159
6.4	Synthesis of zinc complexes:	169
6.5	Synthesis of ammonium metallATE salts:.....	172
6.5.1	Iron:	172
6.5.2	Zinc:	177
6.5.3	Cobalt:.....	181
6.5.4	Manganese:	182
6.5.5	Copper:	183
6.6	Crystal structures determination:	184
6.7	Catalytic oxidation of alcohols:.....	199
6.7.1	General catalytic procedure:	199
6.7.2	Blank reactions:	199
6.7.3	Catalyst optimization:.....	200
6.7.4	Optimization of other parameters:	201
6.7.5	Solvent screening:	202
6.7.6	Experiment in presence of BHT as radical scavenger:	202
6.7.7	GC-Methods:.....	203
6.7.8	GC chromatograms:.....	207
6.7.9	Products characterization:.....	222
6.7.10	Kinetic experiments, Hammett plot:	224
6.7.11	Synthesis of <i>tris</i> (triphenylphosphine)ruthenium dichloride: ^[240]	225
6.7.12	Synthesis of deuterated benzyl alcohol:.....	225
6.8	Synthesis of <i>oxo</i> -bridged iron complexes of PycLen ligands:.....	228
6.9	Cyclic carbonates synthesis from CO ₂ and epoxides:	233
6.9.1	Zinc PycLen complexes:	233
6.9.2	General catalytic procedure:	233
6.9.3	Reaction optimization:	233
6.9.4	Catalyst loading screening:	234
6.9.5	Reaction time optimization:	235

6.9.6	Influence of the pressure of CO ₂ :	236
6.9.7	Catalyst recycling (reaction re-run):	236
6.9.8	Catalyst recovery:	237
6.9.9	Synthesis of Eugenol glycidyl ether:	238
6.10	Iron Pyclen complexes:	239
6.10.1	General catalytic procedure:	239
	Reaction optimization:	239
6.10.2	Catalyst loading screening and blank experiment:	240
6.10.3	Influence of the pressure:	241
6.10.4	Influence of the temperature:	242
6.10.5	Influence of the reaction time:	243
6.10.6	Scale up reaction:	244
6.10.7	Recycling experiment:	244
6.10.8	Catalyst recovery and recycle:	245
6.11	Ammonium ferrates:	246
6.11.1	General catalytic procedure:	246
6.11.2	Reaction optimization:	246
6.11.3	Temperature influence/catalyst screening:	247
6.11.4	Temperature influence:	248
6.11.5	CO ₂ pressure influence:	249
6.11.6	Catalyst recycle experiment:	250
6.11.7	Reaction scale-up:	251
6.11.8	Effect of external nucleophiles:	252
6.11.9	Determination of enantiopurity of the product with (R)-Styrene oxide:	253
6.11.10	DFT calculations:	255
6.11.11	Complete reaction paths from DFT computations:	256
6.11.12	Theoretical estimation of the dissociation of FeCl ₃ Br ⁻ in styrene oxide:	263
6.11.13	Theoretical estimate of the activation energy from experimental data:	264

6.11.14	Complete reaction paths from semiempirical tight binding calculations evaluated through the XTB code:.....	266
6.11.15	Comparison between semiempirical-XTB and DFT-Gaussian results:....	267
6.12	Ammonium zincates:.....	270
6.12.1	General catalytic procedure:.....	270
6.12.2	Catalyst screening:.....	270
6.12.3	Blank experiments:.....	271
6.12.4	Reaction time optimization:.....	271
6.12.5	Reactions at room temperature:.....	273
6.12.6	Reactions at ambient pressure of CO ₂ :.....	274
6.12.7	Influence of catalyst loading at room temperature and ambient pressure: 275	
6.12.8	Final optimization of the reaction conditions:.....	275
6.12.9	Multigram scale-up reaction:.....	276
6.12.10	Catalyst recycling experiments:.....	276
6.12.11	Product characterization:.....	277
6.12.12	Selected NMR spectra of cyclic carbonates: (blue residues of the starting epoxide) 284	
6.13	Cycloaddition of aziridines and CO ₂ , catalyzed by ammonium ferrates:.....	293
6.13.1	Synthesis of 4-Methoxystyrene (17e):.....	293
6.13.2	Synthesis of dimethyl-(1-aryl-2-bromo)-ethyl sulfonium bromides (18a-e): 294	
6.13.3	General synthesis of 1-alkyl-2-arylaziridines:.....	295
6.13.4	Synthesis of 1-Tosyl-2-phenylaziridine (19l): ^[253]	297
6.13.5	Synthesis of trimethylsulfoxonium iodide:.....	298
6.13.6	Synthesis of 1,2-diphenylaziridine (19m):.....	298
6.13.7	Synthesis of 1-(4-nitro)-phenyl-2-phenylaziridine (19n):.....	299
6.13.8	General catalytic procedure:.....	300
6.13.9	GC methods:.....	301
6.13.10	Catalyst screening:.....	302
6.13.11	Kinetic study:.....	303

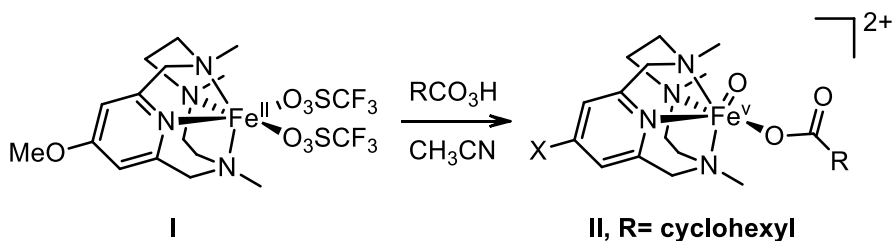
6.13.12	Scale-up of the reaction (gram scale):.....	309
6.13.13	Products characterization:.....	309
6.13.14	DFT studies:	329
6.13.15	Complete energy profiles as obtained by DFT computations. No zero-point correction is considered:.....	329
6.13.16	Visual representation of the intermediates:	333
6.14	Dimerization of aziridines: synthesis of piperazines	335
6.14.1	General catalytic procedure:	335
6.14.2	Work-up procedures:	335
6.14.3	Catalyst screening:.....	336
6.14.4	Lower aziridine concentration experiments:.....	336
6.14.5	Other metallates:.....	337
6.14.6	Control experiments:.....	337
6.14.7	Microwave heating optimization:	338
6.14.8	Temperature optimization:	338
6.14.9	Solvent screening:	339
6.15	Polyethylene terephthalate (PET) depolymerization:	341
6.16	PET glycolysis:	341
6.16.1	General catalytic procedure:	341
6.16.2	Blank experiments, conventional heating:	342
6.16.3	Catalyst screening:.....	342
6.16.4	Influence of reaction time:	343
	Blank experiments, microwave heating (MW):.....	344
6.16.5	Catalyst screening, microwave heating:.....	344
6.16.6	Reaction time influence, microwave heating:.....	345
6.16.7	Influence of temperature, microwave heating:	349
6.16.8	Glycolysis with 1,3-propanediol, microwave heating:	350
6.16.9	Comparison of BHET yield between commercial rPET and untreated water bottle: 350	
6.17	PET methanolysis:.....	351

6.17.1	General catalytic methods:.....	351
6.17.2	PET methanolysis in pressure tubes, catalyst screening:	351
6.17.3	PET methanolysis in autoclave, catalyst screening:	352
6.17.4	PET methanolysis, control experiments in autoclave:	352
6.18	PET hydrolysis:.....	353
6.18.1	General catalytic methods:.....	353
6.18.2	Optimization of the reaction:	353
6.19	PET ammonolysis:.....	354
6.19.1	General catalytic procedure:	354
6.19.2	Synthesis of ammonium carbamate:.....	354
6.19.3	Preliminary results:.....	355
6.19.4	Products characterization:.....	355
7	REFERENCES:.....	373

1 CATALYTIC OXIDATION OF ALCOHOLS WITH PYCLEN IRON(III) COMPLEXES

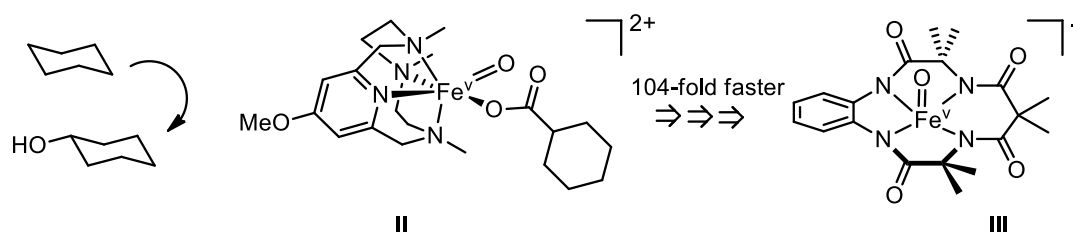
1.1 INTRODUCTION:

“Oxidation and iron” are a binomial largely present in nature: in fact, high valent iron complexes are normally found in nature as oxidative tools for functionalizing inert molecules.^[1] Synthetic models have been studied on mono- and di-nuclear nonheme oxo-iron(IV) which proved to be able to break C-H bonds,^[2] and higher oxidation states such as oxo-iron(V) were proposed as intermediate in Rieske oxygenase cycle^[3]. Macrocyclic nitrogen-based ligand proved to be fundamental in the stabilization of such high valent iron intermediates^[4] and to exploit their catalytic behavior, which is generally described in terms of hydrogen atom abstraction (HAA) and oxygen atom transfer (OAT) reactions. The identification of such high-valent intermediates is not trivial; therefore, the use of macrocyclic nitrogen ligands has allowed a detailed spectroscopic characterization of species that would otherwise be very difficult to identify^[5,6]. Ground-breaking work from Fan and co-workers^[7] was fundamental in this field thanks to the detailed spectroscopic characterization of high valent iron complexes of 12-membered pyridine containing macrocycles. The neutral macrocyclic ligand **MeO-PyNMe₃** allowed the accumulation of a predominant oxo-iron(V) species at -40 °C, starting from its iron(II) precursor (complex **I**, Scheme 1). This high-valent species was previously only hypothesized or detected



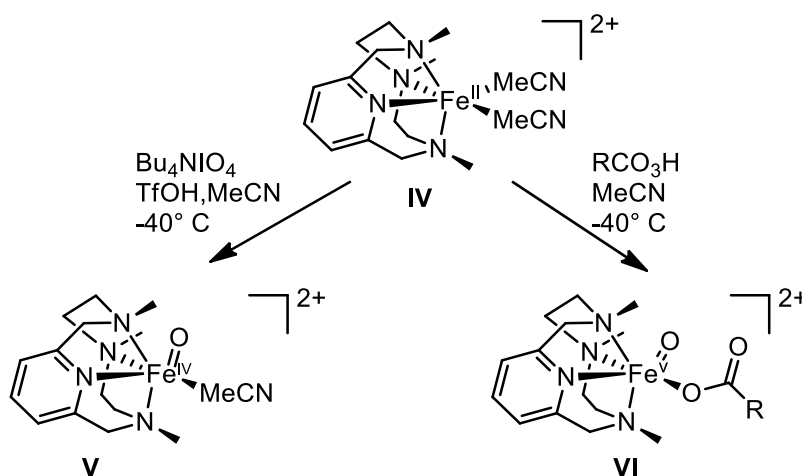
Scheme 1. Synthesis of complex **II** after treatment of **I** with a peracid as minor component in Fe(TPA) systems, and in this case they were instead characterized by EPR. Specifically, in the case of **I** and cyclohexyl peroxyacid, the accumulation of the low-spin ($S=1/2$) oxo-iron(V) compound **II** also allowed the characterization via Mossbauer

to further confirm the true nature of the complex. The activity of those compounds was compared to previously reported TAML iron complex (**III**) in cyclohexane C-H oxidation to cyclohexanol.^[8] The rate for the pyridine-containing macrocycle is 10^4 -fold faster than **III**, which instead is a tetraanionic ligand (Scheme 2). The neutral nature of PyNMe₃ ligand hampers the electrophilicity of the oxo-iron(V) species, significantly increasing its oxidative ability.



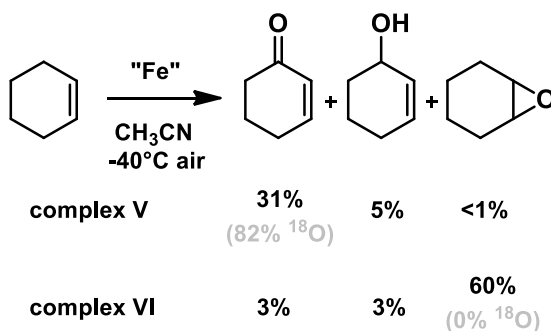
Scheme 2. Comparison of the rate of cyclohexane oxidation by complex **II** and **III**

Another work from Dantignana and co-workers^[9] further investigated the reactivity of high-valent iron complexes of a 12-member pyridine containing macrocycle and in particular the difference between a well-defined oxo-iron(IV) and an oxo-iron(V) complex **V** and **VI**. We previously discussed the oxo-iron(V) compounds generated by the oxidation of iron(II) complexes with peracids and their ability to hydroxylate cyclohexane. The related oxo-iron(IV) compound was obtained by the oxidation of the iron(II) complex **IV** with hypervalent iodine reagents as shown in scheme 3:



Scheme 3. Formation of **V** and **VI** from **IV** and different oxidants.

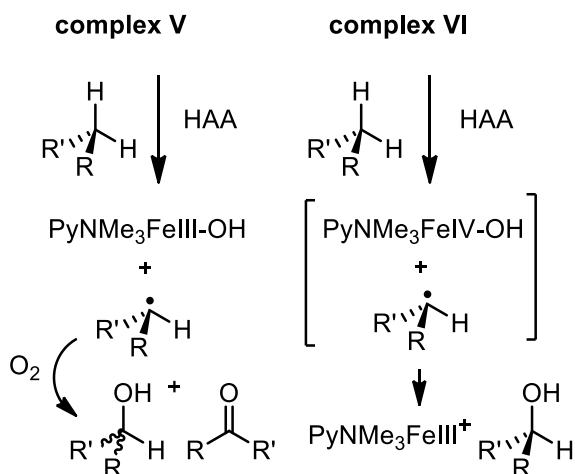
These species were characterized with UV-Vis, Mossbauer, Raman and XAS analysis and the more stable isomer for the oxo-iron(IV) compound is the one with Fe-O bond *trans* to the pyridine nitrogen, with a spin value $S=1$. The reactivity of **V** was compared with the related oxo-iron(V) complex **VI** in different reactions (Scheme 4). In the oxidation of *p*-substituted thioanisoles the reaction rate of **VI** was extremely faster than **V** and so the influence in oxidation and spin state in OAT could not be assessed and the reactivity difference can be addressed to the extreme electrophilicity of **VI**. Instead, the oxidation of hydrocarbons proceeds via a similar transition state for both the complexes, but oxo-iron(V) is 4 to 5 orders of magnitude more reactive. Interestingly, the chemoselectivity of the two iron compounds was found to be completely different at -40°C in CH_3CN under aerobic conditions.



Scheme 4. Selectivity of the oxidation of cyclohexene by complex **V** and **VI** in aerobic conditions.

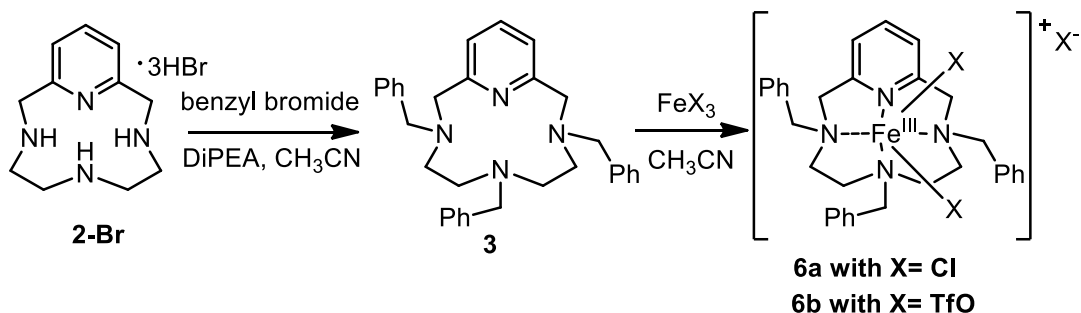
The use of 100 eq. of cyclohexane in the previously described reaction conditions led to the formation of the allylic oxidation products as the major products in the case of **V** and the epoxidation of the double bond for **VI**. This confirms the tendency of the latter to undergo OAT reaction at extremely fast reaction rate and the ability of the oxo-iron(IV) complex to abstract activated C-H hydrogen. Performing the reaction under ^{18}O atmosphere provided important mechanistic insights: the ketone produced by the allylic oxidation incorporated 82% of ^{18}O suggesting that the radical formed after HAA does not undergo rapid rebound but instead interacts with dioxygen. Instead, no isotope labelling into the epoxide was detected, confirming the OAT path. Furthermore, in the case of **VI**, the side-products did not show any incorporation of labelled oxygen. These findings prove the fact that the oxygen rebound with hydroxo-iron(III) formed by **V** is slow and the carbon-centered radical can

diffuse out of the reaction pocket and interact with oxygen. Instead, the putative hydroxo-iron(IV) formed after HAA by **VI** is prone to quickly transfer its hydroxyl ligand.



Scheme 5. Possible reaction pathways of complex **V** and **VI** after HAA step.

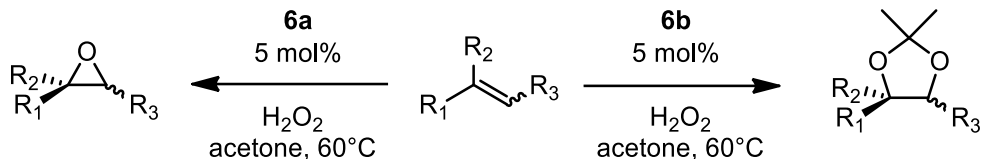
In our group, in the past few years, we proved that high-valent iron complexes can also be obtained by the oxidation of iron(III) with hydrogen peroxide. We were able to report a particular iron based chemoselective catalytic system for the oxidation of olefins, using two different 12-membered functionalized pyridine-containing ligand macrocyclic complexes.^[10] The peculiar iron(III) complexes were obtained as shown in Scheme 6:



Scheme 6. Synthesis of complexes **6a** and **6b**.

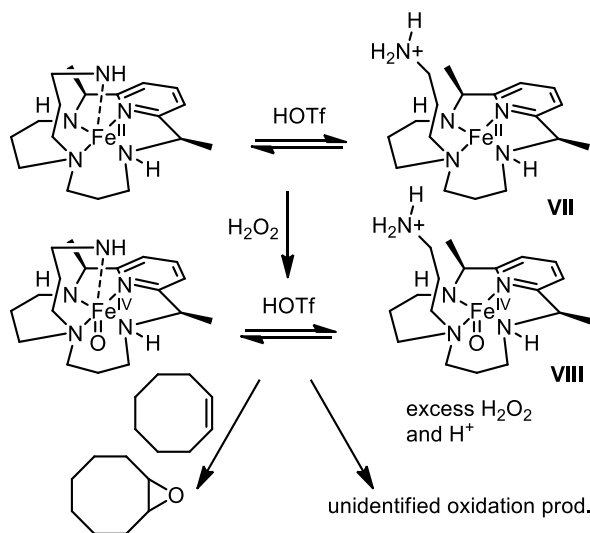
The complexes proved to be active in the oxidation of different olefins in acetone at 60°C, using hydrogen peroxide as oxidant

(Scheme 7). The iron(III) chloride complex **6a** had a mixed spin state ($S=1/2$ and $S=5/2$) and was found to be highly selective to the epoxide formation and, on the contrary, the iron(III) triflate one **6b** ($S=5/2$) was almost fully selective to the formation of acetoneides.



Scheme 7. Chemoselectivity of the oxidation of olefinic substrates by **6a** and **6b**.

Complex **6a** appears to possess high OAT affinity to olefins in presence of hydrogen peroxide, as the epoxide was the only product isolated. In the case of complex **6b**, the chemoselectivity can be addressed by a *syn*-dihydroxylation mechanism but we must take in to account the fact that epoxides can be readily converted in acetoneides in the presence of a Lewis or Bronsted acid in acetone as solvent. The possible presence of catalytic amount of triflic acid in the reaction of olefins with **6b** and hydrogen peroxide can strongly modify the outcome of the overall reaction (Scheme 8). Indeed, the influence of triflic acid on the reactivity of a 14-membered pyridine-containing ligand iron complex was reported by Latifi and co-workers.^[11]



Scheme 8. Formation of complex **VIII** and interaction with triflic acid.

In their study they highlight the influence of the pH on the reactivity of their oxoiron(IV) complex with cyclooctene.

Their proposed ligand, in fact, bears an appended aminopropyl functionality, which interacts with the iron center. The reaction of the iron(II) complex **VII** with hydrogen peroxide leads to the formation of **VIII** (observed with UV-vis technique) and the presence of one equivalent of acid accelerates the formation of such species. Excess acid and oxidant leads to the formation of unidentified oxidation products. The acid influences the rate of the reaction by protonating the pendant arm which is therefore not able to coordinate the iron center, resulting in a faster OAT and enhanced catalytic activity toward olefin epoxidation, comparable with a non-functionalized macrocyclic ligand's complex.

Thanks to the knowledge I have gained in my research group on the synthesis of this class of macrocyclic ligands^[4,10,12] and their iron(III) complexes, I decided to investigate their catalytic behavior in the selective oxidation of alcohols, using hydrogen peroxide as oxidant.

The selective oxidation of primary and secondary alcohols respectively to aldehydes and ketones is a fundamental transformation both at the industrial and laboratory scale. In fact, carbonyl compounds have a broad reactivity profile and find place as substrates for both fundamental and fine chemistry.^[13] The process is known since the last century and usually relied on the use of highly toxic metal-oxo reagents (i.e. KMnO_4) and metal oxide surfaces.^[14] Despite the increase of catalytic protocols to improve this process,^[15] in accord with the fundamental principles of green chemistry, the major effort is put in the search for the optimal catalyst, in terms of activity and sustainability. In the several reported methodologies,^[16] the green oxidants employed are O_2 , H_2O_2 and organic peroxides, and in recent years, significant advances have been achieved in the oxidation of benzyl alcohols to benzaldehydes, using homogeneous iron(II),^[17-19] iron(III)^[20-23] and copper(II)^[20] complexes, metallacarboranes,^[23] supported nanoparticles,^[24] MOF,^[25] and organic oxidants.^[26]

Despite the fact that the use of iron and its complexes, among the different transition metals, has received an impressive boost, witnessed by several timely reviews,^[27-29] the call for more sustainable selective oxidation reactions is still open. Heme and

non-heme iron complexes are well known to catalyze alcohol oxidation reactions in presence of an external oxidant,^[30,31] through the formation of high valent species that perform hydrogen atom abstraction from the substrate and the formation of a carbonyl compound.^[32] Usually, large kinetic isotopic effect values confirm this hypothesis, where highly electron-poor porphyrinic complexes are generally more reactive. Another important experimental proof of such behavior is the oxidation of cyclobutanol. The exclusive formation of cyclobutanone is related to a 2-electron mechanism involving a sequential hydrogen atom abstraction and electron transfer.^[33] If a carbon radical is formed and escape the solvent cage, the formation of the ring-opening oxidized product is noticed. Our catalysts are generally cationic non-heme complexes that should therefore be able to perform selectively this transformation. During my first year of my PhD, I focused on the optimization of this reaction, with the aim of designing the best catalyst to achieve high conversion and selectivity, maintaining the most sustainable conditions in terms of quality and quantity of oxidant employed, temperature and solvent. A profound experimental-mechanistic binomial study was performed, to better understand the nature of our catalytic system. As often happens in homogeneous catalysis, the recovery of the catalyst at the end of the reaction is nothing but trivial, and the fate of the catalyst itself is generally hard to predict. In the case of oxidation reactions, when using aqueous hydrogen peroxide as oxidant, the formation of dimeric oxo-bridged compounds is a possible pathway of deactivation of the catalyst. Such dimeric iron species are described in the literature since the '80s as synthetic models for enzymes but they have been described both as active or dead-end species.^[34-40] More recently, as described by Green and co-workers, dimeric iron(III) chloride complexes of non-functionalized pyclen ligands are identified as unactive species in the oxidative coupling of pyrrole and phenyl-boronic acid.^[40] These species have been synthesized by the reaction of the monomeric iron complexes in presence of water and a base, so in this way they can be subsequently studied both from an experimental and spectroscopical point of view. Due to both the similarity of the previously reported examples with our catalysts and the concrete possibility of the formation of such species in our oxidation reactions, we decided to synthesize the related oxo-bridged compounds to assess their structural and spectroscopical characterization, with the final aim to study their catalytic behavior. Beside single crystal X-Ray diffraction structural

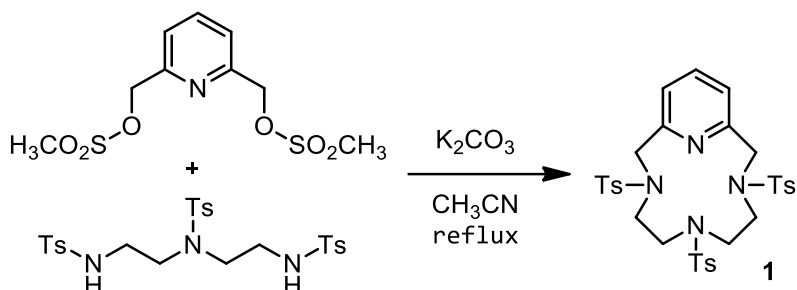
assignment, we proved the nature of the oxo-bridged compounds by means of Raman spectroscopy. The latter is a widely employed analytical technique, discovered by C.V. Raman and co-workers in 1928,^[41] which relies on the inelastic scattering of photons coming from a monochromatic source such as a laser, called Raman scattering. For a molecule to exhibit a Raman effect, there must be a change in its electric dipole-electric dipole polarizability with respect to the vibrational coordinate corresponding to the virtual rotovibrational energetic state. Raman spectroscopy should not be confused with IR spectroscopy where the light absorbed matches the energy gap between the initial and final rotovibronic state. Transitions with large Raman intensity usually has low IR intensity and *vice-versa*. Raman shifts are reported in wavenumbers, which are directly correlated to energy. Raman spectroscopy is used in chemistry, usually in combination with other techniques, to identify and study the nature of chemical bonds in a molecule or material and related to our study, it has been used for the study of the vibrational bands associated with the Fe-O-Fe fragment in proteins and model compounds.^[42-46] Due to the lack of possible analytical technique that can be used to evaluate the nature and purity of paramagnetic iron compounds, Raman spectroscopy proved to be an intuitive and fundamental tool to assess the structure of our compounds and turned out to be a suitable *routine* technique to evaluate the purity of the materials prepared in our laboratory.

1.2 RESULTS AND DISCUSSION

1.2.1 Synthesis of the iron complexes:

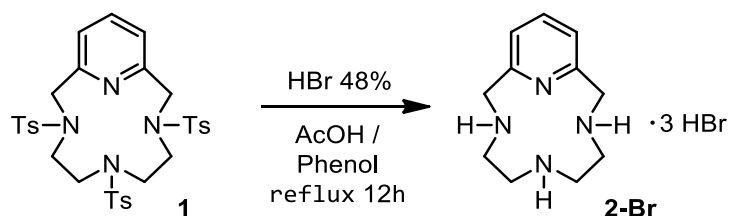
The previously described iron complexes **6a** and **6b** were prepared as reported,^[47] where the first step involved the synthesis of the principal macrocyclic scaffold **1** by a modified Richman-Atkins procedure. A tosyl-protected diethylenetriamine is reacted with a 2,6- substituted pyridine in refluxing acetonitrile, using a heterogeneous base (*i.e.* potassium carbonate) to simulate the high-dilution conditions that promote the macrocycle formation rather than the undesired polymerization of the reactants (Scheme 9). Ligand **1** is obtained usually in very high yield, and after separation of the base and evaporation of the solvent, no extra purification steps are necessary. In certain cases, due to the lack of purity of the reactants or hydration of the carbonate base, the reaction will not proceed to completion and purification of the macrocycle from

byproducts is needed. After evaporation of acetonitrile and extraction of the products, a recrystallization step using ethyl acetate is usually satisfactory in terms of purification from unreacted triamine, which will remain dissolved.



Scheme 9. Synthesis of ligand **1** by modified Richman-Atkins procedure

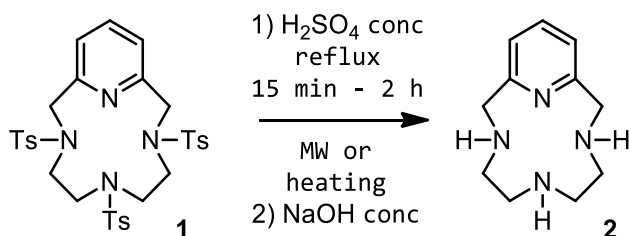
The synthetic path towards differently functionalized ligands continues with the deprotection of tosyl groups by acid hydrolysis in refluxing concentrated HBr to yield ligand **2-Br** (Scheme 10), using excess phenol and acetic acid as solvent, which render the overall reaction conditions quite harsh. The product is obtained by precipitation of the hydrobromide salt with acetone from the reaction mixture, after concentration and cooling.



Scheme 10. Synthesis of ligand **2-Br** by acid hydrolysis with concentrated hydrobromic acid.

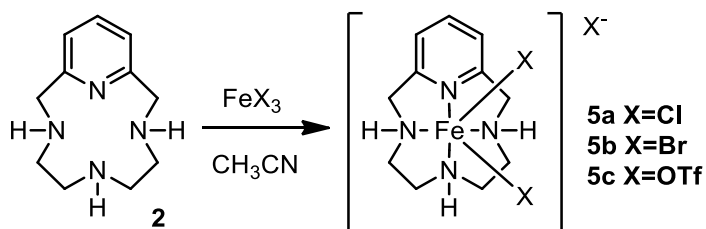
Better yields of the free base ligand **2** can be obtained by acid hydrolysis with concentrated sulfuric acid at 150–200 °C, which requires even shorter reaction time, followed by treatment with NaOH to obtain the free base ligand. As already reported,^[48] with this method less reproducible yields ranging from 60 to 80% are obtained, compared to the deprotection with hydrogen bromide, but the product

can be isolated in high purity after a simple extraction with organic solvents. A modified procedure involved the heating by means of microwaves,^[49] which allows the completion of the reaction in shorter times at lower temperatures (20 minutes at 120 °C). In this case, after cooling the reaction mixture, the hydrogen sulfate salt of ligand **2** is precipitated by direct addition of diethyl ether. The salt is separated from the mixture and treated with concentrated NaOH until pH >14. The free base ligand **2** is then obtained by extraction with dichloromethane, with improved yield compared to the traditional heating method (Scheme 11).



Scheme 11. Synthetic pathway for ligand **2**, by acid hydrolysis with concentrated sulfuric acid, under traditional or MW heating.

Metal complexes **5a-c** were prepared in acetonitrile with the already reported procedure,^[47] involving the slow addition of the metal precursor to a solution of the ligand in acetonitrile at room temperature (Scheme 12). The mixture is stirred for a few hours, even if the precipitation of the complexes is almost immediate. In certain cases, if the precipitation does not occur, the solvent is evaporated, and the residue treated several times with diethyl ether and/or hexane and separated by filtration. Complexes **5a-c** present a lower solubility in non-protic solvents compared to **6a** and **6b** but are highly soluble in water. All the complexes were characterized by means of mass spectroscopy and elemental analysis.



Scheme 12. Synthesis of complex **5a-c** using different metal precursors.

Magnetic moments, μ_{eff} , of 4.67 μB and of 5.42 μB were measured by the Evans' method for complexes **5a** and **5b**, respectively. These room temperature magnetic moments in solid state were also confirmed in solution (d6-DMSO) by Evans NMR method,^[50] where μ_{eff} , of 5.37 μB (**5a**) and of 5.36 μB (**5b**) were calculated and seems to point out to an iron metal center in the high spin state of 5/2.^[51]

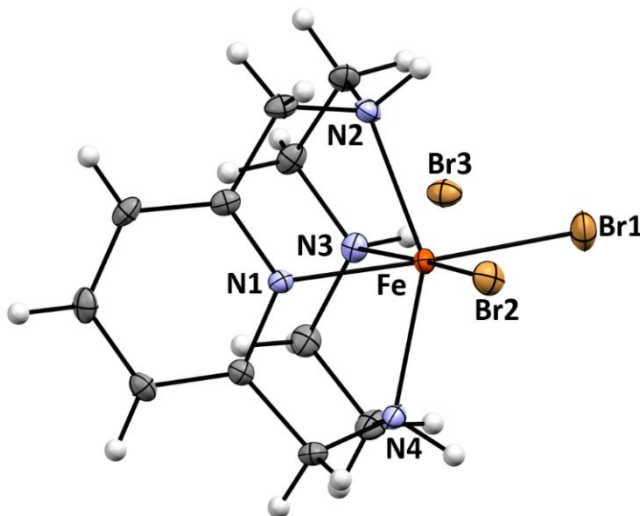
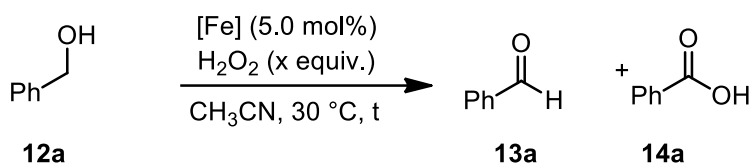


Figure 1. Molecular structure of complex **5b**, full description in the experimental section.

Single crystals suitable for X-ray diffraction were grown by slow evaporation from a water solution of complex **5b**. Figure 1 shows the structure of the complex. The iron center is coordinated by the four nitrogen atoms of the macrocycle and two bromide anions to form a distorted octahedral coordination environment. As shown, the macrocycle ligand chelates the metal in a tetradentate cis- α fashion, with the bromine atoms at the two cis positions.^[52,53] Full description of the structural features of complex **5b** is found in the experimental section.

1.2.2 Iron-catalyzed alcohol oxidations:

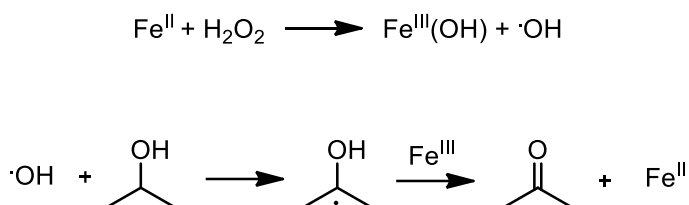
Oxidation of benzyl alcohol **12a** was chosen as benchmark reaction for the optimization of the catalytic conditions. This reaction has been widely studied in recent years, but good results with high selectivities were obtained mainly with heterogeneous catalysts.^[54,55] In terms of homogeneous catalysts, few examples are reported of being capable of yielding selectively benzaldehyde in this transformation, leaving the room for a further optimization of the reaction. This prompted us to test our iron(III) complexes **6a**, **6b**, as a starting point for the evaluation of their catalytic activity which is somehow close to what we have already recently reported for the epoxidation/dihydroxylation reaction of olefins, using hydrogen peroxide as oxidant.



Scheme 13. General reaction scheme for the oxidation of benzyl alcohol

As already mentioned in the introduction of this chapter, high-valent iron oxo compounds can undergo both oxygen atom transfer reaction (OAT) and hydrogen atom abstraction (HAA). The latter is generally considered an important reaction step in the oxidation of alcohols, both in the case oxo-species as catalyst, with the elimination of water, and also for acceptorless dehydrogenative oxidations, where hydrogen is produced. For instance, the interaction of **6a** and **6b** with hydrogen peroxide has already been proved to produce such high-valence iron oxo species, as discussed in the introduction, which can be suitable catalyst for the oxidation of alcohols. Typical reactions were performed by adding the catalyst and benzyl alcohol to the solvent and the subsequent addition of the oxidant (H₂O₂, 30%) by slow addition, using a syringe pump, or by repeated sequential additions. All the reactions were followed by ¹H NMR adding CH₂Br₂ as internal standard;^[56] By means of gas chromatography, using dodecane as internal standard, we were able to evaluate the conversion of the starting benzyl alcohol **12a** and

the selectivity for benzaldehyde **13a** or benzoic acid **14a**. All the conversion and yield values are obtained by calibration curves, previously prepared using pure products. Oxidations by means of hydrogen peroxide catalyzed by Fenton's reagent (ferrous ion, Scheme 14) have received considerable scrutiny since last century,^[57] while the use of ferric salts have been given considerably less attention.



Scheme 14. Oxidation of alcohols by Fenton's reagents, by HAA of an hydroxyl radical.

Nevertheless, simple iron(III) chloride, in the absence of a ligand, is able to catalyze the oxidation of benzylic primary aromatic alcohols to aldehydes, by using a three-fold excess of hydrogen peroxide and water as solvent at room temperature, albeit in very modest yields and with concomitant over-oxidation to benzoic acids.^[22] Moreover, Martin and Garrone have reported in 2003, that FeBr_3 can catalyze efficiently the selective oxidation of benzylic alcohols using hydrogen peroxide, under solvent free conditions.^[58] To the best of our knowledge, ferric salts have been since then neglected in such oxidation reaction, until recent reports on the use of $\text{Fe}(\text{OTs})_3$ for the selective oxidation of benzyl alcohol^[21] and on the efficient use of $\text{Fe}(\text{OTf})_3$ as the catalyst for the solvent free oxidation of cyclohexane.^[59] We were thus interested in comparing the results of the use of simple iron(III) salts under our conditions, in acetonitrile as solvent at room temperature (Table 1). Under our conditions, blank control experiments in the absence of any catalyst gave no conversion of the starting aldehyde. All the tested ferric salts catalyzed a fast decomposition of H_2O_2 , but if a large excess of the oxidant was used, 20-fold excess with respect to the alcohol (Table X, entries 1,2,3), a good conversion could be achieved in 24 hours. However, only using FeBr_3 an acceptable selectivity was observed, and benzaldehyde was obtained as the major product (83% selectivity, Table X, entry 3) comparable

with the results of Martin. If the addition of the oxidant was slow, using a syringe pump in 2 hours, its quantity can be drastically reduced and sustainable conversions, 76%, and selectivity, 83%, were obtained also when using only 4 equivalents of hydrogen peroxide in respect to the alcohol (Table 1, entry 4).

Table 1. Preliminary screening of the oxidation of benzyl alcohol by ferric salts.

Entry	Catalyst	eq H ₂ O ₂	Conv 12a (%)	Select 13a (%)	Select 14a (%)
1	FeCl₃	20	98	6	31
2	Fe(OTf)₃	20	72	31	21
3	FeBr₃	20	84	83	5
4		4	76	83	4

After a very detailed optimization procedure, we noticed that complex **6b** seems to be much more active as catalyst and higher conversion was observed but a better selectivity was obtained using catalyst **6a** (5 mol% loading) by adding only one equivalent of oxidant at 0 °C and stirring the reaction at room temperature for further 1.5 hours. Under those conditions a very low conversion was observed (30% conversion and 77% selectivity for benzaldehyde). The unsatisfactory results are exasperated by the fact that they are comparable, despite harsher conditions are needed, to the ones obtained with simple ferric salts as catalysts, and the use of such functionalized ligands in such conditions was therefore not justified. The use of non-functionalized polyazamacrocyclic ligands in oxidation reactions was always considered detrimental, where free N-H bonds can be sensitive to strong oxidants and affect the complex stability, but nevertheless, it is also reported that N-alkylation of the ligand can cause a change in the spin state configuration at iron, resulting in a lower catalytic activity.^[60]

Table 2. Optimization of the reaction with complex **6a** and **6b**.

Entry	Catalyst	eq H ₂ O ₂	Conv 12a (%)	Select 13a (%)	Select 14a (%)
1	6b	4	56	43	9
2	6a	4	30	77	23

We were thus interested in studying the catalytic activity of our iron(III) complexes **5a-c**, that in the solid state were shown to possess a high-spin iron center which should hamper the reactivity towards the oxidation, despite the presence of the aforementioned unprotected N-H functionalities. Interestingly, complexes **5a** and **5c**, which showed a sluggish solubility in CH₃CN, when using 20 equivalents of oxidant at room temperature for 24 hours, compares quite well with their respective salt precursors, and in particular for complex **5a** a slightly better selectivity in benzaldehyde was observed. On the other hand, complex **5b**, under those conditions was less active and less selective than ferric bromide alone when a 20-fold excess of the oxidant was added.

Table 3. Preliminary screening with complexes **5a-c**.

Entry	Catalyst	eq H ₂ O ₂	Conv 12a (%)	Select 13a (%)	Select 14a (%)
1	5a	20	95	11	27
2	5c	20	86	19	20
3	5b	20	66	55	11

But if the oxidant was added in small portions, the catalytic system based on complex **5b** was much more selective and, for instance, if 1 equivalent of hydrogen peroxide was added every 15 minutes to the reaction mixture, a reasonable selectivity for benzaldehyde with good conversion (78% conversion, 76% selectivity, table 4, entry 1) in just 3h was observed (in total 12 equivalents of hydrogen peroxide). A huge boost in selectivity was obtained by slowly adding 2 equivalents of the oxidant by syringe pump in 2 h and allowing the reaction mixture to stir at 30 °C for further 22 h (Table 4, entry 2). This indicates that the simultaneous addition of large quantities of oxidants is detrimental and can lead to undesired

byproducts formation or catalyst deactivation. Finally, the best compromise between conversion and selectivity in terms of the overall process was obtained by the slow addition of 4 equivalents of oxidant and allowing the reaction to stir at 30 °C for 24 h (Table 4, entry 3).

Table 4. Optimization of the reaction with complex **5b** as catalyst.

Entry	Catalyst	eq H ₂ O ₂	Conv 12a (%)	Select 13a (%)	Select 14a (%)
1	5b	12	78	76	3
2	5b	2	50	98	2
3	5b	4	96	90	10

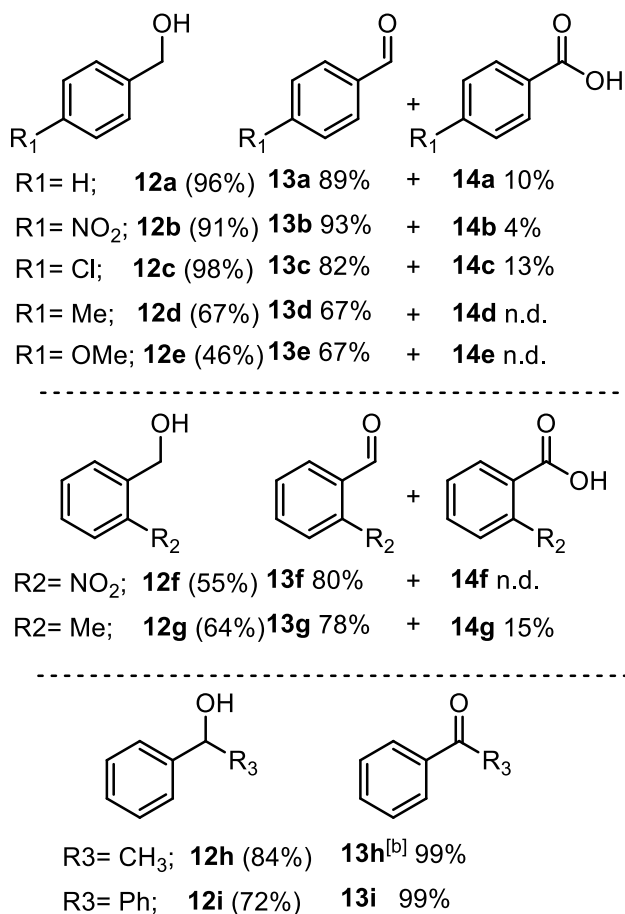
Interestingly, under identical reaction conditions, pure FeBr₃ was almost inactive (<24% conversion) and less selective (<75%). This evidence might discriminate the activity of the iron salt itself and the one which is coordinated by the pycnen ligand, where the latter can favor the formation and stabilization of high valence species that are responsible for the transformation. The mechanism of action of pure iron bromide with hydrogen peroxide is even today under discussion, where it can act both as source of high-valence species or simply by promoting bromine catalyzed oxidations, as recently reported by He and co-workers.^[61] We next checked the effect of the solvent, and higher selectivity (>99%) was obtained only in AcOEt (Table 5, entry 2), despite a lowering of the conversion. When using acetone as solvent, the diminished conversion (Table X, entry 3) could be accounted to its ability to trap free hydroxyl radicals that can be involved in the reaction.[36] Other solvents such as water and *t*-amylalcohol were not satisfactory (Table 5, entries 4,5).

Table 5. Solvent screening.

Entry	Catalyst	solvent	Conv 12a (%)	Select 13a (%)	Select 14a (%)
1	5b	CH ₃ CN	96	90	10
2	5b	AcOEt	55	99	1
3	5b	Acetone	35	86	-
4	5b	Water	98	1	-
5	5b	<i>t</i> -amylalcohol	10	90	-

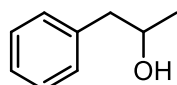
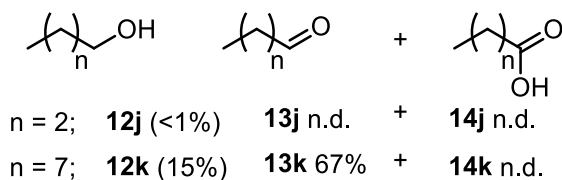
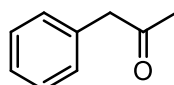
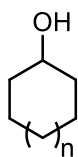
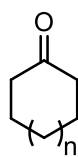
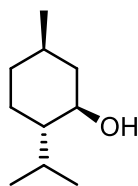
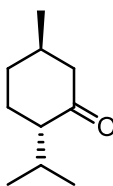
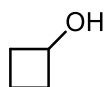
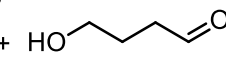
1.2.3 Reaction scope:

We decided to explore the scope of the reaction by using the optimized conditions, 24 hours at room temperature and the addition of 4 equivalents of oxidant with syringe pump over 2 hours. Those conditions were found to give the best compromise between quantitative conversions while keeping high selectivity. Oxidation of para substituted benzyl alcohols proceeded smoothly and high conversions with good selectivity were observed especially with electron withdrawing substituents (products **13b** and **13c**, Table 6). Slightly lower conversions and selectivity were obtained with electron donating substituents (products **13d** and **13e**, Table X). In the case of ortho-substituted benzylic alcohols, lower conversions were obtained (products **13f** and **13g**, Table 6). Secondary alcohols were converted smoothly with full selectivity to the ketone, and products **13h** and **13g** were obtained in 83% and 71% yield respectively. Product **13h** can be selectively obtained in slightly lower yield in just 2 hours by slowly adding the oxidant at 90 °C.

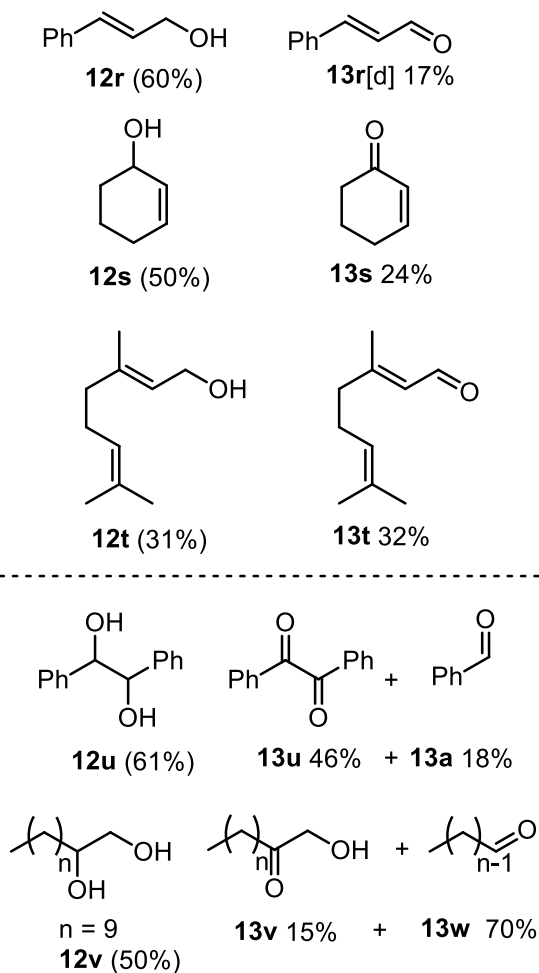
Table 6. Reaction scope: benzylic substrates

Reactions were performed with **5b** (2.5×10^{-2} mmol) in CH₃CN (10 mL) at a cat/alcohol/H₂O₂ ratio of 1:20:80; H₂O₂ (30% sol) was added by syringe pump in 2 h than allowing the reaction mixture to stir at 30 °C for further 22 h. Conversions of the starting alcohol (in brackets) and selectivity were calculated by GC and GC-MS (dodecane as the internal standard), [b] When the same reaction was repeated at 90 °C a 81% conversion was observed in just 2 h and **13h** was obtained with a 88% selectivity

A lower efficacy in the oxidation of both primary and secondary aliphatic alcohols stands out from data reported in Table 7. As a matter of fact, conversions of both nonyl alcohol, **12k**, and 1-pentyl-2-propanol, **12l**, hardly exceeds 15%, although in both cases reasonable selectivity were observed (67% for product **13k** and 99% for **13l**). Cyclic secondary alcohols were oxidized more efficiently to ketones, and products **13m-o** were obtained in good to excellent selectivity. Interestingly, in the oxidation of cyclobutanol, **12p**, cyclobutanone **13p** was the main product with high selectivity (78%), and as discussed before, this product should be the result of a 2-electron process involving a HAA and electron transfer. Anyway, from GC-MS analysis we were able to detect 4-hydroxybutyraldehyde, and γ -butyrolactone as major by-products which are resulting from a probable 1 electron mechanism in which the carbon centered radical escapes the solvent cage and results in the ring opening of the product. The mechanism of this transformation with our catalytic system is not completely determined, and a competitive 2-1 electron process might take place. In order to further test the selectivity of our system, several alcohols having both hydroxy and olefinic units were considered, to evaluate the possibility of preferential reactions. When cinnamyl alcohol, **12r**, was used as substrate, we observed a good conversion (60%), but a poor selectivity towards the expected cinnamaldehyde, **13r** (17%). Interestingly, the low yield in **13r** was accompanied by the formation of benzaldehyde as major byproduct (25%), which comes from the oxidative breaking of the starting double bond, that might be direct or via the formation of epoxide as reaction intermediate.^[62] In any case, the complete absence of products derived from the epoxidation reaction of the double bond was observed also in the case of 2-cyclohexenol **12s** and geraniol **12t**. Finally, we also checked the possibility to selectively oxidize 1,2-diols, whose chemo- and/or regioselective oxidation has still proven to be challenging (Table 8).^[63] When hydrobenzoin **12u** was treated under our optimized conditions, diketone was formed with a 46% selectivity, accompanied even in this case by the formation of benzaldehyde (18%), along with traces of other overoxidation products such as benzoic acid. Interestingly, dodecane-1,2-diol, **12v**, was not efficiently converted into the corresponding hydroxymethyl ketone **13v**, which was observed by GC-MS with high quantities of undecanal as major byproduct, **13w**.

Table 7. Reaction scope: linear and cyclic aliphatic substrates**12l** (17%)**13l** 99%n = 1; **12m** (81%)**13m** 73%n = 3; **12n** (90%)**13n** 99%**12o** (36%)**13o** 78%**12p** (32%)**13p** 78% + [c] 20%

Reactions were performed with **5b** (2.5×10^{-2} mmol) in CH_3CN (10 mL) at a cat/alcohol/ H_2O_2 ratio of 1:20:80; H_2O_2 (30% sol) was added by syringe pump in 2 h than allowing the reaction mixture to stir at 30 °C for further 22 h. Conversions of the starting alcohol (in brackets) and selectivity were calculated by GC and GC-MS (dodecane as the internal standard), [c] The presence of ring opened product was detected by GC-MS and 4-hydroxybutyaldehyde was obtained as major by-product

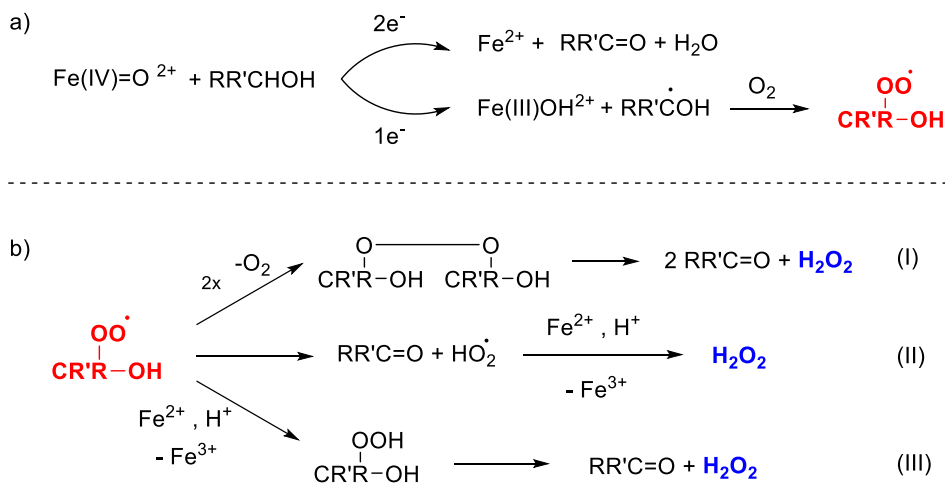
Table 8. Reaction scope: unsaturated substrates and diols.

Reactions were performed with **5b** (2.5×10^{-2} mmol) in CH_3CN (10 mL) at a cat/alcohol/ H_2O_2 ratio of 1:20:80; H_2O_2 (30% sol) was added by syringe pump in 2 h than allowing the reaction mixture to stir at 30 °C for further 22 h. Conversions of the starting alcohol (in brackets) and selectivity were calculated by GC and GC-MS (dodecane as the internal standard), [d] Benzaldehyde was found in large quantities, 25% overall selectivity.

1.2.4 Discussion on the proposed reaction mechanism:

To shed light on the reactivity of our system, we performed a series of experiment in order to assess the different possible reaction pathways followed by our catalyst. First, we evaluated the influence of EWG and EDG on the reaction kinetics using a series of p-substituted benzyl alcohols under the optimized reaction conditions described above, to evaluate the possible formation of a positive charged intermediate in the benzylic position. Plotting the k_{rel} of the reactions ($k_{rel} = k_X/k_H$) and the Hammett parameter we obtained a ρ value of -0.42 (experimental section). The low value of this parameter indicates that the reaction is not strongly influenced by the presence of EWG and EDG therefore the transition state does not involve a strong electrophilic species. The value is comparable with the synthetic Fe(IV)(O)-porphyrin•+ ($\rho = -0.39$).^[64] The kinetic constant (k_D) for the oxidation of the deuterated α,α -d₂-benzyl alcohol was calculated (see experimental section) and a kinetic isotope effect (KIE - k_H/k_D) of 3.52 was found. This relatively low value at 30 °C is typical for other oxo species and can discriminate the absence of any tunnelling effect, which might become predominant at lower temperatures. The rate determining step can be confirmed as the α C-H hydrogen atom abstraction of the alcohols.^[65] Still, the species responsible for this transformation can be formed by two substantial mechanisms: a 1e- mechanism in which O-O of iron(III) hydroperoxo undergoes homolytic cleavage to form Fe(IV)(O)+ •OH or ii) a 2e- mechanism in which the same species undergoes heterolytic cleavage to form Fe(V)(O) and OH- (Scheme 15). In our case, it seems that the bond dissociation energy (BDE) of the α C-H hydrogen atom cannot be neglected. In fact, the conversion of benzylic alcohols (BDE ~80 Kcal/mol) are much higher than the aliphatic ones (BDE ~90+ Kcal/mol).^[65] This might be more predominant for a 2-electron mechanism, given the fact that the mono-electronic mechanism would produce a strongly reactive hydroxyl radical that would discriminate less between different C-H bonds. When we carried out benzyl alcohol oxidation in presence of a radical scavenger (BHT = butylhydroxytoluene) a lowering of the conversion was noticed, and this might be accounted for radical trapping of the intermediates formed. Taking in consideration the long reaction time needed for our system to reach a good conversion of the substrate, we cannot exclude the accumulation of carbon centered radicals deriving from the hydrogen atom abstraction (HAA) which can form organic peroxides and hydroperoxides that are known to be converted into alcohol and

aldehyde/ketone at a very slow rate. Peroxidic substrates can also decompose and produce hydrogen peroxide as shown in scheme 15.



Scheme 15. a) Possible formation of organic peroxides/hydroperoxides and b) decomposition pathways

This very complex behavior is not unusual for iron systems in oxidation reaction. The presence of single electron processes is typical for high-spin iron complexes, and this might lead to a plethora of possible reaction mechanism. Our catalyst presents two cis-labile positions which might be responsible for this peculiarity because once the possible Fe(III)(OOH) is formed, it can both undergo the well-defined homolytic cleavage to Fe(IV)(O) or it can be coordinated in a η^2 fashion and undergo heterolytic cleavage to Fe(V)(O)(OH) (Figure 2).

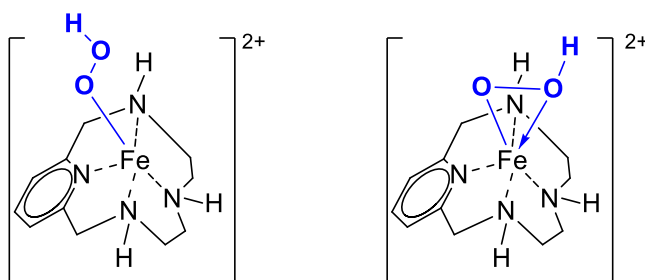


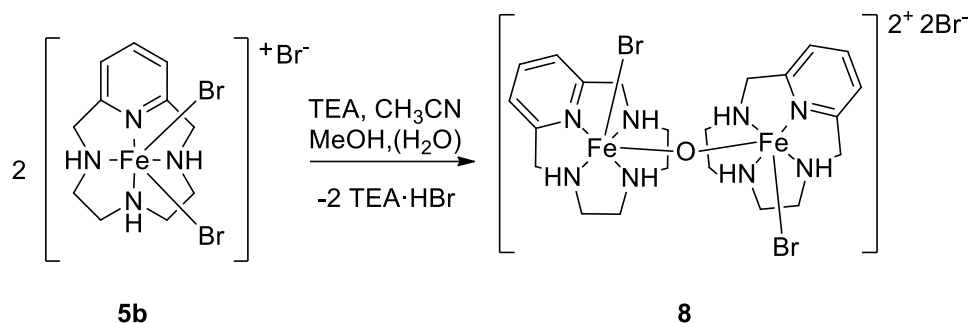
Figure 2. Possible coordination geometries of an “hydroperoxo” bound iron complex of a pycnen ligand.

Trace presence of brominated products were detected by GC-MS analysis. The formation of Br^+ species can be possible, but the very low presence of brominated products might highlight how unfavored this process is in our conditions. We also observed the formation of brominated acetonitrile, and it is well documented that it could be a promoter for $1e^-$ processes that might favor this chemistry.^[66] After 24 h of reaction, the metal complex could only be recovered as a flocculent brown powder that was not active anymore as catalyst in the oxidation reaction. This might be attributed to either the decomplexation of iron or the formation of other inactive dimer species. The investigation of the possible activity of dimeric complexes continued in our research lab, with the aim of a more comprehension of their structural and spectroscopical behavior.

Oxo-bridged iron complexes have been a topic of interest in the field of biomolecular catalysis and modelling since the early 80's, where the focus was on the investigation of the reactivity of enzymes such as Hemerythrin and Oxyhemerythrin.^[42,43,67-70] Another aspect of interest of this peculiar class of iron(III) molecules was related to their magnetic properties, where strong antiferromagnetic coupling was spectroscopically investigated on synthetic model compounds, based on both *heme* and *non-heme* complexes.^[44,65,71,72] As previously stated in the introduction, the role of such dimeric species in a catalytic transformation is still under debate and it is not easy to assess their activity towards, for example, oxidation reactions. In a very recent paper, K. Green and co-workers reported the isolation and characterization of iron(III) oxo-bridged pyclen complexes as intermediates in the C-C coupling of pyrrole and phenylboronic acid and proved their negligible catalytic activity with respect to their monomeric counterparts.^[40] These compounds are obtainable by the interaction of mononuclear iron species with a base in the presence of water. Complex **5b** is strictly related to the one just mentioned and for this reason, inspired by this new findings, we synthesized and characterized three novel symmetric and non-symmetric iron(III) bromide oxo-bridged pyclen complexes **8,9,10**, to evaluate the differences arising from different coordination environment.

1.2.5 Complex 8:

The dimeric oxo-bridged form of complex **5b** was prepared in the same fashion of the previously described syntheses of reported by Green and coworkers and it shows the same conformation, with bromine atoms substituting the chlorine ones.^[40]



Scheme 16. Synthesis of complex **8**.

Complex **5b** was dissolved in acetonitrile with the addition of methanol and after the addition of triethylamine, it has been stirred for 1 hour (Scheme 16). The resulting solution was left to diffuse with a layer of diethyl ether for several days to obtain dark red crystals suitable for XRD. Thanks to the crystal structure determination, we were able to notice that two macrocyclic units of ligand **2** approach and bridge by an oxygen atom to form a highly symmetric compound. Complex **8** crystallizes in the monoclinic crystal system, *s.g.* $C2/m$. The asymmetric unit consists of only one half of the O-Fe(2)Br moiety and a bromide anion in the second coordination sphere, so the structure features two identical iron centres. Both iron atoms are 6-fold coordinated in a distorted octahedral geometry by the linking oxygen, a bromide ligand and the tetraaza-macrocycle **2**, which adopts its usual *cis*-(+++)^[10,73] conformation. The complex is di-cationic and the two bromide anions are required for charge balance. The O atom lies on an inversion centre so that the two O-Fe(2)Br units are symmetrical and placed in a staggered conformation. Furthermore, the Fe-O-Fe fragment is linear with an angle of 180° and a $\text{Fe}\cdots\text{Fe}$ separation of $3.5360(5)$ Å. Comparing this complex with the previously reported by Green, in the latter the Fe-O-Fe unit was slightly bent, and after a search in the CSD database, we were able to notice that the XFe-O-FeX motif with a linear μ -oxo bridge and a staggered conformation of the halide donors also appears in numerous complexes of other tetraaza-macrocyclic or chelating ligands.^[39,74-82]

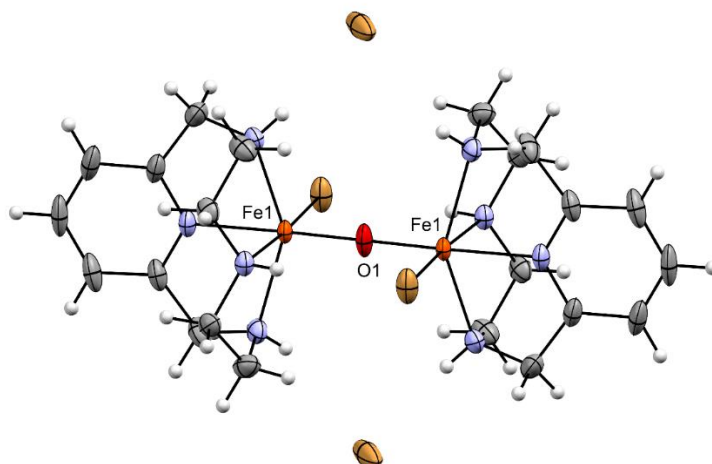
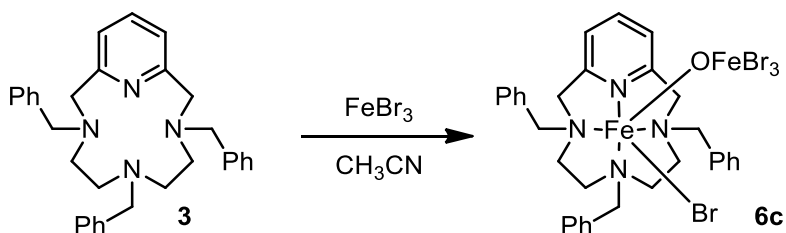


Figure 3. Structure of **8** with thermal ellipsoid at 50 % probability level: Solvent molecules are omitted for clarity (details in experimental section). Selected bond distances (Å): Fe1-O1 1.7680(4) (the two iron atoms are symmetry related by $-x+1, -y, -z+1$).

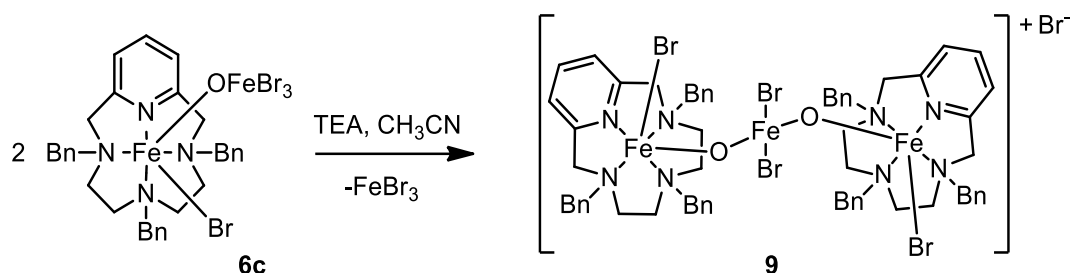
1.2.6 Complex 9:

The synthesis of complex **9** was achieved starting from a metal complex precursor that was somehow unexpected. The treatment of ligand **3** with iron(III) bromide to obtain a complex similar to the already reported **6a** and **6b**, led to the undesired formation of a dimeric complex **6c** in which the coordinated iron in the macrocycle bears a $-\text{OFeBr}_3$ moiety. The structure of this compound was only tentatively assigned using mass spectroscopy and elemental analysis but only thanks to Raman analysis we were able to confirm the dimeric nature and the presence of the Fe-O-Fe fragment (*vide infra*).



Scheme 17. Synthesis of complex **6c**.

Further treatment of **6c** with triethylamine led to the formation of a very interesting trinuclear iron(III) species, complex **9**. The lesser steric hindrance of ligand **3** in comparison with ligand **2** and the presence of a bridging iron unit allows the formation of this trimer with two iron-pyclen moieties bridged by a tetrahedral ferrate anion. Red prismatic crystals of **9** were obtained by slow diffusion of diethyl ether in a solution of acetonitrile/MeOH. Complex **9** crystallizes in the orthorhombic crystal system, s.g. $Pca2_1$. The asymmetric unit contains one molecule of **9** along with a bromide counterion plus disordered molecules of acetonitrile and methanol. The crystal structure is displayed in Figure 4.



Scheme 18. Synthesis of complex **9**.

Each of the two octahedral iron centers, **Fe1** and **Fe3**, interact with four nitrogen donors of the tetraaza-macrocycle, a bromide ligand and the μ -O atom and they are connected by a bridging tetrahedral **FeBr₂O₂** unit *via* μ -oxo linkages. Fe-O-Fe angles are 173.3(3) $^\circ$ for Fe1-O1-Fe2 and 173.4(3) $^\circ$ for Fe3-O2-Fe2, while Fe \cdots Fe distances are 3.5290(4) Å for Fe1 \cdots Fe2 and 3.5470(3) Å for Fe3 \cdots Fe2. Moreover, the octahedral fragments are positioned in such a way that the two bromide ligands point in opposite direction to each other. Even in this case, the macrocycles are folded in *cis*-(+++) *conformation* [40], with the bulky *N*-benzyl substituents that point above the N₄ macrocyclic plane and leave the macrocyclic cavity available for the coordination to the iron atoms. It is worth mentioning that an analogous species with a higher nuclearity was obtained by Brewer and co-workers.^[40] In the presence of a less hindered tetraaza-macrocycle, they crystallized a tetranuclear complex in which three octahedral iron(III) units are connected by a tetrahedral iron(III) centre.

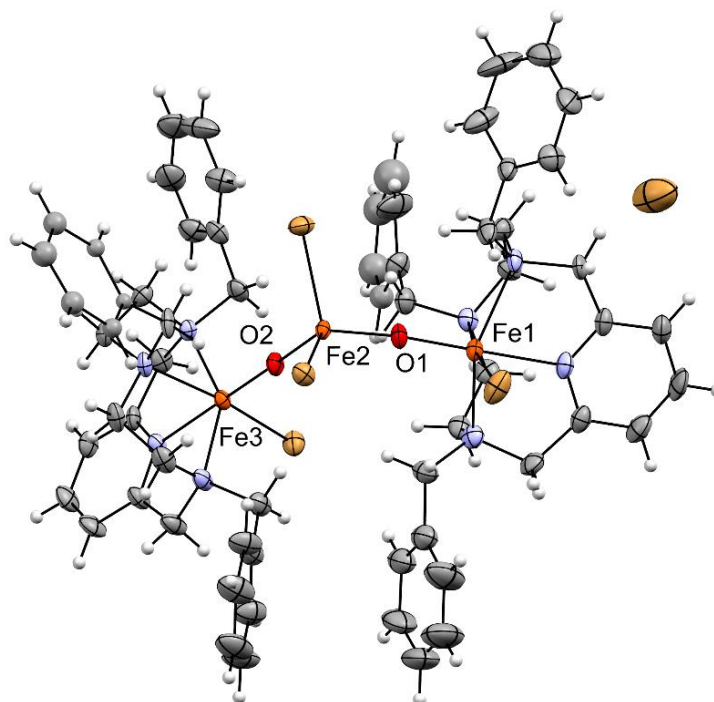
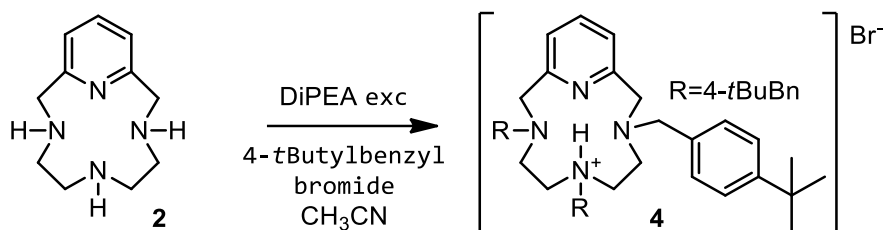


Figure 4. Structure of **9** with thermal ellipsoid at 50 % probability level: Solvent molecules are omitted for clarity and disordered moieties are treated with isotropic models (details in Supporting Information). Selected bond distances (Å): Fe1-O1 1.764(4), Fe3-O2 1.766(4), Fe2-O1 1.770(4), Fe2-O2 1.786(4).

1.2.7 Complex 10:

Ligand **4** were synthesized starting from ligand **2** by N-alkylation with (4-*t*butyl)benzyl bromide in refluxing acetonitrile, in presence of excess DiPEA (Scheme 19).^[83] An inorganic base such as potassium carbonate can be employed with similar results. The reaction proceeds with the formation of the functionalized ligand in low yield (usually around 35%) and most importantly the product is obtained in the protonated form as hydrobromic salt, after precipitation with cold acetone.



Scheme 19. Synthesis of protonated ligand **4**.

This might be due to the inner basicity of the polyamine ligand which is hampered by the substitution of the N atoms with benzylic substituents, that renders the ligand, even in presence of excess DiPEA, the real base of the reaction. The ligand was characterized by XRD analysis, and the structure is reported in figure 5.

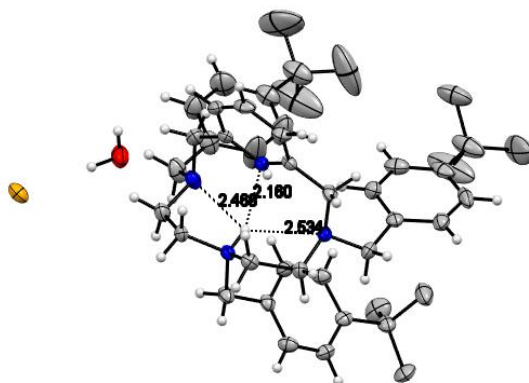
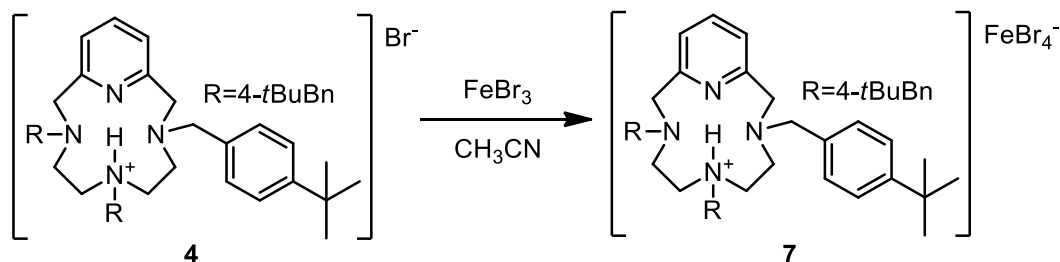


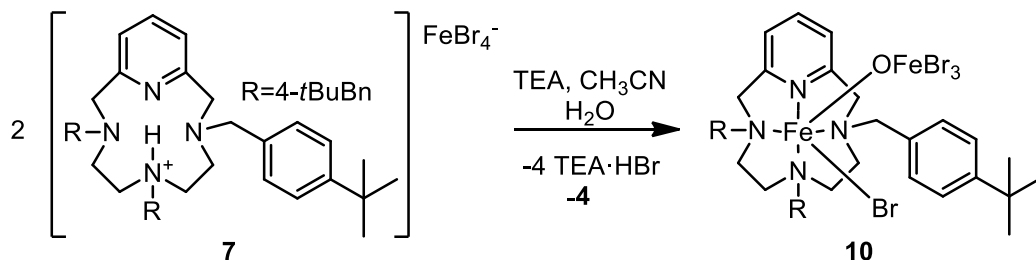
Figure 5. Synthesis of protonated ligand **4**.

When ligand **4** was treated in acetonitrile with FeBr_3 in the previously described procedure for the formation of the other metal complexes (Scheme 20), the reaction proceeded to the formation of a bright red solid product **7** that was later identified as a salt in which the ligand retained the proton inside the cavity and iron was the counterion, in form of tetrabromoferrate.^[83]



Scheme 20. Synthesis of the tetrabromoferrate salt **7**

Unfortunately, all the attempts to crystallize this material have failed and the structural features of compound **7** were only assigned thank again to Raman spectroscopy, in combination with MS and elemental analysis. At this point, after dissolution of **7** in acetonitrile, triethylamine was diluted in acetonitrile and added dropwise (Scheme 21). Slow diffusion of diethyl ether in the acetonitrile solution led to the formation of red block shaped crystals of **10** after several weeks.



Scheme 21. Synthesis of dimeric complex **10**

Crystal structure of the novel compound **10** was obtained by X-Ray diffraction at 150 K (Figure 6). The reaction proceeds with the loss of a ligand **4** molecule to yield a non-symmetrical di-iron(III) complex. It is most likely due to the steric bulkiness of the ligand, which disfavoured the approaching of two identical units. To account for the observed stoichiometry, the bridging μ -oxo atom is furnished by water, which can also be adventitious when working with undistilled solvents, and 4 equivalents of triethylammonium bromide are released. Complex **10** crystallizes in the triclinic crystal system, s.g. $P\bar{1}$. The asymmetric unit comprises one molecule of **10** along with disordered acetamide molecules, formed by basic hydrolysis of acetonitrile. As shown in figure X, the complex has a dimeric nature with two iron atoms in different coordination environments. The overall coordination geometry is similar to that of already reported complexes^[34, 35, 37, 38, 84-86] with a $N_4XFe(\mu\text{-oxo})FeX_3$ core: **Fe1** is hexacoordinated in a distorted octahedral geometry by the four nitrogen donors of the tetraaza-macrocyclic, a bromine atom and a μ -oxo ligand; this μ -oxo bridge connects **Fe1** to the iron centre **Fe2**, which is in tetrahedral geometry, surrounded by three bromine atoms and the linking oxygen atom. The **Fe1-O-Fe2** fragment is bent, with an angle of $153.1(2)^\circ$ and a $Fe\cdots Fe$ distance of $3.4398(9)$ Å. The macrocycle is folded in a *cis*-(+++) *conformation with the N substituents that are positioned above the N4 macrocyclic plane*^[10, 73]. It is important to notice that the conformation of the ligand in **10** greatly differs from the structure of **4**.^[83] In fact, when the ligand is protonated, the bonds between the substituted nitrogen atoms and the corresponding pendants are rotated in such a way that the bulky substituents hinder the macrocyclic cavity. In the case of **10**, instead, the substituents are pointing away from the macrocyclic cavity, allowing the coordination of an iron(III) cation.

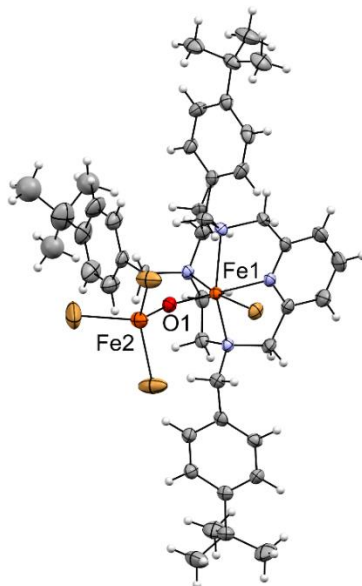


Figure 6. Structure of **10** with thermal ellipsoid at 50 % probability level: Solvent molecules are omitted for clarity and disordered moieties are treated with isotropic models (details in experimental section). Selected bond distances (Å): Fe1-O1 1.788(4), Fe2-O1 1.749(4).

1.2.8 Raman spectroscopy:

Raman spectroscopy is a widely employed analytical technique for the study of the vibrational bands associated to the Fe-O-Fe fragment in proteins and model compounds^[87-91]. Even in our case, Raman spectroscopy turned to be a fundamental tool to characterize the μ -O complexes under investigation. Micro-Raman spectroscopy was carried out using a Horiba LabRam HR evolution at the Dipartimento di Scienze della Terra "A. Desio" of the Università degli Studi di Milano (Figure 7). The spectrometer is equipped with a Nd-Yag 532 nm/100mW with Ultra Low Frequency (ULF) filters. Scattered light was collected by a 100X objective (NA aperture = 0.9) in backscattering geometry; a diffraction grating with 600 lines/mm and the hole set at 200 μ m were used. The spectra have been detected by a Peltier-cooled Charge Couple Detector. To balance signal to noise and to reduce the damage of the highly absorbing samples 3 accumulations for 60 seconds were collected with a laser power set to 0.1%. Instrument calibration was performed before each round of analysis using the peak at 520.70 cm^{-1} of a silicon wafer. We

performed our analysis using an excitation wavelength of 532 nm and collecting the backscattering light from the powdered samples.



Figure 7. The Raman spectrometer used for this study, thanks to prof. Patrizia Fumagalli (Dipartimento di Scienze della Terra, Università degli Studi di Milano)

1.2.9 Complex 5b and 8:

As expected from its crystal structure already reported^[92], in the Raman spectra of the precursor **5b** we found the typical **Fe-Br** stretching modes in the region between **200-300 cm⁻¹** ^[93-95]. In the spectra of compound **8**, the striking difference, that was somehow wanted, from compound **5b** is the presence of a very intense band with a maximum at **409 cm⁻¹** assigned to the symmetric stretching of the **Fe-O-Fe** moiety. The asymmetric stretching vibration band associated to the same fragment, usually found in the region between **750-900 cm⁻¹**, is not present; in fact, according to the selection rules, such vibrational mode is forbidden in the Raman spectrum due to the centrosymmetric nature of **8**. Moreover, bands that can be ascribed to Fe-N stretching vibration bands are present in both the precursor **5b** and complex **8** at **381 cm⁻¹** and **447 cm⁻¹**^[96-98]. (see experimental section).

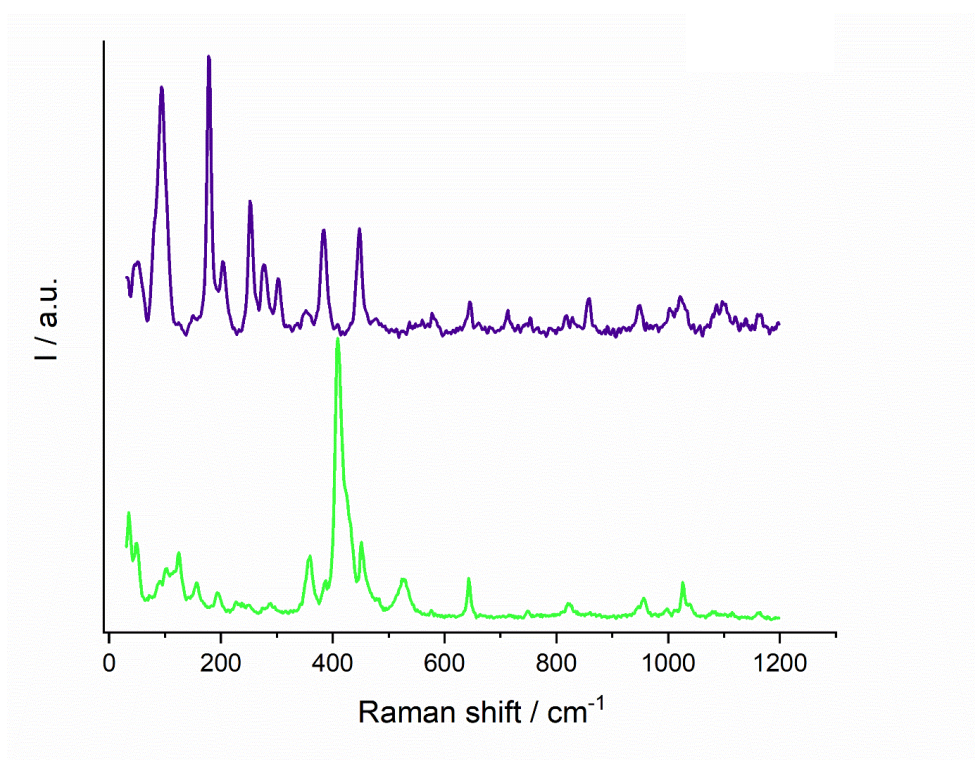
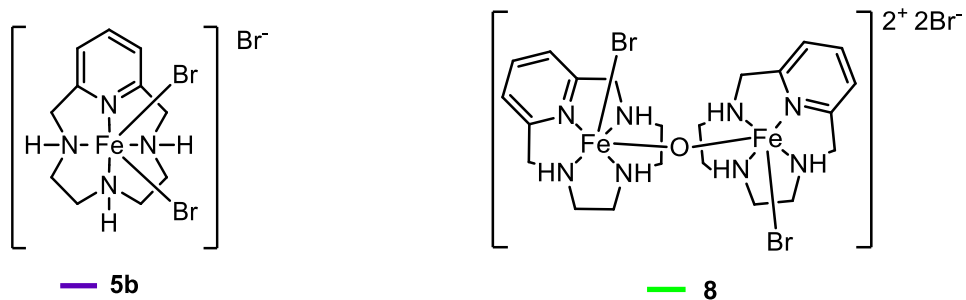
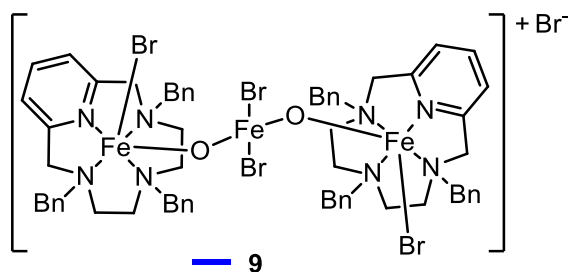
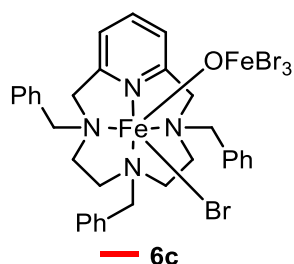


Figure 8. Raman spectra of complex **5b** (violet, top) and **8** (green, bottom).

1.2.10 Complex 6c and 9:

As previously described, at the very beginning the structure of the precursor **6c** was only assigned by elemental analysis and MS. In the case of ESI-MS experiments, the ionization in methanol resulted in the formation of putative (Ligand 3)Fe(OMe); those fragments are clearly not useful for the determination of the structure of **6c** but rather a mere confirmation of the formation of an actual iron complex with the corresponding ligand. All the attempts to crystallize **6c** failed and for this reason Raman Spectroscopy proved to be a fundamental tool to elucidate its true nature. In fact, the spectra of **6c** closely resemble that of complex **7**. Based on these findings, we were able to claim the presence of two non-symmetric iron units bridged by an oxygen atom, with ν_s at 378 cm^{-1} and ν_{as} at 861 cm^{-1} . The reaction of **6c** with a base afforded compound **9** in which two identical octahedral coordinated iron units are connected to an unusual tetrahedral FeO_2Br_2 fragment *via* μ -oxo bridges. As we can see in figure X, the Raman spectra of **9** and the precursor share to a large extent the same features, but with inverted intensities of ν_s and ν_{as} modes. An increasing asymmetry of the two iron centers involved in the vibration has been invoked to account for the enhancement of ν_{as} ^[87,99,100]



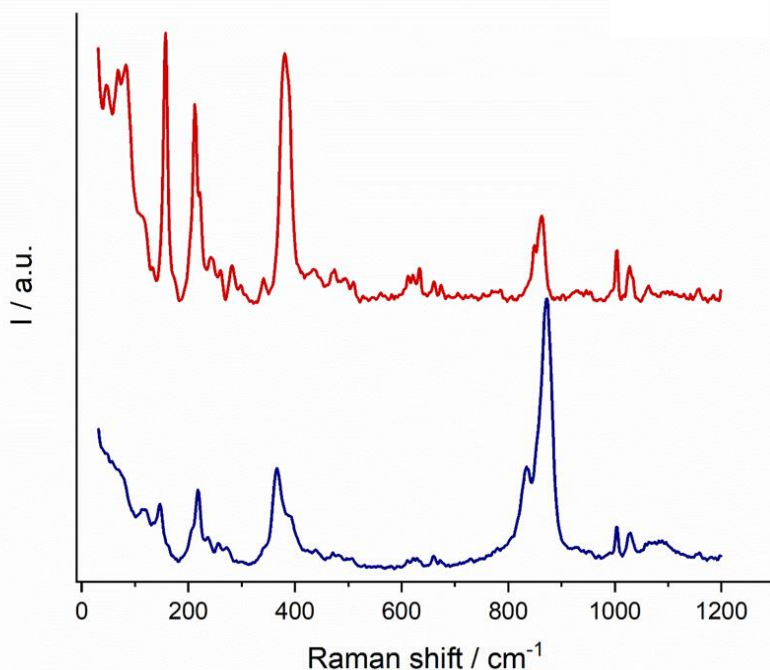


Figure 9. Raman spectra of complex **6c** (red, top) and **9** (blue, bottom)

1.2.11 Complex **7** and **10**:

The Raman spectra of the precursor **7** is a direct proof of the presence of a FeBr_4^- anion. The most intense lines at 203 cm^{-1} and 294 cm^{-1} can indeed be assigned as A_1 and T_2 vibrational bands of the aforementioned tetrahedral unit^[101] and the less intense one at $\sim 90 \text{ cm}^{-1}$ tentatively assigned as the E mode^[102]. As a proof of the formation of the oxo-bridged complex, the Raman spectra of **10** clearly shows the presence of two intense bands at 414 cm^{-1} and 849 cm^{-1} , which can be respectively assigned to the symmetric (ν_s) and asymmetric (ν_{as}) Fe-O-Fe vibration^[87,88,91]. In analogy with related μ -oxo complexes of Ru and Os^[103], the sharp line at $\sim 154 \text{ cm}^{-1}$ might be assigned to the Fe-O-Fe bending vibration (δ), even though this mode was associated to a line at $\sim 210 \text{ cm}^{-1}$ in the $[\text{Cl}_3\text{Fe-O-FeCl}_3]^{2-}$ dianion^[104]. The formation of complex **10** also resulted in the modification of the whole spectra in the region between $200\text{-}300 \text{ cm}^{-1}$, in which Fe-Br stretching bands are usually observed^[93-95], due to a lowering of the overall symmetry by the formation of a $\text{N}_4\text{BrFe(O)FeBr}_3$ unit.

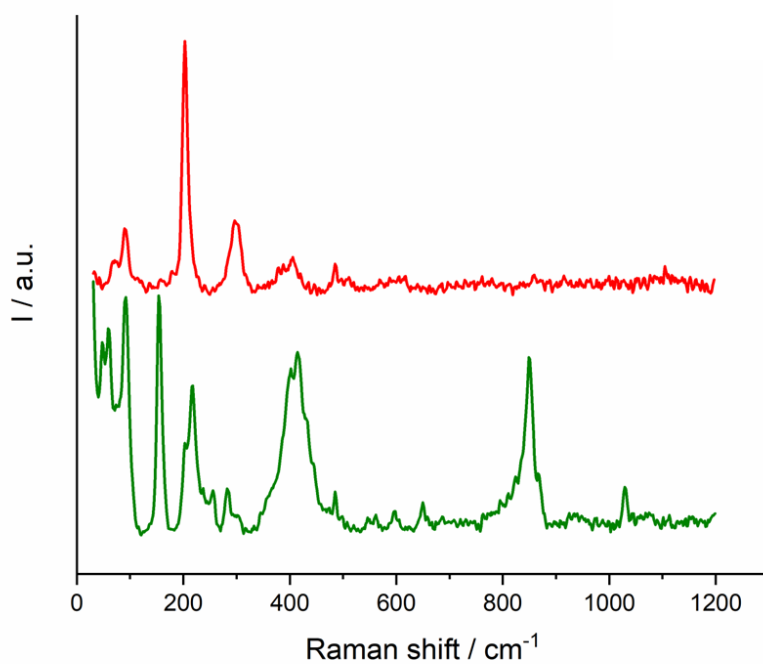
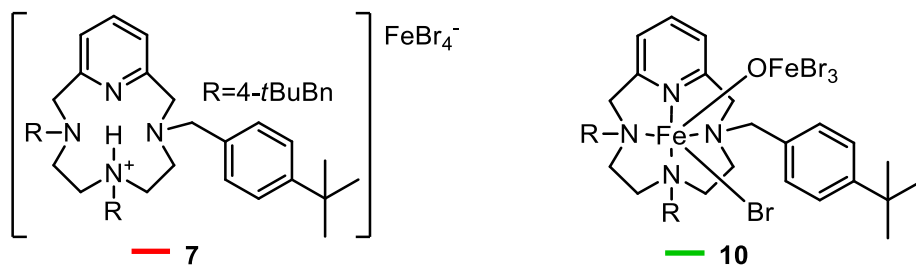


Figure 10. Raman spectra of complex **7** (red, top) and **10** (green, bottom)

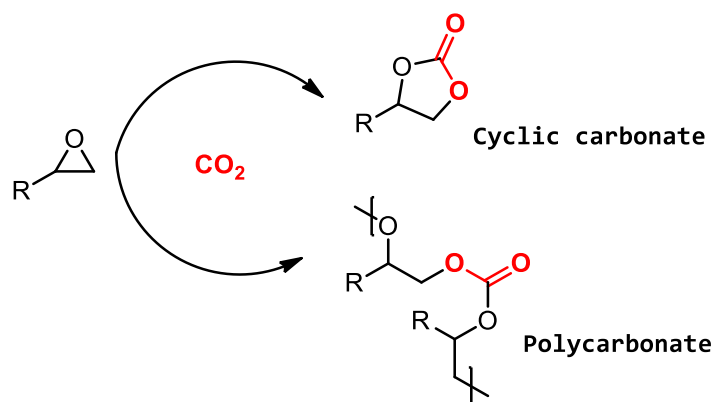
1.3 CONCLUSIONS:

We successfully developed a catalytic system for selective alcohol oxidation, based on iron(III) bromide complex of a non-functionalized pyclen ligand.^[105] The catalyst was very active in the reaction of benzylic substrates, using hydrogen peroxide as oxidant at room temperature, in acetonitrile as solvent. The possible mechanism of the reaction was investigated by means different experiments: the Hammett plot of the reaction of different substituted benzyl alcohols showed a negligible influence of both EDG and EWG, and the KIE value obtained comparing the rate of the reaction of benzyl alcohol and the deuterated compound was similar to other iron-based systems. These findings are in accord with an high valent iron-oxo species that performs hydrogen atom abstraction on the alcohol. A large scope of reaction was performed, with good conversion and selectivity on most of benzylic substrates, slower conversion rate on aliphatic alcohols and worse selectivity on unsaturated alcohols. We then explored the synthesis and characterization of different oxo-bridged compounds which may be produced after oxidation reactions of the monomeric precursor. We obtained the structure by XRD, to evaluate how the bulkiness of the ligand influences the resulting complex. We successfully employed Raman spectroscopy, for the first time in our group, as a useful tool for the determination of the nature of the Fe-O-Fe moiety, in terms of symmetrical and unsymmetrical contribution, in the different coordination environment.^[106] This spectroscopical approach might be exploited in the future as an intuitive probe of the purity of the complexes prepared in our group, as the undesired presence of dimeric species is sometimes noticed.

2 CYCLOADDITION OF CO₂ TO EPOXIDES WITH PYCLEN METAL COMPLEXES AS CATALYSTS

2.1 INTRODUCTION:

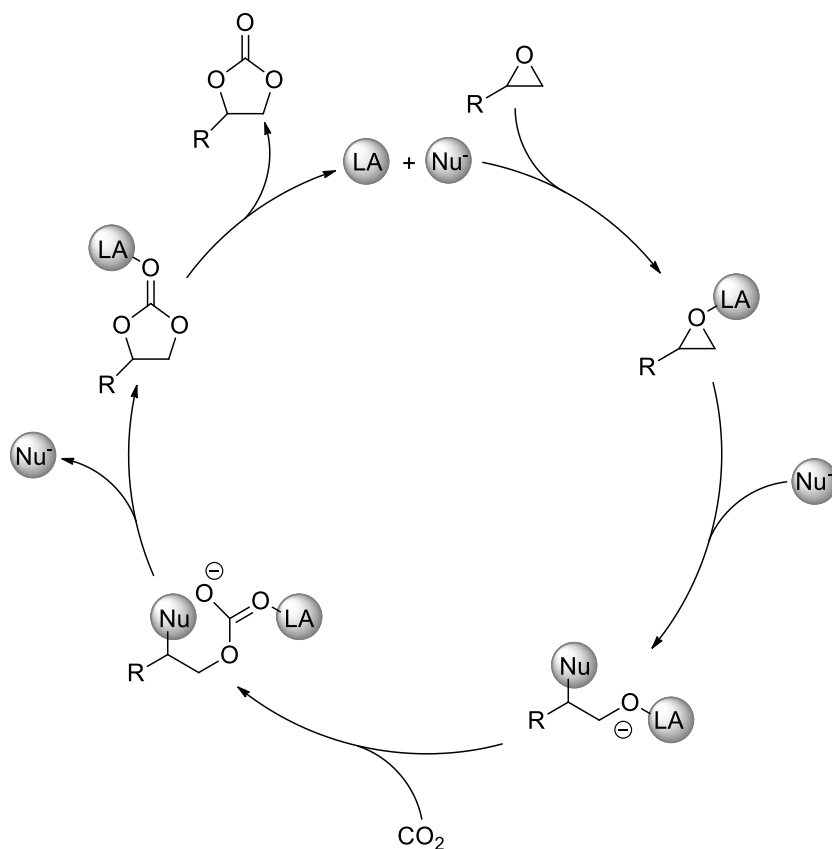
The use of carbon dioxide as a feedstock has aroused large interest since the start of the second half of the last century, but usually, metal-catalyzed transformation of carbon dioxide and organic substrates resulted in low turnovers and selectivity. The intrinsic high thermodynamic stability of CO₂ has strongly limited its employment as C₁ synthon. In this view, the coupling of CO₂ with high free energy substrates such as epoxides to generate polycarbonates and/or cyclic carbonates (Scheme 22) represents one solution, and it is one of the few processes that has been industrialized until now.^[107,108]



Scheme 22. Schematic representation of the reaction of epoxides and carbon dioxide to yield cyclic or polycarbonates

The five membered cyclic carbonates obtained by CO₂ cycloaddition with epoxides are biodegradable liquids with low toxicity^[109] and are mainly employed as aprotic polar solvents,^[107] electrolytes in secondary batteries, intermediates in fine chemical synthesis and monomers for polycarbonate-based polymers.^[110-113] This process has been profoundly studied since it represented a better approach at the

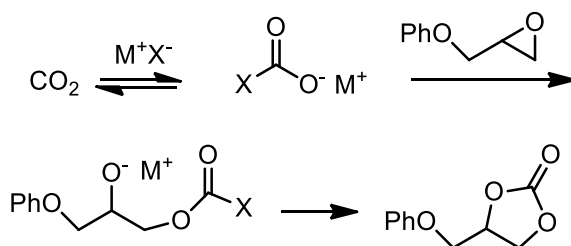
synthesis of those products, where the classical methodology relied on the use of phosgene. Since the first report by Inoue *et al.* in 1969,^[114] who proved to be able to produce polycarbonates from epoxides using $\text{Et}_2\text{Zn}/\text{H}_2\text{O}$, this field has witnessed an impressive boost, where the “bulk” of the works occurred between 70’s and 80’s. Since then, a plethora of catalyst were reported to be active in the production of cyclic and polycarbonates, but the difficulty in finding a particularly active and reproducible catalytic system has slowed down the research in this field for few decades. This problem, however, has been accompanied by a deep understanding of the reaction mechanism (Scheme 23): the reaction begins with a nucleophilic attack on the epoxide that leads to the ring opening product.



Scheme 23. General mechanism of the formation of cyclic carbonates from CO_2 and epoxides, catalyzed by a Lewis acid and a nucleophile

In general, the nucleophiles of choice are represented by organic halides, and the attack is favoured by the presence of a Lewis acid to activate the epoxide either in an *intermolecular* or in an *intramolecular* fashion. Following this, the ring-opened product can undergo either CO₂ insertion to form a carbonate or repetitive epoxide insertion to lead to polyether formation. Carbonate linkages will be favoured in case the CO₂ insertion rate is faster than that of epoxide insertion and this might be controlled by the reaction conditions and the nature of the catalyst, where the cyclic product is still the largely thermodynamically favoured product.

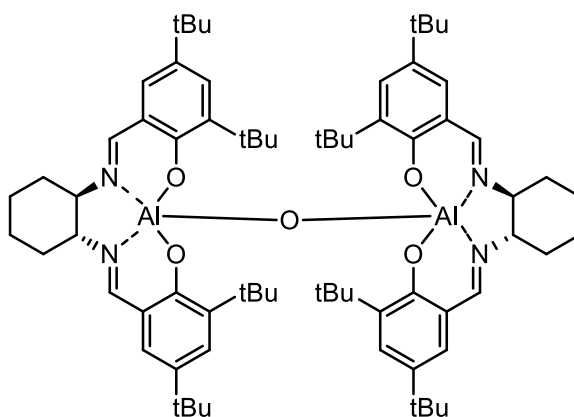
In the case of alkali metals catalyzed synthesis of cyclic carbonates, Rokicki and co-workers reported in 1984 a system^[115] based on alkali metal salts and phase transfer reagents, such as crown ethers. They were able to claim that the reactivity of the catalyst increased with increasing nucleophilicity of the anion and the dimensions of the cation, where the first attack the epoxide to yield an "alcoholate" anion that is stabilized by the activated cation. This intermediate reacts smoothly with CO₂ rather than with another epoxide ring, and the carbonate anion formed is thermodynamically driven to form the cyclic product rather than react with another substrate molecule, thus no copolymerization products were found. This methodology required relatively harsh conditions for long reaction time to obtain good results. A way less acknowledged mechanism proposed by Endo and co-workers^[116] (Scheme 24) involves the initial activation of carbon dioxide by the nucleophile, at very high pressure, forming an ionic species that can interact with the epoxide, but this is still not strongly supported by evidence.



Scheme 24. Alternative method proposed by Endo with activation of carbon dioxide

In a report from Kihara *et al.* it is explained that simple halide nucleophiles are able to catalyze this reaction efficiently, in the order of chloride > bromide > iodide \approx fluoride.^[116] The nucleophilicity is a fundamental aspect in this reaction but also the ability to act as a leaving group is strongly influencing the overall reactivity.

During the course of the years, both main-group and transition metals catalysts have been tested in the synthesis of cyclic carbonates. For main group, aluminium based systems proved to be fairly active, since the discovery of aluminium trichloride in presence of triphenylphosphine as an efficient catalyst for the synthesis of cyclic carbonates, in 1980.^[117] The development of aluminium-based porphyrin systems by Inoue in 1978 is another example of how a finely tuned main group metal complex is a suitable catalyst for this transformation.^[118] In 2010, North and co-workers exploited the activity of aluminium as catalyst using salen-based bimetallic complexes (Scheme 25).^[119] The catalytic system is composed by the metal complex and tetrabutylammonium bromide as co-catalyst.



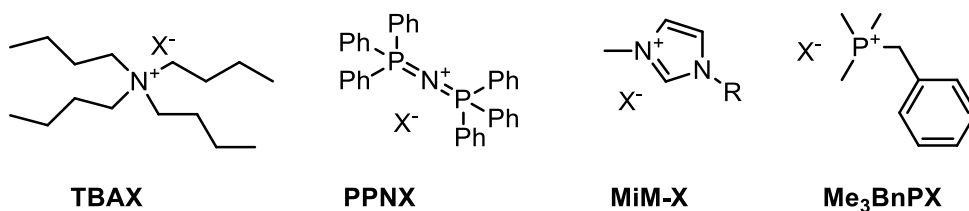
Scheme 25. The bimetallic oxo-bridged aluminum catalyst proposed by North and co-workers in 2010

A deep experimental study was performed to shed light on the role of the co-catalyst and, rather than being a mere supplier of nucleophilic bromide, it was also responsible for the formation of

tributylamine which can contribute to the activation of carbon dioxide and hamper the reactivity of the system. Other transition metal catalysts based on the most disparate ligands were reported to be active in this transformation in the last 20 years, with the large majority that required the presence of a remarkable quantity of added co-catalyst. Very few examples are reported to be active without the addition of an external nucleophilic species, most of them relying on bimetallic systems.

The presence or absence of a co-catalyst in this transformation has laid the background for a questionable topic: which is the real catalyst? The metal complex or the added co-catalyst? Indeed, jumping backwards in 1996, a brilliant review from Darensbourg and Holtcamp^[120] summarizes the metal complexes reported to be active in the synthesis of cyclic and polycarbonates up to that point, and as opening in the first chapter they clearly claim: ***“simple quaternary salts such as alkyl ammonium or phosphonium halides are extremely effective for high-yield conversions of many epoxides with carbon dioxide to form the corresponding cyclic carbonate”***. This is of striking importance in defining the true active catalyst in this kind of transformation, since the turnover frequencies are usually misleadingly reported based on the amount of metal catalyst even in large excess of a nucleophilic co-catalyst as brilliantly reported by Campisciano and co-workers.^[121] Indeed, the evaluation of the efficiency of a catalyst used in very small loading, in presence of a large amount of quaternary ammonium salts (even more than 10-fold in respect to the metal), especially at high temperatures, should be questioned but it is usually overlooked; in any case, I suggest that for clarity, these results should be evaluated in the absence of the metal-based catalyst itself, in control experiments.

Nevertheless, the activity of simple organic halides as catalysts has opened the way to the development of organocatalytic synthesis of cyclic carbonates (Scheme 26). Homogeneous organocatalysts that consists of ionic nucleophile (Lewis bases), typically organic halides, such as quaternary ammonium,^[122-124] bis(triphenylphosphine)iminium salts^[125] and ionic liquids^[126] in the absence of a Lewis acid, however, usually require quite high reaction temperatures and CO₂ pressure to achieve good results, intensive work up procedures for the isolation of the products and of lack of reutilization of the catalytic system due to degradation.^[127]

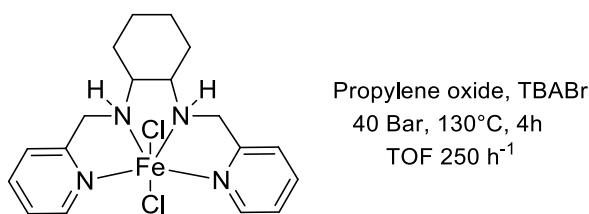


Scheme 26. Examples of organic halides reagents used for this reaction.

In this view, the most active catalytic systems for the cycloaddition of CO₂ to epoxides remain the ones in which there is the presence of a Lewis acid, which is able to coordinate the oxygen atom of the epoxide in order to activate it towards the attack of the nucleophilic Lewis base.^[128] These two active species can be embedded in a single bifunctional catalyst or in a binary system of two separate components. The class of Lewis acids that has been more exploited consist of transition metal complexes, which shows very high activities but whose selectivity towards cyclic or polymeric carbonates is strongly correlated to the nature of the nucleophile and the metal center.

Many examples have been reported in the literature, but in view of my thesis I want to highlight some examples in which non-toxic and Earth-abundant metals were used. Among the different Lewis acid metal catalyst employed, zinc has proved to be very efficient in performing this transformation. However, zinc scarcity might represent a future problem and research efforts have been focused on the development of metal complexes based on the more Earth-abundant, non-toxic metal iron.^[129] Given to its natural and high chemical reactivity, iron is considered one of the most promising metals for homogeneous catalysis.^[130] A broad number of iron complexes have been reported as active catalysts in the chemical fixation of CO₂ with epoxides. One of the earliest example is reported by Wang and co-workers in 2014,^[131] where a N,N'-bis-2-pyridinylmethylene-cyclohexane-1,2-diamine ligand (Scheme 27) is used to obtain an iron complex which was active for the synthesis of propylene oxide, with TBABr as co-catalyst, in relatively harsh conditions. More recently, Capacchione and co-workers brilliantly exploited the activity of an iron(III) complex of an [OSSO] type ligand,^[50] which was previously used in the synthesis of chromium

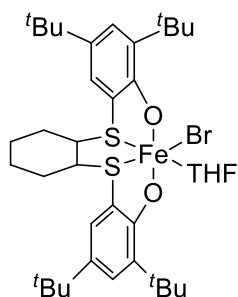
compounds. The complex proposed in this work is a pre-catalyst that in presence of TBABr forms a “ferrate” compound that acts as the real catalyst. The latter proved to be highly active even at low temperature and ambient pressure of CO₂, in presence of a 5-fold quantity of TBABr (Scheme 28).



Wang, 2014

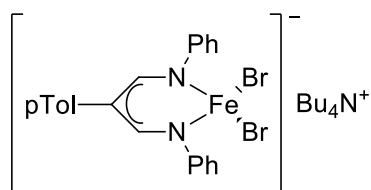
Scheme 27. Catalytic system proposed by Wang and co-workers.

A similar approach was studied by Pescarmona and Otten in 2019,^[132] where a series of formazanate complex of iron were successfully employed as catalyst. In this case, the preformed ferrate catalyst was active without the addition of any external nucleophile, albeit in relatively harsher conditions and lower turnovers (Scheme 28).



Capacchione, 2018

Propylene oxide, TBABr
1 Bar, 35°C, 6h
TOF 108 h⁻¹

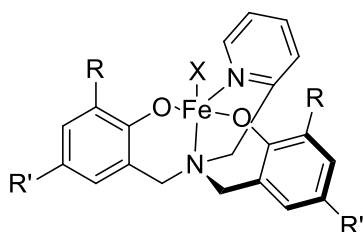


Pescarmona, Otten, 2019

Propylene oxide
12 Bar, 90°C, 18h
TOF 14 h⁻¹

Scheme 28. Ferrate compounds employed as catalysts by Capacchione and Pescarmona.

Other examples were recently reported, in which N_2O_2 ligands were used to prepare active iron(III) catalysts. Kerton and Kozac (Scheme 29) were able to tune the selectivity of the transformation towards the formation of cyclic carbonates or polycarbonates by the modification of their ligands' geometry.^[133] Even in this case, they noticed the formation of a six-coordinate ferrate intermediate when the catalyst was treated with $PPNCl$, by means of MALDI-TOF analysis.

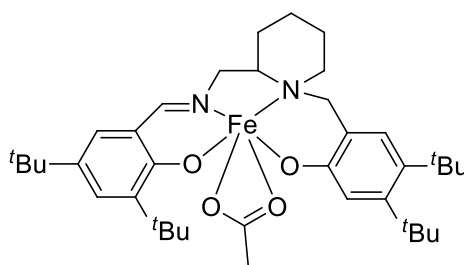


Kerton, Kozac, 2019

Propylene oxide, $PPNCl$

20 Bar, 100°C, 22h

TOF 114 h^{-1}



Jones, 2019

Cyclohexene oxide, TBACl

10 Bar, 80°C, 24h

TOF 153 h^{-1}

Scheme 29. Iron complexes based on N_2O_2 ligands, used as catalyst for epoxides/ CO_2 reactions

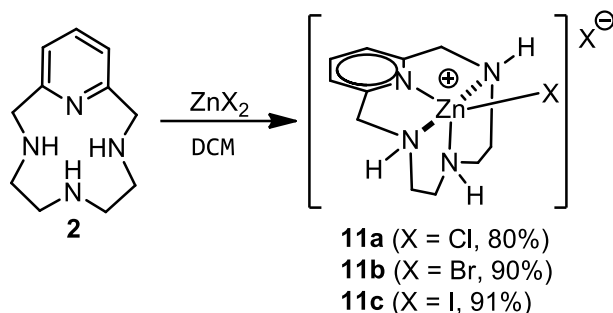
The system based on these complexes proved to be active only in the presence of an excess of phosphonium halide and relatively high pressure of carbon dioxide. Similar examples were reported by Jones and co-workers (Scheme 29),^[134] in which a particular N_2O_2 ligand iron complex proved its activity as catalyst for the synthesis of cyclohexene carbonate from cyclohexene oxide and carbon dioxide. Even in this case the catalyst was active in presence of an excess of TBACl as nucleophilic co-catalyst. This complex was also exploited in the polymerization of *rac*-Lactide to PLA, a biobased polymer largely employed today as biodegradable plastic material.

In this view, due to our long expertise in coordination chemistry in our group, we decided to explore the catalytic activity of different metal complexes based on the pyclen ligand's family. At first, we exploited the activity of different zinc complexes,^[135] since zinc proved to be one of the best metals active in this transformation, thanks to its Lewis acidity. The system was found to be active without the addition of any nucleophilic co-catalyst, probably due to the particular coordination geometry around the metal center. We later decided to transition towards a more sustainable and Earth-abundant metal such as iron. While doing so, we also investigated the possibility to obtain a more soluble complex by functionalization of the pyclen scaffold. In this case, after reaction with iron(III) bromide, we obtained a particular and somehow unexpected ferrate compound which was proved to be a promising active catalyst for the cycloaddition of epoxides and carbon dioxide.^[83]

2.2 RESULTS AND DISCUSSION:

2.2.1 Preparation of the zinc complexes:

The preparation of ligand **2** is described in the previous chapter. Zinc complexes **11a-c** were obtained by slowly addition of the zinc salt to a stirred solution of the macrocyclic ligand **2** in dichloromethane (Scheme 30). Due to the good solubility of the ligand in DCM, a small excess was used to avoid the presence of free zinc metal salt in the product. The series of halogen derivatives was prepared in order to assess the different reactivity in the ring-opening of epoxides. The metal complexes proved to be soluble in different polar media, therefore they were fully characterized by NMR spectroscopy in deuterated DMSO, MS spectrometry and elemental analyses. The ¹H NMR data in DMSO-*d*₆ are consistent with an apparent C_s symmetry of the structure in solution, with two signals for each couple of equivalent methylene groups.



Scheme 30. Synthetic route used to obtain zinc complexes **11a-c** (yield in brackets).

Changing from chloride to bromide anions, the NMR spectra did not show any important variation. Instead, when iodide was present as anion, the difference in the NMR spectra is significant and might be due to the different conformation or steric hindrance around the complex. The ESI-MS analysis resulted for all the complexes in the presence of a principal fragment corresponding to the cationic complex with one halogen anion coordinated to the metal center. To further assess the structure of the metal complexes, single crystals suitable for X-ray crystallography were grown for each complex. The crystal structure of **11c** was satisfactory in terms of clarity of molecular structure but not in terms of refinement value, therefore it has not been discussed deeply. Structural details and geometrical parameters are discussed in detail in the experimental section for complex **11a-b**. Interestingly, for each complex four nitrogen atoms of the macrocycle and a monodentate halide ligand form a distorted square pyramidal environment around the Zn(II) ion, where the additional halide anion balances the positive charge in the second coordination sphere. The macrocycle adopts a *cis*-folded (+++) conformation with the metal atom that is displaced from the N4 macrocyclic cavity.^[73] This arrangement and all the structural parameters are comparable to those of similar complexes which have been already reported in the literature.^[136,137] The Zn-X bond distance in each complex varies consistently with the X⁻ anion size (2.2139 Å for Zn-Cl and 2.3516 Å for Zn-Br). To better describe the geometry of the [Zn^{II}(X)(Pc-L)]⁺ five-coordinated system, the τ -value, which was first introduced by Addison and colleagues,^[138] was calculated. τ is defined as $(\beta - \alpha)/60$, where β and α are the largest angles in the system that define the basal plane of a square-pyramid. The ideal square-pyramidal geometry possesses a τ value of 0, where instead the trigonal-bipyramidal geometry has $\tau = 1$. In the current

study, β and α refer to N2-Zn-N4 and X-Zn-N1 bond angles respectively and N3 represents the axial ligand. Both complexes under investigation lie in the continuum between the two ideal geometries, but it seems that complex **11b** (Figure 12) tends to approach more the square-pyramidal geometry ($\tau = 0.26$), in comparison with complex **11a** (Figure 11) which is slightly distorted ($\tau = 0.35$).

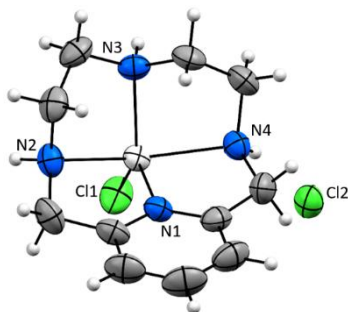


Figure 11. Molecular structure of the complex [Zn(II)(Cl)(2)]Cl·1.5H₂O, **11a** (50% probability thermal ellipsoids). Selected bond lengths. Full crystal structure data are reported in the experimental section.

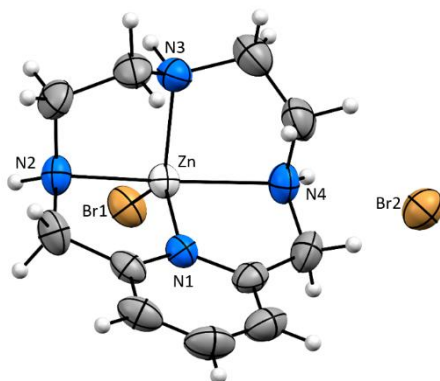
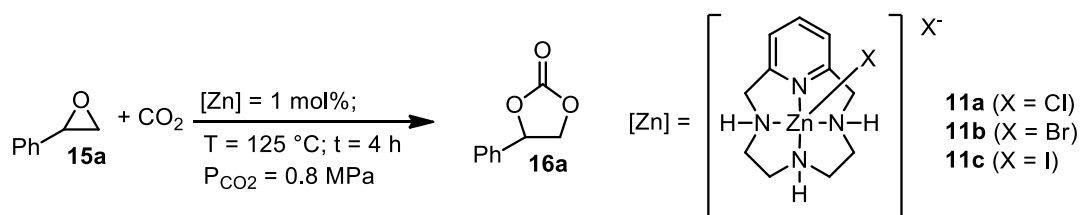


Figure 12. Molecular structure of the complex [Zn(II)(Br)(2)]Br·H₂O, **11b** (50% probability thermal ellipsoids). Selected bond lengths. Full crystal structure data are reported in the experimental section.

2.2.2 Optimization of the reaction:

We decided to compare the catalytic activity of our zinc complexes **11a-c** in the model reaction between CO₂ and styrene oxide **15a** with simple quaternary ammonium halides, which are known to exhibit good activities in carbon dioxide fixation with epoxide.^[139] Efficient binary catalytic systems composed by zinc and ammonium salts have already been reported, as stated in the introduction of this chapter. The presence of both Lewis acid and nucleophile in the binary catalytic system facilitate the ring-opening step, which is often considered as rate-defining, making it less energetically demanding. In our vision, due to the specific coordination geometry, metal-complexes **11a-c** were themselves perfectly suited to act as bifunctional systems, without the addition of nucleophilic co-catalyst, as they already possess an outer sphere nucleophilic halogen anion and a free coordination site on the zinc. To verify this hypothesis, we tested complexes **11a-c** both in the presence and in the absence of tetrabutylammonium halide salts as co-catalysts.



Scheme 31. Model reaction of styrene oxide **15a** and CO₂ with zinc catalysts **11a-c**, to yield styrene carbonate **16a**.

Table 9. Screening of the [Zn(II)(X)(2)]X (**11a-c**) catalysed cycloaddition of CO₂ to styrene oxide **15a**.

Entry	Catalyst	Co-catalyst	Conversion 15a ^[b] (%)	Selectivity 16a ^[b] (%)	TOF ^[c] (h ⁻¹)
1	11a	TBACl	90	95	11
2	-	TBACl	97	99	12
3	11a	-	78	92	19.5
4	11b	TBABr	>99	>99	>12
5	-	TBABr	>99	91	>12
6	11b	-	>99	>99	25
7	11c	TBAI	96	93	12
8	-	TBAI	95	98	12
9	11c	-	97	97	24

Reaction conditions: neat, 250 mL of **15a** (2.19 mmol), [Zn] = 1 mol%, TBAX = 2 mol%, at 125 °C; P(CO₂) = 0.8 MPa; reaction time = 4 h. [b] Conversions and selectivity determined by ¹H NMR using mesitylene as internal standard. [c] Turnover frequency (mol_{15a(converted)}} · mol_{cat}⁻¹ · reaction time⁻¹).

In accord to literature^[140] and with the results reported in table 9, tetrabutylammonium halide salts alone, in these working conditions, can efficiently promote the reaction with only slight differences depending on the nature of the halide. TBABr appears as the most active catalyst (>99% of conversion, TOF >12 h⁻¹, table 9, entry 5), whilst TBACl is the most selective (99% selectivity, table 9, entry 2). We noticed that lowering the catalytic loading, quaternary ammonium salts are less efficient and with only 1 mol% of TBABr the observed conversion was reduced to 60%. The disadvantage of using quaternary ammonium salts in our conditions are the fact that they are very hygroscopic, and this leads to a difficult handling of the reagents and water can alter the selectivity of the products, moreover the organic cation is usually difficult to separate from the product, compared with our complexes which are separated by precipitation. Although complex **11a** alone is a competent catalyst, it demonstrated to be less active than TBACl (Table 9, entries 3 and 2) and even in combination with TBACl as

co-catalyst, only moderate beneficial effect has been observed in terms of conversion (Table 9, entry 1 and 3).^[121] Far better results were obtained with complex **11c**, which is fully comparable in terms of conversion and selectivity both in presence or absence of added co-catalyst (Table 9, entries 8 and 9). The best results were observed with complex **11b**, that in combination with TBABr resulted in complete selectivity and conversion (Table X, entry 4). Most importantly, complex **11b** alone gave the best TOF observed (25 h⁻¹), again with quantitative conversion and full selectivity (Table 9, entry 6). It should be pointed out that the absence of the ammonium salt allows the isolation of styrene carbonate **16a** in almost quantitative yield and excellent purity by simple filtration of the catalyst, followed by precipitation with *n*-hexane. No reaction was observed when using ligand **2** alone as the catalyst.

After the preliminary results, we decided to further optimize the reaction conditions with the most active complexes **11b** and **11c**, in order to maintain high conversions and selectivity while working under milder reaction conditions. At first, we decreased the catalyst loading, maintaining the CO₂ pressure of 0.8 MPa, the temperature at 125 °C and the reaction time of three hours (see experimental section).

Table 10. Screening of the catalyst loading on the model reaction of styrene oxide and CO₂.

Entry	Cat.	Loading (mol%)	Conversion 15a (%) ^[b]	Selectivity 16a (%) ^[b]	TOF (h ⁻¹) ^[c]
1	11b	1	>99	>99	>33
2	11b	0.5	>99	>99	67
3	11b	0.1	53	>99	177
4	11b	0.01	2	>99	67
5	11c	1	>99	95	>33
6	11c	0.5	>99	95	67
7	11c	0.1	83	94	277

Reactions conditions: neat, 250 μL of **15a** (2.19 mmol), at 125 °C; P(CO₂) = 0.8 MPa; reaction time = 3 h. [b] Conversion and selectivity determined by ¹H NMR using mesitylene as internal standard. [c] Turnover frequency (mol_{3a}·mol_{cat}⁻¹·reaction time⁻¹).

The selectivity was not affected by the decreasing of catalyst loading while the conversion started to drastically decrease below 0.5 mol% (Table 10, entry 3 and 4). Complex **11c** maintained a good activity even at very low catalyst loading and with a remarkable TOF of 277 h⁻¹ (Table 10, entry 7). Despite the catalyst loading, higher selectivity was always observed with complex **11b**. With this complex, the desired cyclic styrene carbonate **16a** was obtained as the only reaction product, and almost quantitative conversion (99%) with complete selectivity (>99%) towards **16a** was obtained with only 0.5 mol% loading, without any added co-catalyst (Table 10, entry 2).

We next monitored the effect of the temperature with the aim of working closest to room temperature. With complex **11b**, we observed a dramatic drop in the conversion at lower temperatures (Table 11). This drop in conversion can be due to the lower solubility of the metal complexes in the neat epoxide **15a** at lower temperatures. By addition of 250 μ L of DMSO as co-solvent to the reaction mixture and, even at 75 °C we were able to obtain a 39% conversion with good selectivity for compound **16a** (Table 11, entry 4).

Table 11. Dependence of the temperature with **11b** as catalyst for cycloaddition of CO₂ to styrene epoxide.

Entry	T (°C)	Conversion ^[b] (%)	Selectivity ^[b] (%)	TOF ^[c] (h ⁻¹)
1	100	30	61	15
2	75	10	10	5
3 ^[d]	100	58	97	29
4 ^[d]	75	39	82	19.5

Reaction conditions: neat, 250 mL of **15a** (2.19 mmol), **11b** = 0.5 mol%; P(CO₂) = 0.8 MPa; reaction time = 4 h. [b] Conversions and selectivity determined by ¹H NMR using mesitylene as internal standard. [c] Turnover frequency (mol_{15a(converted)}} · mol_{cat}⁻¹ · reaction time⁻¹). [d] The catalyst was previously dissolved in 250 μ L of dimethyl sulfoxide.

Considering the best results obtained with the zinc bromide complex, we decided to continue with the optimization of the reaction parameters using **11b** as catalyst.

We then investigated the effect of CO₂ pressure on the conversion of **15a** and selectivity for **16a**, and we were pleased to see that the catalytic activity was retained also at very low pressures (Figure 13), with anyway an understandable lowering of the overall activity. Indeed, under CO₂ at atmospheric pressure (0.101 MPa) at 125 °C, we observed a moderate conversion (31%) in just 3 hours, with a good selectivity (77%). It should be noted that, at such low conversion the errors we introduce in measuring the yield in **16a** is quite high and the selectivity might be underestimated. In fact, in the ¹H NMR only the starting epoxide **15a** and the product **16a** are observed, without any by-product.

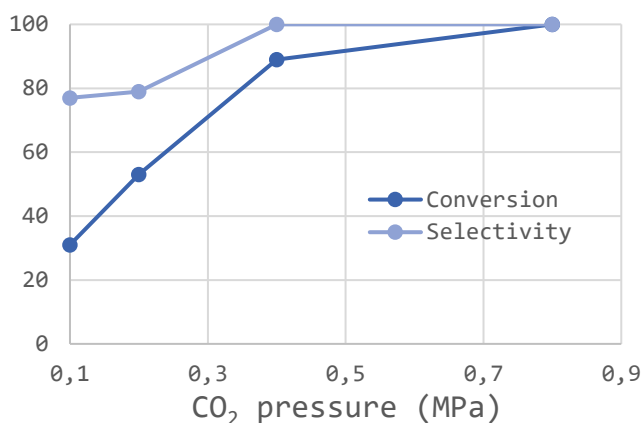


Figure 13. Conversion vs selectivity at different CO₂ pressure, at 125 °C; reaction time = 3h.

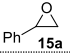
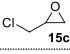


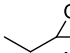
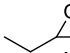
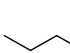
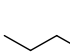


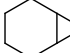
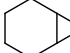
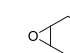
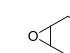
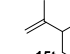
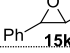
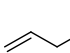
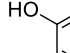
2.2.3 Scope of the reaction:

With these results in our hand, we decided to study the scope of the reaction by using complex **11b** under the optimised reaction conditions (0.5 mol% catalyst loading at 125 °C, PCO₂ = 0.8 MPa; reaction time = 3 h). Reactions were carried out in neat epoxide (250 µL); with solid epoxides or in cases where a very low solubility of **11b** in the reaction media was noticed, 125 µL of propylene carbonate (PC) were added (see experimental section). The choice of this solvent was due to its high polarity and non-toxic nature, and that the fact that complex **11b** solubility was improved during the course of the reaction, when the cyclic carbonate is formed and its concentration increases. Table X summarizes the results obtained in terms of conversion and selectivity, which have been calculated by quantitative ¹H NMR of the crude reaction mixture using mesitylene as internal standard. Most of the products can be easily isolated after the reaction and when necessary purified by column chromatography.

Reactive epoxide such as (+/-)-epichlorohydrin **16c**, due to electronegative effect of its substituent that facilitated the nucleophilic attack to open the epoxide ring,^[141] gave quantitative yield of cyclic carbonate (Table 12, entry 2).

On the other hand, the low solubility of the catalyst in alkyl-substituted epoxides even at high temperatures caused a drop in the reaction yield, whose effect is more pronounced on increasing chain length, as exemplified by the difference between propylene oxide and 1,2-hexene oxide (compare entry 3 with entry 7 in Table 12). However, as cited above, complex **11b** is very soluble in more polar cyclic carbonates even at room temperature. Thus, as previously stated, when the metal complex was previously dissolved in PC, high conversions with excellent selectivity were restored (entries 4, 6 and 8, Table 12). In the case of propylene oxide, the reaction product is the same as the cyclic carbonate employed as the solvent, entry 4, and in this case the reaction product can be isolated in very high purity by addition of chloroform to the reaction mixture because complex **11b** is insoluble in chlorinated solvents and precipitates quantitatively. A simple filtration, followed by evaporation of chloroform under reduced pressure yielded pure **16b** in almost quantitative yield. On the other hand, the reactions of disubstituted epoxides failed to give the desired cyclic carbonates (entries 9-13, Table 12).

Table 12. Substrate scope of **11b** catalyzed cycloaddition of CO₂ to different epoxides

Entry	Substrate	Selectivity ^[b] (%)	Conversion ^[b] (%)	TOF ^[c] (h ⁻¹)
1	 15a	>99	>99	>66
2	 15c	>99	>99	>66
3	 15b	74	>99	>66
4 ^[d]	 15b	>99	>99	>66
5	 15d	19	42	28
6 ^[d]	 15d	96	97	65
7	 15e	15	26	17
8 ^[d]	 15e	94	99	66
9	 15l	-	n.d.	-
10 ^[d]	 15l	-	n.d.	-
11	 15n	-	0	-
12 ^[d]	 15n	40	15	10
13	 15p	99	25	17
14 ^[d]	 15p	>99	80	53
15	 15t	-	7	5
16 ^[d]	 15k	-	0	-
17	 15f	>99	98	65
18	 15m	>99	71	47

Reaction conditions: neat, 250 mL of **15x**, **11b** = 0.5% at 125 °C; P(CO₂) = 0.8 MPa; reaction time = 3h. [b] Conversions and selectivity determined by ¹H NMR using mesitylene as internal standard. [c] Turnover frequency (mol₁₅·mol_{cat}⁻¹·reaction time⁻¹). [d] Complex **11b** was dissolved in 125 μL of propylene carbonate.

Moreover, in the case of 1,1-dimethyloxirane (1,2-epoxy-2-methyl propane), **15i**, we were not able to determine the conversion of the starting product because we noticed a high loss in weight of the sample even when pre-dissolving the catalyst in propylene carbonate, due to the extreme volatility of the substrate under the reaction conditions (entries 9 and 10, Table 12).

A very low conversion (15%), and only prior dissolution of the catalyst in propylene carbonate, was observed in the case of cyclohexene oxide (entry 12, Table 12). However, cyclic carbonate **16n** was obtained with a modest selectivity (40%) with some unidentified by-products. The strong activity of the system towards the cycloaddition reaction of CO₂ on terminal vs. internal epoxides was further demonstrated in the case of 4-vinylcyclohexene dioxide **15p**, where only the terminal exocyclic epoxide (highlighted in red in table) reacted with CO₂ to give 4-(7-oxabicyclo[4.1.0]heptan-3-yl)-1,3-dioxolan-2-one, **16p** (entries 13 and 14, Table 12) in good yields.

No reaction was observed with sterically hindered internal epoxides such as *cis*-limonene 1,2-oxide, **15t**, or *trans* stilbene, **15k** (entries 15 and 16 Table 12).

In the case of unsaturated cyclic carbonates, which are currently gaining increasing attention both from academic and industrial communities as reactive monomers for copolymerization since their activity in crosslinking reactions,^[142] allyl glycidyl ether, **15f**, were almost quantitatively converted to (2-oxo-1,3-dioxolan-4-yl)methyl vinyl ether, **16f** (entry 17, Table 12).

Bio-based eugenol epoxide **15m**, which was prepared in our laboratory (see experimental section), led to a satisfying 71% yield of the corresponding cyclic carbonate (entry 18, Table 12). To the best of our knowledge, cyclic carbonate **16m** was never characterized before, and it can be considered as an interesting building block for bio-based non-isocyanate polyurethane from renewable resources.^[143]

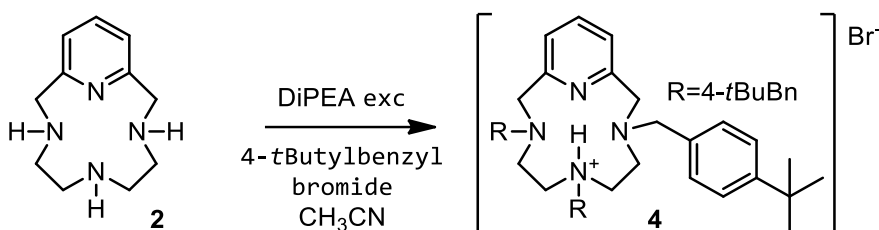
2.2.4 Catalyst recovery and recycle:

The stability and recyclability of a catalyst are of fundamental importance for practical application, and usually a limiting factor in homogeneous catalysis. In order to gain insights to the catalyst stability and its potential reuse, two different tests were conducted under the optimised reaction conditions (**11b** = 0.5 mol% at 125 °C; P(CO₂) = 0.8 MPa; reaction time = 3 h). As previously described, at the end of the reaction after dilution with chlorinated solvent the precipitation of the zinc complex occurs, allowing the recovery by filtration as a white solid. We performed the reaction on 2.5 mL of styrene oxide, **15a**, to reduce possible intrinsic errors by working with higher quantity of substrate and catalyst. It should be mentioned that we indeed noticed a scale up effect, probably due to a less efficient stirring in the reaction vessel, with a maximum conversion of 86%, but with full selectivity for styrene carbonate **16a**. At the end of the catalytic reaction, 4 mL of chloroform were added and the solid metal complex **11b** was recovered by filtration followed by a double washing with 2 mL of chloroform (see experimental section for details). The ¹H NMR spectrum of the recovered solid is perfectly consistent with the starting complex, while the elemental analysis showed a slightly higher content of carbon than expected, probably due to the presence of residual product.

We also decided to restore a catalytic cycle without isolating the catalyst but just adding fresh styrene epoxide and re-running the reaction in the optimized condition, to evaluate the robustness of the system. The details are described in the experimental section. Only at the fourth run we observed a decrease in catalytic activity, but this also be the result of a less efficient stirring, due to the increased solvent volume, or even to a higher dilution of the catalyst. Still, a remarkable TON of 756 mol of styrene oxide per mole of catalyst was achieved.

2.2.5 Preparation of iron complex:

After working with zinc complexes 11a-c and delighted by their activity in optimized reaction conditions for the reaction of different epoxides and CO₂, we wanted to improve the system by two different means: first we wanted to switch from zinc^[135] to the more earth-abundant metal iron and second, we wanted to obtain a functionalized ligand to improve the solubility in epoxides. To do so we started with the synthesis of ligand **4** (Scheme 32) by reacting ligand **2** and (4-*t*Butyl)benzyl bromide, in presence of excess DiPEA, in analogous condition for the obtaining of ligand **3**.



Scheme 32. Synthesis of ligand **4** in analogous condition to the synthesis of ligand **3**.

The initial idea was to obtain a neutral functionalized pyclen ligand but after the reaction, the product was obtained after precipitation with cold acetone in the hydrobromic salt form. This behavior can be due to the fact that while functionalizing the nitrogen atoms of the ligand, the latter can actually become a stronger base than DiPEA, thanks to the ability to coordinate the proton in the macrocyclic cavity, influencing the equilibria of the overall reaction. The product can be further precipitated by repeating the cold acetone adding to yield a second/third crop, but maximum yield obtained was still not very satisfactory, hovering around 35%. The structure of this protonated ligand was also confirmed by XRD (Figure 14). Ligand **4** was subjected to the reaction with iron(III) bromide in acetonitrile, in attempt to obtain the coordination of the iron center in the macrocycle cavity.

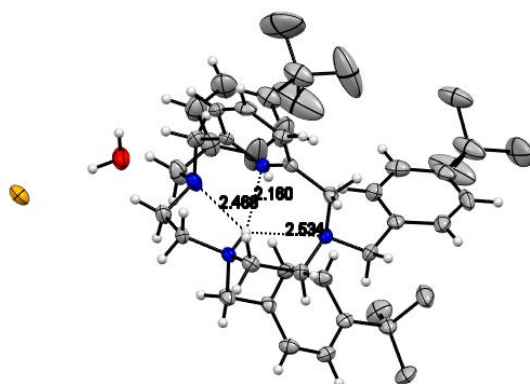
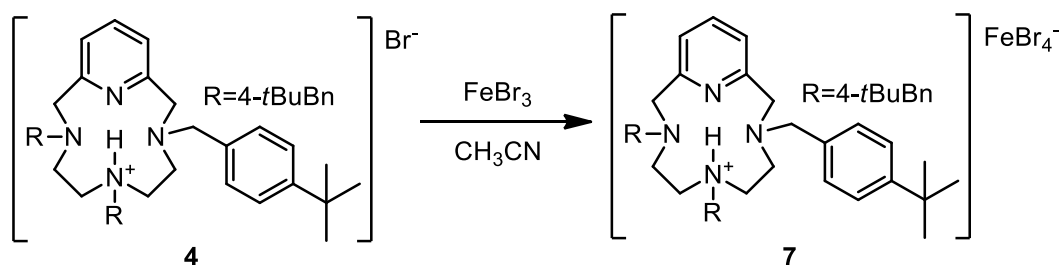


Figure 14. Molecular structure of the bromohydrated ligand, **4** (50% probability thermal ellipsoids). Selected bond lengths (Å): N1..H 2.180, N2..H 2.534, N4..H 2.488 Full crystal structure data of **4** are reported in the experimental section.

We decided to use iron bromide since, as proved for the previous work with zinc complexes, the bromide anion is far more active in respect to chloride and iodide. While trying to obtain the new complex, as initially highlighted by ESI-MS and elemental analysis, we only isolated the protonated ligand **4** in which the bromide anion was exchanged by a tetrabromoferrate anion (Scheme 33).



Scheme 33. Synthesis of complex **7**, starting from protonated ligand **4**.

The formation of such kind of tetrahedral anions by reaction of an iron salt and a source of halide was already known, but we were only able to initially assess this structure by MS and elemental analysis, where in the first, in the ESI negative mode, the peak corresponding to the tetrabromoferrate anion at 375.80 m/z was predominant.

All the attempt to crystallize the resulting complex **7** were unsuccessful, leading to the formation of crystals of **4**. The possible reason behind this is that the ferrate species might be unstable in the crystallization conditions. The final, unmistakable attribution of the proposed structure of **7** was achieved thanks to Raman spectroscopy (major information in the previous chapter and in experimental section). With this technique, combined with the other analysis results, we were able to assess the presence of the tetrahedral tetrabromoferrate anion which possess typical Raman resonances: the most intense lines at **203** cm^{-1} and **294** cm^{-1} are assigned as A_1 and T_2 vibrational bands of the anion^[101] and the one at **~90** cm^{-1} was tentatively assigned as the E mode^[102]

2.2.6 Optimization of the reaction:

We decided to investigate the activity of complex **7** in the model reaction of styrene oxide (SO) and CO_2 , to evaluate how the presence of the ferrate anion influences the reaction outcome. Optimization of the reaction conditions, such as catalyst loading, temperature, pressure and reaction time (see experimental section for more details), gave promising results. At first, we compared the activity of our catalyst with simple tetrabutylammonium bromide, and the latter proved to be far less successful at yielding the cyclic carbonate product, with an almost 5-fold difference in the TOF compared to complex **7** (entry 2 and 6, Table 13). In fact, the latter was able to convert quantitatively SO in 3 hours at 125 °C and 0.8 MPa of CO_2 pressure with only 0.5% mol loading of catalyst (entry 1, Table 13) with a remarkable 79% yield of styrene carbonate (SC) (TON = 198, TOF = 66 h^{-1}). Decreasing the catalyst loading to 0.1% mol resulted in a huge decrease in activity and selectivity (entry 3, Table 13).

The optimal pressure of CO_2 was found to be 0.8 MPa with a loss of activity and selectivity when decreasing the pressure (see experimental section). The right balance between conversion and selectivity was achieved in 4 hours reaction time at 100 °C (entry 7, Table 13). It is well known that simple

Table 13. Optimization of the reaction conditions

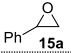
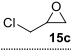
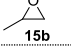
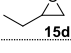
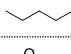
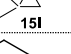
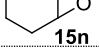
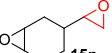
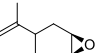
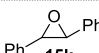
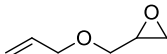
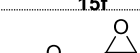
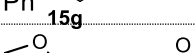
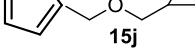

Entry	Cat. (mol%)	Conv. 15a %	Select. 16a %	TOF h ⁻¹
1	3 0.5%	99	80	66
2	3 0.25%	93	86	124
3	3 0.1%	23	54	77
4	FeBr ₃ 0.5%	39	0	26
5	TBAB 2%	86	96	14
6	TBAB 0.25%	25	92	33
7 ^[b]	3 0.25%	99	87	99

Reaction conditions: styrene oxide (SO) 2.19 mmol; T = 125 °C; P = 0.8 MPa; t = 3h. Conversion and selectivity determined by ¹H NMR using mesitylene as internal standard. ^{b)} Styrene oxide (SO) 2.19 mmol; T = 100 °C; P = 0.8 MPa; t = 4h.

2.2.7 Scope of the reaction:

As for the zinc complexes **11a-c** discussed before, alkyl-substituted substrates were by far worse solvents for complex **7** and this resulted in loss of activity, especially when increasing the alkyl chain length. To solve this problem, in certain cases we decided to use propylene carbonate (PC) as a co-solvent, as previously successfully reported, which considerably enhanced the solubility of our complex and boosted the activity. Overall, our complex was active in this transformation for the majority of the epoxides tested, with a remarkable higher activity for terminal ones, and also linear alkyl epoxides **16b,16d,16e** could be converted in high selectivity. Epichlorohydrin was converted to the corresponding carbonate **16c** in high yield and selectivity with a remarkable TOF value of 115 h⁻¹. On the other hand, in our standard conditions, substrates such as cyclohexene oxide **15n** and 2-methyl-1,2-epoxypropane **15l** were found to be converted in very poor yield, and even more sterically hindered epoxides such as stilbene oxide **15k** and limonene oxide **15t** did not react at all. As already proved with the zinc catalyzed reaction, it was interesting to note that in the case of 4-vinylcyclohexene dioxide **15p** the only product obtained when using our pyclen-ferrate system was the terminal carbonate **16p**, in 18% isolated yield.

Table 14. Scope of the cycloaddition of CO₂ to epoxides catalysed by the ferrate complex **7**.

Entry	Substrate	Selectivity ^[b] (%)	Conversion ^[b] (%)	TOF ^[c] (h ⁻¹)
1		86	>99	66
2		94	86	115
3		99	89	89
5		99	16	16
7		54	28	28
10 ^[d]		16	50	33
11 ^[d]		50	16	10
13 ^[d]		60	30	30
15		-	-	-
16 ^[d]		-	-	-
17 ^[d]		99	56	56
18 ^[d]		99	>99	100
19		99	72	75
20 ^[d]		99	35	35
21 ^[d]		96	50	25

Reaction conditions: epoxide 250 μ L; **7** = 0.5 mol% T = 100 $^{\circ}$ C; P (CO₂) = 0.8 MPa; reaction time = 3 - 6h; neat. [b] Conversion and selectivity determined by ¹H NMR using mesitylene as internal standard. Conversion is indicated under each product. Selectivity for the product in brackets. [c] TON = mol_{15(converted)} · mol₇⁻¹; TOF = TON · reaction time⁻¹. [d] propylene carbonate (PC) as solvent.

Glycidyl ethers were generally reactive (**15f**, **15g**, **15j**) and, for that reason, we tested some di-glycidyl ethers derivatives, which find place as monomers in polymer chemistry for epoxides thermosets and NIPUs (non-isocyanate polyurethanes)^[144]. Bisphenol-A diglycidyl ether **15r** was converted to the dicarbonate compound **16r** in good yield (48%) and very high selectivity (96%) in PC as co-solvent at 100 °C in just 4 hours. Di-glycidylether of hydroquinone **15s** was converted into the corresponding di-carbonate **16s** in moderate yield (35%).

2.2.8 Scale up:

A ten-fold scale-up reaction (2.5 mL substrate) was performed to evaluate the activity of our catalytic system in the optimized condition, using propylene oxide **15b** as substrate. The results obtained were highly satisfying with a TON of 396 (TOF = 99 h⁻¹) and isolated yield of 75%. This reaction was then recycled 3 times (total volume of epoxide 7.5 mL) by simple addition of new substrate between each run to evaluate the robustness of the catalyst, and we obtained an overall TON of 1020 (TOF = 85 h⁻¹) thus proving the recyclability of our system.

2.3 CONCLUSIONS:

In summary, we evaluated the catalytic activity of our pyclyen zinc and iron complexes in the cycloaddition of CO₂ to epoxides. We were able to exploit their activity in relatively mild conditions, without the addition of any external nucleophilic co-catalyst. The zinc bromide complex proved to be a competent catalyst, especially in terms of selectivity for the formation of the desired cyclic carbonates but lacked in terms of solubility in a consistent number of epoxydic substrates. Moreover, the use of zinc metal should be limited due to its rapid depletion. Moving to iron complexes, we performed the synthesis of a functionalized ligand **4** that retained a proton in the macrocycle cavity. The latter, upon reaction with iron(III) bromide resulted in the formation of a special ferrate compound **7** which still proved to be active in the formation of cyclic carbonates at mild conditions, which compares well with other iron-based systems reported in the literature. A broad scope of reaction was explored for both zinc and iron-based catalysts, and propylene carbonate was proposed as alternative green solvent when needed.

3 AMMONIUM METALLATES FOR CYCLIC CARBONATES SYNTHESIS FROM EPOXIDES AND CO₂:

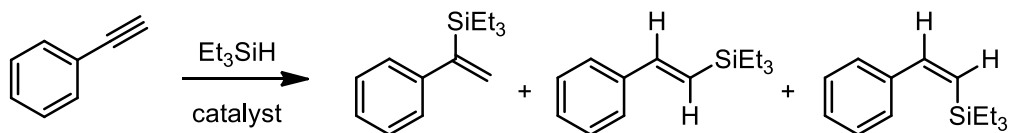
3.1 INTRODUCTION:

Having in mind the results obtained with the ferrate compound **7** obtained by treatment of the protonated ligand **4** with iron bromide, and the remarkable activity of the tetrabromo ferrate anion in the cycloaddition of epoxides and carbon dioxide, together with other examples reported, we wanted to improve the overall sustainability of the process by finding a simpler ferrate “surrogate”. When we first looked at the literature, we were surprised by how few this class of compounds has been exploited in catalytic activities. In fact, most of the tetrahalogeno metallate compounds were studied for their structural, spectroscopical and magnetic properties, but in this introduction, I want to give more attention to the examples related to catalysis.

3.1.1 Chlorometallates for hydrosilylation / hydrogermylation:

Studies in the late 80's about alternative catalysis for hydrosilylation, reported by Lukevics and co-workers,^[145] were based on the fact that the most active catalysts up to that time were based on anionic rhodium and platinum halogen complexes, especially **hexachloroplatinite**, and no experimental data were available on other metals including non-noble ones. To explore the activity of other metals in this reaction, they synthesized a series of metallates by reaction of metal chlorides and triethylbenzylammonium chloride in absolute ethanol. They also studied the possibility of the formation of supported tetrahalogeno compounds by reaction with a polystyrene modified phosphonium halide. They obtained sixteen chlorometallates and nine supported chlorometallates, using **manganese, iron, cobalt, nickel, copper, zinc, rhodium, palladium, indium, tin, antimony, osmium, iridium and platinum**. They wanted to study the activity of metals with different valence and triethylbenzylammonium chloride was chosen as cation for its availability and for its ability to solubilize various anions in non-polar organic solvents, an important aspect in homogeneous catalysis.

They tested the activity of the so obtained compounds in the reaction of phenylacetylene and triethylsilane: this reaction allows the assessment of activity and regio/stereo selectivity by production of different isomers (Scheme 34):



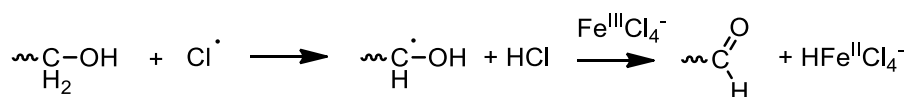
Scheme 34. Reaction of phenylacetylene and triethylsilane, products distribution

The reaction was performed in neat, at 80 °C. At first, it was clear that the activity strongly depends on the nature of the metal, with Mn^{II} , Fe^{II} , Co^{II} , Ni^{II} , Pd^{II} , In^{III} , Sb^{III} , Sb^{V} complexes almost completely inactive in the given conditions. Slightly more activity was observed for Ti^{IV} and $\text{Osmium}^{\text{IV}}$, where the last one unfortunately showed less activity of its precursor hexachloro osmic acid (15 vs 100% conversion). Nevertheless, **high activity** was observed for Fe^{III} , Cu^{II} , Zn^{II} , Rh^{III} , Ir^{III} , Pt^{IV} compounds, with activity trend in the following order: $[\text{RhCl}_4]^- > [\text{PtCl}_6]^{2-} > [\text{IrCl}_6]^{3-} > [\text{CuCl}_4]^{2-} > [\text{ZnCl}_4]^{2-} > [\text{FeCl}_4]^-$. Even though even neutral metal halides show significant activity, the anionic metallate compounds are usually more active, especially in the case of zinc (from 3 to 88% conversion in the same conditions). In the case of iron(III), copper(II) and zinc(II), the alpha isomer was prevalent, with only the trans beta isomer formed as byproduct. All the other period V metals were found to be much more active in beta-addition, especially for the trans isomer. Interestingly, $[\text{FeCl}_4]^-$ catalyzes the alpha addition while the precursor FeCl_3 acts in the opposite, favoring the formation of beta products.

The same catalysts were tested in the hydrogermylation of phenylacetylene, using triethylgermane in TFH.^[146] In this case, the reactivity was limited to noble metals, in the order $\text{Pt} > \text{Pd} > \text{Rh} > \text{Ir}$. Moreover, in this particular transformation, the catalyst proved to be far less active than the benchmark Speier's catalyst (hexachloroplatinic acid in isopropanol).^[147]

3.1.2 Chloroferrate in the polymerization of epoxides:

Rozemberg and co-workers, in 1988, studied the possible reduction of trivalent iron chloride during the polymerization reaction of propylene oxide (PO) and phenylglycidyl ether (PGE).^[148] It was already known at that time that FeCl₃ can undergo reduction to divalent iron during polymerization reactions, to form FeCl₂ and HCl, but up to that point no one studied this reaction using chlorometallate as catalyst. They synthesized [Ph₄P][FeCl₄] and tested it in the aforementioned reaction. They noticed that after addition of the catalyst to PO at a certain temperature, the amount of iron(II) was almost 30% of the initial amount, and remains unchanged during reaction. In the case of PGE, the amount of iron(II) increases during polymerization. The reduction produces chlorine atoms that might reversibly oxidize iron(II) to iron(III) or react with monomers/oligomers, and this might explain the difference of accumulation of divalent species while changing the epoxide (different reactivity towards chlorine), where PGE contains phenyl rings that can indeed be chlorinated. Moreover, it was proved via IR spectroscopy that the oligomers formed during reaction, in the form of hydroxyl terminated chains, react with chlorine to produce oxidized products (aldehydes, Scheme 35). Therefore, PGE polymerization is inhibited by iron(II), while in the case of PO, the kinetic of polymerization is described by first order with respect to the monomer during the whole process, even in presence of iron(II) derived by the iron(III) catalyst.



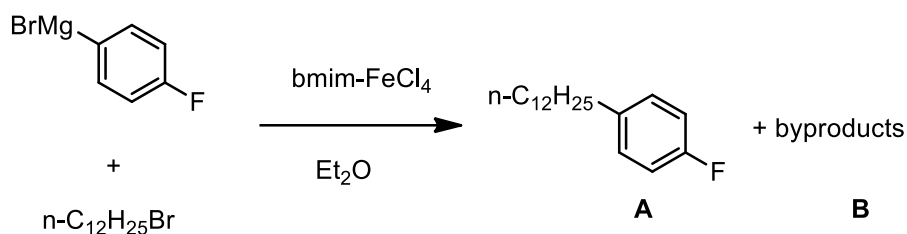
Scheme 35. Oxidation of oligomeric chains by chlorine and reduction of iron(III).

3.1.3 Iron containing ionic liquids for alternative catalysis:

In early 2000's, Holderich and co-workers reported an example of catalytic Friedel-Crafts acylation using iron containing ionic liquids.^[149] The latter were obtained by treatment of 1-Methyl-3-butylimidazolium chloride with anhydrous FeCl₃, to produce an ionic liquid in which the anion is in the form of [FeCl₄]⁻. The ionic liquid was also supported on amorphous silica, to obtain a

heterogeneous catalyst. With the homogeneous ionic liquid, good results were obtained in terms of conversion of mesitylene, anisole and slightly worse results with *m*-xylene. The support of the iron catalyst on silica led to far lower conversion and moreover a large leaching of the metal. This poses a serious question in terms of the possibility of a real heterogeneous catalysis taking place.

The same catalyst was applied to the coupling of alkyl halides to aryl Grignard reagents, in 2005, by Gaertner and Bica.^[150] At that time, they already highlighted how the inexpensive and non-polluting nature of iron was of fundamental interest for its development in catalysis. They successfully exploited the activity of this iron containing ionic liquid on the reaction of 4-fluorophenylmagnesium bromide and dodecyl bromide, together with a broad scope of substrates, with molar loading of catalyst down to 0.5 mol% (Scheme 36). They performed the reaction in diethyl ether at 0 °C, without the need to use anhydrous reagents or inert atmosphere, with the cooling needed to overcome the exothermic addition of the Grignard reagent to the solution, although higher temperatures did not influence the conversion.



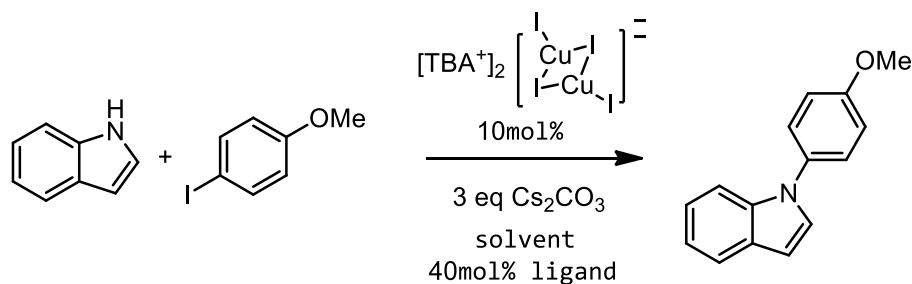
cat loading (mol%)	yield of A	yield of B
10	88.3%	11.1%
5	89.8%	9.7%
1	80.3%	14.8%
0.5	79.4%	15.9%

Scheme 36. Schematic representation of the results obtained with bmim-FeCl₄ as catalyst

The system was recycled at the end of the reaction by extraction of the product with ether and filtration of MgBr_2 , up to 5 times, with almost no loss in conversion and yield of the product.

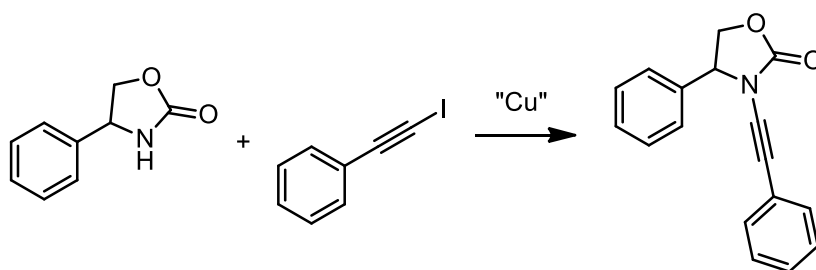
3.1.4 Iodocuprate(I) compound for coupling reactions:

A particular copper(I) compound, in the form of $[\text{TBA}]_2[\text{Cu}_2\text{I}_4]$, was successfully applied in context in which copper(I) catalysis is necessary but limited by the intrinsic low solubility of copper salts in organic media. In fact, the addition of TBAI to CuI leads to the formation of a crystalline compound that is a highly soluble form of a copper(I) compound, in a multigram scale (up to 600g) with high purity. This compound was successfully employed as copper source in the coupling of aryl iodides to indole and other amines (Scheme 37), as reported by Dormer and co-workers.^[151]



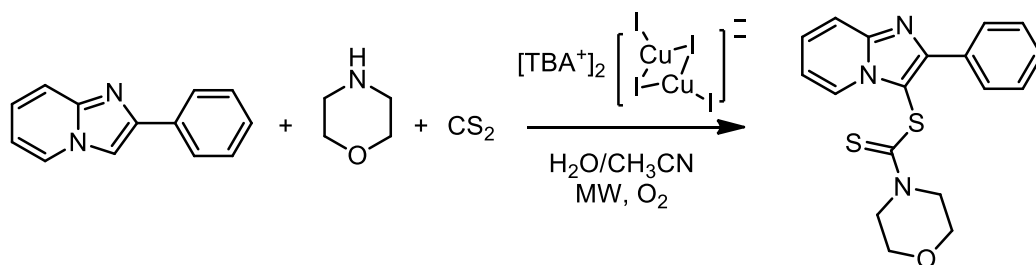
Scheme 37. Coupling reaction of indole and 4-Iodoanisole, catalyzed by soluble copper(I) compound $[\text{TBA}]_2[\text{Cu}_2\text{I}_4]$

This reaction was successfully applied also to other substrates such as oxazolidinones (Scheme 38), a largely present moiety in pharmaceuticals. The activity of the catalyst was not limited to aryl iodides but also bromo and iodo alkynes.

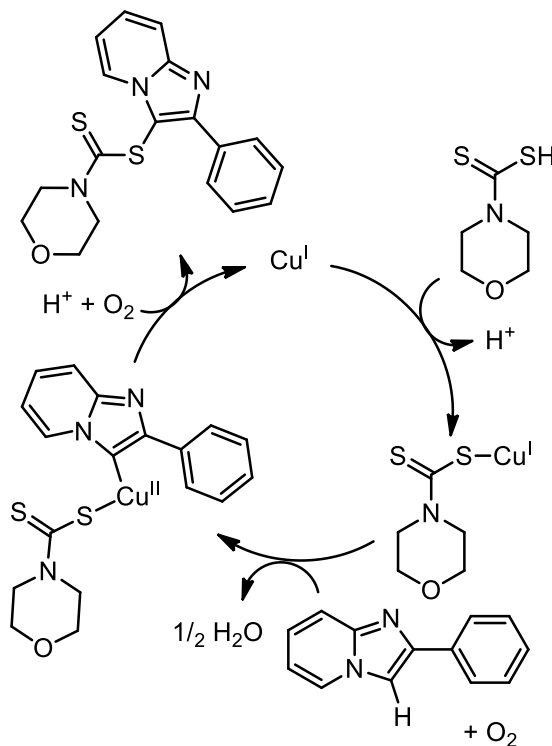


Scheme 38. Reaction of 2-phenyloxazolidinone with alkynyl iodide.

This soluble copper compound was very recently exploited in the formation of dithiocarbamates by the one-pot reaction of imidazopyridines, carbon disulfide and an amine (Scheme 39).^[152] The reaction proceeds in acetonitrile/water media, under microwave heating, in presence of air. This particular heating source allows the completion of the reaction in just 15-45 minutes.



Scheme 39. Model reaction between 2-phenylimidazopyridine, morpholine and carbon disulfide, catalyzed by soluble copper(I) catalyst.

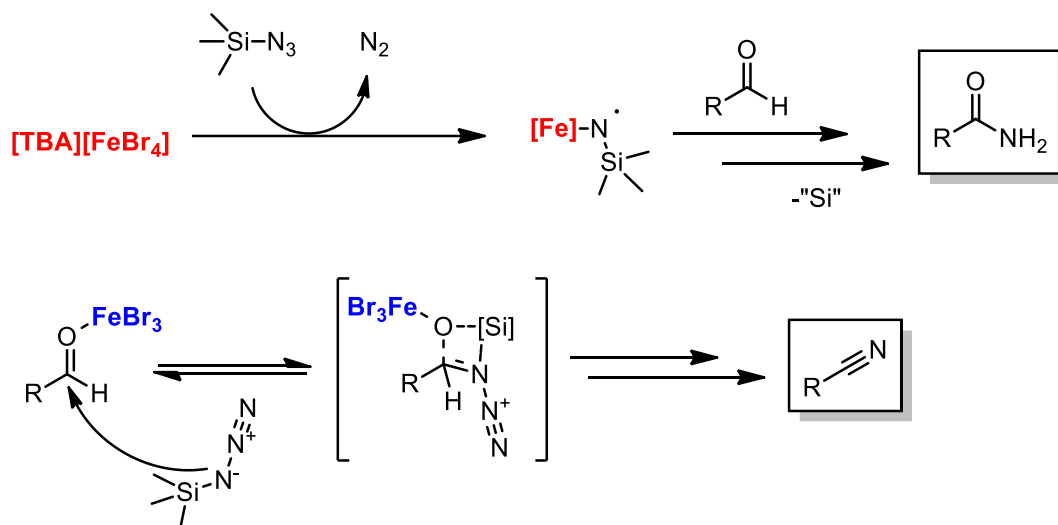


Scheme 40. Proposed reaction mechanism.

The reaction was performed successfully on a broad scope of substrates and the mechanism was investigated by experimental means. Oxygen is necessary to oxidize the product and regenerate the catalyst (Scheme 40). The system was able to be scaled up to 1.5g product scale in 45 min of reaction time.

3.1.5 Controlling the selectivity in aldehyde functionalization by iron catalysts:

It was recently reported that the reaction of aldehydes with trimethylsilyl azide, catalyzed by iron(III) compounds, leads to the formation of different products.^[153] The product selectivity is defined by the nature of the iron compound: when simple iron(III) bromide was used, the reaction led to the formation of nitriles, while the use of [TBA][FeBr₄] shift the selectivity to amides. The proposed explanation in the change of reaction outcome is that iron can act both as a Lewis acid and nitrene transfer reagent. The latter, is efficiently promoted by iron when it is provided in the form of tetrabromo ferrate anion, while Lewis acid iron(III) bromide promotes the nucleophilic attack of the azide to promote the formation of nitriles.



Scheme 41. Different selectivity of the reaction between aldehydes and trimethylsilyl azide, catalyzed by different iron compounds.

The reaction was deeply investigated by crossed experiments, validating the possible mechanism proposed in Scheme 41.

3.1.6 Finding the best candidate:

The ionic couple [TBA][FeBr₄] reported in this work was previously synthesized by Wyrzykowski and co-workers.^[154] They prepared different homo and mixed tetrahalogenoferrate compounds, by reaction of iron(III) halides and tetrabutylammonium halides in ethanol, to evaluate the magnetic, thermal and spectroscopical features of these ferrate compounds. In our view, thanks to the simple preparation procedure and cheapness of the materials required, these species might be active as catalysts in the cycloaddition of epoxides and carbon dioxide, in view of the previously reported results with pyclyen ferrate salt **7**.^[83]

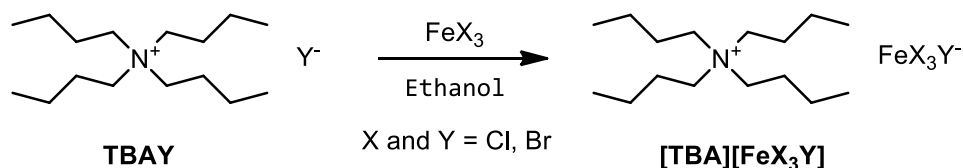
We therefore prepared four homo and mixed ferrate compounds and we tested them in the reaction with styrene oxide and CO₂, as model reaction, and further investigated the nature of the catalytic system by means of experimental and theoretical studies (DFT).

3.2 RESULTS AND DISCUSSION:

3.2.1 Synthesis of tetrabutylammonium tetrahalogenoferrate salts:

The synthesis of a series of tetrabutylammonium (TBA) tetrahalogenoferrate was performed by a reported procedure.^[154] The products are obtained by mixing an ethanolic solution of a TBA halide and an iron(III) halide precursor. In this way, we were able to obtain four homo and mixed ferrate salts using chloride and bromide as halides. When we tried to perform the reaction in presence of iodide, only complex mixtures of products were obtained which have never been successfully characterized. The detailed insight in the synthesis and characterization of the ferrate salts is reported in the experimental section.

Table 15. The four synthesized homo and mixed tetrahalogenoferrate salts and their experimental melting point.



FeX_3	TBA Y	$[\text{TBA}][\text{FeX}_3\text{Y}]$	m. p.
FeCl_3	TBACl	$[\text{TBA}][\text{FeCl}_4]$	113 °C
FeCl_3	TBABr	$[\text{TBA}][\text{FeCl}_3\text{Br}]$	132 °C
FeBr_3	TBACl	$[\text{TBA}][\text{FeBr}_3\text{Cl}]$	129 °C
FeBr_3	TBABr	$[\text{TBA}][\text{FeBr}_4]$	135 °C

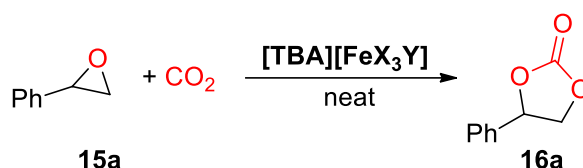
All the compounds were obtained as solid, crystalline materials which proved to be far more air and bench stable in respect to the corresponding precursors. In fact, both tetrabutylammonium salts and iron(III) halides are highly hygroscopic and this is something that renders their use and weighting rather complicated. The possibility to work with solid and stable materials is highly favorable. The melting point of the materials are all above 100°C so they do not fall in the definition of “ionic liquids”. The compounds are strongly

colored, progressively passing from yellow (for TBAFeCl₄) to deep red (for TBAFeBr₄) with increasing bromide content.

3.2.2 Evaluation of the catalytic activity of ammonium ferrates in cyclic carbonate formation:

The activity of the different TBA ferrates was evaluated in the model reaction of styrene oxide and carbon dioxide, in the condition used for the previous work (Table 16).

Table 16. Preliminary results with TBA ferrates in the cycloaddition of carbon dioxide and styrene oxide.



Entry	Cat. mol%	Con. 15a %	Sel. 16a %	TOF ^[b] (h ⁻¹)
1	[TBA][FeCl ₄] 0.5%	73	88	36
2	[TBA][FeCl ₃ Br] 0.5%	83	95	42
4	[TBA][FeBr ₃ Cl] 0.5%	99	70	49
5	[TBA][FeBr ₄] 0.5%	73	88	36
7	TBACl 0.5%	41	95	21
8	TBABr 0.5%	33	>99	17

Reaction conditions: styrene oxide (SO) 2.19 mmol; T = 100 °C; P = 0.8 MPa; t = 4h. Conversion and selectivity determined by ¹H NMR using mesitylene as internal standard. [b] TON = mol_{15a(converted)} · mol_{cat}⁻¹; TOF = TON · reaction time⁻¹

As clearly stated by Table 16, all the tested compounds proved to be catalytically active for this transformation, in just 0.5 mol% loading, with good turnovers. Compared to simple ammonium halides, that are still reported to be competent catalysts for this reaction, the simple incorporation of an iron halide salt strongly impacts the reactivity of the catalyst by almost doubling the rate of the reaction. [TBA][FeCl₃Br] was found to be the most selective catalyst in terms of styrene carbonate formation and for this reason it has been selected as the best catalyst for further optimizations (Figure 15).

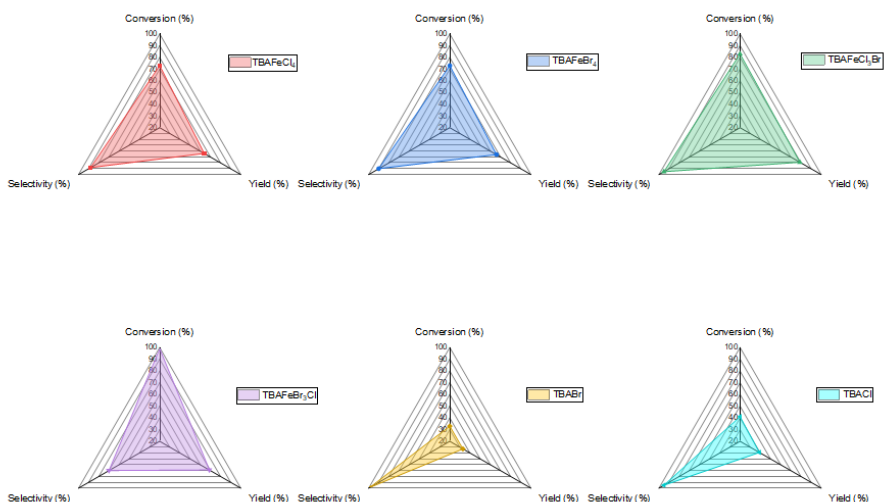


Figure 15. Graphical comparison for the activity of the different ferrates and simple ammonium halides.

Luckily, we observed that in this case, the best catalyst was also the result of the combination of the cheapest precursors used, improving the overall economic sustainability of the system.

Precursor	Price (€/g)
TBABr	0.82
TBACl	2.51
FeBr ₃	6.04
FeCl ₃ • 6 H ₂ O	0.20

The price list is based on the Sigma-Aldrich catalogue and is intended as a mere yet useful comparison on laboratory scale

By looking at the reported prices, the catalyst **TBAFeCl₃Br** should only cost **0.65 €/g**. The cheapness of the catalyst, combined with its activity is an aspect of fundamental importance while trying to obtain high value products starting from a waste material such as CO₂.

3.2.3 Effect of the reaction temperature:

As previously mentioned, the mixed ferrate catalyst **[TBA][FeCl₃Br]** outperform ammonium quaternary halides at at 125 °C but this difference becomes much more relevant at low temperatures (Figure 16). This is in agreement with the role played by the ferric salt as Lewis acid in activating the epoxide towards the nucleophilic attack of the halide. At higher temperatures, this effect become less important, as the nucleophilic attack will still occur. The higher selectivity of simple ammonium halides compared to the ferrate compound might be due to the presence of the Lewis acidic iron that might be responsible for secondary minor reaction paths. Indeed, decreasing the temperature to 100 °C resulted in a striking difference between **[TBA][FeCl₃Br]** and the ammonium halides where the activity of the latter is almost halved while the ferrate salt maintains good values of conversion (83%) of the substrate and high selectivity (95%). The difference between the presence or absence of iron is even more striking at lower temperatures: at 75 °C the ferrate compound still maintains moderate activity (33% conversion, 97% selectivity) while simple ammonium salts practically failed to react. Interestingly, at 50 °C a 12% conversion of the starting epoxide is observed when using 0.5 mol% of ferrate catalyst, leaving the door open for a possible application of this catalyst even at very low temperature.

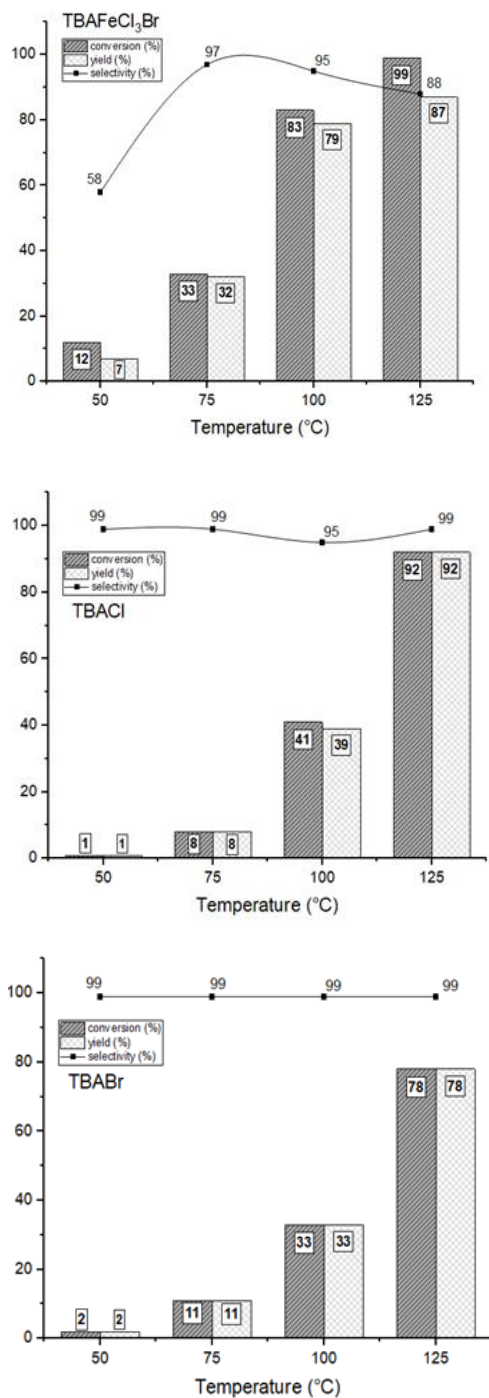


Figure 16. Catalyst activity at different temperature.

3.2.4 Effect of the CO₂ pressure:

Under otherwise identical conditions ($T = 100\text{ }^{\circ}\text{C}$ at $0.5\text{ mol}\%$ catalyst loading) we monitored the dependence of the reaction from the applied CO₂ pressure, with the aim to reduce at maximum quantity of CO₂ used to achieve sufficiently satisfactory results (Figure 17). In this case both [TBA][FeCl₃Br] and the ammonium halides proved to not be strongly influenced by the pressure of CO₂ employed. In the case of ammonium halides, the activity remains constant between 1.6 and 0.4 MPa CO₂ pressure but always lower compared with the ferrate compound. The latter suffers of an expected minor decrease of activity when moving to lower pressure of carbon dioxide but even at 0.4 MPa of CO₂ pressure a 70% conversion in just 4 h of reaction time was observed. The negligible effect of the employed pressure on the reaction will be further confirmed by theoretical investigations which point to a barrierless step of addition of carbon dioxide to the ring-opened epoxide, meaning that the activity is lowered by lowering of the pressure only in terms of less solubilized CO₂ in neat epoxide available for the transformation.

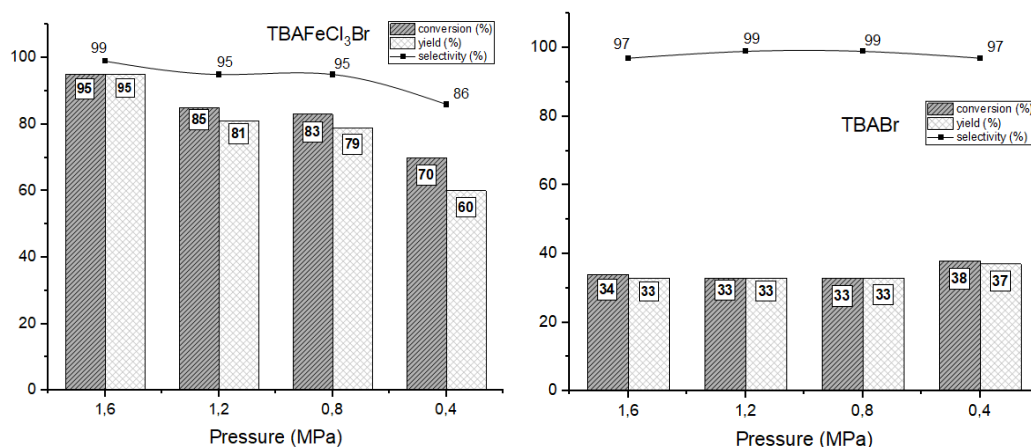
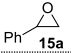
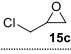
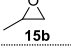
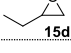
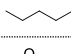
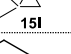
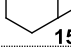
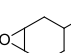
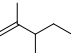
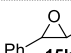
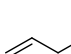
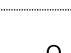
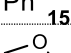
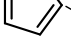



Figure 17. Catalyst activity at different carbon dioxide pressure (The results obtained with TBACl are omitted as they are completely comparable with those obtained with TBABr).

3.2.5 Scope of the reaction:

We investigated the activity of our best catalyst, in the optimized reaction conditions, on a broad scope of different epoxides. In general, our complex proved to be active for the majority of the epoxides, with a remarkable higher activity in the case of terminal ones, as expected by previously reported results. The activated substrate (+-) epichloridrine **15c** was almost quantitatively converted (97%, complete selectivity) in the corresponding cyclic carbonate **16c**. Even with alkyl substituted epoxides we obtained very high selectivity for the formation of cyclic carbonate products with just a slight decrease of conversion while increasing the alkyl chain of the substrate. In the case of propylene oxide **15b** complete selectivity for propylene carbonate was achieved. In this case, the very low boiling point of the epoxide can lead to a small weight loss in the preparation and venting of the autoclave. For less volatile substrates such as 1,2-butylene oxide **15d** and 1,2-hexene oxide **15e**, we obtained full selectivity for the cyclic product with good and comparable conversion values (75% and 76% respectively). Glycidyl ethers confirmed to be very active substrates: allyl glycidyl ether **15f** was converted selectively to the corresponding cyclic carbonate **16f** in 84% yield, furfuryl glycidyl ether **15j** was also converted in the corresponding cyclic carbonate in good yield (75% conversion, 99% selectivity). Phenyl glycidyl ether **15g** was quantitatively converted to phenyl glycidyl carbonate **16g**. The activation of more sterically demanding epoxides such as cyclohexene oxide **15n** is usually tedious but we were pleased to see that the catalyst was active also in this case, without the need of harsh reaction conditions or high catalyst loading. In our case, it was sufficient to increase the catalyst loading to 1 mol%, to obtain a high conversion of cyclohexene oxide (68%) with full selectivity to the cyclic product **16n** without formation of any polymeric by-product. In the case of 4-vinylcyclohexene dioxide **15p**, in which both an internal and a terminal epoxide are present, we obtained the selective conversion of the substrate (73%) to the terminal cyclic carbonate (92%). The formation of the di-carbonate was accounted only for the 6% of product yield. Increasing the substitution of the epoxide substrates, led to poor results. For 1,2-epoxy-1-methylpropane **15l**, only 50% conversion of the substrate was obtained but with a modest 32% yield of the cyclic product. In the case of even more sterically hindered substrates such as t-stilbene oxide and limonene oxide, no satisfactory results were obtained. In the

Table 17. Scope of the cycloaddition of CO₂ to epoxides catalysed by the ferrate salt [TBA][FeCl₃Br].

Entry	Substrate	Selectivity ^[b] (%)	Conversion ^[b] (%)	TOF ^[c] (h ⁻¹)
1		95	83	42
2		99	97	49
3		99	92	46
5		87	75	38
7		99	76	38
10		33	50	25
11		99	68	34
13		92	73	37
15		-	-	-
16 ^[d]		27	11	6
17		99	84	42
18		99	99	50
19		99	75	38
20 ^[d]		89	36	18
21 ^[d]		94	78	39

Reaction conditions: epoxide 250 μ L; cat = 0.5 mol% T = 100 °C; P (CO₂) = 0.8 MPa; reaction time = 4h. [b] Conversion and selectivity determined by ¹H NMR using mesitylene as internal standard. Conversion is indicated under each product. Selectivity for the product in brackets. [c] TON = mol_{15(converted)} · mol_{cat}⁻¹; TOF = TON · reaction time⁻¹. [d] propylene carbonate (PC) as solvent.

end, some particular terminal di-epoxides were used as substrates since the carbonate products could have a possible application as non-isocyanate polyurethane monomers: the bis-carbonate of (bisphenol A)diglycidyl ether (BADGE, **15r**) was obtained in 73% yield (94% selectivity) using only 1 mol% catalyst. In the same condition, 1,4-(bisbenzyloxy)diglycidyl ether **15s** was less active, with a 32% yield and 89% selectivity for the product. Even for this work, propylene carbonate was successfully employed as green co-solvent.

3.2.6 Scale up of the reaction and recycling of the catalyst:

Performing a 20-fold scale-up reaction allowed us to evaluate the activity of our system in such conditions. We used styrene oxide **15a** as the substrate and [TBA][FeCl₃Br] as the catalyst (0.5 mol%). Interestingly, even in this environment the latter proved to be active, with a minimum decrease in the conversion (74%) maintaining high selectivity for the cyclic product **16a**. Pure styrene carbonate was isolated by simple treating the reaction mixture with n-hexane followed by cooling and filtration of the crystalline product (58% isolated yield). The recyclability of the system was tested in the case of the synthesis of propylene carbonate (PC), under the optimized reaction conditions, to evaluate the robustness of the catalytic system. The reaction was recycled by simply adding fresh propylene oxide **15b** three times (total volume 0.750 mL) after each run. In the three consecutive runs, we observed only a minimal drop in the PC yield (from 99% to 96%) that might be due to a higher dilution of the catalyst. In any case, a remarkable TON of 594 was achieved. Full recycling details are discussed in the experimental section.

3.2.7 Density Functional Theory (DFT) investigation:

In view of our experimental findings, we were intrigued by the possibility to shed light on our catalytic system by a theoretical point of view. We decided to select a multi scale approach, since the system presents different degrees of freedom with a broad set of possible reaction paths and conformations to be considered. The semiempirical approach using an algorithm implemented in the xTB code allowed us to perform a brief screening of possible most relevant reactive channels and conformations. The latter were then optimized at the DFT level, using semiempirical geometries of the reaction intermediates and transition states.

First, we discussed the dissolution of [TBA][FeCl₃Br] in styrene oxide, in the ionic compounds [TBA]⁺ and [FeCl₃Br]⁻. As we previously

hypothesized, the ferrate fragment can further dissociate with the release of a chloride or a bromide. The whole ferrate, in fact, prefer to face the epoxide in the carbon direction and by forcing its approach, the epoxide undergoes C-C bond breaking reaction. The activation barrier of this process was found to be quite large (almost 30 Kcal/mol) which renders this reaction a non-viable channel in the experimental conditions. Indeed, we never noticed the presence of C-C bond breaking products in any of our experiments. The dissociation of the ferrate upon solvation instead requires only 9 Kcal/mol for the release of a chloride and 15 Kcal/mol for the bromide. At the experimental conditions considered we can assume that the dissociation favors the ferrate form, where the concentration of chloride is about two orders of magnitude smaller and the bromide is four orders of magnitude lower in molarity, probably excluding it from the possible reacting system. We therefore considered the transformation occurring with a free chloride anion, FeCl_2Br and carbon dioxide in neat styrene oxide.

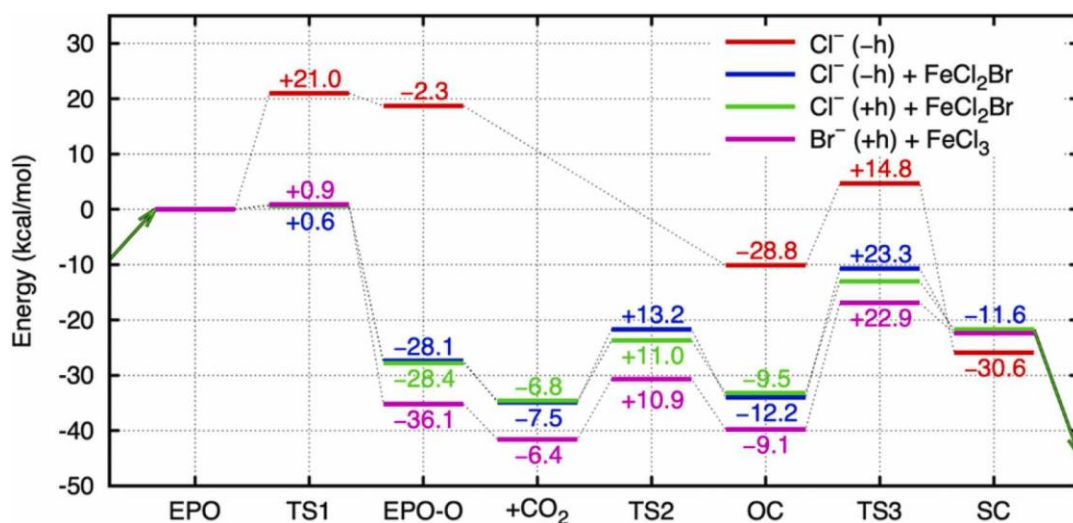


Figure 18 Schematic energy profiles for the relevant step in the reaction studied (see experimental for further details).

Strong Lewis acids (LA) such as FeCl_2Br or FeCl_3 almost annihilate the barrier of epoxide ring opening and largely stabilize the first ring opened intermediate, which, when no LA is present, is very close in energy to the TS and is likely to evolve back to the

reactants. The most favorable reaction path occurs when the epoxide ring is activated by FeCl_2Br and a chloride anion attacks the more hindered carbon of the epoxide. Indeed, when no LA is present the rate determining step of the reaction is the ring opening of the epoxide. Carbon dioxide as weak Lewis acid is much less effective than FeCl_2Br and FeCl_3 in lowering the energy barrier for the epoxide ring opening. The rearrangement of the opened organic carbonate might happen before the ring closing, with just few Kcal/mol barrier (Figure 19, TS2).

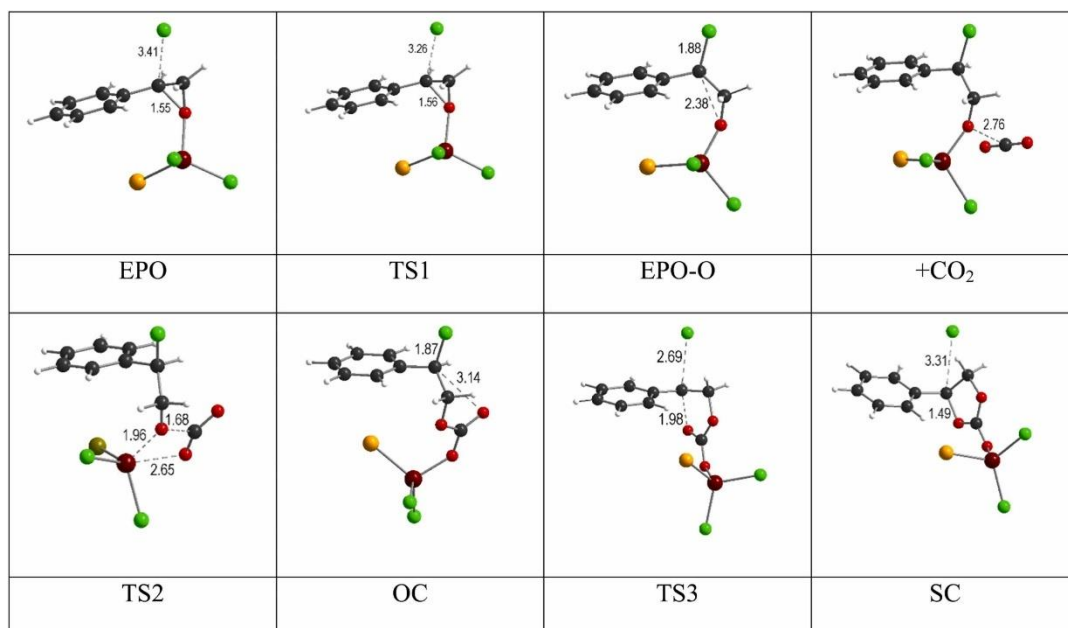


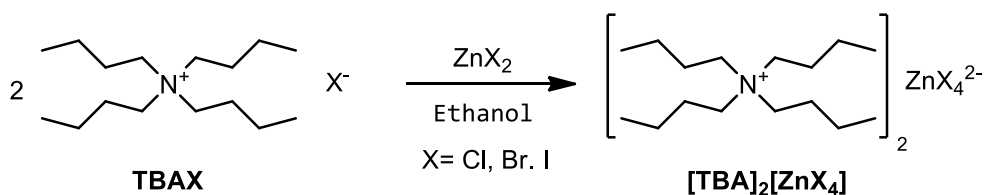
Figure 19 Representation of the relevant geometries in the reaction studied, where the chloride acts as the nucleophile and FeCl_2Br as Lewis acid.

As mentioned, the reaction seems to occur much more favorably when the iron Lewis acid is present. The latter allows the barrier for the ring opening step to drop to less than 1 Kcal/mol, stabilizing the species by almost 21 Kcal/mol (Figure 18). The ring closing step in presence of the Lewis acid implies a barrier of 20 Kcal/mol. This theoretical finding is in accord with the amount of increase in the reaction rate observed in presence of iron, with an overall lowering of about 1 Kcal/mol. It should be pointed out that the presence of iron might also assist the detachment of the halide from the last

intermediate, but we were not able to rule out this hypothesis. At the conditions considered, the monometallic mechanism is the most viable possibility from a thermodynamic point of view.

3.2.8 Synthesis of tetrabutylammonium tetrahalogenozincate salts:

A series of tetrabutylammonium zincates, $[\text{TBA}]_2[\text{ZnX}_4]$, ($\text{X} = \text{Cl}, \text{Br}, \text{I}$) was synthesized by simple mixing of an ethanolic solution of tetrabutylammonium halide with a zinc halide salt, in the appropriate stoichiometric ratio (Table 18). All the ammonium zincates were obtained in decent yields and purity after recrystallization from cold methanol. As pointed out for the analogue ammonium ferrates, a possible equilibrium between the undissociated dianion $[\text{ZnX}_4]^{2-}$ and two solvated forms $[\text{ZnX}_3]^- + \text{X}^-$ and $\text{ZnX}_2 + 2\text{X}^-$ was considered. The ESI(-)-HRMS of the compounds did not show the expected dianion $[\text{ZnX}_4]^{2-}$, but a more persistent monoanion $[\text{ZnX}_3]^-$ was detected in the case of $\text{X} = \text{Cl}, \text{Br}$, while in the case of $[\text{ZnI}_4]^{2-}$ only I^- and I^{3-} were detected most likely due to the higher lability of the compound. For more synthetic and characterization details see experimental section.



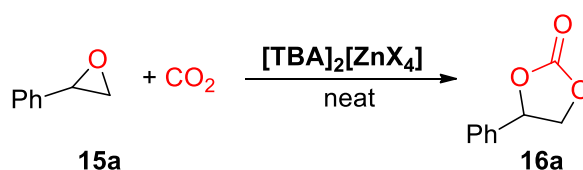
ZnX_2	TBAX	$[\text{TBA}]_2[\text{ZnX}_4]$
ZnCl_2	TBACl	$[\text{TBA}]_2[\text{ZnCl}_4]$
ZnBr_2	TBABr	$[\text{TBA}]_2[\text{ZnBr}_4]$
ZnI_2	TBAI	$[\text{TBA}]_2[\text{ZnI}_4]$

Table 18. The three homo tetrahalogenozincate salts prepared for this study (see experimental section for details)

3.2.9 Evaluation of the catalytic activity of ammonium zincates in cyclic carbonate formation:

Even for this work, we decided to use the model reaction between styrene epoxide **15a** and carbon dioxide to optimize the reaction conditions using different tetrahalogenozincates salts as catalysts. The optimized conditions with the previously described ferrate catalytic system were found to be 0.5 mol% catalyst loading at 100 °C and under 0.8 MPa of CO₂, so we decided to initially use them as starting point for the optimization using the newly prepared zincate compounds. Interestingly, all the zincate catalysts tested gave quantitative conversions of the starting epoxide in 4 h reaction time, with excellent selectivity in the case of the bromide and iodide salts (94 and 95% respectively, entries 2 and 3, Table 19). We decided to halve the reaction time and even in this case we still observed a quantitative conversion, except for [TBA]₂[ZnCl₄] as catalyst (entry 4, Table 19). The most promising catalyst resulted to be [TBA]₂[ZnBr₄] complex, in analogy with the results obtained with the zinc bromide pyclen based catalyst, which in just 1 h of reaction time converted 98% of starting **15a** with 96% selectivity for the cyclic carbonate. An outstanding conversion of 52% was observed in just 15 minutes of reaction time (entry 14, Table 19), corresponding to the remarkable Turnover frequency (TOF) of 416 h⁻¹, a clear sign of a promising truly active catalyst for this transformation.

Table 19. Preliminary optimization of the cycloaddition of carbon dioxide and styrene oxide catalyzed by tetrabutylammonium zincates.



Entry	Cat. 0.5 mol%	t (h)	Con. 15a %	Sel. 16a %	TOF ^[b] (h ⁻¹)
1	[TBA] ₂ [ZnCl ₄]	4	97	86	49
2	[TBA] ₂ [ZnBr ₄]	4	>99	94	50
3	[TBA] ₂ [ZnI ₄]	4	>99	95	50

4	[TBA] ₂ [ZnCl ₄]	2	82	98	82
5	[TBA] ₂ [ZnBr ₄]	2	>99	95	99
6	[TBA] ₂ [ZnI ₄]	2	>99	91	99
7	[TBA] ₂ [ZnCl ₄]	1	56	95	112
8	[TBA] ₂ [ZnBr ₄]	1	98	96	196
9	[TBA] ₂ [ZnI ₄]	1	78	85	156
10	[TBA] ₂ [ZnCl ₄]	0.5	30	93	120
11	[TBA] ₂ [ZnBr ₄]	0.5	87	99	348
12	[TBA] ₂ [ZnI ₄]	0.5	42	99	168
13	[TBA] ₂ [ZnCl ₄]	0.25	11	>99	88
14	[TBA] ₂ [ZnBr ₄]	0.25	52	92	416
15	[TBA] ₂ [ZnI ₄]	0.25	21	86	168
16	TBACl	4	41	99	21
17	TBABr	4	33	99	17
18	TBAI	4	42	99	21
19	-	-	3	n.d.	2

Reactions performed in an autoclave. Reaction conditions: styrene oxide (SO) 250 μ l (2.19 mmol); cat. 0.5 mol%; P(CO₂) = 0.8 MPa; T = 100 °C. Conversion and selectivity determined by ¹H NMR using mesitylene as the internal standard. [b] Turnover number ($\text{mol}_{15a(\text{converted})} \cdot \text{mol}_{\text{cat}}^{-1}$) and Turnover frequency ($\text{mol}_{15a(\text{converted})} \cdot \text{mol}_{\text{cat}}^{-1} \cdot \text{reaction time}^{-1}$).

3.2.10 Effect of temperature and CO₂ pressure:

In view of the strong activity of the zincate salts in the condition previously studied, we decided to explore their use at milder reaction conditions by lowering the reaction temperature and the carbon dioxide pressure. Initially we reduced the CO₂ pressure to 1 atmosphere and reactions were performed in sealed vials with a CO₂ balloon as reservoir at 100 °C. In all cases we noticed a lower conversion of **15a** accompanied by a lower selectivity for the cyclic carbonate product, due to competing rearrangement side reactions of the starting **15a** (entries 1-3, Table 20).

Table 20. Optimization of the reaction temperature while changing the carbon dioxide pressure

Entry	Cat.	T (°C)	P(CO ₂) (MPa)	Con. 15a %	Sel. 16a %	TOF ^[b] (h ⁻¹)
1	[TBA] ₂ [ZnCl ₄]	100	0.1	63	89	31.5
2	[TBA] ₂ [ZnBr ₄]	100	0.1	87	63	43.5
3	[TBA] ₂ [ZnI ₄]	100	0.1	80	83	40
4	[TBA] ₂ [ZnCl ₄]	50	0.1	11	91	5.5
5	[TBA] ₂ [ZnBr ₄]	50	0.1	47	96	23.5
6	[TBA] ₂ [ZnI ₄]	50	0.1	22	82	11
7 ^[c]	[TBA] ₂ [ZnCl ₄]	30	0.8	11	73	0.7
8 ^[c]	[TBA] ₂ [ZnBr ₄]	30	0.8	95	>99	5.9
9 ^[c]	[TBA] ₂ [ZnI ₄]	30	0.8	>99	>99	6.2

Reaction performed in sealed vials with a CO₂ balloon. Reaction conditions: styrene oxide (SO) 2.19 mmol; cat. 0.5 mol%; t = 4h. Conversion and selectivity determined by ¹H NMR using mesitylene as the internal standard. [b] Turnover number (mol_{15a(converted)}}·mol_{cat}⁻¹) and Turnover frequency (mol_{15a(converted)}}·mol_{cat}⁻¹·reaction time⁻¹). [c] Cat loading 1 mol%; t = 16 h. Reaction performed in an autoclave.

The reactions were repeated at 50 °C, to obtain a better solubility of CO₂, and in this case the selectivity improved, unfortunately with a lower conversion (entries 4-6, Table 20). We decided to test the reactivity of the catalytic system at room temperature by using higher pressure of CO₂ (0.8 MPa) in autoclave. In this case, by using a 1 mol% catalyst loading and extending the reaction time to 16 h, both [TBA]₂[ZnBr₄] and [TBA]₂[ZnI₄] gave almost quantitative conversions with full selectivity towards **16a** (entries 8 and 9, Table 20).

3.2.11 Effect of the catalyst loading and final optimization:

We decided to optimize the reaction conditions and to study the scope of the reaction using [TBA]₂[ZnBr₄] as catalyst since this complex proved to be the best in terms of conversion and selectivity in the range of conditions studied. We set room temperature and atmospheric CO₂ pressure as the biggest target and therefore we optimized the catalyst loading in order to maximize the yield of **16a**. We noticed that in the 24 hours of reaction time, the observed conversion of **15a** was not strongly correlated with the catalyst loading. While doubling the amount of the catalyst (from 0.5 mol% to 1 mol%) we obtained 47% of conversion (entry 3, Table 21), in comparison with 34%, with a TOF of 2.0 h⁻¹. Unfortunately, even with a 5 mol% amount of catalyst we obtained the same conversion. We investigated if this effect might be due to inhibition of the catalyst by the product formation or to the diminishing of carbon dioxide concentration during the reaction. Indeed, it is known that rubber balloons are not gas-tight and that carbon dioxide may leak through. To avoid any doubt, we repeated the same reaction by under a constant CO₂ flow at atmospheric pressure and we observed a remarkable increase in conversion (69%, entry 5, Table 21) of the starting epoxide, with complete selectivity in favor of the cyclic carbonate, with a TOF of 4.3 h⁻¹. However, working under constant bubbling of carbon dioxide results in a large waste of gas, we decided to fix the working temperature at r.t. while increasing CO₂ pressure up to 0.8 MPa in autoclave, as successfully investigated in some preliminary results, with the aim to reduce the catalyst loading. With just 0.1 mol% of the catalyst only a 5% of conversion was observed, while a gratifying TOF of 7.3 h⁻¹ was observed with a 0.5 mol% loading of [TBA]₂[ZnBr₄]. In the end, the best compromise between conversion and selectivity was obtained by using a 1 mol% loading of the catalyst, with just 0.2 MPa of CO₂ pressure. In these conditions we obtained almost identical results proving that

pressure is not a limiting factor as long as a sufficient quantity of CO₂ is provided.

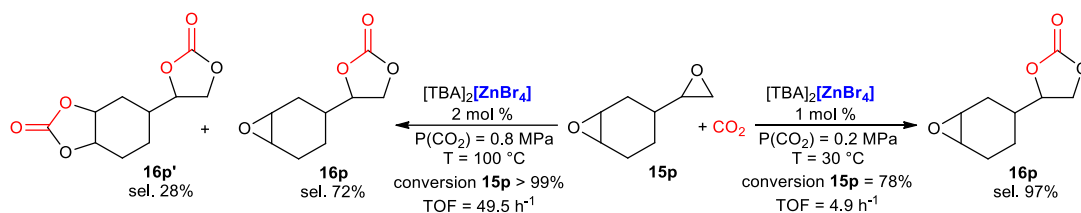
Table 21. Final optimization of the reaction conditions

Entry	Cat. loading (mol%)	P(CO ₂) (MPa)	t (h)	Con. 15a %	Sel. 16a %	TOF ^[b] (h ⁻¹)
1	0.5	0.1	24	34	97	2.8
2	1	0.1	24	47	>99	2.0
3	5	0.1	24	47	>99	0.4
4	1	0.1	16	42	98	2.6
5 ^[c]	1	0.1	16	69	>99	4.3
6 ^[d]	0.1	0.8	16	5	>99	3.1
7 ^[d]	0.5	0.8	16	58	97	7.3
8 ^[d]	1	0.8	16	87	98	5.4
9 ^[d]	1	0.2	16	88	>99	5.5

Reaction performed in sealed vials with a CO₂ balloon, using [TBA]₂[ZnBr₄] as catalyst. Reaction conditions: styrene oxide (SO) 2.19 mmol; T = 25 °C. Conversion and selectivity determined by ¹H NMR using mesitylene as the internal standard. [b] Turnover number (mol_{15a(converted)}}·mol_{cat}⁻¹) and Turnover frequency (mol_{15a(converted)}}·mol_{cat}⁻¹·reaction time⁻¹). [c] Reaction performed under CO₂ flow. [d] Reactions performed in an autoclave.

3.2.12 Reaction scope:

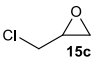
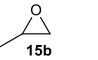
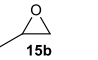
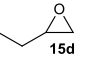
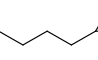
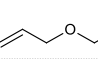
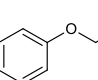
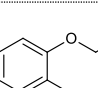
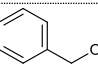
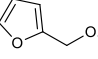
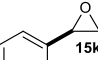
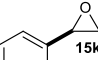
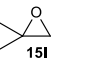
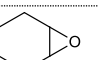
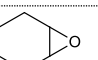
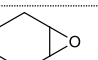
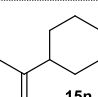
A broad reaction scope was performed, on the same epoxydic substrates employed for the ammonium ferrate work. The results in terms of conversion are quite similar (Table 22), with a high activity of the catalyst at very milder reaction conditions (30 °C, 0.2 MPa CO₂). The catalyst proved to be active on all the substrates beside the more substituted limonene oxide and t-stilbene oxide, which failed to react. Interestingly, we were able to find optimized conditions even for more challenging substrates such as cyclohexene oxide and 1,1-dimethyloxirane, for which we obtained good results at 100 °C and 0.8 MPa carbon dioxide pressure. In the case of **15l** we obtained 56% yield in just 2 hours, with a remarkable TOF of 28. For cyclohexene oxide, almost complete conversion was obtained when increasing the pressure to 1.6 MPa in 16 hours (90% conversion, 89% selectivity). This proved the possibility to finely tune the reactivity of the catalyst by changing the reaction conditions, a feature that is more clearly explained in the case of double epoxydic substrate 4-vinylcyclohexene dioxide **15p**.



Scheme 42. Different reaction outcome with changing the experimental conditions with substrate **15p**.

In fact, when the reaction is performed in the optimized conditions at room temperature and low pressure, only the terminal epoxide is converted to obtain product **16p** in almost complete selectivity. By increasing the temperature and pressure, we noticed the formation of the di-carbonate product **16p'** as a result of the conversion of the internal epoxide. At prolonged reaction time and higher pressure of carbon dioxide we were able to obtain the complete conversion of both the epoxydic moieties to yield selectively product **16p'**.

Table 22. Scope of the cycloaddition of CO₂ to epoxides catalysed by the zincate salt [TBA]₂[ZnBr₄].

Entry	Substrate	T (°C)	P(CO ₂) (MPa)	t (h)	Con. 15 %	Sel. 16 %	TOF ^[b] (h ⁻¹)
1		30	0.2	16	64	>99	4.0
2		30	0.2	16	88	99	5.5
3 ^[c]		30	1.0	16	94	99	5.9
4		30	0.2	16	86	>99	5.4
5		30	0.2	16	>99	>99	6.2
6		30	0.2	16	85	>99	5.3
7 ^[d]		30	0.2	16	75	76	4.7
8 ^[d]		30	0.2	16	75	76	4.7
9		30	0.2	16	99	97	6.2
10		30	0.2	16	87	96	5.4
11 ^[e]		30	0.2	16	-	-	-
12 ^[e]		100	1.6	16	6	80	0.4
13 ^[f]		100	0.8	2	56	77	28.0
14		30	0.2	16	12	-	0.8
15		100	0.8	2	18	99	9.0
16		100	1.6	16	90	89	5.6
17		100	0.8	2	12	-	6.0

Reaction performed in autoclave. Reaction conditions: epoxide 250 ml; cat. 1 mol%. Conversion and selectivity determined by ¹H NMR using mesitylene as the internal standard. [b] Turnover frequency (mol_{15(converted)}}·mol_{cat}⁻¹·reaction time⁻¹). [c] Isolated yield. [d] Unidentified by-products, possibly of polymeric nature, accounted for the rest of the mass balance. [e] CH₃CN (0.5 mL) was added to solubilize 15k. [f] Iso-butyraldehyde was also formed, accounting for the rest of mass balance.

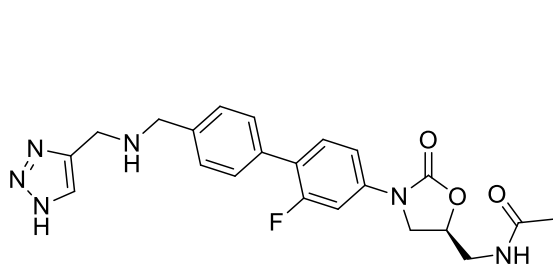
3.3 CONCLUSIONS:

In summary, we synthesized a series of tetrabutylammonium tetrahalogenoferrates and zincates, by mixing ammonium halides and metal halides in ethanol. All the products have been characterized (see experimental section) and proved to be competent catalysts for the cycloaddition of carbon dioxide and epoxides.^[155] In particular, we started by working with the ferrate compounds, which proved to be active at relatively mild condition with high conversion and selectivity for most of the substrates tested, without the addition of any co-catalyst. The best catalyst was found to be [TBA][FeCl₃Br], obtained by the mixing of TBABr and FeCl₃. This catalytic system was investigated by means of DFT calculations, which were in agreement with all the experimental findings. The chloride was found to be the most probable nucleophilic species that is responsible for the ring opening of the epoxide substrate, which is in turn activated by the presence of FeCl₂Br. The rate determining step was found to be the ring closing of the carbonate product. We then moved to the evaluation of the catalytic activity of the relative zincate compounds. They proved to be highly active, far more than the iron-based system, showing high turnovers even at room temperature and ambient pressure of carbon dioxide. The most active catalyst was [TBA]₂[ZnBr₄], which proved its catalytic activity on almost every substrate tested. By tuning the reaction conditions, we were able to convert also highly substituted epoxides and also to tailor the selectivity of the reaction in the case of 4-vinylcyclohexene dioxide. The catalyst was recyclable and confirmed its robustness for three consecutive runs.

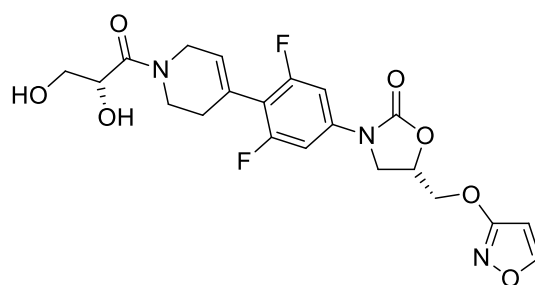
4 SYNTHESIS OF OXAZOLIDINONES FROM AZIRIDINES AND CO₂ CATALYZED BY AMMONIUM FERRATES:

4.1 INTRODUCTION:

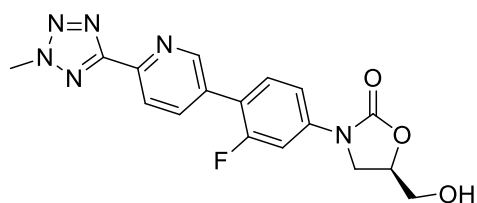
Last decade has witnessed an increase in the use of CO₂ gas as renewable building block in the coupling with reactive molecules.^[156-158] Ring strained small heterocycles, such as aziridines and epoxides, have a prominent role in the field, due to the high energy associated with these molecules that makes the reaction with thermodynamically stable CO₂ smoothly.^[159] These reactions display interesting features in terms of eco-sustainability, since the coupling occurs with 100% of atom-economy, valorizing waste CO₂ to value-added products. In this contest, 1,3-oxazolidin-2-ones are of great interest since they are present as active moieties in several pharmaceutical active molecules. Examples of active oxazolidinones include antibacterial^[160] and antimicrobial drugs (Scheme X).^[161-165] Linezolid^[166] is a potent antimicrobial which is usually administered against gram-positive bacteria. Other examples (Scheme 43) include Tedizolid^[167,168] and Radezolid.^[169,170] Posizolid^[170] is a new pharmaceutical that appears to have excellent, targeted bactericidal activity against all common gram-positive bacteria, regardless of resistance to other classes of antibiotics.



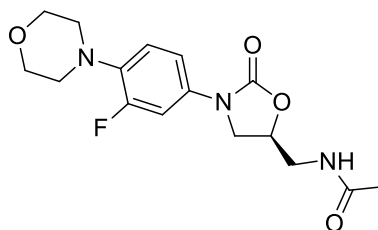
Radezolid



Posizolid



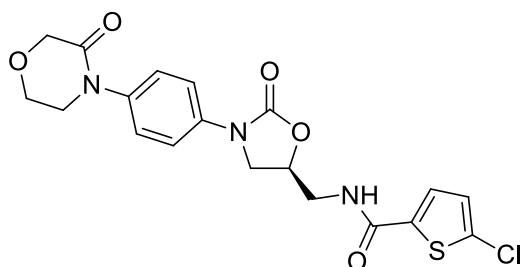
Tedizolid



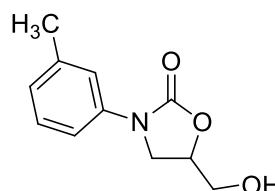
Linezolid

Scheme 43. Examples of pharmaceutically active oxazolidinones

Another example is Rivaroxaban, which is an anticoagulant medication (Scheme 44) specifically used to treat deep vein thrombosis, pulmonary emboli, to prevent blood clots in atrial fibrillation and following hip or knee surgery. It displays high structural similarity to Linezolid.



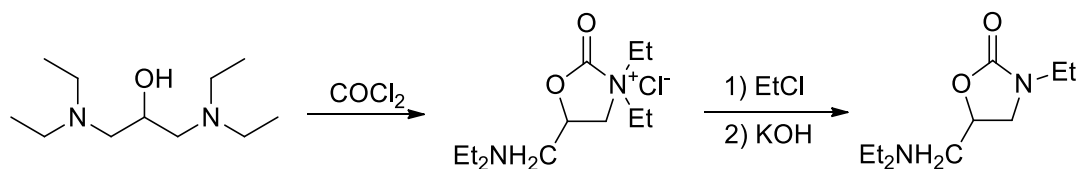
Rivaroxaban



Toloxatone

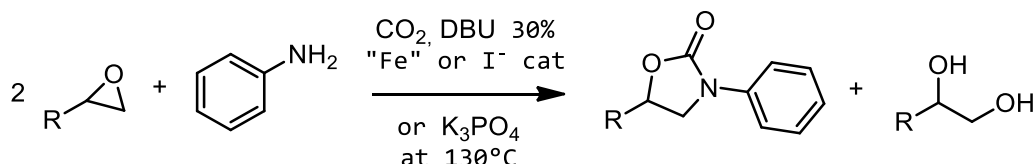
Scheme 44. Rivaroxaban, an anticoagulant drug, and Toloxatone, an antidepressant

Several synthetic strategies have been reported for the construction of the 1,3-oxazolidin-2-one skeleton and to avoid the use of highly hazardous phosgene (Scheme 45),^[171] most of them rely on cycloaddition reactions.



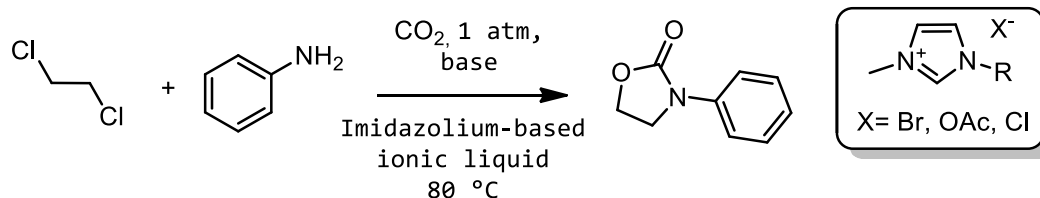
Scheme 45: 2-oxazolidinones synthesis with phosgene

One interesting approach is represented by the three component reaction of CO₂ with anilines and epoxides, which has been recently demonstrated to be efficiently catalyzed under atmospheric CO₂ pressure by pyridine-bridged pincer-type Fe(II) complexes at 90 °C,^[172] by potassium phosphate at 130 °C^[173] or with a binary catalytic system composed of organocatalysts and DBU at 90 °C (Scheme 46).^[174]



Scheme 46. Synthesis of aryl oxazolidinones through reaction of epoxides and anilines by different catalysts.

Anilines can also be efficiently employed in this transformation by reaction with dichloroalkanes and CO₂ (atmospheric pressure, T = 70 °C in the presence of 2 eq. of CsCO₃) catalyzed by a particular ionic liquid (Scheme 47),^[175] or with epoxides and dimethyl carbonate with the use of rare-earth metal amides as catalysts.^[176]

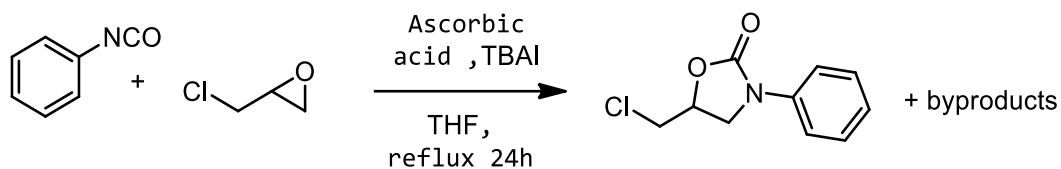


Scheme 47. Synthesis of oxazolidinones from anilines and dichloroalkanes catalyzed by imidazolium-based ionic liquids.

Aniline-derived amino alcohols have also been shown to react smoothly with CO₂ (0.5 MPa) at room temperature in the presence of an external base and *p*-toluenesulfonyl chloride (TsCl) as sacrificial reagent.^[177,178] All these methods are synthetically efficient since they are highly selective for differently substituted oxazolidinones but suffer from some limitations such as the need of high temperatures, the use of over-stoichiometric base or sacrificial reagents.

A different approach was recently reported by Poater, D'Elia and co-workers (Scheme 48): they proposed an efficient organocatalytic

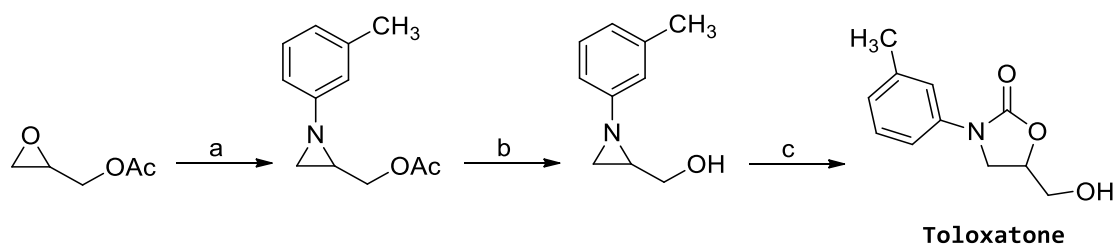
synthesis of 5-substituted 3-aryl-oxazolidin-2-ones by cycloaddition of isocyanates to epoxides, by using ascorbic acid as hydrogen bond donor and TBAI as catalysts in refluxing THF.^[178]



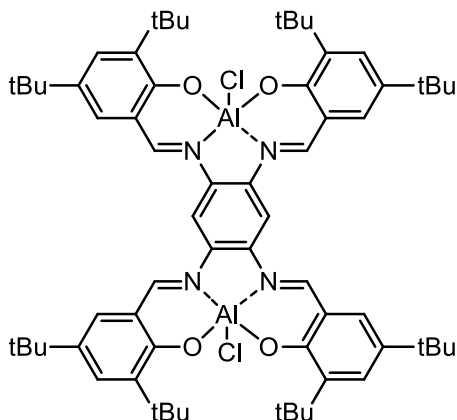
Scheme 48: Example of the synthesis of N-aryloxazolidinones by reaction of epoxides and isocyanates catalyzed by the combination of ascorbic acid and TBAI.

Another 100% atom-economic process is represented by the cycloaddition reaction of CO₂ to aziridines that occurs at very high temperatures and pressure.^[179-181] This reaction can be efficiently promoted by several homogeneous^[182-185] and heterogeneous^[186-191] catalysts by applying more sustainable conditions such as lower temperatures and lower CO₂ pressures.

Toloxatone (Scheme 49) is an antidepressant drug that contains an oxazolidinone moiety. Interestingly, the total synthesis of Toloxatone that was proposed by North and coworkers^[192] (Scheme 48) is bright example of the exploiting of a cycloaddition reaction using CO₂ and 1-(3-methyl)-phenyl-2-hydroxymethylaziridine-to form the desired product, as a demonstration of the power and high applicability of this reaction, by using a particular aluminum binuclear complex (Scheme 50)

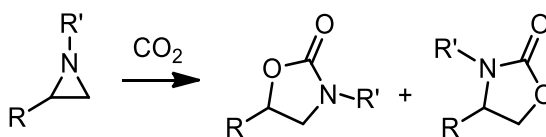


Scheme 49: Total synthesis of Toloxatone. a: 1) 3-methylaniline, 50°C, 2 days. 2) PPh₃/Br₂ (1 eq.), Et₃N (2 eq.), acetonitrile, 0°C-RT, 24 h. 80% yield. b: NaOH (2 eq.), water, RT, 16 h. 91% yield. c: Al-based catalyst CO₂ (10 bar), 100°C, 24h. 70% yield.



Scheme 50: the bis-salphen aluminum-based catalyst employed by North and co-workers

At a big difference from the CO₂ coupling with epoxides that yields univocally a single stereoisomer, the corresponding reaction with an aziridine can produce two different regioisomers if the starting aziridine is not symmetrically substituted (Scheme 51). Moreover, epoxides are industrial products, and they are therefore commercially available. Aziridines, on the contrary, are not commercially available and their synthesis is tedious (see experimental section). For these reasons, this particular reaction, in comparison to the cycloaddition of carbon dioxide and epoxides, has been less studied. Even in this case, it is recognized that both an electrophilic and a nucleophilic species are concomitantly required for the efficient CO₂ insertion into the aziridine ring.^[193] In general, the nucleophiles of choice are represented by organic halide salts, and, in case of *N*-alkyl-2-aryl aziridines, the attack is favored on the most substituted carbon atom.^[192] Following this, the ring-opened product undergoes CO₂ insertion to form a carbamate, which *via* a fast backbiting of the intermediate leads to the formation of 5-substituted 1,3-oxazolidin-2-ones when starting from 2-substituted aziridines.



Scheme 51: The two possible isomers arising from the reaction of un-symmetrical aziridines with carbon dioxide.

After having successfully reported the use of our catalytic systems in the cycloaddition of CO₂ and epoxides, especially in the case of simple ammonium metalates, we decided to study this reaction using our ferrate salts as catalysts. We selectively obtained 5-substituted 1,3-oxazolidin-2-ones at room temperature and 1 atm of CO₂ pressure. It is important to note that such mild conditions are rarely used and either higher CO₂ pressures or temperatures are usually needed.

4.2 RESULTS AND DISCUSSION:

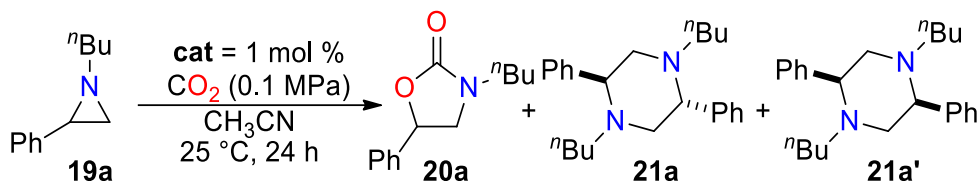
4.2.1 Synthesis of aziridines:

For the full detailed description of the synthesis of aziridines see experimental section.

4.2.2 Initial optimization of the reaction conditions:

1-butyl-2-phenyl aziridine **19a** was selected as the benchmark substrate to optimize the reaction conditions. We decided to investigate the catalytic activity of the series of tetrabutylammonium ferrates employed in the previous work for the cycloaddition of carbon dioxide and epoxides. The reactions were performed in acetonitrile (1 mL) as solvent, under CO₂ atmosphere and room temperature for 24 hours. All the ferrate salts showed a striking selectivity in the formation of the desired 3-butyl-5-phenyl-1,3-oxazolidin-2-one **20a** (Table 23) and traces of the 4-substituted isomer were detected only in the case of [TBA][FeCl₄] and [TBA][FeCl₃Br] as catalysts (entries 1 and 2, Table 23). In certain cases, we noticed the appearance of a mixture of two diastereoisomeric piperazines **21a** and **21a'** (meso-1,4-dibutyl-2,5-diphenylpiperazine and (±)-1,4-dibutyl-2,5-diphenylpiperazine, respectively). These products arise from the coupling of two aziridine molecules, which account for the rest of the reaction mass balance.

Table 23. Preliminary investigation in the formation of oxazolidinones catalyzed by ferrate salts.



Entry	Catalyst	Conversion 19a % ^[b]	Selectivity 20a % ^[b]	TOF ^[c] (h ⁻¹)
1	[TBA][FeCl ₄]	58	96 ^[d]	2.4
2	[TBA][FeCl ₃ Br]	90	98 ^[d]	3.8
3	[TBA][FeBr ₃ Cl]	94	97	3.9
4	[TBA][FeBr ₄]	>99	97	4.1
5	FeBr ₃	88	84	3.7
6	TBABr	12	>99	0.5
7	FeBr ₃ + TBABr	>99	99	4.1

Reaction conditions: 1-butyl-2-phenyl aziridine, **19a**, (1 mmol) and catalyst (1 mol%) in CH₃CN (1 mL) under CO₂ atmosphere (P = 0.1 MPa) at T = 25 °C; t = 24 h. [b] Conversion and selectivity determined by ¹H NMR using dibromomethane as the internal standard and confirmed by GC (decane as ISTD) [c] Turnover frequency (mol_{19a}(converted) · mol_{cat}⁻¹ · reaction time⁻¹). [d] Traces of the 3-butyl-4-phenyl-1,3-oxazolidin-2-one isomer were detected (d.r. = 97:3).

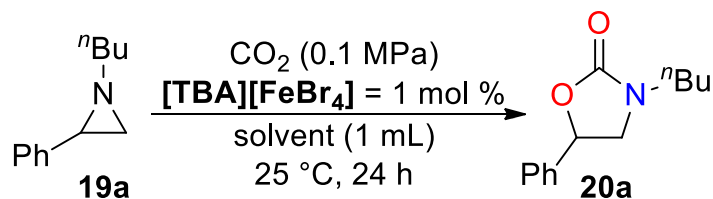
The highest TOFs were obtained in the case of “bromo” ferrates (entries 3-4, Table 23). Indeed, the activity of simple iron(III) bromide as Lewis acid in 1 mol% amount, was enough to observe a good conversion of the starting aziridine **19a** (88%), but with a lower selectivity for the oxazolidinone formation (entry 5, Table X). As in the case of reactions with epoxides, TBABr alone yielded pure **20a**, but in very poor yield (12%, entry 6, Table 23). As a proof of concept, since ammonium ferrates are formed at room temperature under vigorous stirring by the mixing of a quaternary ammonium salt and an iron(III) halide, we decided to perform a reaction in which the compound is formed *in situ* under our catalytic conditions. Indeed, results obtained are almost identical to those observed for the preformed ammonium ferrate [TBA][FeBr₄] (entry 7, Table 23).

Nevertheless, as already mentioned in the previous chapter, tetrabutylammonium ferrates are much easier to handle in respect to the corresponding precursor and their synthesis is quite straight forward. For these reasons they have been preferentially employed as preformed catalysts rather than formed *in situ*.

4.2.3 Solvent screening:

We investigated the effect of different solvents, concentration, and pressure in the model reaction, using $[TBA][FeBr_4]$. Polar and non-polar aprotic solvents were found to be suitable reaction media, where good conversions of **19a** were observed (Table 24). THF, instead, proved to not be suitable, probably competing with the aziridine in the coordination to iron (entry 4, Table 24). Even using a protic solvent such as MeOH (entry 6, Table 24) provided a very low selectivity. It should be noted that in all cases, except for dichloromethane, variable amounts of 2,5-diphenylpiperazines, **21a** and **21a'**, were also formed.

Table 24. Solvent screening for the reaction of **19a** with carbon dioxide catalyzed by $[TBA][FeBr_4]$



Entry	Solvent	Conversion 19a % ^[b]	Selectivity 20a % ^[b]	TOF ^[c] (h ⁻¹)
1	DCM	85	>99	3.5
2	CH ₃ Cl	75	83	3.1
3	Acetone	92	84	3.8
4	THF	38	92	1.6
5	AcOEt	90	93	3.8
6	MeOH	41	34	1.7
7	Dimethyl carbonate	75	89	3.1

Reaction conditions: 1-butyl-2-phenyl aziridine (1 mmol) and catalyst (1 mol%) in the solvent (1 mL) under CO_2 atmosphere ($P = 0.1$ MPa) at $T = 25$ °C; $t = 24$ h. [b] Conversion and selectivity determined by 1H NMR using dibromomethane as the internal standard. [c] Turnover frequency ($mol_{19a}^{(converted)} \cdot mol_{cat}^{-1} \cdot reaction\ time^{-1}$).

4.2.4 Optimization of the reaction:

While performing the reactions under a gentle flow of carbon dioxide, in order to keep its concentration constant, with 1 mol% of catalyst, we observed a 97% conversion of the starting aziridine **19a**, with very high selectivity for **20a** (entry 1, Table 25). When we repeated the same reaction, by using a CO₂ balloon as reservoir, we obtained lower conversion of **19a** and a higher formation of piperazine byproducts (entry 2, Table 25). This result is in agreement with the one obtained in the case of zincate catalyzed formation of cyclic carbonate while using a carbon dioxide balloon, which is not properly gas-tight^[194], and the concentration of CO₂ tends to diminish over time leading to poor results. Under CO₂ flow, using a 2.5 mol% loading of [TBA][FeBr₄] we were able to reduce the reaction time to 16 hours, obtaining good results (entry 3, Table 25), where a further increase in the amount of the catalyst (5 mol%) was detrimental, since piperazines started to be formed as the major by-products (entry 4, Table 25).

Table 25. Optimization of the reaction conditions with [TBA][FeBr₄] as catalyst

Entry	Cat (mol%)	t (h)	P (MPa)	Conversion 19a % ^[b]	Selectivity 20a % ^[b]	TOF ^[c] (h ⁻¹)
1	1	16	0.1	92	98	5.8
2 ^[d]	1	16	0.1	76	70	4.8
3	2.5	16	0.1	>99	97	2.5
4	5	16	0.1	>99	82	1.2
5 ^[e]	1	24	0.1	5	>99	0.2
6 ^[e]	5	24	0.1	32	91	0.3
7 ^[f]	1	16	0.1	71	43	4.4
8	1	24	0.4	>99	98	4.1
9 ^[g]	1	24	0.4	88	83	3.7

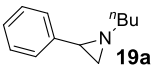
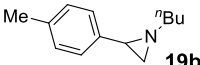
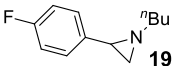
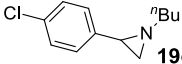
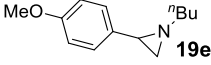
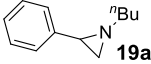
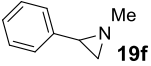
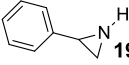
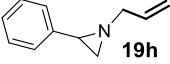
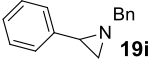
Reaction conditions: 1-butyl-2-phenyl aziridine (1 mmol) and catalyst (x mol%) in CH₃CN (1 mL) under CO₂ atmosphere at T = 25 °C; under stirring. [b] Conversion and selectivity determined by ¹H NMR using dibromomethane as the internal standard. [c] Turnover frequency (mol_{19a(converted)}·mol_{cat}⁻¹·reaction time⁻¹). [d] Reaction performed under a CO₂ balloon. [e] 10 mL of CH₃CN were used (**19a**, 0.1 M). [f] 0.1 mL of CH₃CN were used (**19a**, 10 M). [g] FeBr₃ 1 mol% as the catalyst.

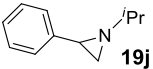
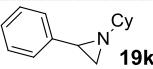
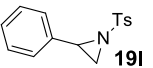
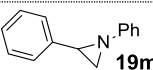
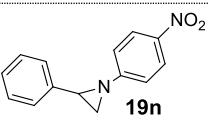
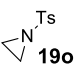
A 10-fold diluted sample (0.1 M solution of **19a**) resulted in complete drop of activity (only 5% conversion), but with a complete selectivity in favor of **20a** (entry 5, Table 25). On the contrary, increasing the concentration of **19a** to 10M resulted in a lowering of selectivity (43%) for **20a** and in this case, rather than being byproducts, piperazines **21a** and **21a'** (57%) were recovered as main products (entry 7, Table 25). By following a typical reaction with GC analysis, repeated in the first 2 h of reaction, we observed the initial formation of a slight amount of piperazines (ca. 2%) together with **20a**. Interestingly, the amount of piperazine by-products remains constant after the first 30 min of reaction, and the formation of oxazolidinone becomes predominant, with a final complete conversion of the substrate after 24 h and a global selectivity of 97% in **20a**. We were able to isolate pure piperazines **21a** and **21a'**, by performing the reaction under N₂ atmosphere instead of CO₂. This confirms that in the absence of CO₂ a fast reaction, catalyzed by a Lewis acid between two molecules of **19a**, leads to the formation of the piperazine product. Indeed, the concentration of carbon dioxide plays a fundamental role by favoring the entrapping of the ring-opened product and oxazolidinone formation; we performed the reaction at room temperature in autoclave under 0.4 MPa pressure of CO₂ (entry 8, Table 25), and the obtained results were very close to those observed working under CO₂ flow.

4.2.5 Kinetic study:

We performed the reaction of 2-phenyl aziridines bearing different substituents in para position on the phenyl ring. The presence of electron-donating groups (EDG) stabilizes the formation of a positive charge at the benzylic position, while electron-withdrawing groups (EWG) should destabilize it. Stabilization of the carbocation at the benzylic position after the ring opening of the aziridine ring is expected to increase the rate of the reaction. To better compare the effect of the substituents, the reactions were performed with a lower catalyst loading at room temperature and atmospheric CO₂ pressure, to avoid the complete conversion of the starting aziridine. As expected, the presence of EDGs in para position led to a faster but less selective conversion of the starting product. Aziridine **19b** was converted almost quantitatively in just 16 h at room temperature, but the selectivity in product **20b** was only 85% (entry 2, table 26). By means of GC analysis, we noticed a fast formation of piperazines **21b-21b'** at the beginning Table 26.

Optimization and reaction scope of the cycloaddition of aziridines and carbon dioxide

Entry	Substrate	Cat. (mol%)	Conv. 19 % ^[b]	Sel. 20 % ^[b]	TOF (h ⁻¹) ^[c]
1	 19a	1	92	98	5.8
2	 19b	1	94	85	5.9
3	 19c	1	87	99	5.4
4	 19d	1	83	99	5.2
5	 19e	1	95	48	5.9
6	 19a	2.5	>99	97	2.5
7	 19f	2.5	>99	84 ^[d]	2.5
8	 19g	2.5	>99	90	2.5
9	 19h	2.5	>99	>99	2.5
10	 19i	2.5	>99	96	2.5

11 ^[e]		2.5	>99	30 ^[f]	2.5
12 ^[e]		2.5	85	24 ^[g]	2.1
13 ^[e]		2.5	45	40 ^[h]	1.1
14 ^[e]		2.5	>99	n.d. ^[i]	2.5
15 ^[e]		2.5	>99	32 ^[1]	2.5
16 ^[e]		2.5	40	90	1.0

Reaction conditions: aziridine (1 mmol) and catalyst (x mol%) in CH₃CN (1 mL) under CO₂ atmosphere at T = 25 °C; under stirring; t = 16 h. [b] Conversion and selectivity determined by ¹H NMR using dibromomethane as the internal standard. [c] Turnover frequency (mol_{1a}(converted)·mol_{cat}⁻¹·reaction time⁻¹). [d] Traces of the 3-methyl-4-phenyl-1,3-oxazolidin-2-one isomer were detected (d.r. = 98:2). Piperazines **21f** (mixture of diastereoisomers) accounted for the rest of mass balance. [e] Reaction performed in a steel autoclave at 100 °C for 16 h and 1.6 MPa of CO₂. [f] Piperazines **21j** (mixture of diastereoisomers) were formed with a global 70% selectivity. [g] Piperazines **21k** (mixture of diastereoisomers) were formed with a global 76% selectivity. [h] Several by-products were present in the reaction crude, including probably piperazines **21l** and **21l'**. [i] Only piperazines **21m** (mixture of diastereoisomers) were detected with a global 88% selectivity. Others unidentified by-products accounted for the rest of the mass balance. [1] Several other unidentified by-products accounted for the rest mass balance.

of the reaction, with a 10% selectivity in the first hour (see experimental section for further details). After one hour, this side reaction rapidly stopped, and the formation of oxazolidin-2-one product **20b** predominated until the complete consumption of aziridine. Plotting the conversion of the starting aziridine over time for **19a** and **19b** confirmed that the presence of an EDG on the phenyl ring increase the rate of conversion. We could not address a clear first order kinetic in the aziridine consumption since the side reaction (the formation of piperazines) probably follows a second order kinetic. On the other hand, the presence of EWG slows

down rate of the reaction by disfavoring the nucleophilic attack, and a lower conversion of the starting aziridines **19c** and **19d** was observed (entries 3 and 4, Table 26). Aziridine **19e** was readily converted in just 16 h (entry 5, Table 26), but with very low selectivity for product **20e**.

4.2.6 Reaction scope:

We decided to perform the scope of the reaction in the optimized conditions at room temperature and atmospheric pressure of carbon dioxide. In this case we used a 2.5 mol% catalytic loading, to obtain an almost quantitative conversion of aziridine. N-methyl aziridine **19f** was converted quantitatively but with a low selectivity (84% entry 7, Table X). In this case, the formation of 1-4-dimethyl-2,5 diphenylpiperazines **21f-21f'** is favored due to the reduced steric hinderance. Unprotected aziridine **19g** was efficiently converted with a very good selectivity (entry 8, Table 26). Good conversions and selectivity were observed for allyl and benzyl N-substituted aziridines **19h** and **19i** (entries 9 and 10, Table 26). We noticed that substrates bearing a secondary alkyl substituent were not converted in the usual conditions, requiring the increase of temperature and pressure. Aziridines **19j** and **19k** were converted at T = 100 °C, P(CO₂) = 1.6 MPa but with very modest selectivity (entries 11 and 12, Table 26). The possible reason behind this is the fact that the Lewis acid suffers from the steric hindrance of the substituent while approaching the nitrogen atom of the aziridine. Indeed, the same negative results were observed for tosyl protected aziridine **19l**, due to the presence of electron-withdrawing sulfonyl group at the nitrogen atom,[53] and unfortunately also with aryl substituted aziridines **19m** and **19n** (entries 13-15, Table 26). Surprisingly, aziridine, **19o**, was selectively converted to 3-tosyl-1,3-oxazolidin-2-one **20o**, in modest yield (entry 16, Table 26). When we tried to react di-substituted aziridine **19p**, even at harsher reaction conditions, we only obtained several unidentified by-products, among which benzaldehyde (probably due to aza-Cope rearrangement).

4.2.7 Scale up experiments:

A gram-scale reaction, using 1 g of aziridine **19a** as substrate, was performed in a steel autoclave at 25 °C for 24 hours under CO₂ atmosphere (0.4 MPa) using the tetrabromoferrate compound as catalyst. The crude reaction mixture showed a quantitative conversion with a high selectivity for the formation of **20a** that was obtained in 81% isolated yield by extraction with AcOEt/water.

4.2.8 Mechanistic investigation:

As in the case of cycloaddition of epoxides and carbon dioxide, we performed an extended set of ab initio computations to shed light on the mechanism of this transformation.

First, we considered that the ferrate species might undergo dissociation in this reaction environment as in the previous studied case. We determined that the dissociated form of the ferrate anion into FeBr_3 and Br^- , is thermodynamically favored by 6 kcal/mol in respect to the undissociated ferrate when interacting with aziridine **19f**.

Second, even in this case we did not consider any bimetallic mechanism, since based on our calculations the reaction may proceed even with just a single iron-based catalyst molecule.

Third, we assumed that, as proven experimentally, the nucleophilic attack and C-N bond breaking in the aziridine **19f** happens on the benzylic carbon atom, since only 5-substituted 1,3-oxazolidin-2-ones were obtained. Computational results obtained in this study confirmed this choice since the barrier for aziridine ring opening is slightly larger when the halide attacks the less hindered carbon atom of the ring.

Fourth, the cation was not included in the reaction environment since its role is not relevant from an energetic point of view.[50]

Computed data are described in the experimental section, along with the molecular structures of all reaction intermediates and transition states.

We first considered the formation of a complex between aziridine and the Lewis acid and then with the upcoming bromide anion. The first transition state involved the aziridine ring opening upon attack of the bromide on the benzylic carbon atom, and consequent breaking of a carbon-nitrogen bond in a concerted way; the second transition state is an internal rearrangement between CO_2 , the LA and the nitrogen atom; the third transition state involves the ring closing step and the formation of the product. The barrier for TS3, corresponding to the ring closure, is by far the largest and accounts for about 23.0 kcal/mol, and it defines the rate-determining step of the reaction. This value is overall consistent with the conversion times measured during laboratory experiments. It is important to see that the energy path for the release of the Lewis acid, FeBr_3 ,

and the bromide from the product is unfavorable when surrounded by acetonitrile. Anyway, for bromide the interaction energies with the product and the reactant are almost equivalent, paving the way to a possible migration from **20f** to another molecule of **1f**.

Most importantly, the entire reaction process is exothermic, with an enthalpy of -25.7 kcal/mol. It is also important to note that FeBr₃ is less bound to the product in respect to the reactant by a considerable amount of energy (12 kcal/mol). Even in this case, this feature is likely to play a key role for the catalyst to abandon the product at the end of the reaction to activate another substrate molecule.

According to experimental evidence, the reaction might proceed also in absence of a Lewis acid. In this case, carbon dioxide must act as a weak Lewis acid itself from the very beginning of the reaction. If this condition is not satisfied, the aziridine ring opening upon attack of bromide does not produce any stable intermediate that will evolve in a product. Indeed, carbon dioxide interacts very weakly – and hence reversibly – with the nitrogen atom of aziridine, and the only relevant resulting conformer is concurrent with many others that are not useful to the reaction. It is therefore unlikely to imagine that carbon dioxide in respect to iron bromide, when acting as a Lewis acid, can strongly activate a substrate molecule for the ring opening, and that this process might only become predominant at very high carbon dioxide pressure. Beside this critical aspect, the conversion of the reactant into the product requires three energy barriers to be overcome. The first TS is negligible and corresponds to an internal conformation conversion between CO₂ and aziridine. The second transition state is the aziridine ring opening upon attack of bromide, and the third transition state corresponds to the ring closing of the product. Even in this case the largest one in terms of energy required is the latter, with a barrier of 9.3 kcal/mole.

4.3 CONCLUSIONS:

In summary we successfully exploited the catalytic activity of tetrabutylammonium ferrates in the reaction of aziridines and carbon dioxide to produce oxazolidinones.^[195] The tetrabromoferrate proved to be the most active catalyst in this transformation, with good results in very mild reaction conditions (room temperature, 0.1-0.4 MPa CO₂). The activity of the system is however limited mainly to N-alkyl substituted aziridines, with other substrates that failed to react or resulted in the formation of byproducts (usually piperazines). Both a kinetic and theoretical investigation have shed light on the mechanism of the reaction, where the rate determining step is the ring-closing of the product when the catalyst activate the aziridine ring, with an overall exothermic process.

5 CHEMICAL RECYCLING OF POLYETHYLENE TEREPHTHALATE (PET):

5.1 INTRODUCTION:

5.1.1 The era of plastics:

Plastics are the material that revolutionized completely our society and way of living. It allowed us to produce inexpensively a huge variety of products, with uses in both industry and everyday life. The first synthetic polymers invented were polystyrene (PS) in 1839, polyvinyl chloride (PVC) in 1835 and Bakelite in 1907.^[196] The production of plastics began to grow around 1950, when the market reached almost 2 million tons/years, and it is today expected to exponentially increase up to 30000 million tons/years in 2050 (Figure 20).^[197]

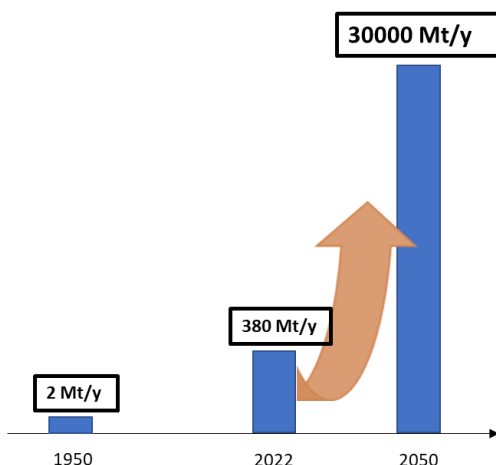


Figure 20. Expected exponential increase in plastics production until 2050.

One of the biggest responsible for the development of plastics production in the last century is without any doubt the Italian chemist Giulio Natta. Together with German chemist Karl Ziegler, he developed a series of catalysts based on titanium and aluminum,^[198] which actively catalyzed the reaction of propylene to isotactic polypropylene.^[199] During those years he was working at the

Politecnico of Milan and thanks to the funding of Montecatini and the collaboration with CNR he was able to develop his studies on the stereochemistry of polymers, culminating in the study of stereospecific polymerization and the Nobel Prize winning in 1963, together with Ziegler (Figure 21).



Figure 21. Nobel Prize assignment ceremony in 1963 with Ziegler (on the left) and Natta (center).

One of the overlooked aspects in the work of Natta, is the fact that since the initial discovery of polypropylene in 1954, it only required three years for the innovation to reach the full industrial level, with the Moplen plant of Montecatini in 1957. Moplen (Figure 22) was the registered trademark of isotactic polypropylene, which revolutionized the everyday life of Italians in the postwar.



Figure 22. Famous advertisement of Moplen with the motto: “e mo... e mo... Moplen!” in the Carosello advertisement on Italian television in the 50-60’s

5.1.2 Development of polyesters:^[200]

During the last century, in 1941 the company Calico Printers Association developed a high molecular weight polyester based on terephthalic acid, called polyethylene terephthalate (PET), in the form of fiber (Terylene, Dacron, Lavsan), film (Melinex, Mylar) and a material which rapidly became a promising candidate for the production of blow molded bottles. Only in 1960s, Du Pont developed high crystalline grade PET containing additives to control morphology, and also co-polymers with enhanced properties. It rapidly replaced glass and metal in the manufacture of different products and today it is used to produce filaments, fibers, films, tire cord and packaging resins, especially food-grade bottles (Figure 23), in a quantity that ranges around 90 million tons/years making it the fourth-most produced polymer in the world.



Figure 23. Typical PET containers (for food/beverages and for other products) with the corresponding recycling symbol.

PET possesses excellent mechanical, electrical and thermal properties,^[201,202] and an example of the most important characteristics is listed below:

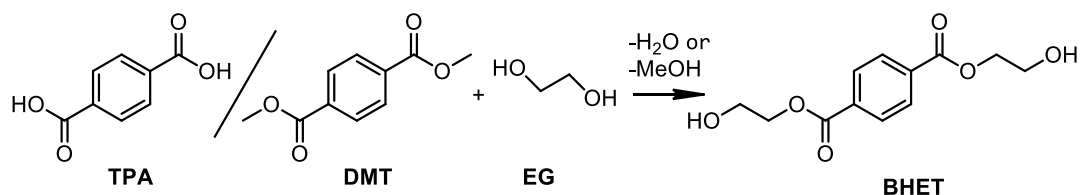
- Transparent and lightweight
- Good resistance to thermal aging
- Low flavor absorption
- Important dimensional stability
- Chemical and electrical resistance
- Economic availability and processability
- Excellent recyclability

PET can be produced in semicrystalline or amorphous structure: the higher crystallinity, the higher the glass transition temperature,

resulting in a polymer with increased hardness, tensile strength and resistance. The density of crystalline PET is 1.455 g/cm³ whereas for amorphous PET is around 1.333 g/cm³.^[203] In the case of films, crystallinity is induced by mechanical operations (i.e., biaxially oriented PET films) or thermal recrystallization.

5.1.3 Synthesis of polyethylene terephthalate:

The synthesis of PET involves the reaction of terephthalic acid (TPA) and ethylene glycol (EG), typically in four main steps: (1) transesterification/direct esterification, (2) prepolymerization, (3) melt condensation, (4) solid-state polycondensation. The formation of the polymer can occur through esterification of acid moieties of TPA and hydroxyl groups of EG, or by transesterification of other esters.

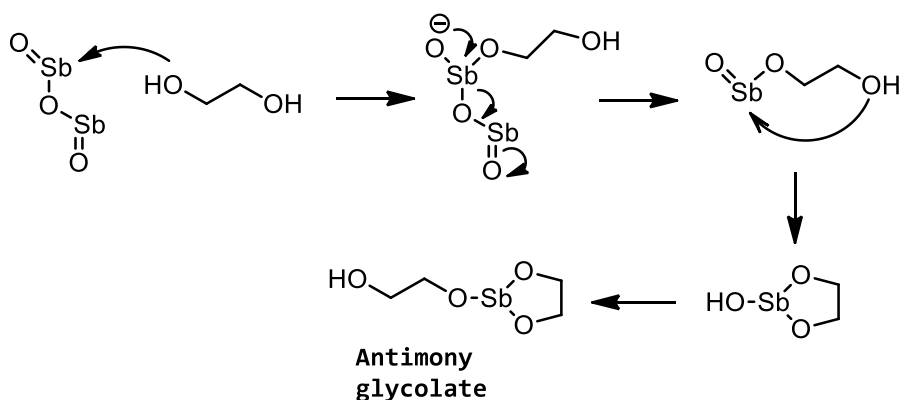


Scheme 52. Synthesis of BHET from TPA or DMT by reaction with EG.

- (1) Formation of BHET (bis(hydroxyethyl)terephthalate and some oligomers by esterification of TPA or transesterification of dimethyl terephthalate (DMT) or BHET. The transesterification is preferred in the production of fibers, and it is performed with catalysts based on manganese, zinc, cobalt and also calcium. In the direct esterification process catalyzed by titanium tetrabutoxide, the formation of diethylene glycol chains, as an etherification byproduct, results in a polymer that has lower melting point, poor thermic resistance and less UV stability.
- (2) Formation of linear oligomers of BHET, with a polymerization degree (DP) of almost 30, at temperatures ranging between 150-200°C and pressure of 100 kPa.

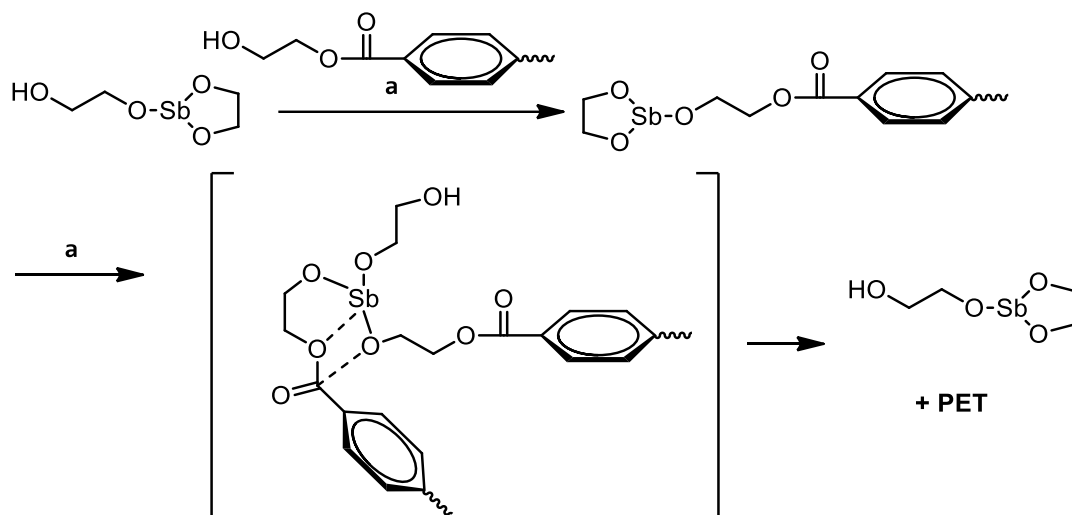
- (3) Continued polymerization up to DP \approx 100
- (4) The final step is the solid-state polycondensation to DP \approx 150, using antimony trioxide as catalyst. Other catalysts based on germanium and titanium have also been used. In this step, chain extenders molecules are added in 0.5-2% to increase the production rate and also to improve the color of the end product. The solid-state procedure is applied in one third of all the PET global production.

The antimony trioxide catalyst is very active in the polymerization step thanks to the formation of antimony glycolate in presence of EG. The probable mechanism of the reaction is described in scheme 53.^[204]



Scheme 53. Formation of antimony glycolate by reaction of antimony trioxide with ethylene glycol.

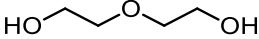
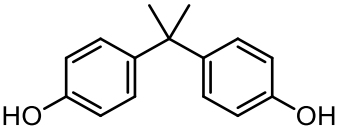
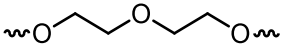
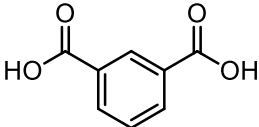
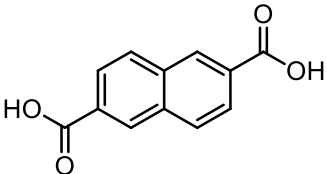
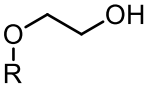
The so formed glycolate can react with an acidic end group of a polymer chain (a) to form a coordinated diester, which undergoes polymerization with a second ester unit to increase the polymer molecular weight, regenerating the catalyst (scheme 54).



Scheme 54. Polymerization between two different chains, catalyzed by antimony glycolate.

To modify the properties of the polymer, different additives can be added during polymerization step.^[205] The most important examples are reported in table 27. The synthesis of PET requires high purity starting materials, since the purification of the polymer is very difficult at the end of the process. EG is easily purified by vacuum distillation, while terephthalic acid is recrystallized several times. Moreover, the temperature of the chain propagation step must be controlled, to avoid the possible undesired decomposition to acetaldehyde and other by-products. The average molecular weight of crystalline PET obtained in this way is around 35000 g/mol.

Table 27. Reagents used in PET synthesis for the modification of the resulting polymer's properties.

Additive	Properties
 <p>Diethylene glycol</p>	<p>Improves dyeability of fibers, lowers melting point</p>
 <p>Bisphenol A</p>	<p>Improves stiffness of the polymer</p>
 <p>bDEG units</p>	<p>Lowers melting point, modify the mechanical properties</p>
 <p>Isophthalic acid</p>	<p>Improves stress-cracking resistance and higher melting temperature</p>
 <p>2,6-Naphtalenedicarboxylic acid</p>	<p>Improves the mechanical properties of the polymer and reduces gas permeability</p>
 <p>Terminated EG groups</p>	<p>Reduces hydroxyl value, improvement of thermal stability</p>

5.1.4 Plastics waste life cycle:

The exponential growth of plastic production is due to three main reasons:^[197,206]

- (1) The development of novel plastic materials, by changing the structure or processing conditions, allows the use of plastics in alternative applications
- (2) Improvement of economic situation in developing countries leads to the increase of plastic production and use
- (3) Decreasing of the cost of plastic production

This increase in the production of plastic was not balanced with a proper increase of its recycling rate, probably due to a lack of education and information regarding the consequences of mismanagement of plastic waste. Today almost **32%** of all plastics end up in **dumps or oceans** (figure 24),^[207] mainly through rivers, but potentially, every waste on land can reach ocean since it is the ultimate sink of earth. Plastic materials leaks into the environment through improper disposal and transport, where they can degrade to microplastics (especially fibers), which are small fragments (less than 5mm) that are extremely difficult to recover, becoming almost ubiquitous.^[208] The problems associated with microplastics are still being evaluated, but the impact on marine and freshwater animals is well studied. Microplastics were also found in the troposphere. Almost **40%** of plastics is **landfilled** in ground protected landfills to avoid the leakage into the environment, but in some cases the absence of such protection leads to a potential problem.^[209] Even in the case of modern technology landfills in the US, almost 1 million metric ton of plastic (3% of all plastic waste) is leaked into the environment. **14%** of plastic waste is **burned for energy recover**: this process in terms of energy produced but it poses serious environmental problems of greenhouse gases generation. Only **14%** of plastics are **recycled** today, and **8%** end up in **lower quality products** (cascaded recycling) and only **2%** are efficiently recovered in a **closed loop** view to replace virgin materials.

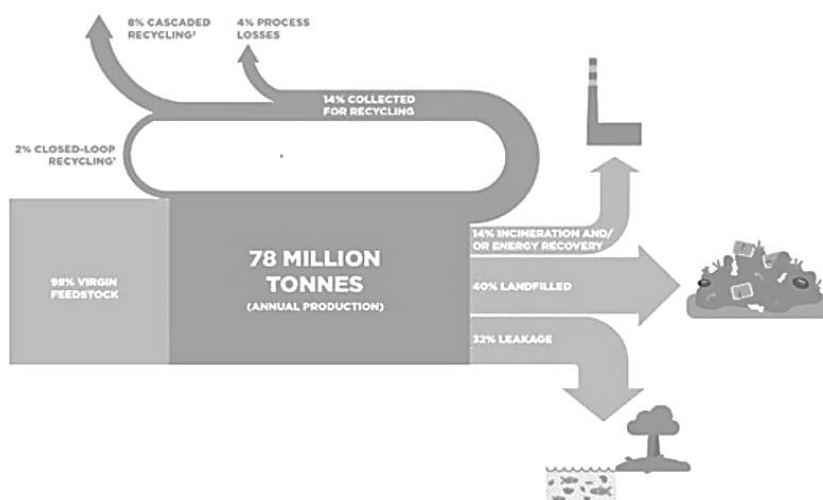


Figure 24. Sankey diagram of the life cycle of plastics (source: Ellen McArthur Foundation, 2018).^[210]

5.1.5 Life cycle of PET:

Today almost **90 million tons** of PET are **consumed** each year, especially for beverage packaging like water bottles. Only a very small portion of this PET, **less than 2 million tons**, is recovered from bottles and **recycled**. Essentially, plastic wastes are collected and transported to facilities in which different components are separated (Figure 25). Food-grade PET is separated from other plastics and other contaminants and collected in bales to be further processed. Usually, bottles are separated also depending on their color. All this recovered and separated PET waste is processed by **mechanical recycling**, in which it is first grinded to flakes to become rPET after washing and separation from polypropylene and polyethylene residues.^[211] Of this little portion, only **30%** is returned to **bottles production**, while almost **70%** is going to **downgraded products** or energy recovery. This is due to the fact that mechanical recycling leads to an intrinsic degradation of the polymer, decreasing its crystallinity and molecular weight.^[212,213] To produce bottles from rPET, during manufacturing, virgin resin is added to improve the properties of the material. In this view we are still far from a closed loop from bottle to bottle. Nevertheless, technology in this field is growing fast, and good results are being obtained by mechanical recycling.

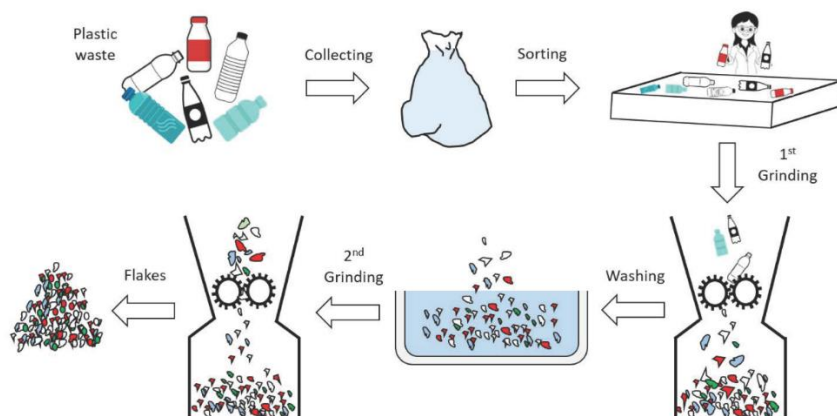


Figure 25. Typical steps in mechanical recycling of PET. In the washing step, PE and PP contaminants are removed thanks to the difference in density.

The traditional use of rPET is in the field of textiles, where the flakes are melted and extruded to obtain PET fibers used to manufacture clothes. **Patagonia** was the first company to introduce this concept in **1993**, where plastic bottles were used to produce Synchronia jackets.^[214] Today, they claim that almost 91% of the polyester used in the manufacture of their technical products comes from recycling, reducing the dependence from oil feedstock and the emission of CO₂.^[214] They also started a program in which they recover garments from customers to produce new polyesters, through the ECOCIRCLE™ process of Teijin, a PET manufacturer in Japan. In the “common thread garment recycling program” they did an analysis on the impact of their recycling program in terms of energy of the process and reduction of carbon dioxide emission.^[215] They confirmed how the recycling of the garments strongly impact the overall sustainability of the production, especially in the case of locally collected materials (reduction of emission linked to transport).

5.1.6 The situation in Italy:

Current PET recycling management is controlled for 53% of the total volume of waste by CORIPET, a consortium between recyclers, converters and producers of plastic bottles, with the aim in accomplish a bottle-to-bottle recycling of PET.^[216] CORIPET has two main businesses:

- (1) the management of local collected waste, the sorting and production of PET bales which are then sold to converters and producers to be mechanically recycled and used to produce bottles.
- (2) The installing of eco-compactors all over Italian territory, especially in big point of interests, to incentivize the collection and sorting of food-grade plastics directly by people. In this case, the collection-sorting-baling path would be prevented, with an overall diminishing of carbon dioxide emission.

Today almost 700 eco-compactors are installed (Figure 26), with the plan to reach a total of 5200 in the next few years. Every compactor has the capacity of processing 1500-2000 plastic bottles/day. An optical reader is installed to prevent the collection of undesired products.

The engine of this new business is fueled by the fact that current normative impose the use of 25% rPET in plastic bottles production within 2025, up to 30% in 2030. Moreover, the percentage of plastic bottles recovered after emission on the marked must reach 90% within 2029. All these reasons have contributed to the increase in the interest of recovery and mechanical recycling of PET, with the rPET price in continuous rise.



Figure 26. Plastic bottles eco-compactor installed by CORIPET in Italy.

Coca-Cola HBC recently converted an old production site in Gaglianico (BI) in an industrial plant for mechanical recycling of PET, with an investment of 31M €. ^[217] The plant is 100% fueled by renewable energy and it is able to process 30k tons/year of PET into bottle preforms (Figure 27). The interest of the company in reducing carbon footprint and improving the recycling is notable, with almost 130M € invested in the last 10 years in Italy. Nevertheless, we should consider the fact that the process is viable today only because the recycled bottles used to produce rPET are not 100% composed by already recycled PET, in view of the fact of the continuous degradation after each mechanical recycling process. This aspect applies an “expiring date” to this approach, since the large-scale production of 100% rPET bottles will auto-limit the future production of the same. For this reason, in my opinion, in the next few years the development of chemical recycling of PET, which produces monomers from recycled plastics, will consequentially rise.

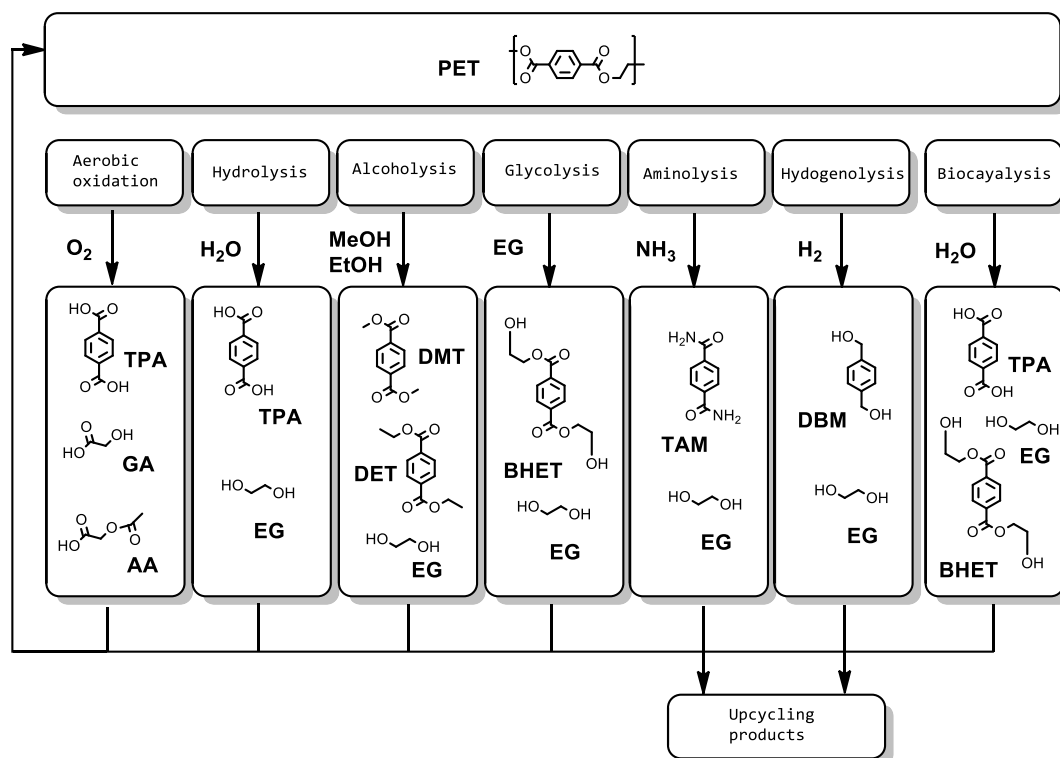


Figure 27. PET bottles preforms, which are then blow molded to produce the desired bottle shape.

5.1.7 Chemical recycling of PET:

The true alternative to mechanical recycling, beside the inefficient energy-recovering incineration of wastes, is the chemical recycling. In the case of PET, chemical recycling (Scheme 55) is the route to obtain pure monomers from recycled waste such as bottles and fibers, especially terephthalic acid (TPA) and its esters together with ethylene glycol (EG). The limitation of chemical recycling, in respect to the mechanical counterpart, is the relatively higher cost and the intrinsic danger in chemical processing. The differences in

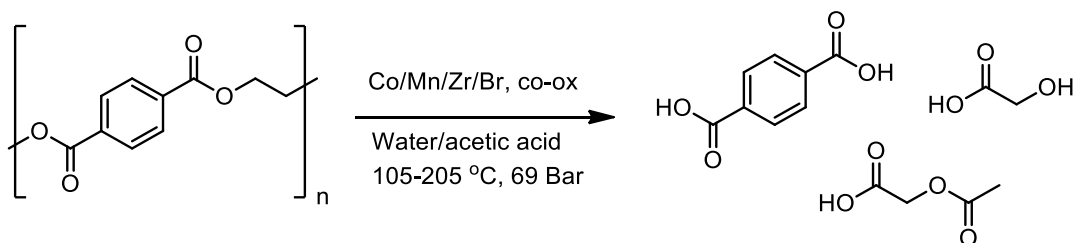
product selectivity in chemical recycling of PET depends essentially by the solvent used for the reaction; the main processes studied today are hydrolysis, glycolysis, alcoholysis, aminolysis and hydrogenolysis. Other approaches involve the aerobic oxidation and biocatalysis.



Scheme 55. Schematic representation of the possible chemical depolymerization of PET and respective products.

5.1.8 Aerobic oxidation:

In presence of a catalyst and heating at high temperatures, PET can be oxidized to TPA and different EG oxidation byproducts. Acetic acid (4-20 wt% solutions) catalyzes this transformation, especially in presence of metals such as Co/Mn/Zr and bromide.^[218] This chemistry is based on the extensive works on autoxidation of hydrocarbons by metal/bromide catalysis.^[219]

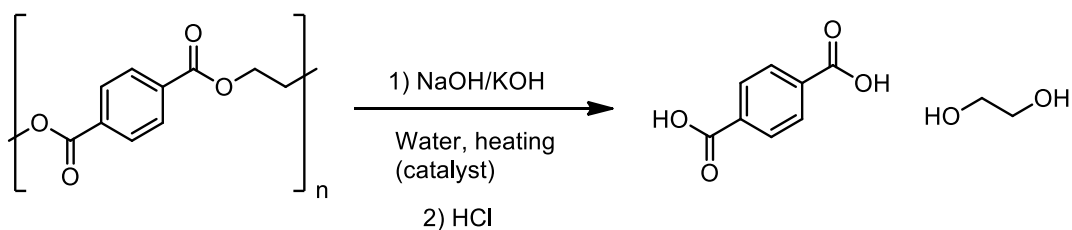


Scheme 56. Typical conditions for aerobic oxidation of PET.

5.1.9 Hydrolysis:

PET hydrolysis can be conducted in either basic, acidic or neutral water solution. The products are TPA and EG. One major drawback of hydrolysis is the fact that large volume of water is required, and stoichiometric quantities of inorganic salts are generated. At industrial scale, it was calculated that to hydrolyze 1 Kg of PET waste, 20-50 L of water would be required, with the generation of 5 Kg of salts.^[220]

Basic hydrolysis requires the use of NaOH or KOH solutions in water, at temperatures around 200 °C and pressure between 15-20 Bar. The product of the reaction is the sodium (or potassium) salt of terephthalic acid, which has to be protonated with an acid, generating large amount of salts (Scheme 57). By LCA analysis, it was noticed that the volume of water is the fundamental aspect in determining if the process is sustainable.^[220] A quaternary ammonium salt can catalyze the reaction by lowering the temperature and pressure needed to obtain good conversion values.^[221] Also microwave heating can be successfully exploited in the alkaline hydrolysis of PET,^[222] in combination with an aforementioned phase transfer reagent.



Scheme 57. Basic hydrolysis of PET.

Acid hydrolysis is usually performed in concentrated (>50 wt%) sulfuric acid at relative low temperature and pressure, to obtain highly pure TPA. The major limitation for industrial development is the corrosion caused by concentrated acid solutions and the difficulty in isolating EG at the end of the reaction. In the case of nitric acid, beside the production of TPA, EG was also oxidized to oxalic acid, a value-added product. Even for acid hydrolysis, ionic liquids can be used both as solvents and catalyst, as reported by Liu and co-workers.^[223]

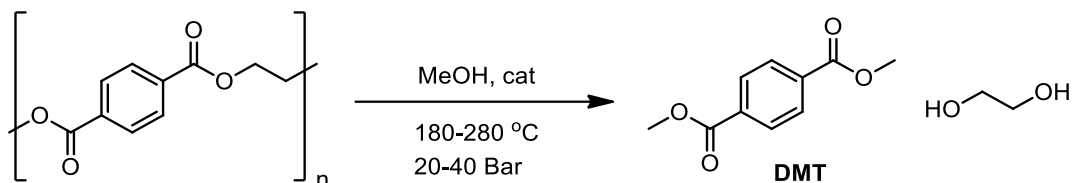
Neutral hydrolysis is naturally ways preferable in respect to basic or acid hydrolysis, as at the end of the reaction no salts are formed, and the products can be recovered by simple filtration. However, this process yields a more impure product and usually high temperatures are required (up to 300 °C) along with high pressures. The use of large volumes of water also renders the isolation of EG somehow more difficult, and it was reported that in this case the addition of xylene as co-solvent helps in decreasing reaction temperature and recovery of EG. Zhang reported that polyoxometallates are active catalyst for neutral hydrolysis at relatively low temperature (145 °C) in only 3 hours reaction time, obtaining up to 93% yield of TPA.^[224] Interestingly, Stanica and Matei found that marine water is a suitable solvent for neutral hydrolysis of PET,^[225] in which you can find sodium, calcium and potassium salts that act as catalysts for this transformation at 200 °C and 40 Bar of pressure.

5.1.10 Alcoholysis:

The reaction of PET with alcohols is a simple transesterification, that leads to the formation of terephthalic acid esters and EG. The most common example is methanolysis, in which methanol is used as solvent and reactant, but other alcohols can be used.

Methanolysis of PET leads to the production of dimethyl terephthalate (DMT, Scheme 58). This monomer has been widely used in the production of PET directly or after hydrolysis to TPA. The limiting factors of this approach have been the difficulty in the separation of products after the reaction, increasing the cost of the procedure, and the need of high temperature and pressure.^[226] The pressure is needed to maintain the methanol in liquid form during the process. The typical catalyst for production of DMT from PET waste are the ones used for transesterification reactions, such as zinc acetate, magnesium acetate, cobalt acetate or metal oxides.

Without the presence of a catalyst, supercritical methanol is required, with temperatures above 300 °C and pressure of 110 Bar, making this process too cost intensive for industrial application. This reaction has been widely studied with different approaches and catalysts such as alkali salts (i.e., K_2CO_3 or $LiOMe$) or using microwave heating as innovative source of heat.



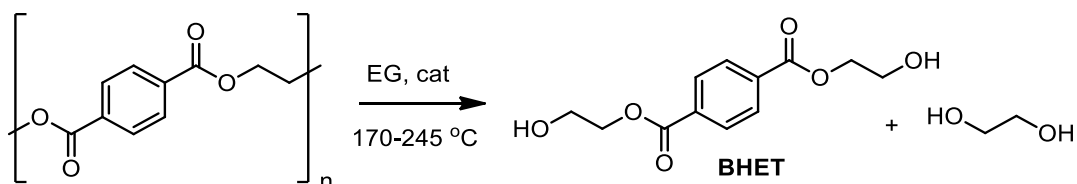
Scheme 58. Typical conditions of methanolysis of PET.

Ethanolysis is similar to methanolysis, using ethanol to produce diethyl terephthalate (DET). This approach can be particularly advantageous in particular areas in which ethanol production is predominant, i.e., Brazil.^[227]

5.1.11 Glycolysis:

This is by far the most studied approach to chemical depolymerization of PET, leading to the development of industrial applications. Glycolysis is the transesterification of PET with excess glycol, usually EG, to generate bis(hydroxyethyl)terephthalate BHET, the monomer resulting from the initial esterification of TPA with EG in the production of PET (Scheme 59). This reaction can occur in absence of a catalyst in the temperature range of 200-240 °C at relatively low pressure, leading to the formation of BHET and oligomers.^[228] Early studies in 1991 by Chen and co-workers,^[229] highlighted that high pressure favors the reaction and excess EG is needed to produce BHET. As in the case of other transesterification reaction of PET, metal acetates have been successfully used as catalysts, since 1989. Manganese acetate showed promising results,^[230] with an almost quantitative yield of BHET in 1.5 hours at 190 °C. Another type of catalyst that is rising in interest in this field are ionic liquids. Iron containing ionic liquid^[231] proved to be particularly active even at lower temperature (140 °C) and other metal containing ILs also proved to be effective in the production of BHET in different conditions.

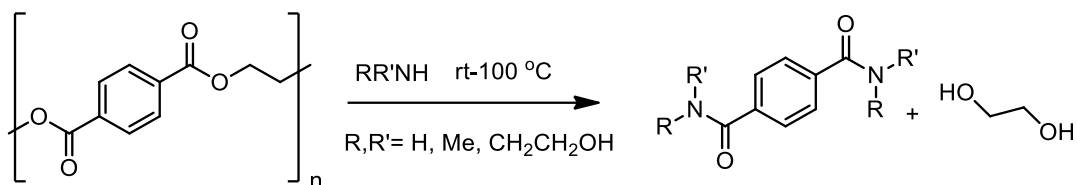
Deep eutectic solvents (DES) have also been studied as suitable media and catalysts for PET glycolysis due to their low cost, low toxicity and simple preparation. Early results in 2015 by Wang show that DES catalyze PET glycolysis at 170 °C in only 30 minutes with a BHET yield of 83%, where the activity is probably due to the presence of a series of hydrogen bonds that activate EG for the reaction. Heterogeneous catalysts have been studied but usually they have been found to be less active in comparison with the homogeneous systems, but completely recyclable for several reaction cycles. Even for glycolysis, microwave heating proved to be highly beneficial, facilitating the reaction and the formation of BHET in shorter reaction times (up to 5 minutes). Other glycols can be employed instead of EG, i.e., propanediol and butanediol, to produce high-value products for PET upcycling.^[232]



Scheme 59. Glycolysis of PET using EG as diol to produce BHET.

5.1.12 Aminolysis:

The depolymerization of PET in presence of amines (or ammonia) leads to the formation of terephthalamides and EG. This reaction is more favored by a thermodynamic point of view, so less harsh conditions can be used, in respect to other depolymerization processes.^[233] The obtained monomers can be used in different upcycling applications, both in the polymer industry or different fields. The reaction is still today not applied in large industrial scale, probably due to the corrosivity of amines at high temperatures. The direct depolymerization of PET with ammonia (ammonolysis) produces a monomer which might find interest as bulk chemical,^[234] but the reaction is still today not optimized and requires quite harsh conditions. Catalysts are usually not used in this transformation, while the presence of a co-solvent proved to be beneficial. The reaction with ethanolamine is widely studied, as the product can be used in the synthesis of polyurethanes.



Scheme 60. Products of aminolysis (or ammonolysis) of PET.

5.1.13 Industrial application of chemical recycling of PET:

A Swiss start-up named **DePoly** applied a process for room temperature basic hydrolysis of PET in presence of titanium dioxide and UV light, previously studied at EPFL in Lausanne.

Circ is a US based company that use high pressure alkaline water in hydrothermal conditions to depolymerize PET fibers, even in presence of other materials.

Gr3n is a Swiss start-up, now called **D3meto**, that opened a pilot plant in Chieti, Italy in 2021 for the microwave assisted hydrolysis of PET in EG as solvent. The plant can treat 60 Kg of plastic stream per hour, and brine derived by the process are used by another company to produce alkali and chlorine. D3meto recently obtained a funding to develop its technology in the middle East.

Loop Industries is a Canadian company that aims at the global market for PET methanolysis. Their technology is based on the use of methanol, a co-solvent and an inorganic alkoxide catalyst, at low temperature and no added pressure.

Eastman Chemical has recently signed a plan to build a 100 ktons/year plant for PET methanolysis in Tennessee, with an investment of 250 million dollars.

JEPLAN, a Japanese start-up, applied the glycolysis of PET in their pilot plant, producing high purity BHET.

Ioniq is a spin-off of Eindhoven University that developed a process for glycolysis catalyzed by immobilized ionic liquids on magnetic nanoparticles. They signed a deal with large producers of consumer-packaged goods companies, with the aim of treating 10 ktons/year of PET waste.

IBM developed a process (**VolCat**) for the recovery of a glycolysis catalyst, which consist in the evaporation of the catalyst and its

recovery by distillation at the end of the process, with a recently announced deal with different commercial partners.

Carbios is a company based in France who launched a demo plant in 2021 for the biocatalytic depolymerization of PET. They raised over 126 million dollars and they currently treat 1.2 kttons/year of waste, aiming at the goal of 40 kttons/year by 2025.

5.1.14 Our approach:

After reading interesting results of metal-containing ionic liquids in the glycolysis of PET waste, we were intrigued by the possibility to apply our metallate catalysts in the same reaction. We performed the synthesis of different metallate species of tetramethylammonium, as it is reported that a small cation favors the interaction with the polyester chain during the reaction. We initially evaluated the glycolysis of PET in ethylene glycol by conventional thermal heating, using ferrates and other metal species. The reaction proved to be much more effective when we switched to microwave heating, with a striking shortening of reaction time. After successful development of microwave assisted glycolysis with EG, we investigated the reaction with other glycols to obtain value added products. We then moved to methanolysis, using metallate catalysts, producing pure DMT in good yield (up to 80%) in just 3 hours of reaction time in a stainless-steel autoclave. A deep investigation of the reaction conditions and catalyst choice was performed. We also investigated the efficiency of basic and neutral hydrolysis in our microwave assisted approach. Finally, we managed to perform direct ammonolysis of PET waste using a peculiar procedure not applied before to the best of our knowledge. All the results are discussed below and in the experimental section.

5.2 RESULTS AND DISCUSSION:

The synthesis of different tetramethylammonium metallates was performed in the same procedure of other tetrabutylammonium salts, and it is described in the experimental section.

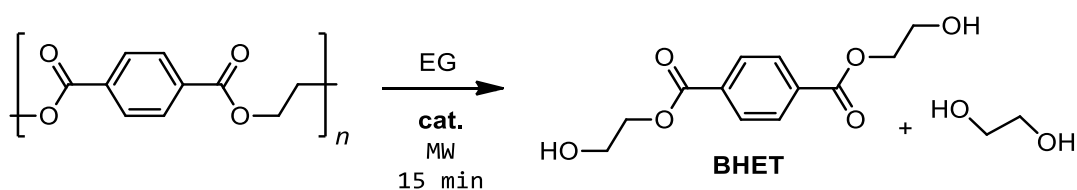
5.2.1 Glycolysis:

Catalytic glycolysis of PET was performed by conventional heating in sealed screw cap glass vials, using an aluminum heating block. Commercial grade clear rPET (125 mg), obtained from grinding of PET bottles, and ethylene glycol (EG, 0.8 mL) were placed in the glass vials equipped with a magnetic stirrer and heated at 170 °C for 16

hours. At the end of the reaction, the resulting mixture was added to hot water and filtered to eliminate residual unreacted PET and insoluble oligomers. The filtrate was concentrated in vacuum and cooled at 4 °C overnight. BHET is formed as white needle-like crystals which are filtered, dried in vacuum and weighted to calculate the yield of the reaction. Conversion of PET was calculated by weighting eventual residues in the first filtration, compared to the starting PET.

The preliminary evaluation between simple metal halides and quaternary ammonium metalates, in these particular conditions using 5 mol% loading, shows comparable results in terms of conversion between the two kinds of catalyst (see experimental section). In the case of zincate catalyst, the yield of BHET was worse than simple zinc chloride. Interestingly in the case of iron, the addition of the quaternary ammonium salt was highly beneficial in terms of BHET yield. In contrast with the fact that smaller cations should ideally be more active during the transformation, in this case the best results were obtained with tetrabutylammonium cation (Table 28, entries 3-6).

Table 28. Comparison in the glycolysis of PET with different iron compounds.



Entry	Catalyst	Conversion %	Yield BHET %
1	-	0	0
2	TMACl	0	0
3	FeCl ₃ ·6H ₂ O	56.1	9.0
4	[TMA][FeCl ₄]	89.0	33.8
5	[TBA][FeCl ₄]	86.6	51.1
6	[Ph ₄ P][FeCl ₄]	91.9	47.3

Reaction performed in MW glass tubes, temperature= 170 °C, catalyst loading= 5 mol%, reaction time= 15min.

In all cases, with the most active catalysts, the reaction proceeded to reach an equilibrium between monomer and oligomers and the results after 16 hours are basically the same after 24 hours (Table 29).

Table 29. Influence of reaction time

Entry	Catalyst	Time (h)	Conversion %	Yield BHET %
1	[TMA][FeCl ₄]	3	45.0	5.4
2	[TMA][FeCl ₄]	16	89.0	33.8
3	[TMA][FeCl ₄]	24	93.7	29.6
4	[TMA] ₂ [MnCl ₄]	3	11.1	0
5	[TMA] ₂ [MnCl ₄]	16	78.5	59.6
6	[TMA] ₂ [MnCl ₄]	24	94.3	57.1
7	[TMA] ₂ [CoCl ₄]	3	16.1	0
8	[TMA] ₂ [CoCl ₄]	16	95.2	48.8
9	[TMA] ₂ [CoCl ₄]	24	93.0	50.1

Reaction performed in screw cap glass tubes, temperature= 170 °C, catalyst loading= 5 mol%.

These results were not enough satisfactory and for this reason we decided to see, based on published reports, if microwave heating would influence this equilibrium to reach better yields of BHET.

Indeed, microwave heating allowed us to obtain full conversion of PET with good yields for BHET in just 15 minutes of reaction.

Table 30. Results obtained with ferrate catalysts and microwave heating.

Entry	Catalyst	Conversion %	Yield BHET %
1	[TMA][FeCl ₄]	100	54.1
2	[TBA][FeCl ₄]	100	27.8
3	[PPh ₄][FeCl ₄]	100	47.2

Reaction performed in MW glass tubes, temperature= 170 °C, catalyst loading= 5 mol%, reaction time= 15min.

In this case, tetramethylammonium cation resulted in the best activity, probably due to a better dielectric heating of the reaction (Table 30, entry 1).

With this catalyst we optimized the reaction time, with a complete conversion after 5 minutes and maximum yield at 30 minutes.

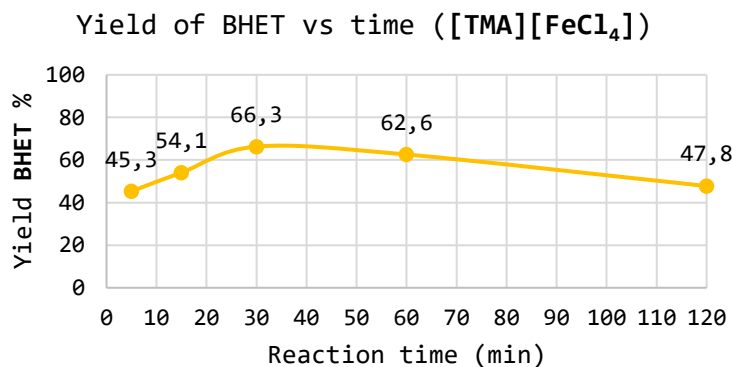


Figure 28. Correlation between reaction time and yield of BHET using [TMA][FeCl₄] as catalyst, with microwave heating.

We evaluated the influence of temperature on the most active catalysts, and we noticed how they behave differently from each other at different temperature. In any case, iron poses the best compromise between activity and sustainability, both from economic and environmental point of view.

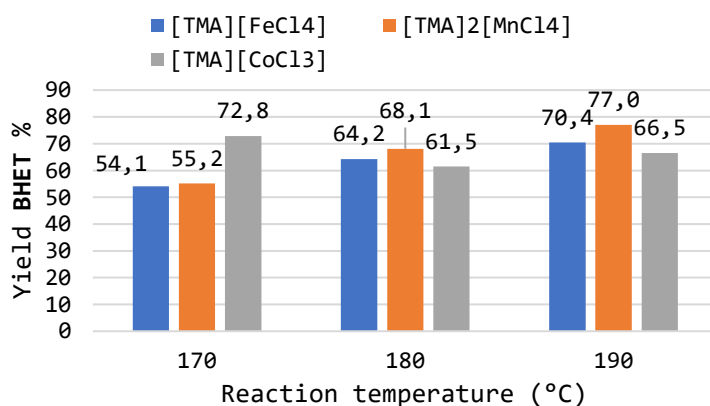


Figure 29. Correlation between reaction temperature and yield of BHET using different catalysts, with microwave heating for 15 minutes.

In the same experimental conditions, we performed the reaction using 1,3-propanediol and 1,4-butanediol as different glycol source, to obtain value added products. The reaction with 1,4-butanediol was unsuccessful due to probable oxidation of the diol, while the reaction with 1,3-propanediol afforded bis(3-hydroxypropyl) terephthalate (BHPT) in good yields, especially in the case of iron catalysts (see experimental section).

5.2.2 Methanolysis:

Catalytic methanolysis of PET was initially performed by conventional heating in sealed glass pressure tubes and later in stainless-steel autoclaves, using an aluminum heating block in both cases. Commercial clear rPET and methanol were placed in the selected reactor vessel with a magnetic stirrer and heated at 130-170 °C for 3-16 hours. Interestingly, at the end of the reaction the monomeric product dimethyl terephthalate (DMT) can be recovered by filtration as crystals by simply cooling the vessel. The so obtained product can be further recrystallized by hot ethyl acetate. For the reaction at 130 °C, after 16 hours the collected amount of DMT was not satisfactory, beside in the case of iron and cobalt catalysts. Especially in the case of iron, good yield of DMT was obtained even after 8 hours (Table 31, entry 7). Zinc and manganese catalysts resulted only in very poor results (Table 31, entries 4-6).

Table 31. Optimization of methanolysis, reaction performed at 130 °C for 16 hours.

Entry	Catalyst	Conversion %	Yield DMT %
1	[TMA][FeCl ₄]	100	64.1
2	[TMA] ₂ [CoCl ₄]	100	72.4
3	[TMA][CoCl ₃]	55.0	17.5
4	[TMA] ₂ [MnCl ₄]	4.6	0
5	[TMA][MnCl ₃]	36.9	22.2
6	[TMA][ZnCl ₄]	9.7	0
7 ^[b]	[TMA][FeCl ₄]	72.4	56.6
8 ^[b]	[TMA] ₂ [CoCl ₄]	28.3	18.1

Reaction performed in glass pressure tubes, 250 mg rPET, 4 mL MeOH, catalyst loading= 5 mol%, reaction time= 16h, T= 130°C. [b] reaction time= 8h.

By increasing the temperature to 170 °C, using a stainless-steel autoclave, we were able to obtain interesting results after just 3 hours of reaction time. Even in this case, iron and cobalt resulted in the highest activity (Table 32, entries 9-10). The cost of cobalt chloride, in comparison to iron chloride, is by far higher, and its use as catalyst poses serious problems both from an environmental and economical point of view. The only benefit in using cobalt catalyst is the higher purity of the material obtained, comparable with commercially available DMT, without the presence of any leaked metal (confirmed by ICP-OES see experimental section). In this view, the use of iron should be preferred, with the aim of optimizing the conditions and purity of the obtained DMT.

Table 32. Optimization of methanolysis, reaction performed at 170 °C for 3 hours.

Entry	Catalyst	Conversion %	Yield DMT %
9	[TMA][FeCl ₄]	100	70.4
10	[TMA] ₂ [CoCl ₄]	100	69.8
11	[TMA][CoCl ₃]	74.3	64.5
12	[TMA] ₂ [MnCl ₄]	74.3	49.8
13	[TMA][MnCl ₃]	58.5	49.9
14	[TMA][ZnCl ₄]	12.5	0
15 ^[b]	[TMA][FeCl ₄]	99	44.7
16 ^[b]	[TMA] ₂ [CoCl ₄]	35.8	30.6

Reaction performed in autoclave, 1 g rPET, 16 mL MeOH, catalyst loading= 5 mol%, reaction time= 3h, T= 170°C. [b] reaction time= 1.5h

5.2.3 Ammonolysis:

Direct ammonolysis of PET with ammonia is a sluggish process that was not successfully developed and studied up to now. We decided to explore this transformation by exploiting the reactivity of ammonium carbamate in ethylene glycol. Ammonium carbamate is the intermediate compound produced during industrial urea synthesis, on multi million tons scale. This compound undergoes thermal degradation to its fundamental components, ammonia and carbon dioxide. We decided to use ammonium carbamate in EG to avoid the presence of corrosive

aqueous ammonia and exploiting the rapid initial glycolysis of PET, which should speed up the reaction. Ammonium carbamate was synthesized by reaction of liquid ammonia and dry ice (see experimental section).

Catalytic ammonolysis of PET was performed by conventional heating in glass pressure tubes, using an aluminum heating block. Clear rPET (125 mg) and ethylene glycol (EG) as solvent (4 mL) were placed in the reaction vessel with a magnetic stirrer. Ammonium carbamate was added, and the reaction was heated at the desired temperature for a certain amount of time. The monomeric product terephthalamide (TAM) can be recovered as white powder directly at the end of the reaction, after washing with water and drying in vacuum.

In 16 hours at 120 °C we obtained 72% yield of pure TAM, without any catalyst. The reaction needs the presence of a large excess of ammonium carbamate but in principle, at the end of the reaction its component can be recovered and recycled to produce again ammonium carbamate. Other ammonia surrogates such as ammonium bicarbonate were not successful.

A tandem process of glycolysis/ammonolysis can be performed and was tested by reaction of BHET in aqueous 14 wt% ammonia solution, at room temperature for 16 hours. The reaction produced quantitative yield of TAM. The same approach can be applied in the ammonolysis of DMT, but in the same reaction conditions we obtained only 50% of yield of TAM.

5.3 CONCLUSIONS:

We developed an “holistic” approach at the chemical depolymerization of PET waste by means of ammonium metallate catalysts, especially by exploiting of microwave heating. The overall sustainability of the process is satisfied when ammonium ferrate is used as catalyst. Different chemical depolymerization routes were explored, with the successful production of BHET (glycolysis) and DMT (methanolysis). Other uncommon routes were also explored, with the production of BHPT (by glycolysis with 1,3-propandiol) and TAM (with ammonium carbamate as ammonia surrogate). Basic hydrolysis was also preliminary investigated successfully by microwave heating. The activity of the catalysts, together with the low energy requirement of microwave heating, can pave the way to a future industrial application of this procedures for the recycling of PET waste.

Our project ELEVATE on the chemical depolymerization of PET was awarded with fundings from the Seed4Innovation initiative 2022 by UNIMI and Fondazione Unimi, as one the best 8 among more than other 90 projects.

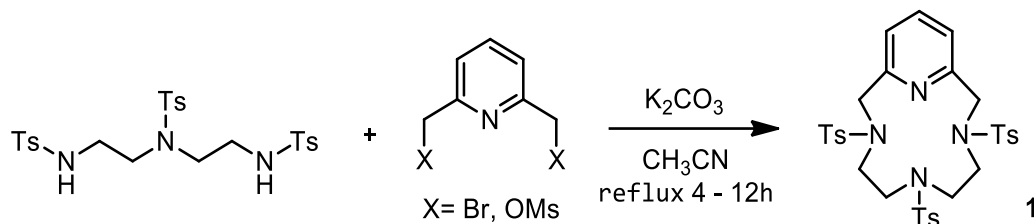
6 EXPERIMENTAL SECTION

6.1 GENERAL EXPERIMENTAL DETAILS:

All the reactions that involved the use of reagents sensitive to oxygen or to hydrolysis were carried out under an inert atmosphere. The glassware was previously dried in an oven at 110 °C and was set with cycles of vacuum and nitrogen. All chemicals and solvents were commercially available and used as received except where specified. ¹H NMR analyses were performed with 300 or 400 MHz spectrometers at room temperature. The coupling constants (J) are expressed in hertz (Hz), and the chemical shifts (δ) in ppm. Low resolution MS spectra were recorded with instruments equipped with electron ionization (EI), electrospray ionization (ESI)/ion trap (using a syringe pump device to directly inject sample solutions), or fast atom bombardment (FAB) sources. High resolution MS spectra were acquired on a Q-ToF SYNAPT G2-Si HDMS 8K instrument (Waters) equipped with a Zspray™ ESI source (Waters). Synthesis of the ligands and iron complexes is described in the experimental section. GC experiments were conducted on a Shimadzu GC-2010 Pro instrument using an SBL™-5ms fused silica capillary column (10 m x 0.1 mm x 0.1 μm film thickness, SigmaAldrich - Supelco). X-ray data collection for the crystal structure determination was carried out by using Bruker Smart APEX II CCD diffractometer with the Mo K radiation (λ=0.71073) at 296 K.

6.2 SYNTHESIS OF LIGANDS:

Synthesis of tosylated pyclen (1):



2,6-bis(methanesulfonyloximethyl)pyridine (5.3 mmol) in CH₃CN (40 mL) was added dropwise to a hot suspension of K₂CO₃ (15 mmol) and N,N',N''-tritosyldiethylenetriamine (5.3 mmol) in CH₃CN (160 mL). The reaction was allowed to react to reflux for 4-12 hours. The solvent was then removed in vacuum and water was added (50.0 mL). The mixture was washed with DCM (3 x 50.0 mL). The organic phases were concentrated in vacuum leading to the pure product as a white powder.

Yield: 99%

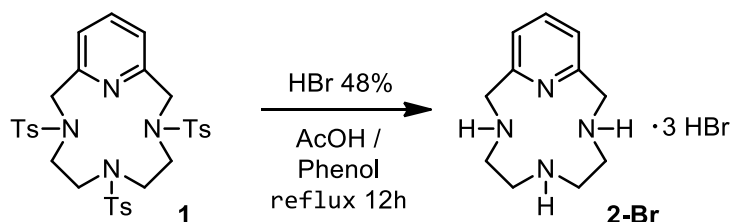
Additional information: 2,6-bis(bromomethyl)pyridine can be also used with similar results. The quality of potassium carbonate is important in terms of yield of the reaction: hydration of the base leads to the formation of sesquicarbonate that is not efficient for this transformation. If the product is not pure and contains unreacted triamine, recrystallisation with warm ethyl acetate will provide pure product.

¹H NMR (300 MHz; CDCl₃; T = 300 K)

δ 7.80 - 7.69 (m, 7H), 7.66 (d, J = 8.2 Hz, 2H), 7.44 (d, J = 7.7 Hz, 2H), 7.36 (d, J = 8.1 Hz, 4H), 7.29 (d, J = 7.9 Hz, 2H), 4.30 (bs, 4H), 3.33 (t, J = 7.5 Hz, 4H), 3.22 - 3.07 (m, 2H), 2.77 (bs, 2H), 2.46 (s, 6H), 2.42 (s, 3H).

Data are in agreement with the literature.^[235]

Deprotection of (1) with hydrogen bromide:



Ligand **1** (1.85 mmol) and phenol (16.0 mmol) were dissolved in acetic acid (5.0 mL). HBr 48% (20.0 mL) was added carefully and the mixture was refluxed for 7-12 hours. The solvent was then evaporated, and the red sticky crude was cooled in ice bath and treated with ice-cold acetone, leading to the formation of **2-Br** as a heavy white precipitate. The product was filtered, washed with cold acetone and dried in vacuum.

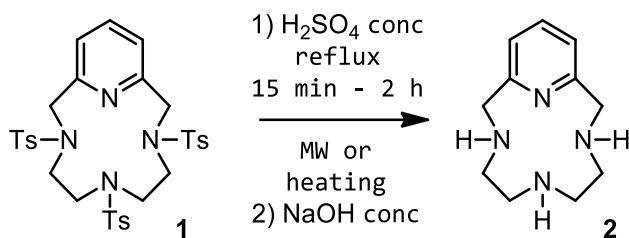
Yield: 88%

Additional information: upon heating, the mixture will develop copious amount of corrosive fumes: work under a fume hood and avoid the contact with corrodible parts.

$^1\text{H NMR}$ (300 MHz; D_2O ; $T = 300 \text{ K}$)

δ 8.06 (t, $J = 7.8 \text{ Hz}$, 1H), 7.58 (d, $J = 7.8 \text{ Hz}$, 2H), 4.70 (s, 4H), 3.40 (br, 4H), 3.24 (br, 4H)

Data are in agreement with the literature.^[47]

Deprotection of (1) with sulfuric acid:

Ligand **1** (17 mmol) was dissolved in concentrated sulfuric acid (15.0 mL). The mixture was heated to 250°C for 1-2h. A change in color is observed upon heating, leading to a dark brown mixture. The latter was cooled and diluted with water (25 mL) then extracted with DCM (2 x 25mL). To the aqueous phase, NaOH 30% was added until pH > 14. This solution was extracted with DCM (5 x 25 mL) and the organic phase was dried with NaSO_4 and evaporated in vacuum. The product was obtained as a yellowish waxy solid.

Yield: 60-80%

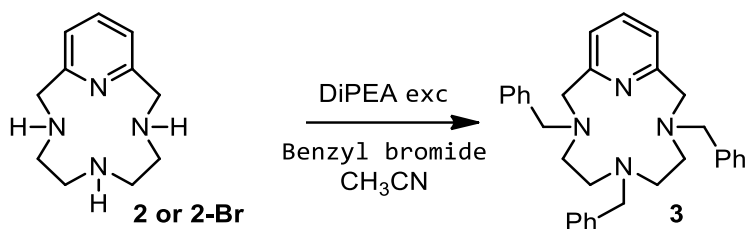
Additional information: The same reaction can be performed using MW as heating source. Ligand **1** is dissolved in concentrated sulfuric acid (2.5 mL every 500 mg of **1**) in a microwave vial. The mixture is heated at 120°C for 20 minutes and then placed in an ice bath. Diethyl ether is slowly added, and a precipitate is formed and filtered. The product is dissolved in the minimum amount of water and solid NaOH is added until pH is >14. After 3 extractions with DCM and evaporation of the solvent, ligand **2** is obtained as light brown solid, usually in higher yields and purity compared to the traditional heating method.

^1H NMR (300 MHz; CDCl_3 ; T = 300 K)

δ 7.51 (t, $J = 7.6$ Hz), 6.99 (d, $J = 7.6$ Hz), 3.96 (s, 4H), 3.23 (bs, 3H), 2.83 – 2.64 (m, 4H), 2.26 (bs, 4H).

Data are in agreement with the literature.^[235]

Synthesis of ligand benzylated Pyclyen ligand (3):



Ligand **2** or **2-Br** (1.251 mmol) was suspended in CH_3CN (30.0 mL), then DIPEA (1.5 mL) and benzyl bromide (4.251 mmol) were added. The mixture was left to react at room temperature overnight. The solvent was then evaporated, the crude was dissolved in CH_2Cl_2 (20 mL) and washed with brine (3 x 15 mL). The organic phases were treated with Na_2SO_4 , filtered and dried in vacuum. The crude was purified by silica gel flash column chromatography using DCM/MeOH (gradient from 98:2 to 9:1) as eluent.

Yield: 72%

^1H NMR (400 MHz; CDCl_3 ; T = 300 K)

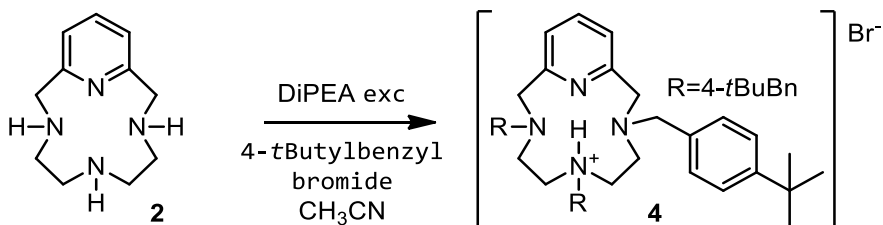
δ 7.61 (t, J = 7.6 Hz, 1H), 7.36 – 7.27 (m, 10H), 7.19 – 7.10 (m, 5H), 7.08 (d, J = 7.6 Hz, 2H), 3.79 (s, 4H), 3.74 (s, 4H), 3.40 (s, 2H), 2.70 (dd, J = 9.1, 6.0 Hz, 4H), 2.46 (dd, J = 9.1, 6.1 Hz, 4H).

^{13}C NMR (101 MHz, D_2O)

δ 157.9, 139.7, 137.1, 133.4, 129.7 – 126.3, 122.6, 119.8, 60.1, 59.7, 49.4, 48.5.

Data are in agreement with the literature.^[47]

Synthesis of protonated functionalized ligand (4):



Ligand **2** (2.55 mmol, 525 mg) and 4-^tbutylbenzyl bromide (8.4 mmol, 1.5 mL) were stirred for 5h in dry CH₃CN (15.0 mL) in presence of DiPEA (1.5 mL). After this time, the solvent was evaporated, and cold acetone was added to the resulting oil. A white precipitate of ligand **4** is formed (347 mg). A second crop of the ligand is obtained by leaving the acetone solution at -20 °C (401 mg).

Yield: 41%

Additional information: 4-^tbutylbenzyl bromide is highly irritating and lacrimator, work under a fume hood. The product can also be obtained as pale pink powder that can be purified by washing with cold acetone.

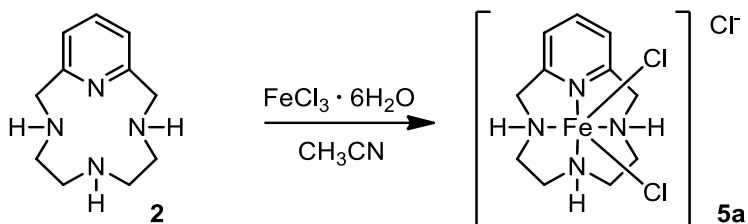
¹H NMR (400 MHz, CDCl₃)

δ 7.50 (t, *J* = 7.6 Hz, 1H), 7.35-7.22 (dd, 8H), 7.11 (dd, 4H), 6.89 (d, *J* = 7.6 Hz, 2H), 4.04 (s, 2H), 3.97-3.83 (bd, 4H), 3.72 (s, 4H), 3.65 (bs, 4H), 3.16-2.99 (bd, 4H), 1.26 (s, 18H), 1.22 (s, 9H).

Data are in agreement with the literature.^[236]

6.3 SYNTHESIS OF IRON COMPLEXES:

Synthesis of complex (5a):^[237]



To a stirring solution of ligand 2 (0.48 mmol) in acetonitrile (10 mL) at 40°C, iron(III) chloride hexahydrate was added (0.48 mmol) and the reaction mixture was left stirring for 4 h. An immediate colour change was observed and the precipitation of a solid was noticed. Complexes 5a was collected by filtration and washed with diethyl ether, then dried under vacuum to obtain a yellow powder.

Yield: 66%

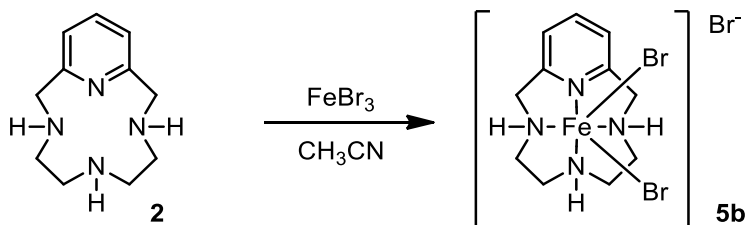
MS (ESI) m/z (%) = calculated for C₁₁H₁₈Cl₃FeN₄: 385.01, found: 332.06 (100) [M⁺ -Cl]

Elem. An. C₁₁H₂₀Cl₃FeN₄O Calculated: C 34.18, H 5.22, N 14.50; found: C 34.72, H 4.90, N 14.20

μ_{eff} (solid state): 4.67

μ_{eff} (DMSO-d⁶solution): 5.37

Synthesis of complex (5b):^[237]



The synthesis was performed as for complex **5a**. The product was precipitated and filtered as a red powder.

Yield: 61%

MS (ESI) m/z (%) = calculated for $\text{C}_{11}\text{H}_{18}\text{Br}_3\text{FeN}_4$: 500.84, found: 421,95 (40) $[\text{M}^+-\text{Br}]$

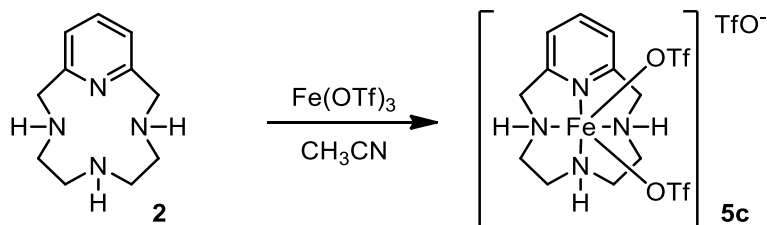
Elem. An. $\text{C}_{11}\text{H}_{18}\text{Br}_3\text{FeN}_4$ Calculated: C 26.33, H 3.62, N 11.16; found: C 26.38, H 3.66, N 11.30

μ_{eff} (solid state): 5.42

μ_{eff} (DMSO- d^6 solution): 5.36

Structure of complex **5b** was obtained by SCXRD. The crystal suitable for the experiment was obtained by slow evaporation of an aqueous solution. The structure and the experimental description are collected in the specific section.

Synthesis of complex (5c):^[237]



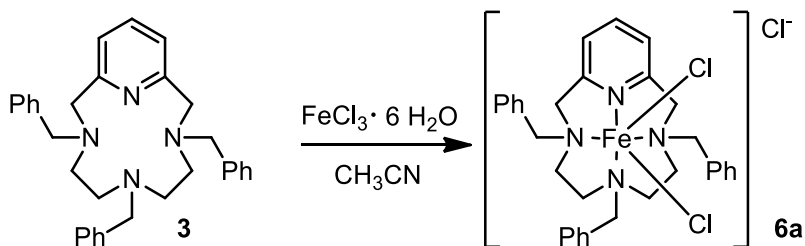
The synthesis was performed as for complex **5a** and **5b**. The product was obtained as brown powder after evaporation of the solvent and several washing with hexane.

Yield: 84%

MS (ESI) m/z (%) = calculated for $\text{C}_{14}\text{H}_{18}\text{F}_9\text{FeN}_4\text{O}_9\text{S}_3$: 708.94, found: 411 (100), $[\text{M}^+ - 2\text{OTf}]$

Elem. An. $\text{C}_{14}\text{H}_{18}\text{F}_9\text{FeN}_4\text{O}_9\text{S}_3$ Calculated: C 23.71, H 2.56, N 7.90; found: C 24.17, H 2.95, N 7.52

μ_{eff} (DMSO-d^6 solution): 4.84

Synthesis of complex (6a):

A solution of $\text{FeCl}_3 \cdot 6\text{H}_2\text{O}$ (0.36 mmol) in acetonitrile (4.0 mL) was added dropwise to a solution of ligand 3 (0.36 mmol) in acetonitrile (4.0 mL). The mixture was left to react for 1 hour at room where a change of color from orange to dark brown was noticed. The solvent was evaporated in vacuum and the crude was treated with Et_2O (5 mL) and left under stirring at room temperature for 30 minutes. The product obtained as dark brown solid was then filtered and dried in vacuum.

Yield: 94%

MS (FAB) m/z (%) = calculated for $\text{C}_{32}\text{H}_{40}\text{Cl}_3\text{FeN}_4\text{O}_2$: 567 (100), found: 569 (62) [$\text{M}^+ - 2\text{Cl}$]

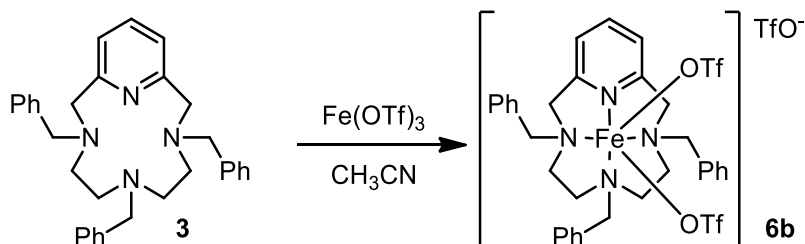
Elem. An. $\text{C}_{32}\text{H}_{40}\text{Cl}_3\text{FeN}_4\text{O}_2$ Calculated: C 56.95; H 5.37; N 8.30; found: C 56.83; H 5.73; N 8.08

μ_{eff} (solid state): 3.73 μB

EPR (9.55 GHz; 300 K) G 1560 ($g = 4.38$), 3312 (br, $g = 2.05$, $\Delta\text{Hpp} = 300$ Gauss);

EPR (9.55 GHz; 77 K) G 1575 ($g = 4.32$, $\Delta\text{Hpp} = 370$ Gauss), 3215 ($g_{\perp} = 2.120$), 3850 ($g_{\parallel} = 1.77$).

Data are in agreement with the literature.^[47]

Synthesis of complex (6b):

Complex **6b** was prepared with the same procedure for complex **6a** and was isolated as a dark brown powder.

Yield: 93%

MS (FAB)+ m/z (%) 830 (100), 831 (37) [M+ -OTf]

MS (ESI-) m/z (%) 148.99 (100) [M-] (CF₃O₃S -)

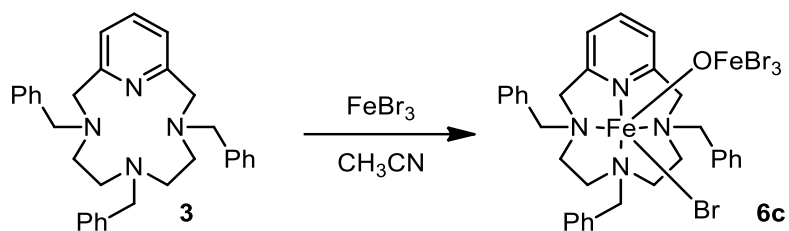
Elem. An. C₃₅H₃₆F₉FeN₄O₉S₃ Calcd: C 42,91; H 3,70; N 5,72; found: C 42,34; H 4,04; N 6,08

μ_{eff} 3.88

EPR (9.55 GHz; 300 K) G 880 (br, g = 7.75), 1575 (g = 4.32, ΔH_{pp} = 170 Gauss), 3290 (g= 2.07);

EPR (9.55 GHz; 77 K) G 880 (br, g = 7.75), 1575 (g = 4.32, ΔH_{pp} = 85 Gauss), 3290 (g= 2.07).

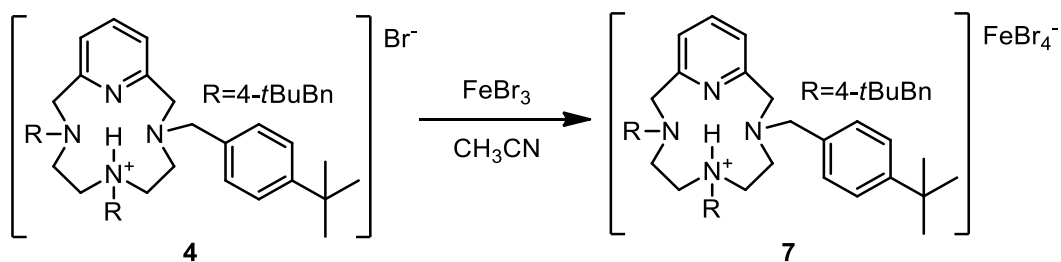
Data are in agreement with the literature.^[47]

Synthesis of di-nuclear complex (6c):^[238]

Complex **6c** was prepared with the same procedure of complex **6a** and **6b** but using an excess of iron(III) bromide. The species was isolated as a dark red powder. The structure was assigned with the help of Raman spectroscopy (see Raman section for further details).

Raman: 861 cm^{-1} (ν_{as} Fe-O-Fe), 378 cm^{-1} (ν_{s} Fe-O-Fe), 212 cm^{-1} (ν Fe-Br), 158 cm^{-1} (δ Fe-O-Fe).

Synthesis of complex (7):



To a stirring solution of ligand **4** (0.17 mmol, 123 mg) in acetonitrile (5.0 mL) at room temperature, a solution of iron(III) bromide (0.17 mmol, 50 mg) in acetonitrile (3.0 mL) was slowly added and the reaction mixture was left stirring for 1 h. The solvent was evaporated under vacuum and the residue was washed several times with *n*-hexane to yield a bright red powder.

Yield: 81%

MS (ESI+) $m/z(\%) =$ calculated for $\text{C}_{44}\text{H}_{61}\text{N}_4$ 645.48, found: 645.51 (100%, M^+)

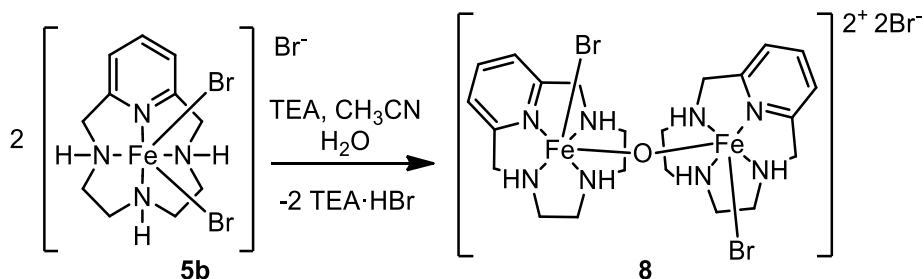
MS (ESI-) $m/z(\%) =$ calculated for FeBr_4 375.60, found: 375,80(100%, FeBr_4^-).

Elem. An. $\text{C}_{44}\text{H}_{61}\text{Br}_4\text{FeN}_4$ Calculated: C, 51.74; H, 6.02; N, 5.49; found: C, 51.41; H, 6.01; N, 5.42

Raman: 294 cm^{-1} (ν Fe-Br), 203 cm^{-1} (ν Fe-Br), 90 cm^{-1} (δ Br-Fe-Br).

Data are in agreement with the literature.^[236,238]

Synthesis of dimeric complex (8):^[238]



Complex **5b** (0.035 mmol) was dissolved in 4 mL of acetonitrile and 10 μL (0.07 mmol) of triethylamine were added. The solution was stirred for 1h. XRD quality brown block crystals were collected by slow diffusion of diethyl ether in the mixture.

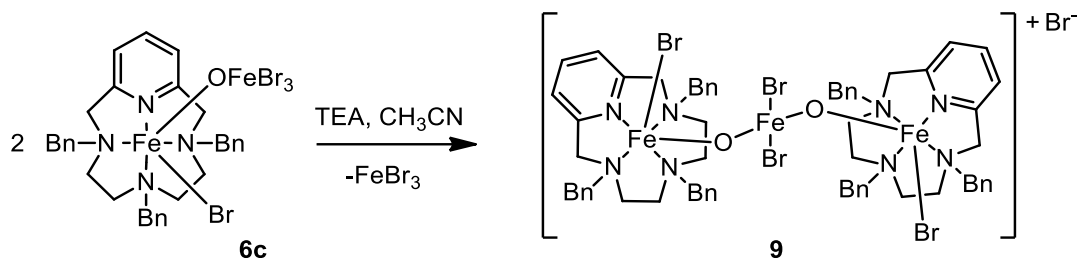
Additional information: the product can also be obtained in the same procedure using a mixture of water/methanol as solvent, where black needle-like crystals are obtained by slow evaporation.

MS (ESI+) in methanol (L stands for ligand): 572.18 ($\text{LFe}(\text{OMe})\text{OFeL}$), 540.51 (LFeOFeL), 320.24 ($\text{LFe}(\text{OMe})_2\text{-2H}$), 260.28 (LFe-2H).

Elem. An. Calculated for $\text{C}_{22}\text{H}_{36}\text{Br}_4\text{Fe}_2\text{N}_8\text{O}$ C, 30.78; H, 4.22; N, 13.03; found: C, 30.05; H, 4.04; N, 12.78.

Raman: 451 cm^{-1} (ν Fe-N), 409 cm^{-1} (ν_s Fe-O-Fe).

Synthesis of tri-nuclear complex (9):^[238]



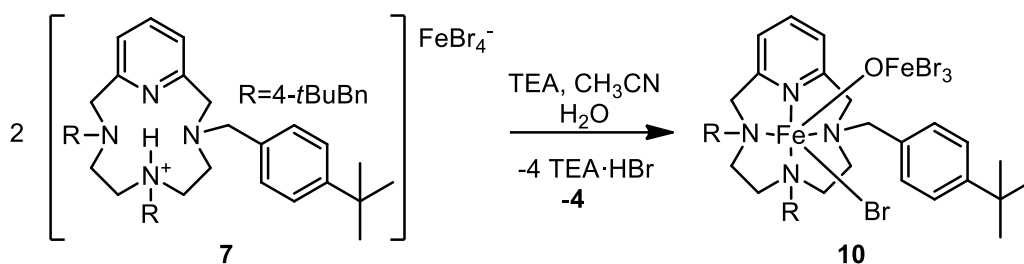
Complex **6c** (0.026 mmol) was dissolved in acetonitrile (4 mL) and 10 μ L (0.07 mmol) of triethylamine were added. The solution was stirred for 1h. XRD quality red prismatic crystals were collected by slow diffusion of diethyl ether in the mixture.

MS (ESI +) in methanol (L stands for ligand): 594.36 (LFe(OMe)₂), 563.57 (LFeOMe).

Elem. An. The quantity of product isolated was not enough to perform an elemental analysis.

Raman: 873 cm⁻¹ (ν_{as} Fe-O-Fe), 367 cm⁻¹ (ν_s Fe-O-Fe), 217 cm⁻¹ (ν Fe-Br).

Synthesis of di-nuclear complex (10):^[238]



Complex 7 (0.035 mmol) was dissolved in acetonitrile (4 mL) and 10 μL (0.07 mmol) of triethylamine were added. The solution was stirred for 1h. XRD quality dark red prismatic crystals were collected by slow diffusion of diethyl ether in the mixture.

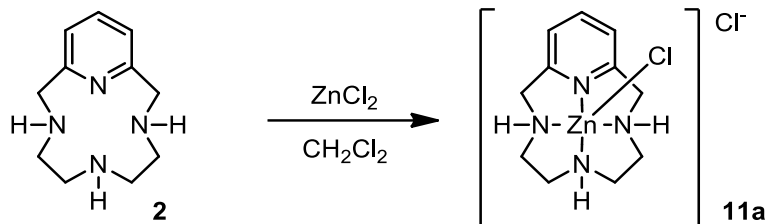
MS (ESI +) in methanol (L stands for ligand): 810.35 (LFeBrOMe), 762.67 (LFe(OMe)₂), 731,81 (LFe(OMe)), 645,97 (LH⁺)

Elem. An. Calculated for $\text{C}_{44}\text{H}_{60}\text{Br}_4\text{Fe}_2\text{N}_4\text{O}$ C, 48.38; H, 5.54; N, 5.13; found: C, 48.81; H, 6.04; N, 5.24

Raman: 849 cm^{-1} (ν_{as} Fe-O-Fe), 414 cm^{-1} (ν_{s} Fe-O-Fe), 217 cm^{-1} (ν Fe-Br), 154 cm^{-1} (δ Fe-O-Fe), 92 cm^{-1} (δ Br-Fe-Br).

6.4 SYNTHESIS OF ZINC COMPLEXES:

Synthesis of complex (11a):^[135]



Zinc(II) chloride (0.65 mmol) was slowly added to a solution of ligand 2 (0.75 mmol) in DCM (20.0 mL). The mixture was stirred room temperature for 1.5 hours. The reaction mixture was then filtered and washed with DCM (5.0 mL x 2), with cold MeOH (few drops), and again with DCM (5.0 mL). The product was recovered as a white powder and dried under vacuum.

Yield: 80%

¹H NMR (300 MHz, d₆-DMSO)

δ 8.11 (t, J = 7.7 Hz, 1H), 7.52 (d, J = 7.7 Hz, 2H), 4.86 (m, 1H), 4.68 (m, 2H), 4.37 (dd, J = 17.6, 6.7 Hz, 2H), 3.90 (d, J = 17.6 Hz, 2H), 2.90 (m, 2H), 2.74 (m, 2H), 2.38 (m, 2H), 2.18 (m, 2H)

¹³C NMR (75 MHz, d₆-DMSO)

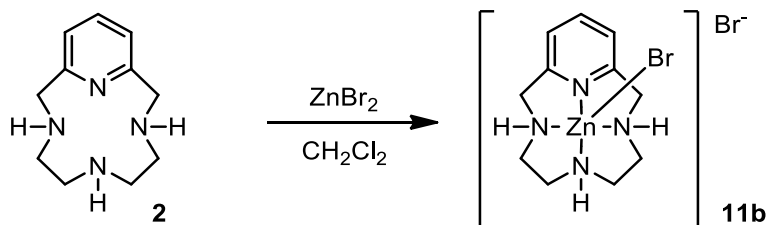
δ 155.6, 141.7, 122.4, 51.6, 47.7, 46.2

MS (ESI +) m/z (%) = calculated for C₁₁H₁₈Cl₂N₄Zn: 340.02, found: 305 (100) [M⁺ -1Cl]

Elem. An. C₁₁H₁₈Cl₂N₄Zn·2H₂O Calculated: C 34.90, H 5.86, N 14.80; found: C 34.60, H 5.59, N 14.49

Single crystals suitable for XRD were obtained by slow evaporation of a water solution of the complex.

Synthesis of complex (11b):^[135]



Complex **11b** was prepared with the same procedure of complex **11a** and isolated as white powder.

Yield: 90%

¹H NMR (300 MHz, d₆-DMSO)

δ 8.11 (t, J = 7.7 Hz, 1H), 7.53 (d, J = 7.7 Hz, 2H), 4.82 (m, 1H), 4.67 (m, 2H), 4.36 (dd, J = 17.6, 6.7 Hz, 2H), 3.91 (d, J = 17.6 Hz, 2H), 2.91 (m, 2H), 2.75 (m, 2H), 2.39 (m, 2H), 2.17 (m, 2H)

¹³C NMR (75 MHz, d₆-DMSO)

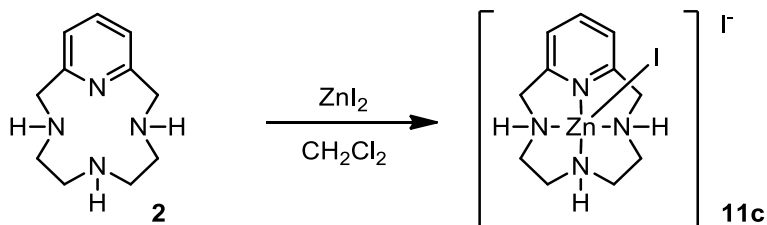
δ 155.7, 141.9, 122.5, 51.5, 47.8, 46.2

MS (ESI +) m/z (%) = calculated for C₁₁H₁₈Br₂N₄Zn: 427,92, found: 351 (100), [M+ -1Br]

Elem. An. C₁₁H₁₈Br₂N₄Zn·2H₂O Calcd: C 28.26, H 4.74, N 11.98; found: C 28.51, H 4.30, N 11.84

Single crystals suitable for XRD were obtained by slow evaporation of a water solution of the complex.

Synthesis of complex (11c):^[135]



Complex **11c** was prepared with the same procedure of complex **11a** and complex **11b**. The product was isolated as pale-yellow powder.

Yield: 91%

¹H NMR (300 MHz, d₆-DMSO)

δ 8.09 (t, J = 7.7 Hz, 1H), 7.51 (d, J = 7.7 Hz, 2H), 4.71 (m, 2H), 4.36 (dd, J = 17.6, 7.0 Hz, 2H), 4.25 (m, 1H), 3.87 (d, J = 17.6 Hz, 2H), 2.87 (m, 2H), 2.77 (m, 2H), 2.50 (m, 2H) overlapping with DMSO residue signal, 1.81 (m, 2H)

¹³C NMR (75 MHz, d₆-DMSO)

δ 155.7, 141.6, 122.2, 52.0, 49.3, 46.3

MS (ESI +) m/z (%) = calculated for C₁₁H₁₈I₂N₄Zn: 523,89, found: 397 (100) [M+ -1I]

Elem. An. C₁₁H₁₈Br₂N₄Zn·2H₂O Calculated: C 25.14, H 3.45, N 10.66; found: C 25.43, H 3.28, N, 10.28

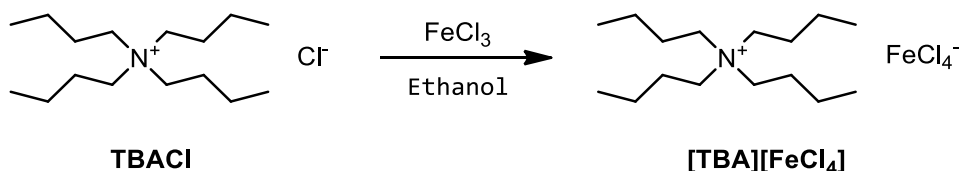
Single crystals suitable for XRD were obtained by slow evaporation of a water solution of the complex.

6.5 SYNTHESIS OF AMMONIUM METALLATE SALTS:

All the metallate salts were synthesized following a procedure previously reported in the literature.^[154]

6.5.1 Iron:

Synthesis of tetrabutylammonium tetrachloroferrate ([TBA][FeCl₄]):



A solution of iron(III) chloride hexahydrate (0.36 mmol, 97 mg) in ethanol (10 mL) was slowly added to a solution of tetrabutylammonium chloride (0.36 mmol, 100 mg) in ethanol (10 mL). If the addition is slow enough, the product is formed as yellow needle-like crystals; in the other case, a yellow powder is formed. The product can be recrystallized by cooling a concentrated solution in ethanol overnight at -20 °C

Yield: 94%

Additional information: TBACl is highly hygroscopic: preferentially use freshly recrystallized TBACl, dried and stored under nitrogen. The synthesis can also be performed using anhydrous iron(III) chloride. The solvent can be replaced with dichloromethane and the product precipitated with diethyl ether at room temperature. The product is slightly light-sensitive, best kept in the dark.

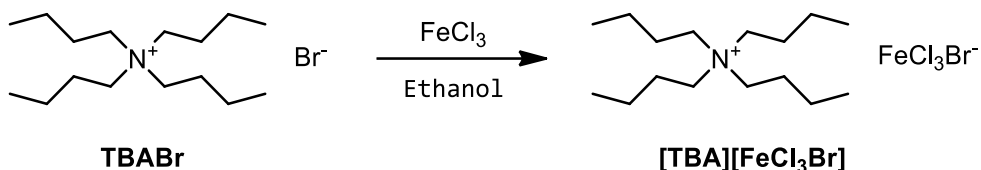
MS (ESI +) m/z (%) calculated for C₁₆H₃₆N: 242.28, found: 242.32 (100%, M⁺).

HRMS (ESI -) m/z (%) calculated for FeCl₄: 193.8150, found: 193.8147 (100%, FeCl₄⁻), 158.8461 (40%, FeCl₃).

Elem. An. C₁₆H₃₆Cl₄FeN Calculated: C, 43.66; H, 8.25; N, 3.18; found: C, 43.82; H, 8.23; N, 3.16.

Melting point: 113 °C

Synthesis of tetrabutylammonium bromotrichloroferrate ([TBA][FeCl₃Br]):



A solution of iron(III) chloride hexahydrate (0.31 mmol, 84 mg) in ethanol (10 mL) was slowly added to a solution of tetrabutylammonium bromide (0.31 mmol, 100 mg) in ethanol (10 mL). If the addition is slow enough, the product is formed as orange needle-like crystals; in the other case, an orange powder is formed. The product can be recrystallized by cooling a concentrated solution in ethanol several days at -20 °C.

Yield: 96%

Additional information: anhydrous iron(III) chloride can also be used.

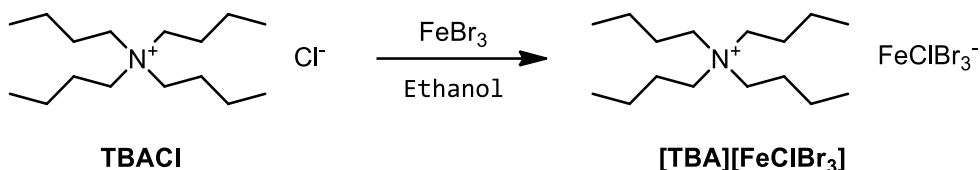
MS (ESI +) m/z (%) calculated for C₁₆H₃₆N: 242.28, found 242.40 (100%, M⁺).

HRMS (ESI -) m/z (%) calculated for FeCl₃Br: 237.7645, found 237.7644 (5%, FeCl₃Br⁻), 197.8150 (100%, FeCl₄⁻), 158.8462 (40%, FeCl₃).

Elem. An. C₁₆H₃₆BrCl₃FeN calculated: C, 39.66; H, 7.49; N, 2.89; found: C, 39.98; H, 7.51; N, 2.86.

Melting point: 132 °C

Synthesis of tetrabutylammonium tribromochloroferrate ([TBA][FeClBr₃]):



A solution of iron(III) bromide (0.36 mmol, 106 mg) in ethanol (10 mL) was slowly added to a solution of tetrabutylammonium chloride (0.36 mmol, 100 mg) in ethanol (10 mL). If the addition is slow enough, the product is formed as light red needle-like crystals; in the other case, a red powder is formed. The product can be recrystallized by cooling a concentrated solution in ethanol several days at -20 °C.

Yield: 97%

Additional information: the scrambling of halides in solution is consistent with the values found in MS analysis. This particular species seems to be the least stable in the series of ammonium ferrates prepared.

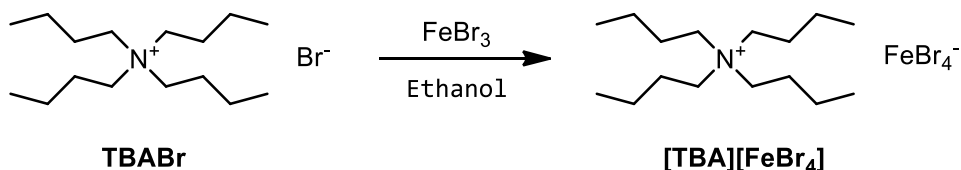
MS (ESI +) m/z (%) calculated for C₁₆H₃₆N: 242.28, found: 242.35 (100%, M⁺).

HRMS (ESI -) m/z (%) calculated for FeClBr₃: 325.6635, found: 325.6632 (5%, FeClBr₃⁻), 281.7137 (10%, FeCl₂Br₂⁻), 237.7645 (40%, FeCl₃Br⁻), 197.8150 (100%, FeCl₄⁻), 158.8463 (50%, FeCl₃).

Elem. An. calculated for C₁₆H₃₆Br₃ClFeN C, 33.51; H, 6.33; N, 2.44; found: C, 33.68; H, 6.22; N, 2.56.

Melting point: 129 °C

Synthesis of tetrabutylammonium tetrabromoferrate ([TBA][FeBr₄]):



A solution of iron(III) bromide (0.31 mmol, 91 mg) in ethanol (10 mL) was slowly added to a solution of tetrabutylammonium bromide (0.31 mmol, 100 mg) in ethanol (10 mL). If the addition is slow enough, the product is formed as dark red needle-like crystals; in the other case, a red powder is formed. The product can be recrystallized by cooling a concentrated solution in ethanol overnight at -20 °C.

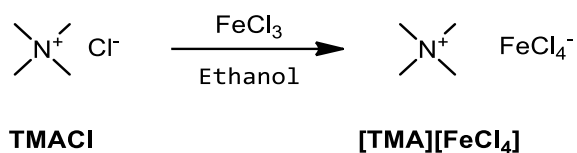
Yield: 98%

MS (ESI +) m/z (%) calculated for C₁₆H₃₆N: 242.28, found: 242.34(100%, M⁺).

HRMS (ESI -) m/z (%) calculated for FeBr₄: 369.6130, found 369.6121 (100%, FeBr₄⁻), 290.6942 (10%, FeBr₃).

Elem. An. calculated for C₁₆H₃₆Br₄FeN C, 31.10; H, 5.87; N, 2.27; found: C, 30.98; H, 5.86; N, 2.00.

Melting point: 135 °C

Synthesis of tetramethylammonium tetrachloroferrate ([TMA][FeCl₄]):

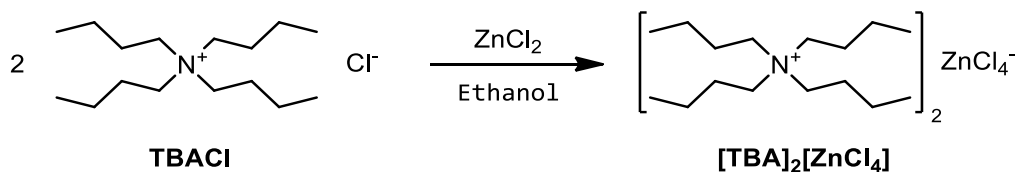
A solution of iron(III) chloride hexahydrate (20 mmol) in ethanol (75 mL) and a solution of tetramethylammonium chloride (20 mmol) in ethanol (75 mL) were mixed and left to react for 3 hours at room temperature. During this time, the product precipitates as a yellow/orange powder that was filtered and dried in vacuum.

Yield: 74%

Elem. An. calculated for C₄H₁₂Cl₄FeN C, 17.68; H, 4.45; N, 5.15; found: C, 17.65; H, 4.40; N, 5.07.

6.5.2 Zinc:

Synthesis of bis-tetrabutylammonium tetrachlorozincate ([TBA]₂[ZnCl₄]):^[239]



A solution of zinc(II) chloride (3 mmol, 408 mg) in ethanol (15 mL) was slowly added to a solution of tetrabutylammonium chloride (6 mmol, 1.67 g) in ethanol (15 mL). After stirring for 1h at 40°C, the solution was concentrated in vacuum and the residue dissolved in the minimum amount of methanol and placed at -20°C overnight. The product was obtained as a white solid.

Yield: 63%

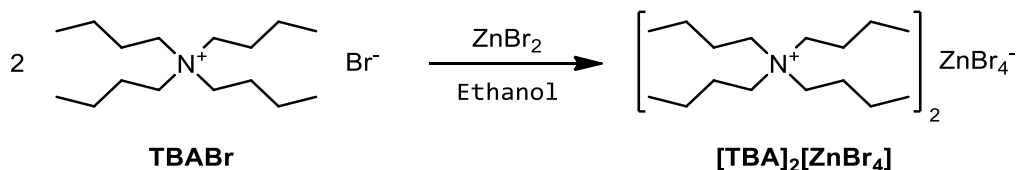
Additional information: the high hygroscopicity of both tetrabutylammonium chloride and zinc(II) chloride can lead to the formation of a hydrated species with formula [TBA]₃[Zn₂Cl₇(H₂O)], confirmed by Raman spectroscopy.

HRMS-(ESI +) m/z (%) calculated for C₁₆H₃₆N 242.28, found: 242.28 (100%, TBA⁺).

HRMS-(ESI -) m/z (%) calculated for ZnCl₃ 170.83, found: 170.833 (100%, ZnCl₃⁻).

Elem. An. calculated for C₃₂H₇₂Cl₄ZnN₂ C, 55.53; H, 10.49; N, 4.05; found: C, 54.89; H, 9.92; N, 3.58.

Synthesis of bis-tetrabutylammonium tetrabromozincate ([TBA]₂[ZnBr₄]):^[239]



A solution of zinc(II) bromide (3 mmol, 675 mg) in ethanol (15 mL) was slowly added to a solution of tetrabutylammonium bromide (6 mmol, 1.93 g) in ethanol (15 mL). After stirring for 1h at 40°C, the solution was concentrated to almost dryness, dissolved in methanol and placed at -20°C overnight. The product was obtained as a white solid.

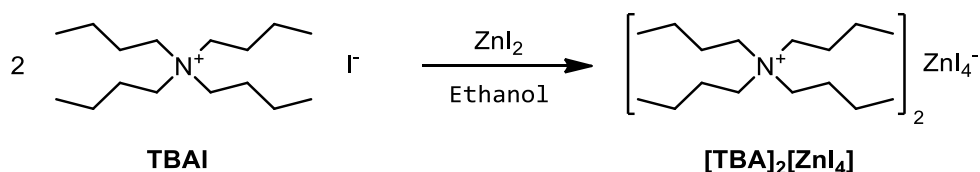
Yield: 71%

HRMS-(ESI +) m/z (%) calculated for C₁₆H₃₆N 242.28, found: 242.28 (100%, TBA⁺).

HRMS-(ESI -) m/z (%) calculated for ZnBr₃ 304.68, found: 304.679 (100%, ZnBr₃⁻).

Elem. An. calculated for C₃₂H₇₂Br₄ZnN₂ C, 44.18; H, 8.34; N, 3.22; found: C, 44.60; H, 8.60; N, 3.35.

Synthesis of bis-tetrabutylammonium tetraiodozincate ($[\text{TBA}]_2[\text{ZnI}_4]$):^[239]



A solution of zinc(II) iodide (4.6 mmol, 1.47 g) in ethanol (15 mL) was slowly added to a solution of tetrabutylammonium iodide (9.2 mmol, 3.40 g) in ethanol (15 mL). After stirring for 1h at 40°C, the solution was filtered and concentrated to a third of the volume and placed at -20°C overnight. The product was obtained as a pale-yellow solid.

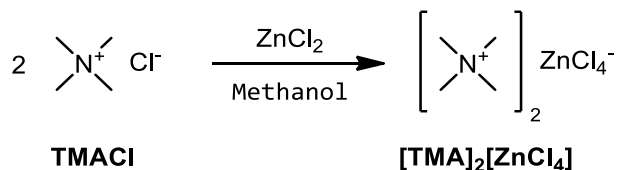
Yield: 88%

HRMS-(ESI +) m/z (%) calculated for $\text{C}_{16}\text{H}_{36}\text{N}$ 242.28, found: 242.28 (100%, TBA^+).

HRMS-(ESI -) m/z (%) only I^- , NaI_2^- and I_3^- where found after the ionization of the material.

Elem. An. calculated for $\text{C}_{32}\text{H}_{72}\text{I}_4\text{ZnN}_2$ C, 27.91; H, 5.27; N, 2.03; found: C, 27.92; H, 5.23; N, 1.92.

Synthesis of bis-tetramethylammonium tetrachlorozincate ([TMA]₂[ZnCl₄]):



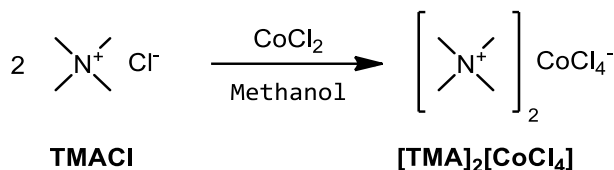
Zinc(II) chloride (1 mmol) was dissolved in methanol (5 mL) and slowly added to a solution of tetramethylammonium chloride (2 mmol) in methanol (5 mL). After stirring overnight at 40 °C, the solution was concentrated under reduced pressure and the product obtained as a white solid.

Yield: 95%

Elem. An. calculated for C₈H₂₄Cl₄N₂Zn C, 27.03; H, 6.81; N, 7.88; found: C, 26.88; H, 6.75; N, 7.11.

6.5.3 Cobalt:

Synthesis of bis-tetramethylammonium tetrachlorocobaltate ([TMA]₂[CoCl₄]):

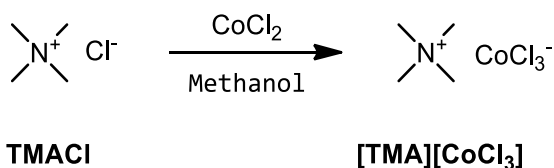


Cobalt(II) chloride (1 mmol) was dissolved in methanol (5 mL) and slowly added to a solution of tetramethylammonium chloride (2 mmol) in methanol (5 mL). After stirring overnight at 40 °C, the solution was concentrated under reduced pressure and the product obtained as a blue powdery solid.

Yield: 88%

Elem. An. calculated for C₈H₂₄Cl₄N₂Co C, 27.53; H, 6.93; N, 8.03; found: C, 27.52; H, 6.67; N, 7.55.

Synthesis of tetramethylammonium trichlorocobaltate ([TMA][CoCl₃]):

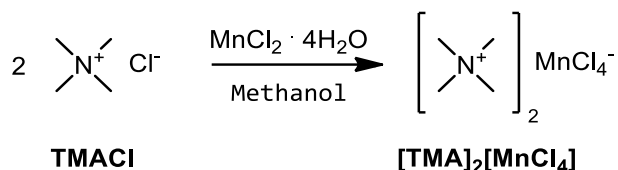


Cobalt(II) chloride (1 mmol) was dissolved in methanol (5 mL) and slowly added to a solution of tetramethylammonium chloride (1 mmol) in methanol (5 mL). After stirring overnight at 40 °C, the solution was concentrated under reduced pressure and the product obtained as a blue powdery solid.

Yield: 86%

Elem. An. calculated for C₄H₁₂Cl₃NCo C: 20.07; H: 5.05; N: 5.85; found: C: 17.87; H: 5.85; N: 5.77;

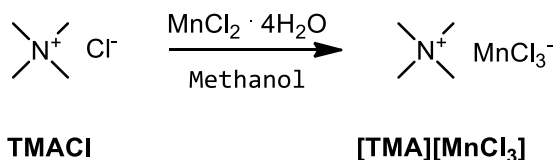
6.5.4 Manganese:

Synthesis of tetramethylammonium tetrachloromanganate ([TMA]₂[MnCl₄]):

Manganese(II) chloride tetrahydrate (1 mmol) was dissolved in methanol (5 mL) and slowly added to a solution of tetramethylammonium chloride (2 mmol) in methanol (5 mL). After stirring overnight at 40 °C, the solution was concentrated under reduced pressure and the product obtained as a pale pink crystalline solid.

Yield: 87%

Elem. An. calculated for C₈H₂₄Cl₄N₂Mn C: 27.85; H: 7.01; N: 8.12; found: C: 27.90; H: 7.04; N: 8.10;

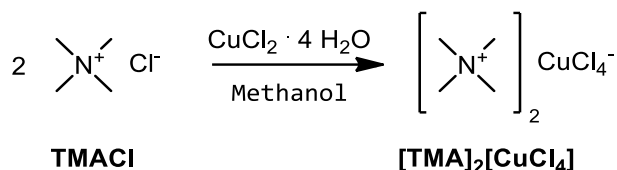
Synthesis of tetramethylammonium trichloromanganate ([TMA][MnCl₃]):

Manganese(II) chloride tetrahydrate (1 mmol) was dissolved in methanol (5 mL) and slowly added to a solution of tetramethylammonium chloride (1 mmol) in methanol (5 mL). After stirring overnight at 40 °C, the solution was concentrated under reduced pressure and the product obtained as pale pink solid.

Yield: 82%

Elem. An. calculated for C₄H₁₂Cl₃NMn C: 20.41; H: 5.14; N: 5.95; found: C: 20.73; H: 5.20; N: 6.07;

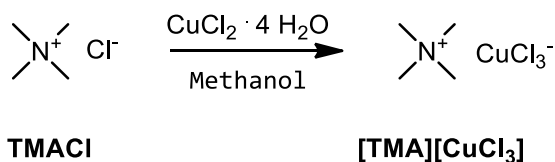
6.5.5 Copper:

Synthesis of tetramethylammonium tetrachlorocuprate ([TMA]₂[CuCl₄]):

Copper(II) chloride tetrahydrate (1 mmol) was dissolved in methanol (5 mL) and slowly added to a solution of tetramethylammonium chloride (2 mmol) in methanol (5 mL). After stirring overnight at 40 °C, the solution was concentrated under reduced pressure and the product obtained as a yellow powder.

Yield: 82%

Elem. An. calculated for C₈H₂₄Cl₄N₂Cu C, 27.17; H, 6.84; N, 7.92; found: C, 27.15; H, 6.73; N, 6.65.

Synthesis of tetramethylammonium trichlorocuprate ([TMA][CuCl₃]):

Copper(II) chloride tetrahydrate (1 mmol) was dissolved in methanol (5 mL) and slowly added to a solution of tetramethylammonium chloride (1 mmol) in methanol (5 mL). After stirring overnight at 40 °C, the solution was concentrated under reduced pressure and the product obtained as yellow solid.

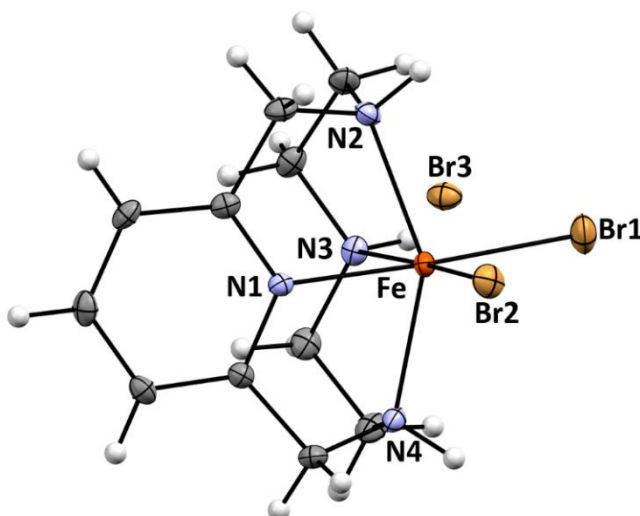
Yield: 84%

Elem. An. calculated for C₄H₁₂Cl₃NCu C: 19.69; H: 4.96; N: 5.74; found: C: 18.91; H: 5.02; N: 5.01;

6.6 CRYSTAL STRUCTURES DETERMINATION:

The single crystal X-ray diffraction experiments were performed on a Bruker Smart APEX II CCD diffractometer with graphite monochromated Mo-K α radiation ($\lambda = 0.71073 \text{ \AA}$). Data were collected at 180 K in the ω -scan mode within the range $3.5^\circ < 2\theta < 53.0^\circ$. The frames were integrated and corrected for Lorentz-polarization effects with the Bruker SAINT software package. The intensity data were then corrected for absorption by using SADABS. No decay correction was applied. The structures were solved by direct methods (SIR-97) and refined by iterative cycles of full-matrix least squares on F_o^2 and ΔF synthesis with SHELXL-97 within the WinGX interface.

Complex 5b:^[237]



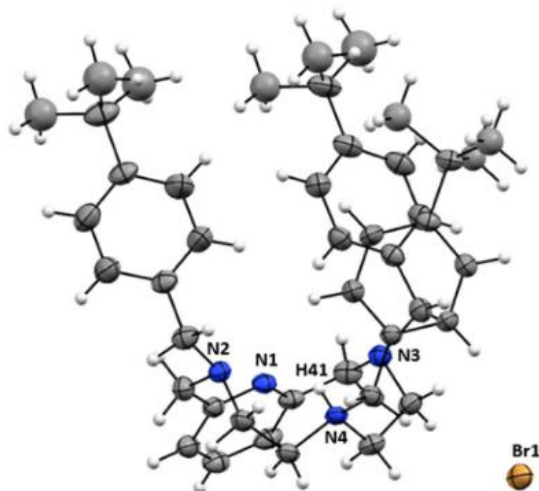
Complex **5b** block red crystals, with formula $[\text{Fe}(\text{C}_{11}\text{N}_4\text{H}_{18})\text{Br}_2]\text{Br} \cdot \frac{1}{2}\text{H}_2\text{O}$, suitable for X-ray analysis were isolated by slow evaporation from an aqueous solution of complex **5b** at room temperature. Compound (**5b**) crystallizes in the monoclinic space group $P2_1/c$ ($n^\circ 13$), $Z = 4$. All atoms are in general position except for the water oxygen atom which is located on the 2-fold axes. Hydrogen atoms of the ligand were placed in geometrically calculated positions and then refined using a riding model based on the positions of the parent atoms with $U_{\text{iso}} = 1.2 U_{\text{eq}}(\text{C})$. The hydrogen atom of water molecule (H1W) was located from a difference Fourier map and refined isotropically. A restrain was applied to the $\text{H} \cdots \text{H}$ distance in order to obtain a reasonable

value for the H-O-H angle. All non-hydrogen atoms were refined with anisotropic displacement parameters.

Full crystallographic data have been deposited with the Cambridge Crystallographic Data Centre (CCDC No. 2016034). A copy of the data can be obtained free of charge on application to CCDC, 12 Union Road, Cambridge CB2 IEZ, UK (Fax: +44 1223 336 033; e-mail: deposit@ccdc.cam.ac.uk).

Empirical formula	C ₁₁ H ₁₉ Br ₃ Fe N ₄ O _{0.50}	
Formula weight	510.88	
Temperature	180(2) K	
Wavelength	0.71073 Å	
Crystal system	Monoclinic	
Space group	<i>P</i> 2/ <i>c</i>	
Unit cell dimensions	a = 12.2711(8) Å	α = 90°.
	b = 8.9801(6) Å	β = 108.537(9)°.
	c = 15.866(1) Å	γ = 90°.
Volume	1657.7(2) Å ³	
Z	4	
Density (calculated)	2.047 Mg/m ³	
Absorption coefficient	8.138 mm ⁻¹	
F(000)	992	
Crystal size	0.2 x 0.09 x 0.03 mm ³	
Theta range for data collection	1.750 to 26.465°.	
Index ranges	-15 ≤ h ≤ 15, -11 ≤ k ≤ 11, -19 ≤ l ≤ 19	
Reflections collected	13113	
Independent reflections	3430 [R(int) = 0.0179]	
Completeness to theta = 25.242°	100.0 %	
Refinement method	Full-matrix least-squares on F ²	
Data / restraints / parameters	3430 / 1 / 181	
Goodness-of-fit on F ²	1.034	
Final R indices [I > 2σ(I)]	R1 = 0.0204, wR2 = 0.0558	
R indices (all data)	R1 = 0.0284, wR2 = 0.0575	
Largest diff. peak and hole	0.551 and -0.656 e.Å ⁻³	

Table X. Crystal data and structure refinement for complex **5b**

Ligand 4:^[236]

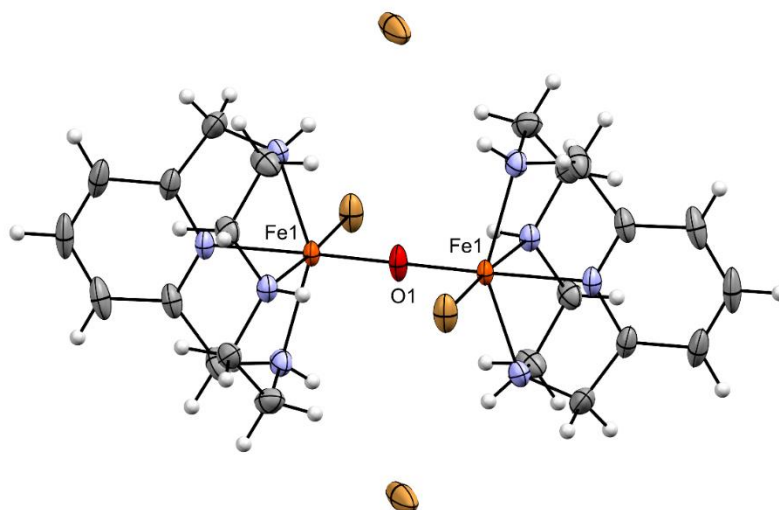
Block colourless crystals of compound **4** suitable for X-ray analysis were grown by slow diffusion of water in an ethanolic solution of compound **7**. Ligand **4**, formula $C_{44}H_{61}N_4Br \cdot H_2O$, crystallizes in monoclinic space group $P 2_1/c$ ($n^\circ 14$), $Z = 8$. Total number of reflections recorded to $\theta_{max} = 23.255^\circ$, was 46762 of which 11992 were unique ($R_{int} = 0.0327$); 8943 were ‘observed’ with $I > 2\sigma(I)$. Final R-values: $wR_2 = 0.1521$ and $R_1 = 0.0764$ for all data; $R_1 = 0.0543$ for the ‘observed’ data. There are two crystallographically independent formula units in the asymmetric unit having the same structure. All atoms are in general position and refined anisotropically, except those of the disordered parts of the molecules. Five out of the six ^tbutyl groups were found to be disordered over two positions which were refined isotropically with occupation factors constrained to sum to unity. Final occupancies are 0.51/0.49, 0.62/0.38, 0.68/0.32, 0.61/0.39 and 0.62/0.48. An orientational disorder of a benzene ring is also observed and refined over two orientations with refined-site occupancy factors of 0.57 and 0.43. All hydrogen atoms attached to carbon atoms were placed in geometrically calculated positions and then refined using a riding model based on the positions of the parent atoms with $U_{iso} = 1.2 U_{eq}$ (1.5 U_{eq} in the case of methyl groups). The hydrogen atoms bound to N4 and N7 (protonated nitrogens) were located from a difference Fourier map and refined isotropically, whereas it was not possible to determine and obtain a satisfactory refinement for the position of the hydrogens bound to O1 and O2 (water molecules). Some restraints were applied to the bond distances in the disordered

tbutyl moieties in order to ensure reasonable values of the C-C bond lengths.

Full crystallographic data have been deposited with the Cambridge Crystallographic Data Centre (CCDC-2071881). A copy of the data can be obtained free of charge on application to CCDC, 12 Union Road, Cambridge CB2 1EZ, UK (Fax: +44 1223 336 033; e-mail: deposit@ccdc.cam.ac.uk).

Empirical formula	C ₄₄ H ₆₃ BrN ₄ O	
Formula weight	743.87	
Temperature	298(2) K	
Wavelength	0.71073 Å	
Crystal system	Monoclinic	
Space group	P2 ₁ /c	
Unit cell dimensions	a = 24.150(2) Å	α = 90°.
	b = 18.654(2) Å	β = 100.100(1)°.
	c = 18.822(2) Å	γ = 90°.
Volume	8347.8(14) Å ³	
Z	8	
Density (calculated)	1.181 Mg/m ³	
Absorption coefficient	1.021 mm ⁻¹	
F(000)	3168	
Crystal size	0.250 x 0.212 x 0.131 mm ³	
Theta range for data collection	1.387 to 23.255°.	
Index ranges	-26 ≤ h ≤ 26, -20 ≤ k ≤ 20, -20 ≤ l ≤ 20	
Reflections collected	46762	
Independent reflections	11992 [R(int) = 0.0327]	
Completeness to theta = 23.255°	100.0 %	
Refinement method	Full-matrix least-squares on F ²	
Data / restraints / parameters	11992 / 75 / 896	
Goodness-of-fit on F ²	1.054	
Final R indices [I > 2σ(I)]	R1 = 0.0543, wR2 = 0.1454	
R indices (all data)	R1 = 0.0764, wR2 = 0.1621	
Largest diff. peak and hole	0.831 and -0.612 e.Å ⁻³	

Table X. Crystal data and structure refinement for ligand **4**

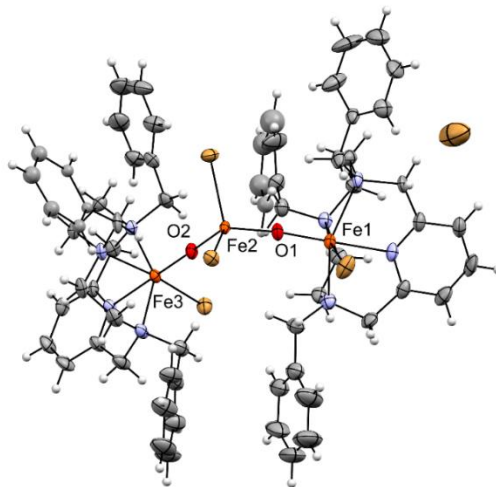
Complex 8:

Crystals suitable for XRD were obtained by slow evaporation of a water/methanol solution of complex **8**. Formula: $C_{22}H_{36}Br_4Fe_2N_8O \cdot 3CH_3OH$, monoclinic space group $C2/m$, $Z = 2$. Total number of reflections recorded to $\theta_{max} = 28.433^\circ$ was 8126 of which 2301 were unique ($R_{int} = 0.0145$); 2107 were 'observed' with $I > 2\sigma(I)$. Final R-values: $wR2 = 0.0762$ and $R1 = 0.0319$ for all data; $R1 = 0.0293$ for the 'observed' data. All non-hydrogen atoms of the complex were refined anisotropically. The hydrogen atoms of the ligands were located from the Fourier-difference synthesis, placed geometrically and refined using a riding model based on the positions of the parent atom with $U_{iso} = 1.2 U_{eq}$. Two molecules of methanol in the structural model (C7-O2 and C8-O3) were found disordered over special positions and were refined isotropically with adequate fractional occupancies (0.5 for C7-O2 and 0.25 for C8-O3). It was not possible to determine and refine the position of the corresponding hydrogen atoms.

Full crystallographic data have been deposited with the Cambridge Crystallographic Data Centre (CCDC-2175108). A copy of the data can be obtained free of charge on application to CCDC, 12 Union Road, Cambridge CB2 1EZ, UK (Fax: +44 1223 336 033; e-mail: deposit@ccdc.cam.ac.uk).

Empirical formula	(C ₂₂ H ₃₆ Br ₄ Fe ₂ N ₈ O) · 3(CH ₃ OH)
Formula weight (g mol ⁻¹)	943.96
Temperature (K)	150(2)
Wavelength (Å)	0.71073
Crystal system	Monoclinic
Space group	<i>C</i> 2/ <i>m</i>
Unit cell dimensions	
a (Å)	12.414(1)
b (Å)	17.616(1)
c (Å)	8.5625(7)
α (°)	90
β (°)	109.113(1)
γ (°)	90
Volume (Å ³)	1769.3(4)
Z	2
Calculated density (Mg m ⁻³)	1.772
Absorption coefficient (mm ⁻¹)	5.379
F(000)	932
Crystal size (mm ³)	0.332 x 0.297 x 0.203
Theta range for data collection (°)	2.086 to 28.433
Index ranges	-16 ≤ h ≤ 16, -23 ≤ k ≤ 23, -11 ≤ l ≤ 11
Reflections collected	8126
Independent reflections	2301 [R _(int) = 0.0145]
Max. and min. transmission	0.7454 and 0.5636
Refinement method	Full-matrix least-squares on F ²
Data / restraints / parameters	2301 / 3 / 115
Goodness-of-fit on F ²	1.059
Final R indices [I > 2σ(I)]	R ₁ = 0.0293, wR ₂ = 0.0748
R indices (all data)	R ₁ = 0.0319, wR ₂ = 0.0762
Largest diff. peak and hole (e Å ⁻³)	1.134 and -0.930
CCDC deposition number	2175108

Table X. Crystal data and structure refinement for complex **8**

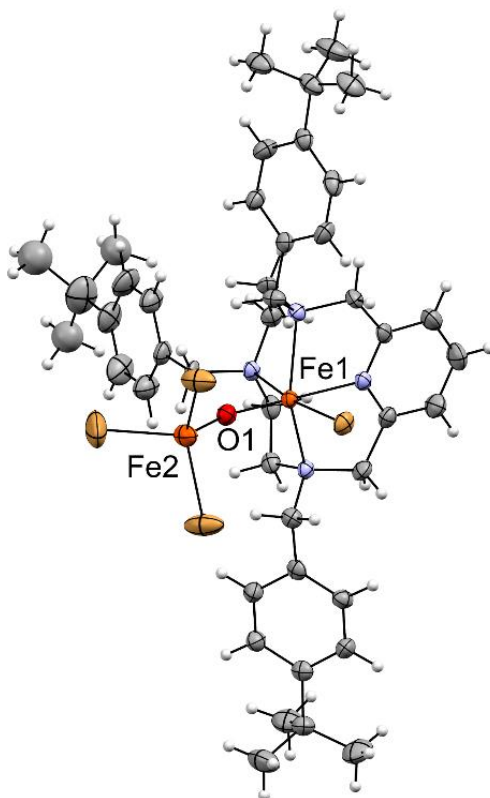
Complex 9:

Crystals suitable for XRD were obtained by slow diffusion of ether in an acetonitrile/methanol solution of complex **9**. Formula: $C_{64}H_{72}Br_5Fe_3N_8O_2 \cdot 1.5(CH_3CN) \cdot 2(CH_3OH)$, orthorhombic space group $Pca2_1$, $Z = 4$. Total number of reflections recorded to $\theta_{max} = 28.759^\circ$ was 67187 of which 19058 were unique ($R_{int} = 0.0390$); 16573 were 'observed' with $I > 2\sigma(I)$. Final R-values: $wR2 = 0.1094$ and $R1 = 0.0585$ for all data; $R1 = 0.0451$ for the 'observed' data. All non-hydrogen atoms of the complex were refined anisotropically, except for those of two benzene rings of the ligand. Each of these units was found disordered over two different positions and was refined by using two isotropic models with adequate fractional occupancies (0.4 for the ring defined by C27, C282, C292, C302, C312, C32 and 0.6 for the ring defined by C27, C281, C291, C301, C311, C32, SHELX FLAT restrain was employed to ensure the planarity of such rings; 0.5 for the rings defined by C591, C601, C611, C621, C631, C641 and C592, C602, C612, C622, C632, C642). The hydrogen atoms of the ligands and of the methyl groups of the solvent molecules were located from the Fourier-difference synthesis, placed geometrically and refined using a riding model based on the positions of the parent atom with $U_{iso} = 1.2 U_{eq}$ ($1.5 U_{eq}$ for methyl groups). Disordered solvent molecules of methanol and acetonitrile were refined isotropically and with fractional occupancies (0.5 for O5-C65, O6-C66, C71-C70-N10; 0.55 for O71-C671, 0.45 for O72-C672). It was not possible to determine and refine the position of the hydrogens attached to the oxygen atoms of the methanol molecules

Full crystallographic data have been deposited with the Cambridge Crystallographic Data Centre (CCDC-2175109). A copy of the data can be obtained free of charge on application to CCDC, 12 Union Road, Cambridge CB2 1EZ, UK (Fax: +44 1223 336 033; e-mail: deposit@ccdc.cam.ac.uk).

Empirical formula	(C ₆₄ H ₇₂ Br ₅ Fe ₃ N ₈ O ₂) · 1.5(CH ₃ CN) · 2(CH ₃ OH)
Formula weight (g mol ⁻¹)	1676.04
Temperature (K)	150(2)
Wavelength (Å)	0.71073
Crystal system	Orthorhombic
Space group	<i>Pca</i> 2 ₁
Unit cell dimensions	
a (Å)	22.073(2)
b (Å)	13.646(2)
c (Å)	24.473(3)
α (°)	90
β (°)	90
γ (°)	90
Volume (Å ³)	7371(2)
Z	4
Calculated density (Mg m ⁻³)	1.510
Absorption coefficient (mm ⁻¹)	3.344
F(000)	3392
Crystal size (mm ³)	0.353 x 0.306 x 0.102
Theta range for data collection (°)	1.492 to 28.759
	-29 ≤ h ≤ 29,
Index ranges	-18 ≤ k ≤ 18,
	-33 ≤ l ≤ 33
Reflections collected	67187
Independent reflections	19058 [R _(int) = 0.0390]
Max. and min. transmission	0.7458 and 0.5648
Refinement method	Full-matrix least-squares on F ²
Data / restraints / parameters	19058 / 12 / 786
Goodness-of-fit on F ²	1.07
Final R indices [I > 2σ(I)]	R ₁ = 0.0451, wR ₂ = 0.1033
R indices (all data)	R ₁ = 0.0585, wR ₂ = 0.1094
Largest diff. peak and hole (e Å ⁻³)	1.820 and -1.627
CCDC deposition number	2175109

Table X. Crystal data and structure refinement for complex **9**

Complex 10:

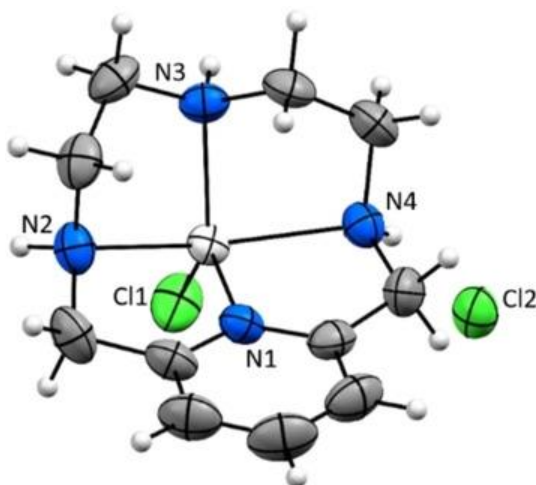
Crystals suitable for XRD were collected by diffusion of diethyl ether in a solution of compound **7** in acetonitrile. Molecules of acetamide were found in the crystal lattice, resulting from basic hydrolysis of acetonitrile. Acetamide itself acted as a base to yield complex **10** in situ. Formula: $C_{44}H_{60}Br_4Fe_2N_4O \cdot 1.35(CH_3CONH_2) \cdot 0.6(CH_3CN)$, triclinic space group $P-1$, $Z = 2$. Total number of reflections recorded to $\theta_{max} = 24.860^\circ$ was 18530 of which 9739 were unique ($R_{int} = 0.0638$); 6141 were 'observed' with $I > 2\sigma(I)$. Final R-values: $wR2 = 0.1622$ and $R1 = 0.1023$ for all data; $R1 = 0.0563$ for the 'observed' data. All non-hydrogen atoms of the complex were refined anisotropically, except for a disordered t-Butyl moiety. The hydrogen atoms of the macrocycle were located from the Fourier-difference synthesis, placed geometrically and refined using a riding model based on the positions of the parent atom with $U_{iso} = 1.2 U_{eq}$ ($1.5 U_{eq}$ for methyl groups). The disordered t-Butyl moiety

of the ligand was refined with two isotropic models around the 3-fold rotation axis. The refined fractional occupancies of the corresponding methyl groups are 0.56 for C42A, C43A, C44A and 0.44 for C42B, C43B and C44B. The disordered molecules of acetamide and acetonitrile in the structural model were refined isotropically with adequate fractional occupancies (0.5 for O2, C45, C46 and N5; 0.45 for O3, C47, C48 and N6; 0.4 for O4, C49, C50 and N7; 0.6 for C51, C52 and N8). C52 from an acetonitrile molecule and O4 from an acetamide molecule share the same site and were constrained to have the same ADP. A series of restraints was applied to the disordered ^tbutyl moiety and solvent molecules to ensure reasonable values of 1,2- and 1,3-distances. It was not possible to locate and refine the position of the hydrogen atoms attached to the solvent molecules.

Full crystallographic data have been deposited with the Cambridge Crystallographic Data Centre (CCDC-2175110). A copy of the data can be obtained free of charge on application to CCDC, 12 Union Road, Cambridge CB2 1EZ, UK (Fax: +44 1223 336 033; e-mail: deposit@ccdc.cam.ac.uk).

Empirical formula	(C ₄₄ H ₆₀ Br ₄ Fe ₂ N ₄ O)· 1.35(CH ₃ CONH ₂)·0.6(CH ₃ CN)
Formula weight (g mol ⁻¹)	1188.06
Temperature (K)	150(2)
Wavelength (Å)	0.71073
Crystal system	Triclinic
Space group	<i>P</i> $\bar{1}$
Unit cell dimensions	
a (Å)	9.745(3)
b (Å)	15.884(6)
c (Å)	19.997(7)
α (°)	78.260(4)
β (°)	76.346(4)
γ (°)	72.282(4)
Volume (Å ³)	2836(3)
Z	2
Calculated density (Mg m ⁻³)	1.391
Absorption coefficient (mm ⁻¹)	3.368
F(000)	1200
Crystal size (mm ³)	0.283 x 0.126 x 0.121
Theta range for data collection (°)	1.360 to 24.860
Index ranges	-11 ≤ h ≤ 11, -18 ≤ k ≤ 18, -23 ≤ l ≤ 23
Reflections collected	18530
Independent reflections	9739 [R _(int) = 0.0638]
Max. and min. transmission	0.7449 and 0.5207
Refinement method	Full-matrix least-squares on F ²
Data / restraints / parameters	9739 / 28 / 550
Goodness-of-fit on F ²	0.988
Final R indices [I > 2σ(I)]	R ₁ = 0.0563, wR ₂ = 0.1443
R indices (all data)	R ₁ = 0.1023, wR ₂ = 0.1622
Largest diff. peak and hole (e Å ⁻³)	1.138 and -1.355
CCDC deposition number	2175110

Table X. Crystal data and structure refinement for complex **10**

Complex 11a:

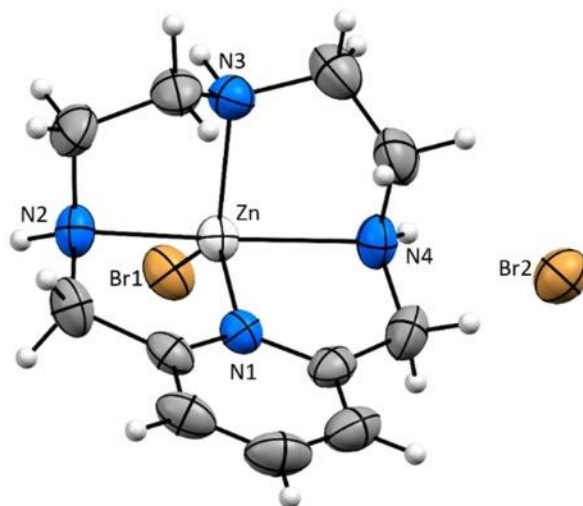
Prismatic colourless crystals suitable for X-ray analysis were grown by slow evaporation from an aqueous solution of **11a** at room temperature. The structure highlights an uncommon square pyramidal geometry of the zinc center in complex **11a**. This feature might be responsible for the enhanced Lewis acidity of zinc and the nucleophilicity of the external chloride anion. Formula: $C_{11}H_{18}ClN_4Zn^+Cl^- \cdot 3/2 H_2O$, triclinic space group $P-1$ ($n^{\circ}2$), $Z = 2$. Total number of reflections recorded to $\theta_{max} = 26.369^{\circ}$ was 6179 of which 3277 were unique ($R_{int} = 0.0098$); 3144 were 'observed' with $I > 2\sigma(I)$. Final R-values: $wR2 = 0.0579$ and $R1 = 0.0229$ for all data; $R1 = 0.0216$ for the 'observed' data. All atoms are in general position. A water molecule (oxygen atom O2) is located very close to a cell vertex (site symmetry -1, Wyckoff letter a) and refined with an occupancy of 0.5. A second water molecule is present which shows a disorder over two positions (site symmetry 1, Wyckoff letter i) of its oxygen atom. The two sites, O1A and O1B, share the same hydrogens and were refined with a sof of 0.5. The hydrogen atoms of the ligand were placed in geometrically calculated positions and then refined using a riding model based on the positions of the parent atoms with $U_{iso} = 1.2 U_{eq}$. The hydrogen atoms (H12 and H13) attached to O1A and O1B were located from a difference Fourier map and refined isotropically, whereas it was not possible to determine the position of the hydrogens bound to O2. Restraints were applied to the distances between the oxygen and the hydrogen atoms (H12 and H13) of the O1A and O1B water molecules. A restraint was applied to

the H12-H13 distance as well in order to obtain a reasonable value for the H-O-H angle.

Full crystallographic data have been deposited with the Cambridge Crystallographic Data Centre (CCDC-2064861). A copy of the data can be obtained free of charge on application to CCDC, 12 Union Road, Cambridge CB2 1EZ, UK (Fax: +44 1223 336 033; e-mail: deposit@ccdc.cam.ac.uk).

Empirical formula	C ₁₁ H ₂₀ Cl ₂ N ₄ O _{1.5} Zn
Formula weight (g mol ⁻¹)	368.58
Temperature (K)	298(2)
Wavelength (Å)	0.71073
Crystal system	Triclinic
Space group	<i>P</i> $\bar{1}$
Unit cell dimensions	
a (Å)	7.8000(4)
b (Å)	8.9923(7)
c (Å)	12.1580(9)
α (°)	78.255(1)
β (°)	88.493(1)
γ (°)	75.167(1)
Volume (Å ³)	806.79(10)
Z	2
Calculated density (Mg m ⁻³)	1.517
Absorption coefficient (mm ⁻¹)	1.855
F(000)	380
Crystal size (mm ³)	0.500 x 0.174 x 0.142
Theta range for data collection (°)	1.711 to 26.369
	-9 ≤ h ≤ 9,
Index ranges	-11 ≤ k ≤ 11,
	-15 ≤ l ≤ 15
Reflections collected	6179
Independent reflections	3277 [R _(int) = 0.0098]
Refinement method	Full-matrix least-squares on F ²
Data / restraints / parameters	3277 / 7 / 198
Goodness-of-fit on F ²	1.044
Final R indices [I > 2σ(I)]	R ₁ = 0.0216, wR ₂ = 0.0567
R indices (all data)	R ₁ = 0.0229, wR ₂ = 0.0579
Largest diff. peak and hole (e Å ⁻³)	0.382 and -0.277

Table X. Crystal data and structure refinement for complex **11a**

Complex 11b:

Prismatic colorless crystals of compound **11b** were obtained from slow evaporation of mother liquor (methanol and chloroform) after reaction purification process (where **11b** was used as catalyst). Formula: $C_{11}H_{18}BrN_4Zn^+Br^- \cdot H_2O$ triclinic space group $P-1$ ($n^\circ 2$), $Z = 2$. Total number of reflections recorded to $\theta_{max} = 26.368^\circ$ was 6583 of which 3317 were unique ($R_{int} = 0.0124$); 2786 were 'observed' with $I > 2\sigma(I)$. Final R-values: $wR2 = 0.0744$ and $R1 = 0.0355$ for all data; $R1 = 0.0275$ for the 'observed' data. All atoms are in general position. The hydrogen atoms of the ligand were placed in geometrically calculated positions and then refined using a riding model based on the positions of the parent atoms with $U_{iso} = 1.2 U_{eq}$. The hydrogen atoms of the water molecule (H1W and H2W) were located from a difference Fourier map and refined isotropically. Their distance to the oxygen atom O was restrained to be equal within a standard deviation of 0.02. Furthermore, the distance H1W-H2W was restrained to a target value in order to retain a reasonable value for the H-O-H angle.

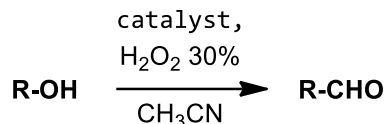
Full crystallographic data have been deposited with the Cambridge Crystallographic Data Centre (CCDC-2064860). A copy of the data can be obtained free of charge on application to CCDC, 12 Union Road, Cambridge CB2 1EZ, UK (Fax: +44 1223 336 033; e-mail: deposit@ccdc.cam.ac.uk).

Empirical formula	C ₁₁ H ₂₀ Br ₂ N ₄ OZn
Formula weight (g mol ⁻¹)	449.50
Temperature (K)	298(2)
Wavelength (Å)	0.71073
Crystal system	Triclinic
Space group	<i>P</i> $\bar{1}$
Unit cell dimensions	
a (Å)	8.3278(8)
b (Å)	9.2464(9)
c (Å)	10.631(1)
α (°)	81.269(1)
β (°)	89.239(1)
γ (°)	89.991(1)
Volume (Å ³)	809.0(1)
Z	2
Calculated density (Mg m ⁻³)	1.845
Absorption coefficient (mm ⁻¹)	6.454
F(000)	444
Crystal size (mm ³)	0.214 x 0.152 x 0.121
Theta range for data collection (°)	1.938 to 26.368
Index ranges	-10 ≤ h ≤ 10, -11 ≤ k ≤ 11, -13 ≤ l ≤ 13
Reflections collected	6583
Independent reflections	3317 [R _(int) = 0.0124]
Max. and min. transmission	0.7463 and 0.5747
Refinement method	Full-matrix least-squares on F ²
Data / restraints / parameters	3317 / 2 / 180
Goodness-of-fit on F ²	1.027
Final R indices [I > 2σ(I)]	R ₁ = 0.0275, wR ₂ = 0.0712
R indices (all data)	R ₁ = 0.0355, wR ₂ = 0.0744
Largest diff. peak and hole (e Å ⁻³)	0.898 and -0.480

Table X. Crystal data and structure refinement for complex **11b**

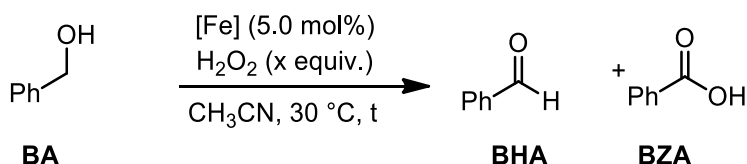
6.7 CATALYTIC OXIDATION OF ALCOHOLS:

6.7.1 General catalytic procedure:



The catalyst (0.025 mmol) and the substrate (0.5 mmol) were dissolved in acetonitrile (10.0 mL) at 30°C. H₂O₂ (30%, 2.0 mmol) was added in 2 hours using a syringe pump, and the mixture was stirred for 24h. After this period, 1 mL of the reaction mixture was collected, an aliquot of dodecane was added as ISTD, the solution was diluted to 10 mL and further analysed by GC. To selected reactions, the remaining reaction mixture was filtered through a PTFE 0.20 µm filter to remove the catalyst and concentrated in vacuum. The so obtained crudes were analysed by ¹H NMR (CH₂Br₂ as internal standard) to identify the products and to confirm the GC values.

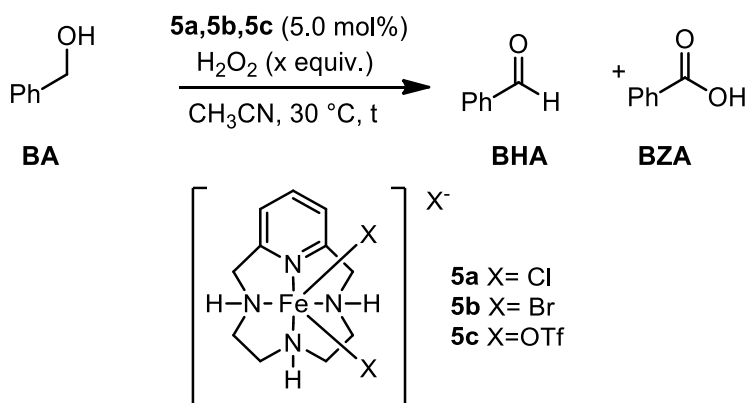
6.7.2 Blank reactions:



Entry	Catalyst	eq H ₂ O ₂	BA Conv (%) ^[b]	BHA Select (%) ^[b]	BZA Select (%) ^[b]
1	FeCl ₃	20	98	6	31
2	Fe(OTf) ₃	20	72	31	21
3	FeBr ₃	20	84	83	5
4 ^[c]		4	76	83	4

Reactions were performed with [Fe^{III}] (2.5 × 10⁻² mmol) in CH₃CN (10 mL) at a cat/alcohol ratio of 1:20 at 30 °C; H₂O₂ (30% sol; equiv. as reported) was added in a single addition, unless otherwise stated. [b] Conversions and selectivity were calculated after 24 h by ¹H NMR using CH₂Br₂ as the internal standard and confirmed by GC (dodecane as the internal standard). [c] H₂O₂ (30% sol) was added dropwise by a syringe pump in 2 h.

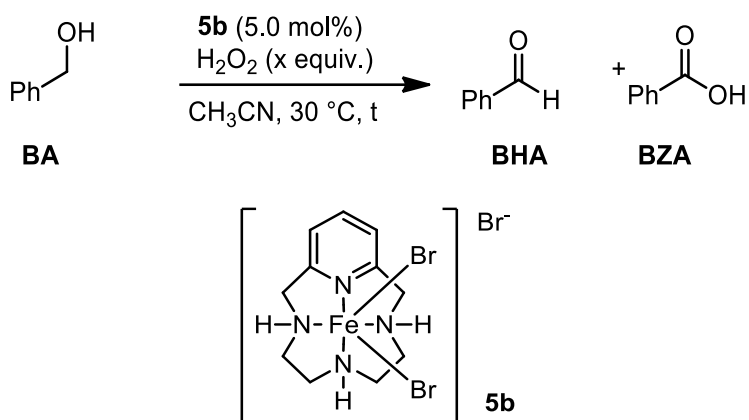
6.7.3 Catalyst optimization:



Entry	Catalyst	eq H_2O_2	Time (h)	BA Conv (%) ^[b]	BHA Select (%) ^[b]	BZA Select (%) ^[b]
5	5a	20	24	95	11	27
6 ^[c]	5a	4	1	33	55	3
7 ^[c]	5a	8	2	46	52	7
8	5b	20	24	66	55	11
9 ^[c]	5b	4	2	30	57	-
10 ^[c]	5b	8	1	60	72	2
11	5c	20	24	86	19	20
12 ^[c]	5c	4	2	69	36	32
13 ^[c]	5c	8	1	85	26	39

Reactions were performed with $[\text{Fe}^{\text{III}}]$ (2.5×10^{-2} mmol) in CH_3CN (10 mL) at a cat/alcohol ratio of 1:20 at 30 °C; H_2O_2 (30% sol; equiv. as reported) was added in a single addition, unless otherwise stated. [b] Conversions and selectivity were calculated after 24 h by ^1H NMR using CH_2Br_2 as the internal standard and confirmed by GC (dodecane as the internal standard). [c] 1 eq. of H_2O_2 was added every 15 min to the reaction.

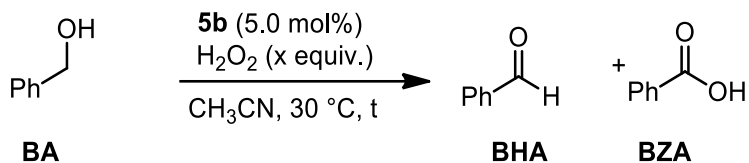
6.7.4 Optimization of other parameters:



Entry	eq H_2O_2	Time (h)	BA Conv (%) ^[b]	BHA Select (%) ^[b]	BZA Select (%) ^[b]
14 ^[c]	12	3	78	76	3
15 ^[d]	2	2	29	93	3
16 ^[d]	2	24	50	98	2
17 ^[d]	4	2	45	87	2
18^[d]	4	24	96	90	10
19 ^[d]	8	2	58	88	2
20 ^[d]	8	24	87	92	2
21 ^[d,e]	4	24	49	82	2
22 ^[d,f]	4	2	76	89	7

Reactions were performed with $[\text{Fe}^{\text{III}}]$ (2.5×10^{-2} mmol) in CH_3CN (10 mL) at a cat/alcohol ratio of 1:20 at $30\text{ }^\circ\text{C}$; H_2O_2 (30% sol; equiv. as reported) was added in a single addition, unless otherwise stated. [b] Conversions and selectivity were calculated after 24 h by ^1H NMR using CH_2Br_2 as the internal standard and confirmed by GC (dodecane as the internal standard). [c] 1 eq. of H_2O_2 was added every 15 min to the reaction. [d] H_2O_2 was added with a syringe pump in 2h. [e] Cat/alcohol ratio 1:40. [f] $T=60\text{ }^\circ\text{C}$.

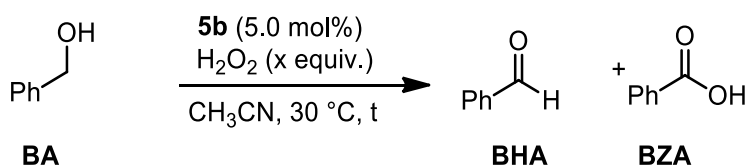
6.7.5 Solvent screening:



Entry	Solvent	BA Conv (%) ^[b]	BHA Select (%) ^[b]	BZA Select (%) ^[b]
18	CH ₃ CN	96	90	10
23	AcOEt	55	99	1
24	Acetone	35	86	-
25	t-amylalcohol	<10	90	-
26	water	98	<1	-

Reactions were performed with [Fe^{III}] (2.5 x 10⁻² mmol) in solvent (10 mL) at a cat/alcohol ratio of 1:20 at 30 °C, for 24 hours; H₂O₂ was added with a syringe pump in 2h. [b] Conversions and selectivity were calculated after 24 h by ¹H NMR using CH₂Br₂ as the internal standard and confirmed by GC (dodecane as the internal standard).

6.7.6 Experiment in presence of BHT as radical scavenger:



Entry	BA Conv (%) ^[b]	BHA Select (%) ^[b]	BZA Select (%) ^[b]
27	7	99	-

Reactions were performed with [Fe^{III}] (2.5 x 10⁻² mmol) in CH₃CN (10 mL) at a cat/alcohol/BHT/H₂O₂ ratio of 1:20:80:80, at 30 °C for 24 hours; H₂O₂ was added with a syringe pump in 2h. [b] Conversions and selectivity were calculated after 24 h by ¹H NMR using CH₂Br₂ as the internal standard and confirmed by GC (dodecane as the internal standard).

6.7.7 GC-Methods:

Gas-chromatographic analyses were performed with GC-FAST technique using a Shimadzu GC-2010 equipped with a Supelco SLB™-5ms capillary column. Dodecane was used as ISTD. The samples were prepared with a concentration of 0.1-0.3 mg/mL in DCM.

Method A:***PTV parameters:***

Temperature = 220 °C

Injection mode: SPLIT

Pressure = 2.74 bar

Total flow = 11.2 mL/min

Column flow = 0.33 mL/min

Linear velocity = 33.7 cm/sec

Purge flow = 1 mL/min

Split Ratio = 30.0

FID parameters:

Temperature = 290 °C

Make-up gas: N₂/air

H₂ flow = 40 mL/min

Make-up flow = 30 mL/min

Air flow = 400 mL/min

Column program:

RATE	Temperature	Holding Time
-	100 °C	2 min
30 °C/min	170 °C	0 min
50 °C/min	270 °C	1 min

Method B:***PTV parameters:***

Temperature = 220 °C

Injection mode: SPLIT

Pressure = 2.74 bar

Total flow = 12.2 mL/min

Column flow = 0.36 mL/min

Linear velocity = 34.9 cm/sec

Purge flow = 1 mL/min

Split Ratio = 30.0

FID parameters:

Temperature = 290 °C

Make-up gas: N₂/air

H₂ flow = 40 mL/min

Make-up flow = 30 mL/min

Air flow = 400 mL/min

Column program:

RATE	Temperature	Holding Time
-	80 °C	0 min
10 °C/min	120 °C	0 min
60 °C/min	270 °C	0 min

Method C:***PTV parameters:***

Temperature = 220 °C

Injection mode: SPLIT

Pressure = 2.74 bar

Total flow = 21.1 mL/min

Column flow = 0.33 mL/min

Linear velocity = 33.7 cm/sec

Purge flow = 1 mL/min

Split Ratio = 60.0

FID parameters:

Temperature = 290 °C

Make-up gas: N₂/air

H₂ flow = 40 mL/min

Make-up flow = 30 mL/min

Air flow = 400 mL/min

Column program:

RATE	Temperature	Holding Time
-	100 °C	2 min
10 °C/min	145 °C	0 min
5 °C/min	165 °C	0 min
60 °C/min	270 °C	0.3 min

Method D:***PTV parameters:***

Temperature = 220 °C

Injection mode: SPLIT

Pressure = 2.74 bar

Total flow = 12.8 mL/min

Column flow = 0.38 mL/min

Linear velocity = 35.6 cm/sec

Purge flow = 1 mL/min

Split Ratio = 30.0

FID parameters:

Temperature = 290 °C

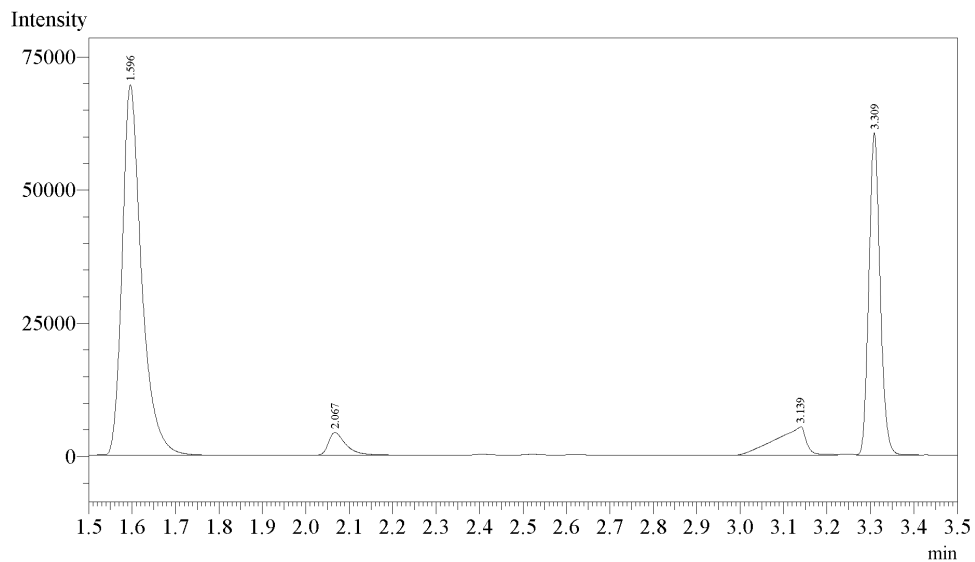
Make-up gas: N₂/airH₂ flow = 40 mL/min

Make-up flow = 30 mL/min

Air flow = 400 mL/min

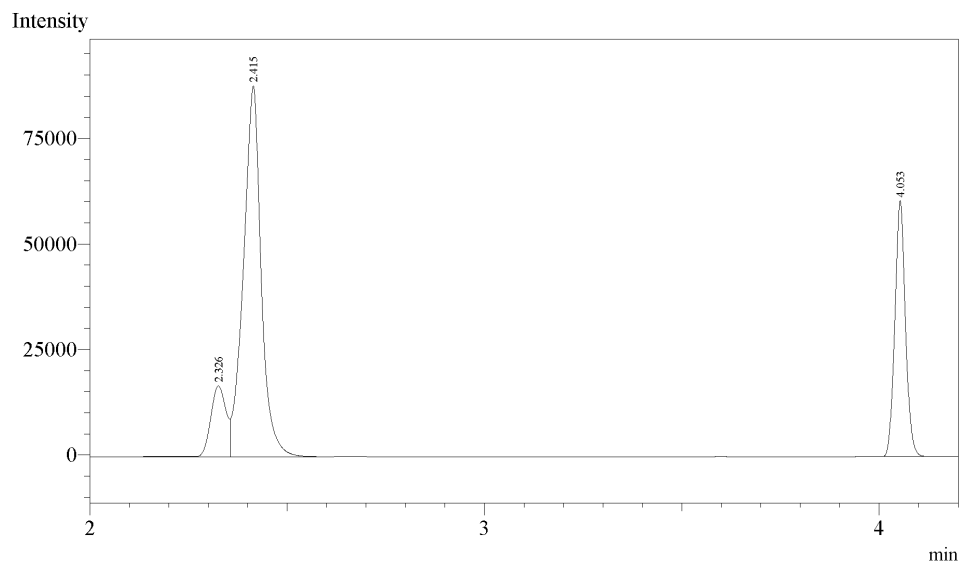
Column program:

RATE	Temperature	Holding Time
-	70 °C	3 min
25 °C/min	90 °C	0 min
60 °C/min	270 °C	0 min

6.7.8 GC chromatograms:**Benzyl alcohol oxidation (method A)**

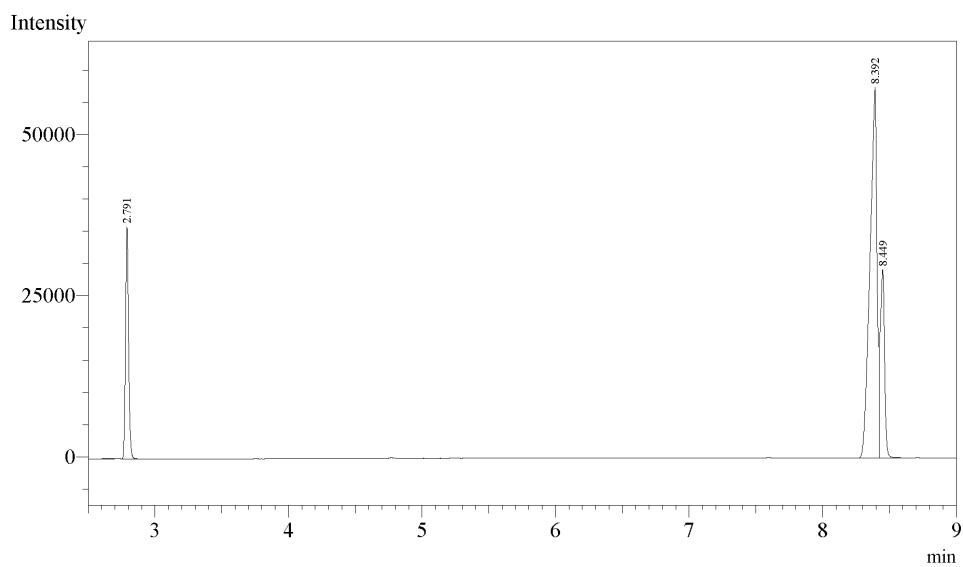
Substance	Retention time (min)	yield
Benzaldehyde, 13a	1.596	86%
Benzyl alcohol, 12a	2.067	4%
Benzoic acid, 14a	3.139	10%
Dodecane (ISTD)	3.309	-

1-Phenylethanol oxidation (method B)



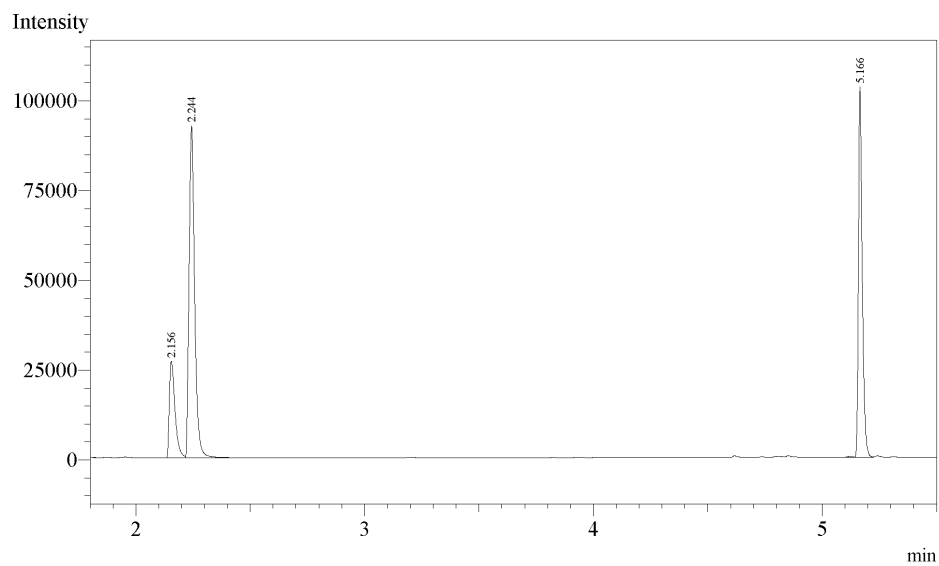
Substance	Retention time (min)	yield
1-Phenylethanol, 12h	2.326	16%
Acetophenone, 13h	2.415	84%
Dodecane (ISTD)	4.053	-

Benzhydrol oxidation (method C)



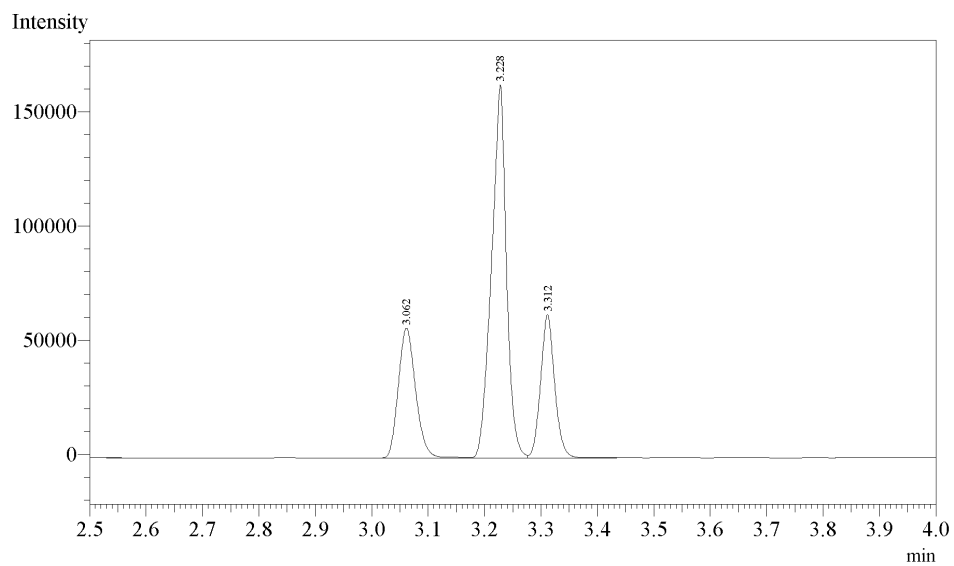
Substance	Retention time (min)	yield
Dodecane (ISTD)	2.791	-
Benzophenone, 13i	8.392	71%
Benzhydrol, 12i	8.449	28%

Cyclohexanol oxidation (method D)

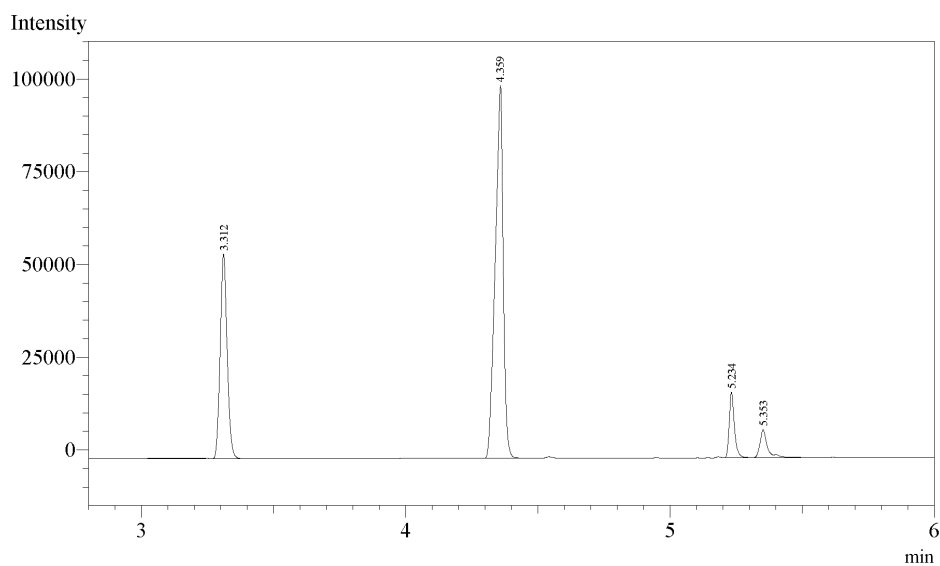


Substance	Retention time (min)	yield
Cyclohexanol, 12m	2.156	19%
Cyclohexanone, 13m	2.244	59%
Dodecane (ISTD)	5.166	-

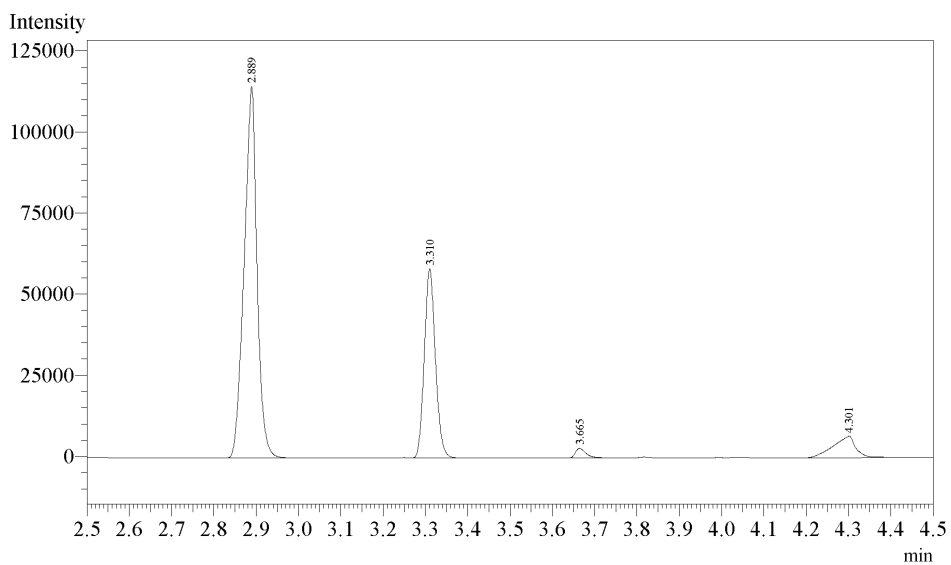
Menthol oxidation (method A)



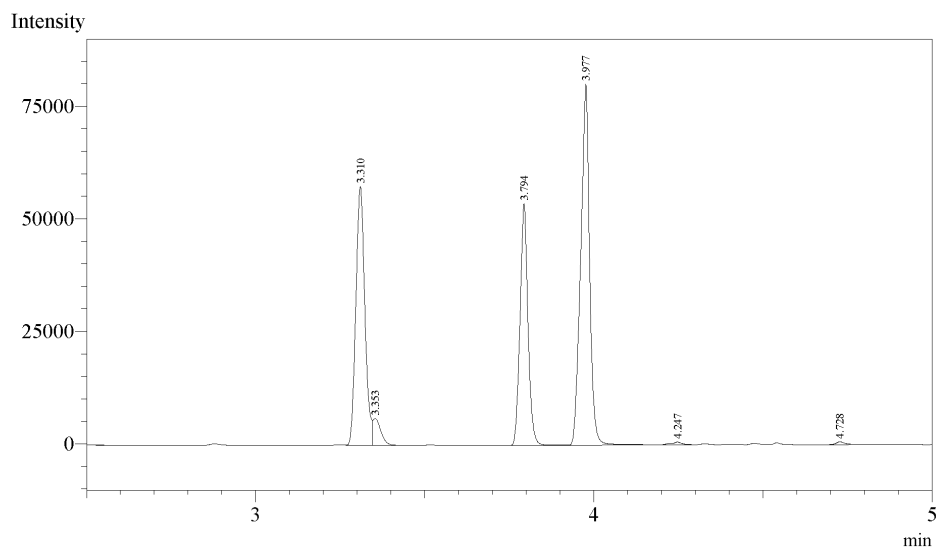
Substance	Retention time (min)	yield
Menthone, 13o	3.062	28%
Menthol, 12o	3.228	64%
Dodecane (ISTD)	3.312	-

p-nitrobenzyl alcohol oxidation (method A)

Substance	Retention time (min)	yield
Dodecane (ISTD)	3.312	-
<i>p</i> -nitrobenzaldehyde, 13b	4.359	85%
<i>p</i> -nitrobenzyl alcohol, 12b	5.234	9%
<i>p</i> -nitrobenzoic acid, 14b	5.353	4%

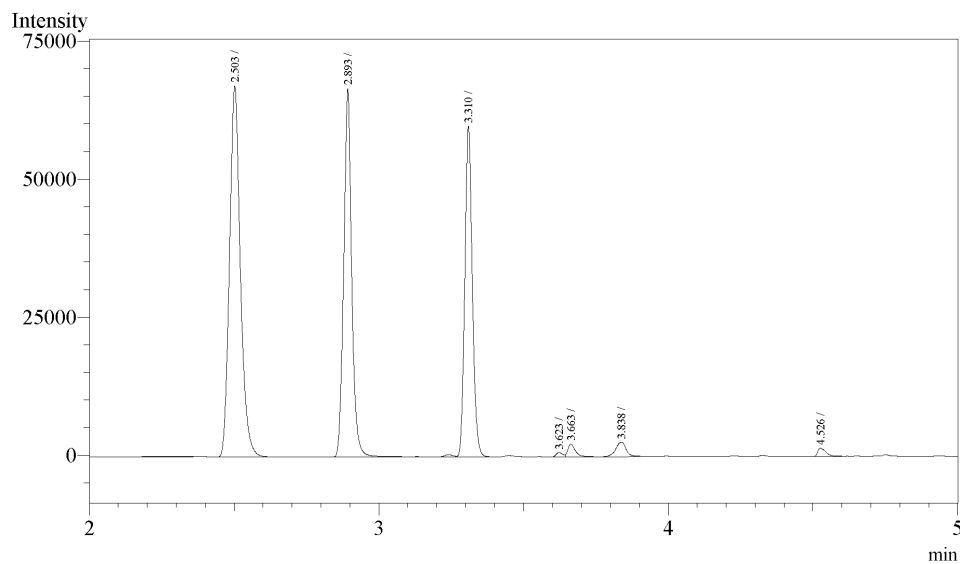
p-chlorobenzyl alcohol oxidation (method A)

Substance	Retention time (min)	yield
<i>p</i> -chlorobenzaldehyde, 13c	2.889	80%
Dodecane (ISTD)	3.310	-
<i>p</i> -chlorobenzyl alcohol, 12c	3.665	2%
<i>p</i> -chlorobenzoic acid, 14c	4.301	13%

p-methoxybenzyl alcohol oxidation (method A)

Substance	Retention time (min)	yield
Dodecane (ISTD)	3.310	-
<i>p</i> -methoxybenzaldehyde, 13e	3.794	31%
<i>p</i> -methoxybenzyl alcohol, 12e	3.977	54%

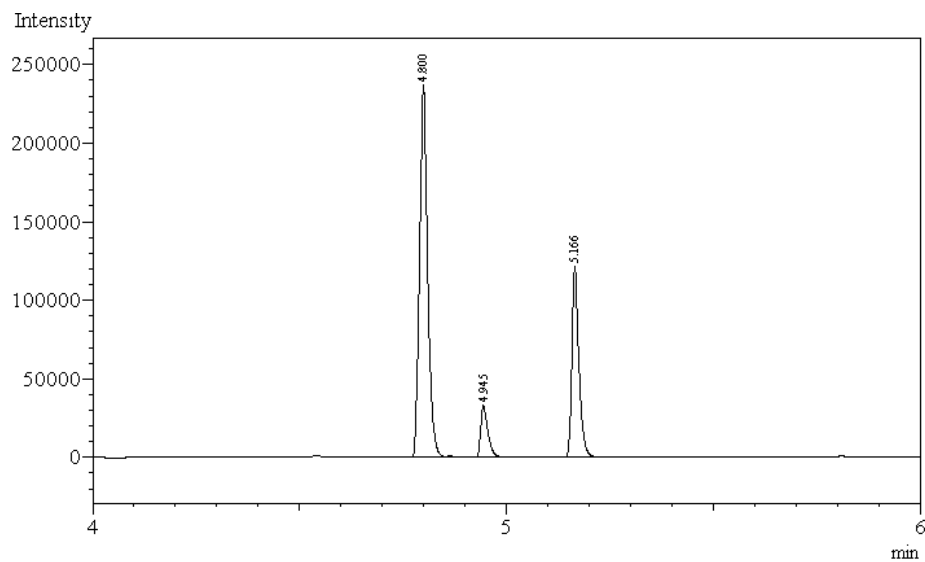
Overoxidation products after min 4

p-methylbenzyl alcohol oxidation (method A)

Substance	Retention time (min)	yield
<i>p</i> -methylbenzaldehyde, 13d	2.503	45%
<i>p</i> -methylbenzyl alcohol, 12d	2.893	33%
Dodecane (ISTD)	3.310	-

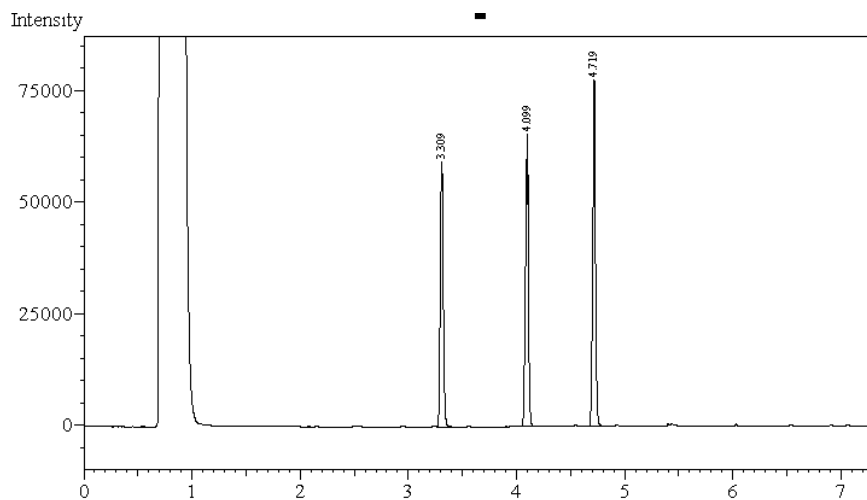
Overoxidation products after min 3.5

Cyclooctanol oxidation (method D)



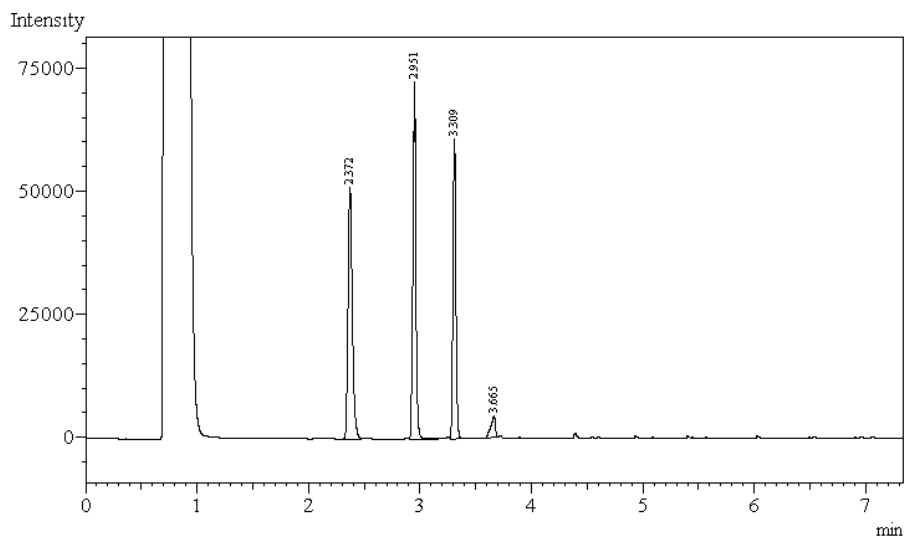
Substance	Retention time (min)	yield
Cyclooctanone, 13n	4.800	89%
Cyclooctanol, 12n	4.945	10%
Dodecane (ISTD)	5.166	-

2-Nitrobenzyl alcohol oxidation (method A)



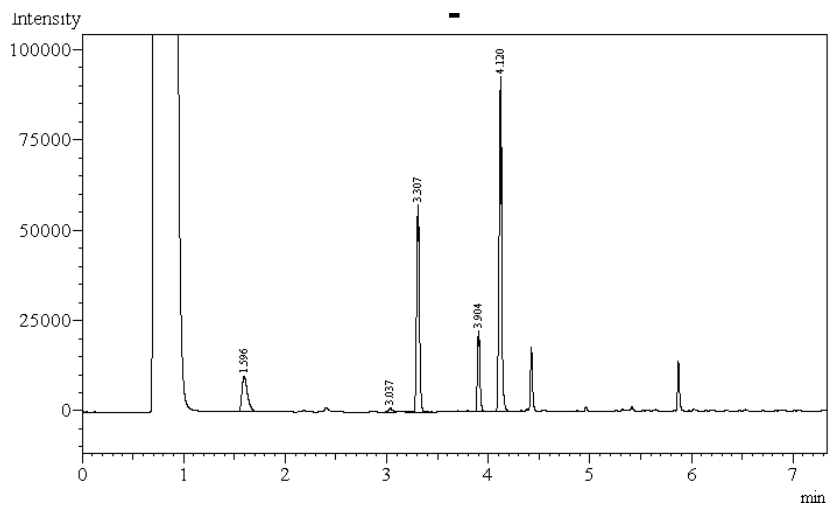
Substance	Retention time (min)	yield
2-Nitrobenzaldehyde, 13f	4.099	44%
2-Nitrobenzyl alcohol, 12f	4.719	45%
Dodecane (ISTD)	3.309	-

2-Methylbenzyl alcohol oxidation (method A)



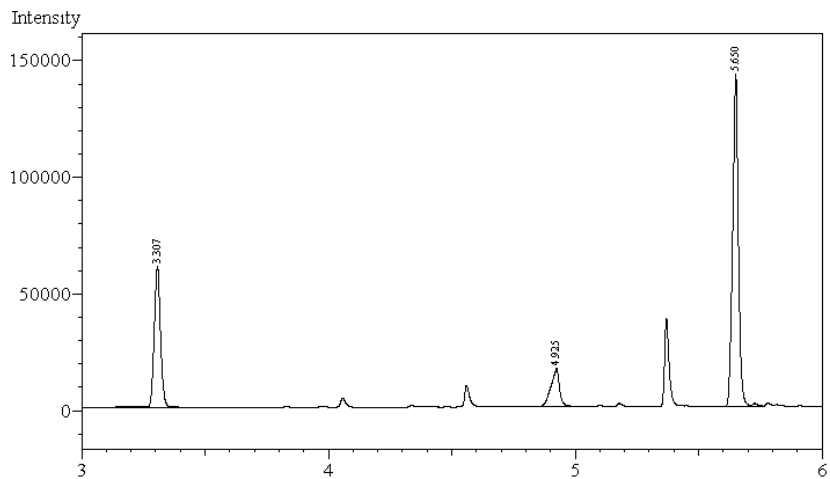
Substance	Retention time (min)	yield
2-Methylbenzaldehyde, 13g	2.372	50%
2-Methylbenzyl alcohol, 12g	2.951	36%
2-Methylbenzoic acid, 14g	3.665	10%
Dodecane (ISTD)	3.372	-

Cinnamyl alcohol oxidation (method A)



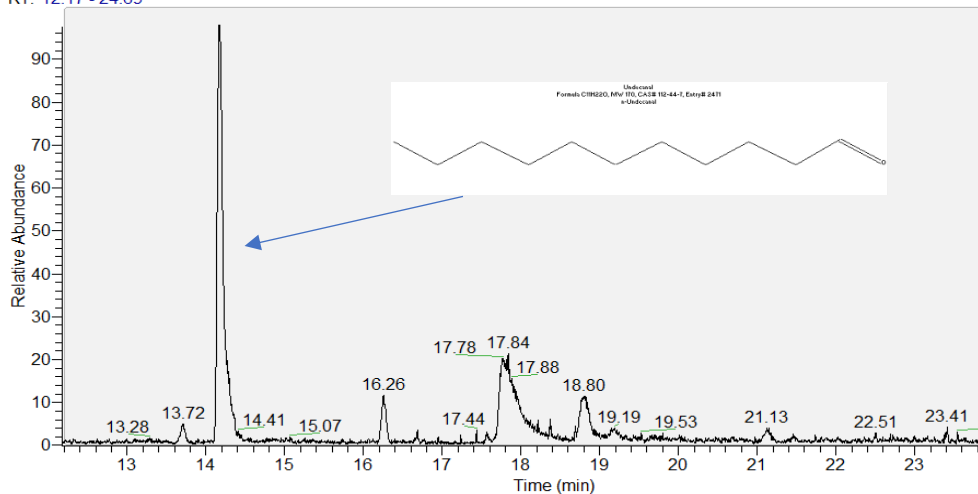
Substance	Retention time (min)	yield
Benzaldehyde, 13a	1.596	15%
Cinnamaldehyde, 13r	3.904	10%
Cinnamyl alcohol, 12r	4.120	40%
Dodecane (ISTD)	3.307	-

1,2-dodecanediol oxidation (method A)

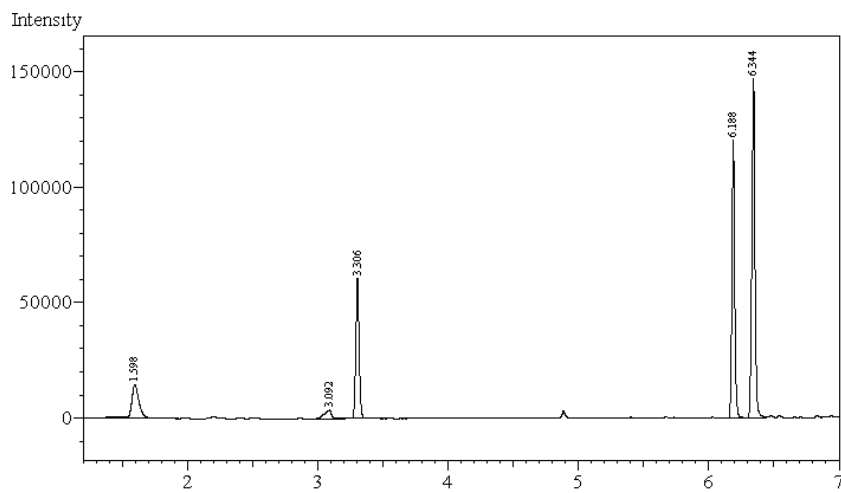


Substance	Retention time (min)	yield
Undecanal (confirmed by GC-MS), 13w	4.925	35%
1,2-dodecanediol, 12v	5.650	50%
1-hydroxy-2-dodecanone, 13v	5.365	7,5%
Dodecane (ISTD)	3.307	-

RT: 12.17 - 24.69

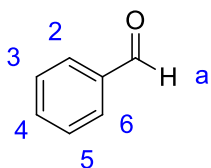


Hydrobenzoin oxidation (method A)



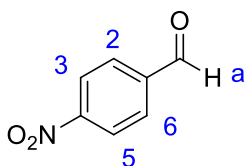
Substance	Retention time (min)	yield
Benzaldehyde, 13a	1.598	11%
Benzoic acid, 14a	3.092	1%
Benzyl (diketone), 13u	6.188	28%
Hydrobenzoin, 12u	6.344	39%
Dodecane (ISTD)	3.306	-

6.7.9 Products characterization:

**Product 13a:**

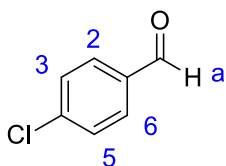
$^1\text{H NMR}$ (300 MHz; CDCl_3 ; T = 300K)

δ 10.05 (s, 1H, H_a), 7.91 (d, 2H, $\text{C}_{2,6}$), 7.64 – 7.56 (m, 3H, $\text{C}_{3,5,4}$).

**Product 13b:**

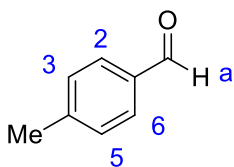
$^1\text{H NMR}$ (300 MHz; CDCl_3 ; T = 300K)

δ 10.18 (s, 1H, H_a), 8.39 (d, 2H, $\text{H}_{3,5}$), 8.08 (d, 2H, $\text{H}_{2,6}$).

**Product 13c:**

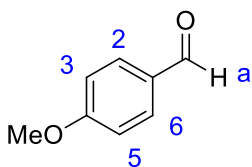
$^1\text{H NMR}$ (300 MHz; CDCl_3 ; T = 300K)

δ 9.98 (s, 1H, H_a), 7.82 (d, 2H, $\text{H}_{3,5}$), 7.51 (d, 2H, $\text{H}_{2,6}$).

**Product 13d:**

$^1\text{H NMR}$ (300 MHz; CDCl_3 ; T = 300K)

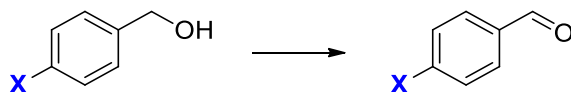
δ 9.93 (s, 1H, H_a), 7.76 (d, 2H, $\text{H}_{2,6}$), 7.32 (d, 2H, $\text{H}_{3,5}$), 2.43 (s, 3H, Me).

**Product 13e:**

$^1\text{H NMR}$ (300 MHz; CDCl_3 ; T = 300K)

δ 9.87 (s, 1H, H_a), 7.85 (d, 2H, $\text{H}_{2,6}$), 7.02 (d, 2H, $\text{H}_{3,5}$), 3.90 (s, 3H, OCH_3).

6.7.10 Kinetic experiments, Hammett plot:



The reaction has been performed on different substituted benzylic alcohols. The rate constants were calculated by mean of conversion of the substrate at different times.

X	K (s ⁻¹)
H	6,1·10 ⁻⁵
Me	8,7·10 ⁻⁵
Cl	4,1·10 ⁻⁵
NO ₂	3,1·10 ⁻⁵

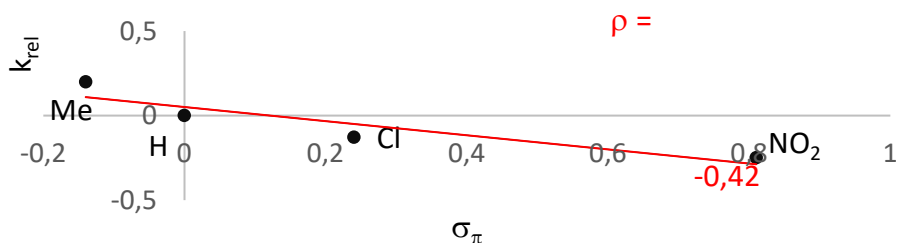
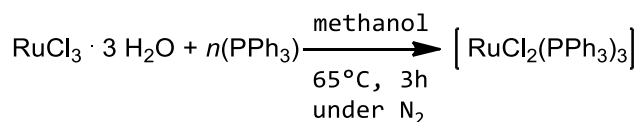


Figure E1. Hammett plot of the oxidation of benzyl alcohol **12a** by complex **5b**

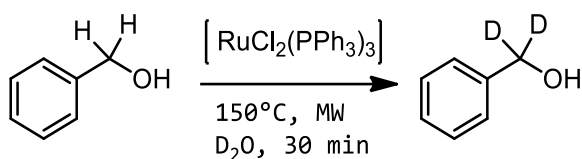
6.7.11 Synthesis of *tris*(triphenylphosphine)ruthenium dichloride: ^[240]



Ruthenium trichloride trihydrate (3.8 mmol) was dissolved in refluxing methanol under nitrogen atmosphere and stirred until dissolution. After cooling, triphenylphosphine (23 mmol) was added and the mixture was again refluxed for 3 hours. The product precipitates on cooling as black shiny crystals. From the filtrate, upon cooling, another product precipitates which was identified as *tetrakis*(triphenylphosphine)ruthenium dichloride.

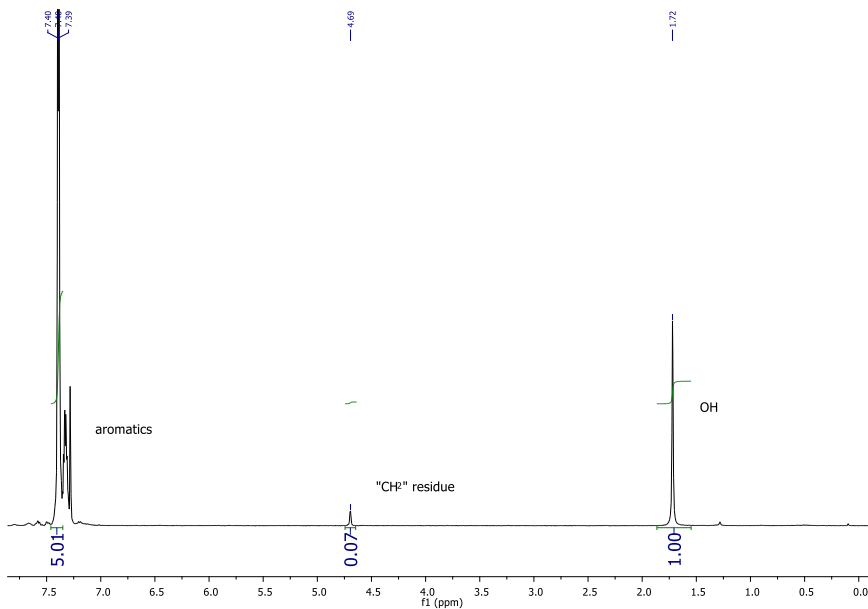
The product was used without further purification, both *tris*- and *tetrakis*- complex.

6.7.12 Synthesis of deuterated benzyl alcohol:

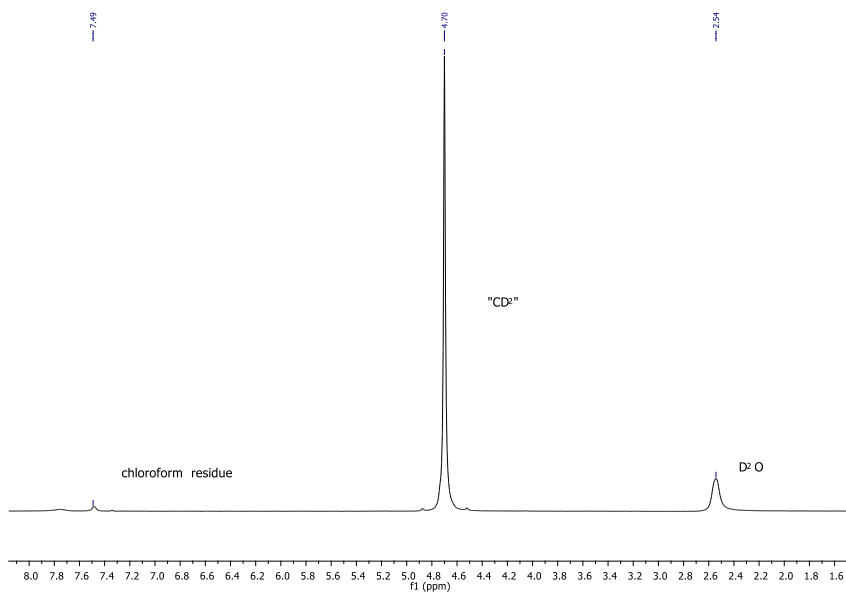


Synthesis of $\alpha,\alpha\text{-d}^2$ -benzyl alcohol was carried out following an already reported procedure^[241], using $\text{RuCl}_2(\text{PPh}_3)_3$ as a catalyst and D_2O as deuterium source under microwave heating. The ruthenium complex was synthesized as reported in literature. ^1H and ^2H NMR spectral data of $\alpha,\alpha\text{-d}^2$ -benzyl alcohol are in agreement with those reported in the literature.

Additional information: the reaction can be performed both with *tris*- and *tetrakis*- complex, prolonging the reaction further up to 1 hour.



^1H NMR of $\alpha,\alpha\text{-d}_2$ -benzyl alcohol in CDCl_3



^2H NMR of $\alpha,\alpha\text{-d}_2$ -benzyl alcohol in CHCl_3

Kinetic isotopic effect:

The evaluation of KIE was done by calculating the rate constant of the conversion of benzyl alcohol vs deuterated benzyl alcohol, catalyzed by complex **5b**.

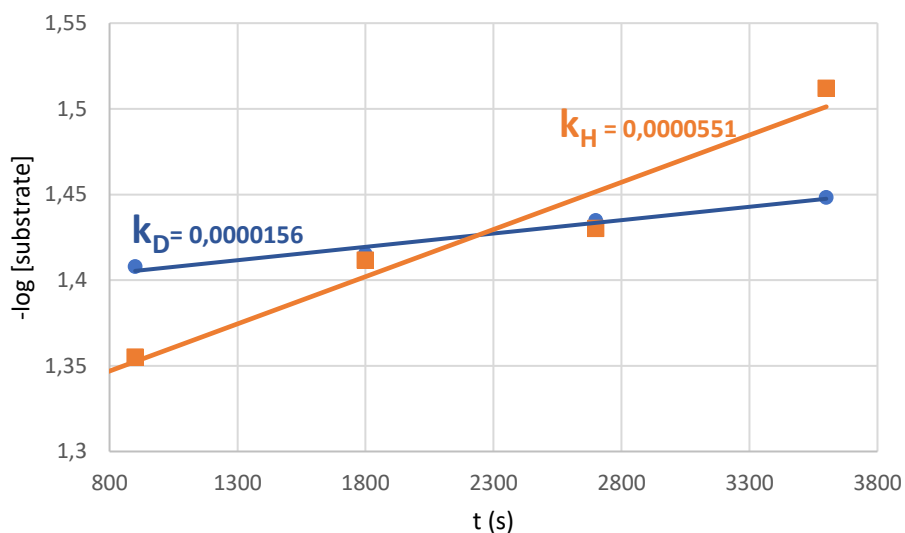


Figure E2. KIE experimental rate slopes for the oxidation of benzyl alcohol by complex **5b**

The kinetic constant of the oxidation of α,α -d²-benzyl alcohol was found to be $1.56 \cdot 10^{-5} \text{ s}^{-1}$ and thus the KIE, expressed as (k_H/k_D) , is equal to **3.52**.

6.8 SYNTHESIS OF OXO-BRIDGED IRON COMPLEXES OF PYCLEN LIGANDS:

The synthesis and structural characterization of the iron complexes is described in the previous chapters (see experimental section).

Identification code	10	9	8
Empirical formula	(C ₄₄ H ₆₀ Br ₄ Fe ₂ N ₄ O)· 1.35(CH ₃ CONH ₂)·0.6(CH ₃ CN)	(C ₆₄ H ₇₂ Br ₃ Fe ₃ N ₈ O ₂)· 1.5(CH ₃ CN) ·2(CH ₃ OH)	(C ₂₂ H ₃₆ Br ₄ Fe ₂ N ₈ O) ·3(CH ₃ OH)
Formula weight (g mol ⁻¹)	1188.06	1676.04	943.96
Temperature (K)	150(2)	150(2)	150(2)
Wavelength (Å)	0.71073	0.71073	0.71073
Crystal system	Triclinic	Orthorhombic	Monoclinic
Space group	<i>P</i> $\bar{1}$	<i>Pca</i> 2 ₁	<i>C</i> 2/ <i>m</i>
Unit cell dimensions			
a (Å)	9.745(3)	22.073(2)	12.414(1)
b (Å)	15.884(6)	13.646(2)	17.616(1)
c (Å)	19.997(7)	24.473(3)	8.5625(7)
α (°)	78.260(4)	90	90
β (°)	76.346(4)	90	109.113(1)
γ (°)	72.282(4)	90	90
Volume (Å ³)	2836(3)	7371(2)	1769.3(4)
Z	2	4	2
Calculated density (Mg m ⁻³)	1.391	1.510	1.772
Absorption coefficient (mm ⁻¹)	3.368	3.344	5.379
F(000)	1200	3392	932
Crystal size (mm ³)	0.283 x 0.126 x 0.121	0.353 x 0.306 x 0.102	0.332 x 0.297 x 0.203
Theta range for data collection (°)	1.360 to 24.860	1.492 to 28.759	2.086 to 28.433
Index ranges	-11 ≤ h ≤ 11, -18 ≤ k ≤ 18, -23 ≤ l ≤ 23	-29 ≤ h ≤ 29, -18 ≤ k ≤ 18, -33 ≤ l ≤ 33	-16 ≤ h ≤ 16, -23 ≤ k ≤ 23, -11 ≤ l ≤ 11
Reflections collected	18530	67187	8126
Independent reflections	9739 [R _(int) = 0.0638]	19058 [R _(int) = 0.0390]	2301 [R _(int) = 0.0145]
Max. and min. transmission	0.7449 and 0.5207	0.7458 and 0.5648	0.7454 and 0.5636
Refinement method	Full-matrix least-squares on F ²	Full-matrix least-squares on F ²	Full-matrix least-squares on F ²
Data / restraints / parameters	9739 / 28 / 550	19058 / 12 / 786	2301 / 3 / 115
Goodness-of-fit on F ²	0.988	1.07	1.059
Final R indices [I > 2σ(I)]	R ₁ = 0.0563, wR ₂ = 0.1443	R ₁ = 0.0451, wR ₂ = 0.1033	R ₁ = 0.0293, wR ₂ = 0.0748
R indices (all data)	R ₁ = 0.1023, wR ₂ = 0.1622	R ₁ = 0.0585, wR ₂ = 0.1094	R ₁ = 0.0319, wR ₂ = 0.0762
Largest diff. peak and hole (e Å ⁻³)	1.138 and -1.355	1.820 and -1.627	1.134 and -0.930
CCDC deposition number	2175110	2175109	2175108

Table E1. Summary of structural information of complex **10**, **9** and **8**

Raman characterization:

Micro-Raman spectroscopy was carried out using a Horiba LabRam HR evolution at the Dipartimento di Scienze della Terra “A. Desio” of the Università degli Studi di Milano. The spectrometer is equipped with a Nd-Yag 532 nm/100mW with Ultra Low Frequency (ULF) filters. Scattered light was collected by a 100X objective (NA aperture = 0.9) in backscattering geometry; a diffraction grating with 600 lines/mm and the hole set at 200 μm were used. The spectra have been detected by a Peltier-cooled Charge Couple Detector. To balance signal to noise and to reduce the damage of the highly absorbing samples 3 accumulations for 60 seconds were collected with a laser power set to 0.1%. Instrument calibration was performed before each round of analysis using the peak at 520.70 cm^{-1} of a silicon wafer.

5b	8	6c	9	7	10	Assignment
		861	873		849	ν_{as} (Fe-O-Fe)
447	451					ν (Fe-N)
	409	378	367		414	ν_{s} (Fe-O-Fe)
381						ν (Fe-N)
302				294		
277						
252						ν (Fe-Br)
		212	217		217	
				203		
		158			154	δ (Fe-O-Fe)
94				90	92	δ (Br-Fe-Br)

Resonance values are expressed in cm^{-1}

Table E2. Summary of Raman resonance values of complexes **8,9,10** and the corresponding precursor.

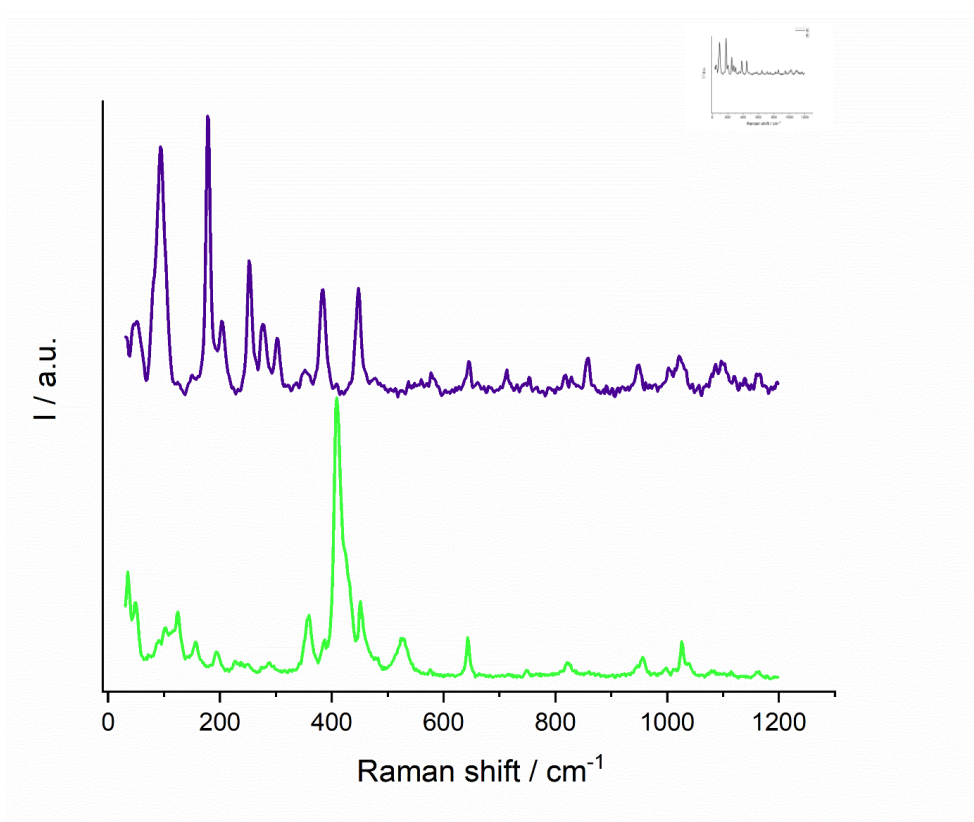
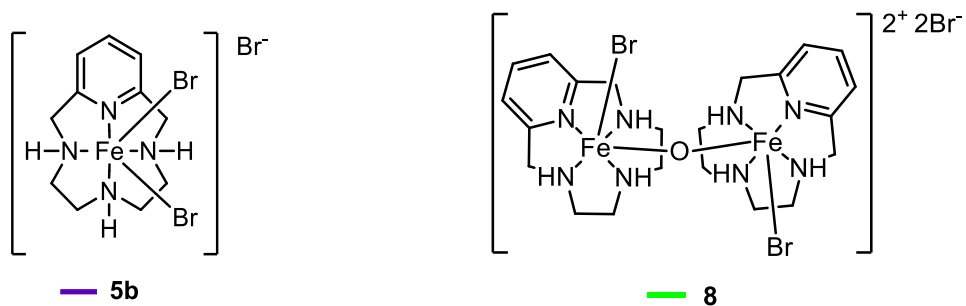


Figure E3. Raman spectra of complex **5b** and **8**

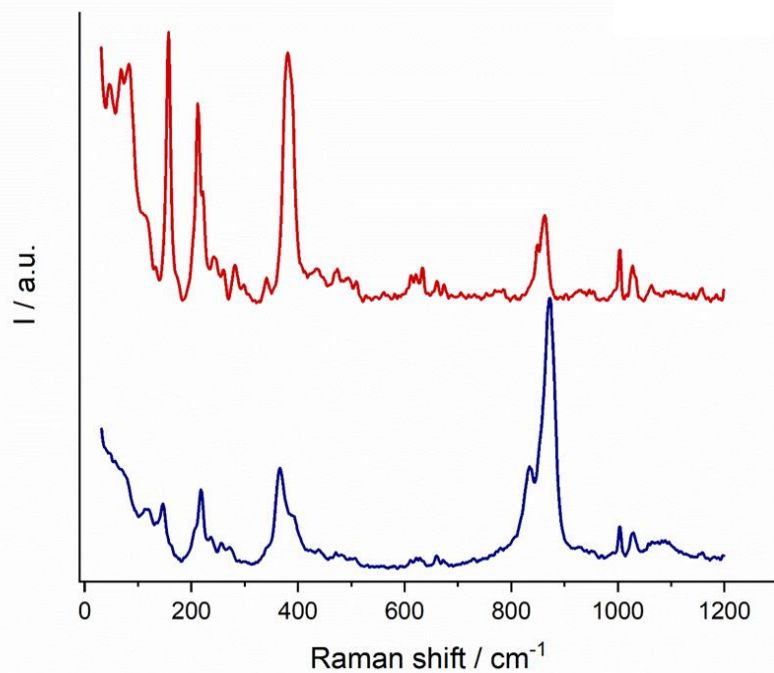
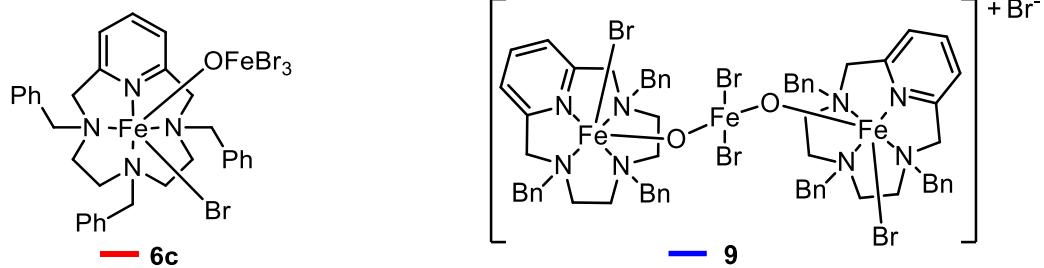


Figure E4. Raman spectra of complex **6c** and **9**

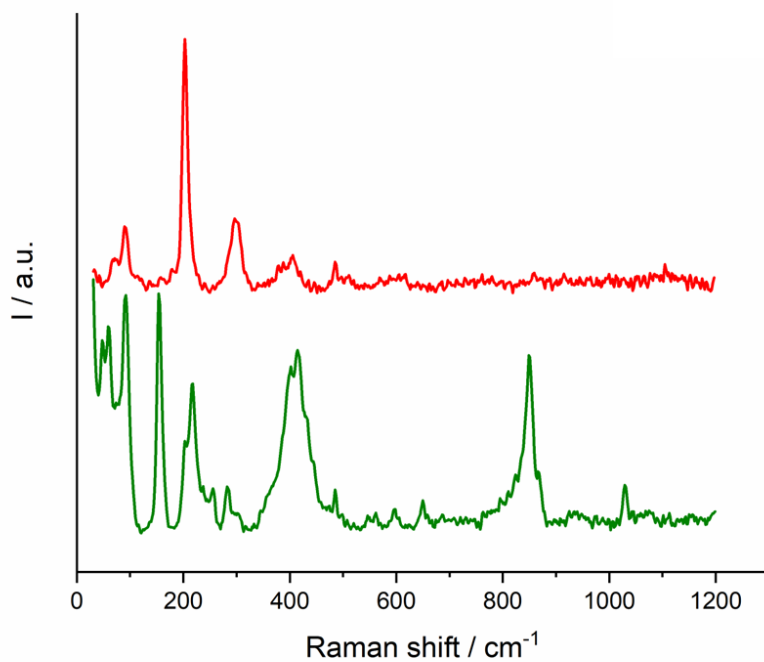
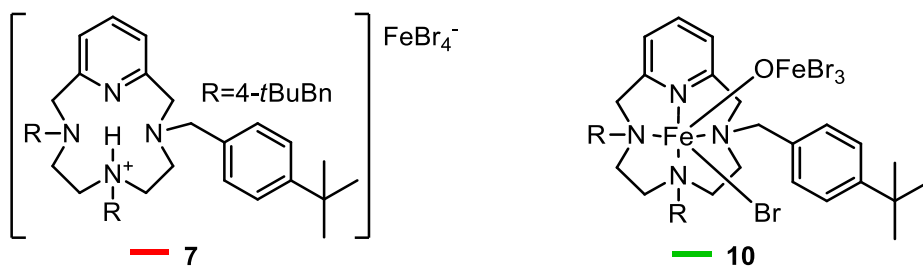


Figure E5. Raman spectra of complex **7** and **10**

6.9 CYCLIC CARBONATES SYNTHESIS FROM CO₂ AND EPOXIDES:

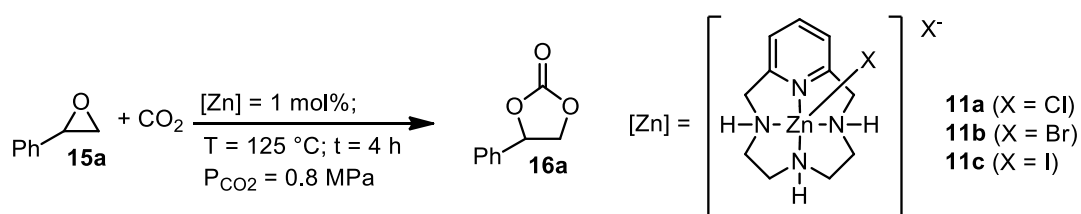
6.9.1 Zinc PycLen complexes:

The synthesis and characterization of the zinc complexes is described in the previous chapters (see experimental section, synthesis of ligands and their complexes).

6.9.2 General catalytic procedure:

In a 2.5 mL glass liner equipped with a screw cap and glass wool, the catalyst and the epoxide (250 μ L) were added. The vessel was transferred into a 250 mL stainless-steel autoclave; CO₂ was charged at room temperature (0.2 or 0.4 or 0.8 MPa). The autoclave was placed in a preheated oil bath (at 75 or 100 or 125 °C) and it was left to react under stirring for 2 to 4 hours, then it was cooled to room temperature in an ice bath and vented. The crude was treated with chloroform (700 μ L) and a sample (150 μ L) was analysed by quantitative ¹H NMR spectroscopy by using mesitylene as ISTD.

6.9.3 Reaction optimization:



Entry	Catalyst	Conversion 15a (%) ^[b]	Selectivity 16a (%) ^[b]	TOF (h ⁻¹) ^[c]	TON ^[d]
1	TBACl (2%)	97	99	12	48,5
2	TBACl (1%)	70	97	17,5	70
3	11a (1%) - TBACl (2%)	90	95	11	45
4	11a (1%)	78	92	19,5	78
5	ZnCl ₂ (1%)	22	-	5,5	22

6	TBAB (2%)	99	91	12	49,5
7	TBAB (1%)	60	96	15	60
8	11b (1%)- TBAB (2%)	>99	>99	12	49,5
9	11b (1%)	>99	>99	25	>99
10	ZnBr ₂ (1%)	99	-	25	99
11	TBAI (2%)	95	99	12	47,5
12	TBAI (1%)	52	99	13	52
13	2c (1%)- TBAI (2%)	96	93	12	48
14	11c (1%)	99	97	25	99
15	Ligand 2 (1%)	5	-	-	-

Reactions conditions: neat, 250 μ L of **15a** (2.19 mmol), at 125 $^{\circ}$ C; P(CO₂) = 0.8 MPa; reaction time = 4 h. [b] Conversion and selectivity determined by ¹H NMR using mesitylene as internal standard. [c] Turnover frequency ($\text{mol}_{3a} \cdot \text{mol}_{\text{cat}}^{-1} \cdot \text{reaction time}^{-1}$). [d] Turnover number ($\text{mol}_{3a} \cdot \text{mol}_{\text{cat}}^{-1}$).

6.9.4 Catalyst loading screening:

Entry	Cat.	Loading (mol%)	Conversion 15a (%) ^[b]	Selectivity 16a (%) ^[b]	TOF (h^{-1}) ^[c]	TON ^[d]
16	11b	1	>99	>99	>33	>99
17	11b	0.5	>99	>99	67	200
18	11b	0.1	53	>99	177	530
19	11b	0.01	2	>99	667	200
20	11c	1	>99	95	>33	>99
21	11c	0.5	>99	95	67	200
22	11c	0.1	83	94	277	830

Reactions conditions: neat, 250 μ L of **15a** (2.19 mmol), at 125 $^{\circ}$ C; P(CO₂) = 0.8 MPa; reaction time = 3 h. [b] Conversion and selectivity determined by ¹H NMR using mesitylene as internal standard. [c] Turnover frequency ($\text{mol}_{3a} \cdot \text{mol}_{\text{cat}}^{-1} \cdot \text{reaction time}^{-1}$). [d] Turnover number ($\text{mol}_{3a} \cdot \text{mol}_{\text{cat}}^{-1}$).

Temperature optimization experiments:

Entry	Cat.	T (°C)	Conversion 15a (%) ^[b]	Selectivity 16a (%) ^[b]	TOF (h ⁻¹) ^[c]	TON ^[d]
23	11b	100	30	61	15	60
24	11b	75	10	10	5	20
25 ^[e]	11b	100	58	97	29	116
26 ^[e]	11b	75	39	82	19,5	78
27	11c	100	93	84	42	168
28	11c	75	42	12	12	24

Reactions conditions: neat, 250 μL of **15a** (2.19 mmol), catalyst loading 0.5 mol%, $P(\text{CO}_2) = 0.8$ MPa; reaction time = 4 h. [b] Conversion and selectivity determined by ¹H NMR using mesitylene as internal standard. [c] Turnover frequency ($\text{mol}_{3a} \cdot \text{mol}_{\text{cat}}^{-1} \cdot \text{reaction time}^{-1}$). [d] Turnover number ($\text{mol}_{3a} \cdot \text{mol}_{\text{cat}}^{-1}$). [e] The catalyst is previously dissolved in 250 μL of DMSO as co-solvent.

6.9.5 Reaction time optimization:

Entry	Cat.	Time (h)	Conversion 15a (%) ^[b]	Selectivity 16a (%) ^[b]	TOF (h ⁻¹) ^[c]	TON ^[d]
29	11b	1	22	>99	22	22
30	11b	2	86	>99	43	86
31	11b	2.5	94	>99	38	94
32	11b	3	99	>99	33	99
9	11b	4	>99	>99	25	>99

Reactions conditions: neat, 250 μL of **15a** (2.19 mmol), **11b** = 1 mol%, TBAB = 2 mol%, at 125 °C; $P(\text{CO}_2) = 0.8$ MPa. [b] Conversion and selectivity determined by ¹H NMR using mesitylene as internal standard. [c] Turnover frequency ($\text{mol}_{3a} \cdot \text{mol}_{\text{cat}}^{-1} \cdot \text{reaction time}^{-1}$). [d] Turnover number ($\text{mol}_{3a} \cdot \text{mol}_{\text{cat}}^{-1}$).

6.9.6 Influence of the pressure of CO₂:

Entry	Cat.	P CO ₂ (MPa)	Conversion 15a (%) ^[b]	Selectivity 16a (%) ^[b]	TOF (h ⁻¹) ^[c]	TON ^[d]
9	11b	0.8	>99	>99	25	>99
33	11b	0.4	>99	89	22	89
34	11b	0.2	79	53	13	53
35	11b	0.1	77	31	8	31

Reactions conditions: neat, 250 μ L of **15a** (2.19 mmol), **11b** = 1%, at 125 $^{\circ}$ C; reaction time = 4 h. [b] Conversion and selectivity determined by ¹H NMR using mesitylene as internal standard. [c] Turnover frequency ($\text{mol}_{3a} \cdot \text{mol}_{\text{cat}}^{-1} \cdot \text{reaction time}^{-1}$). [d] Turnover number ($\text{mol}_{3a} \cdot \text{mol}_{\text{cat}}^{-1}$).

6.9.7 Catalyst recycling (reaction re-run):

Three vials (see general catalytic method) were subjected to the reaction. At the end, after the venting of the autoclave, the reaction mixture in the first vial was diluted with chloroform (700 μ L), and a sample (150 μ L) was analysed by quantitative ¹H NMR spectroscopy by using mesitylene as the internal standard. Fresh styrene oxide (**15a**) (250 μ L, 2.19 mmol) was added to the remaining 2 vials. The autoclave was charged again with CO₂ and left to react in the exact same conditions for additional 3 h. At the end of the second run, the procedure was repeated on the second vial. In the end, fresh styrene oxide (**15a**) (250 μ L, 2.19 mmol) was added to the reaction mixture into the third vial. The autoclave was charged again with CO₂ and left to react in the exact same conditions for additional 3 h. At the end of the third run, fresh styrene oxide (**15a**) (250 μ L, 2.19 mmol) was directly added to the reaction mixture into the remaining vial, then the autoclave was charged again with CO₂ and left for further 3 h. At the end of the last cycle of reaction, the crude was treated diluted chloroform (700 μ L). An aliquot (150 μ L) was analysed by quantitative ¹H NMR spectroscopy by using mesitylene as the internal standard.

The results, in terms of conversion of **15a** and selectivity for **16a**, are summarized in the following table:

Entry	Cat.	Run	Conversion 15a (%) ^[b]	Selectivity 16a (%) ^[b]	TOF (h ⁻¹) ^[c]	TON ^[d]
36	11b	1 st	>99	99	66	200
37	11b	2 nd	>99	95	63	390
38	11b	4 th	>99	88	59	756

Reactions conditions: neat, 250 μ L of **15a** (2.19 mmol), **11b** = 0.5%, at 125 $^{\circ}$ C; P(CO₂) = 0.8 MPa; reaction time = 3 h. [b] Conversion and selectivity determined by ¹H NMR using 1,3,5-trimethylbenzene as internal standard (see Catalyst recycle). [c] Turnover frequency (mol_{3a}·mol_{cat}⁻¹·reaction time⁻¹). [d] Turnover number (mol_{3a}·mol_{cat}⁻¹).

6.9.8 Catalyst recovery:

In a 3 mL glass liner equipped with a screw cap and glass wool, the catalyst (**11b**) (0.050 g, 0.5 mol%) and the styrene oxide (**15a**) (2.5 mL, 21.9 mmol) were added. The vessel was transferred into a 250 mL stainless-steel autoclave; three vacuum-nitrogen cycles were performed, and CO₂ was charged at room temperature (0.8 MPa). The autoclave was placed in a preheated oil bath (125 $^{\circ}$ C) and it was left to react under stirring (for 3 hours), then it was cooled at room temperature in an ice bath and slowly vented. The crude was treated with chloroform (4.0 mL) to precipitate the catalyst. The latter was filtered and washed with chloroform (2.0 mL). An aliquot of the filtrate (200 μ L) was analysed by ¹H NMR spectroscopy by using mesitylene as ISTD.

The recovered catalyst (0.038 g) was analysed by elemental analysis and by ¹H NMR spectroscopy. The analyses showed no traces of catalyst degradation; however, the elemental analysis showed a slightly higher content of carbon and lower nitrogen than expected.

Elem. An. (Fresh) C₁₁H₁₈Br₂N₄Zn·2H₂O Calculated: C 28.26, H 4.74, N 11.98; found: C 28.51, H 4.30, N 11.84

Elem. An. (Recovered) C₁₁H₁₈Br₂N₄Zn·2 H₂O Calculated: C 28.26, H 4.74, N 11.98; found: C 29.54, H 3.87, N 8.67

¹H NMR (400 MHz, in d₆-DMSO)

δ 8.10 (t, J = 7.7 Hz, 1H), 7.52 (d, 2H), 4.79 – 4.75 (m, 1H), 4.69 – 4.65 (m, 2H), 4.38 (d, J = 6.8 Hz, 1H), 4.34 (d, J = 6.7 Hz, 1H), 3.92 (s, 1H), 3.88 (s, 1H), 2.97 – 2.83 (m, 2H), 2.78 – 2.73 (m, 2H), 2.46 – 2.35 (m, 2H), 2.15 – 2.11 (m, 2H).

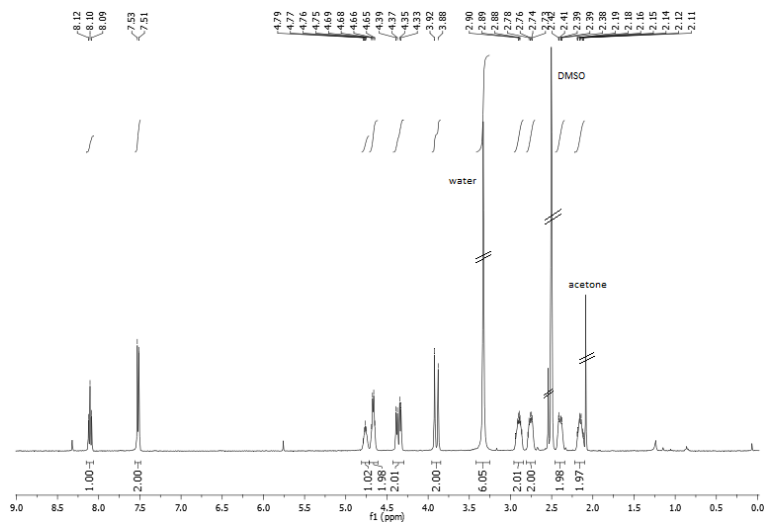


Figure E6. ^1H NMR spectra of recovered **11b** after a catalytic run.

6.9.9 Synthesis of Eugenol glycidyl ether:

Synthesis of eugenol epoxide (**15m**):^[242]

A solution of m-CPBA (80%) (1.7257 g, 10 mmol) was added dropwise to a solution of eugenol (0.8211 g, 5 mmol) in chloroform (25.0 mL) in 15 minutes at 0 °C under stirring. The mixture was left to react under nitrogen at room temperature for 2 hours. The reaction mixture was washed with a saturated aqueous solution of NaHCO_3 (10 mL x 3) and H_2O (10 mL x 3). The reunited organic phases were treated with Na_2SO_4 , filtered and the solvent was evaporated under vacuum at room temperature. The crude was purified via flash chromatography over silica gel, using hexane-diethyl ether as eluent (9:2). The product was isolated as a brownish oil.

Yield: 60%

^1H NMR (300 MHz; CDCl_3 ; T = 300 K)

δ 6.88 (d, J = 8.0 Hz, 1H), 6.78 (s, 1H), 6.75 (d, J = 1.5 Hz, 1H), 5.58 (s, 1H), 3.91 (s, 3H), 3.24 – 2.99 (m, 1H), 2.82 (dd, J = 8.2, 3.3 Hz, 3H), 2.56 (dd, J = 4.9, 2.7 Hz, 1H).

Data are consistent with the literature.

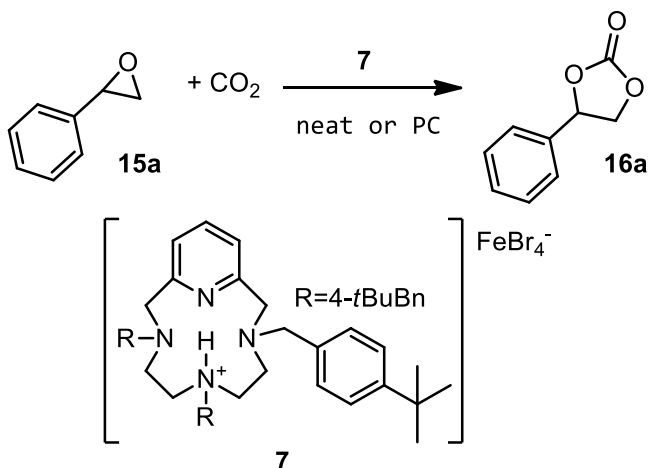
6.10 IRON PYCLEN COMPLEXES:

The synthesis and characterization of the iron complex **7** is described in the previous chapters (see experimental section).

6.10.1 General catalytic procedure:

A 250 mL stainless steel autoclave reactor was equipped with three 2.5 mL glass vials, containing the catalyst/epoxide mixture (0.25 mol% in 250 μ L of substrate). In certain cases, propylene carbonate was added as a solvent (in the case of solid epoxides). The vials were equipped with magnetic stirring bars and sealed with specific caps. The autoclave was then charged with 0.5 MPa CO₂ and vented-off. This operation was performed twice and then the autoclave was charged with 0.8 MPa CO₂ and placed in the heating bath for 4 hours. The reactor was then cooled and the CO₂ released. To each vial the appropriate amount of internal standard (mesitylene) and 1,0 mL of chloroform were added. 300 μ L of the solution were taken and diluted with 350 μ L of CDCl₃ to perform quantitative ¹H NMR analysis.

Reaction optimization:



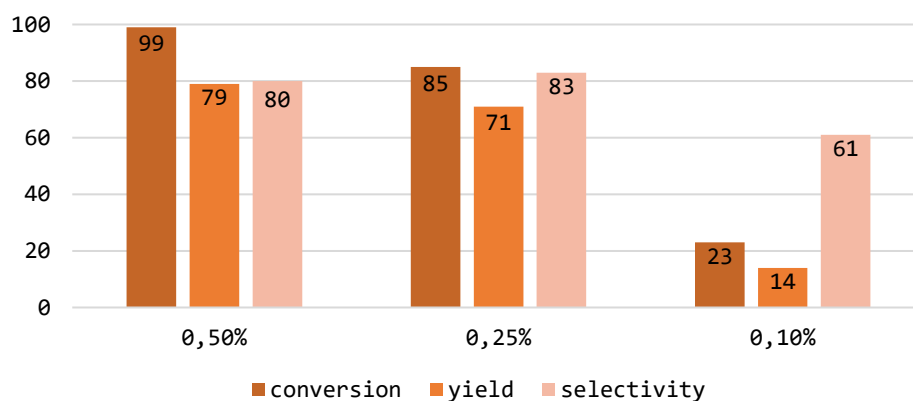
Scheme E1. Synthesis of styrene carbonate from styrene oxide and carbon dioxide.

6.10.2 Catalyst loading screening and blank experiment:

Entry	Catalyst loading (mol%)	Conversion 15a ^[b] %	Selectivity 16a ^[b] %	TOF (h ⁻¹) ^[c]
1	7 (0.5%)	99	80	50
2	7 (0.25%)	85	83	85
3	7 (0.1%)	23	61	57
4	FeBr₃ 0.5%	39	0	20

Reaction conditions: styrene oxide (SO) 2.19 mmol; T = 100 °C; P = 0.8 MPa; t = 4 h. [b] Conversion and selectivity determined by ¹H NMR using mesitylene as internal standard. [c] Turnover frequency ($\text{mol}_{15a(\text{converted})} \cdot \text{mol}_{\text{cat}}^{-1} \cdot \text{reaction time}^{-1}$).

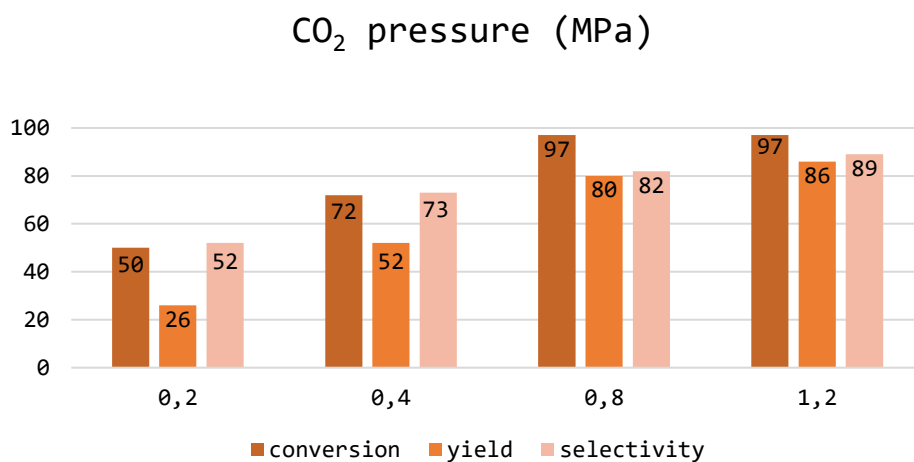
Catalyst loading



6.10.3 Influence of the pressure:

Entry	pCO ₂ (MPa)	Conversion 15a ^[b] %	Selectivity 16a ^[b] %	TOF (h ⁻¹) ^[c]
5	0.2	50	52	33
6	0.4	72	73	48
7	0.8	97	82	65
8	1.2	97	89	65

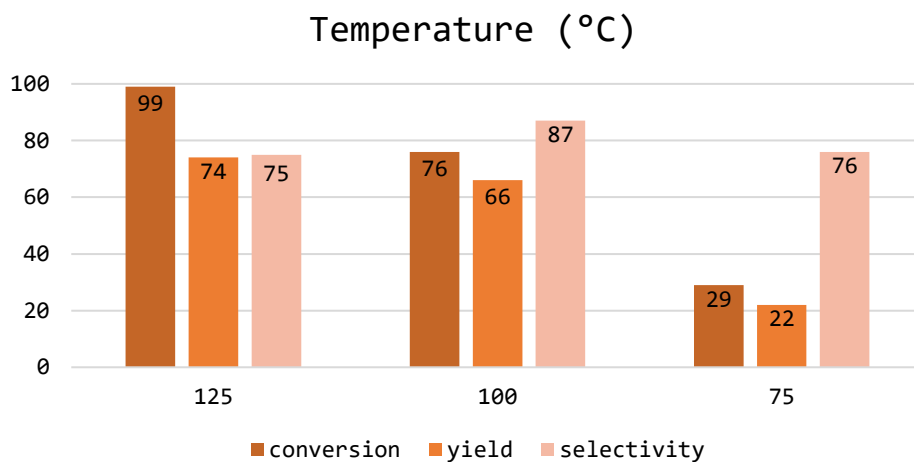
Reaction conditions: styrene oxide (SO) 2.19 mmol; cat. loading 0.5 mol%; T= 100°C; t = 3 h. [b] Conversion and selectivity determined by ¹H NMR using mesitylene as internal standard. [c] Turnover frequency (mol_{15a(converted)}·mol_{cat}⁻¹·reaction time⁻¹).



6.10.4 Influence of the temperature:

Entry	T (°C)	Conversion 15a ^[b] %	Selectivity 16a ^[b] %	TOF (h ⁻¹) ^[c]
8	75	29	76	39
9	100	76	87	101
10	125	99	75	132

Reaction conditions: styrene oxide (SO) 2.19 mmol; catalyst loading 0.25 mol%; P = 0.8 MPa; t = 3 h. [b] Conversion and selectivity determined by ¹H NMR using mesitylene as internal standard. [c] Turnover frequency (mol_{15a(converted)}} · mol_{cat}⁻¹ · reaction time⁻¹).

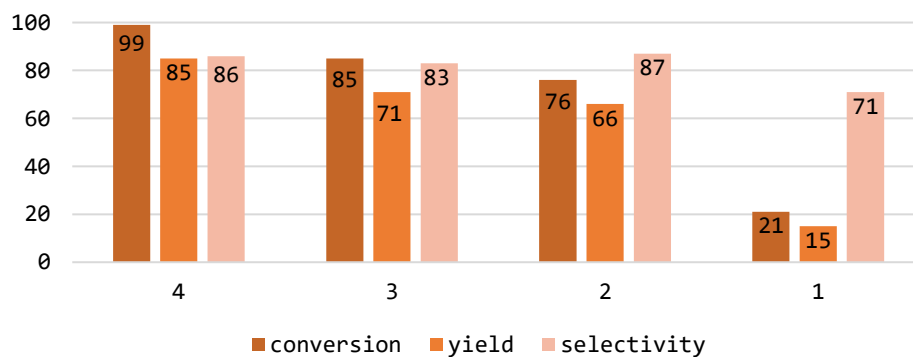


6.10.5 Influence of the reaction time:

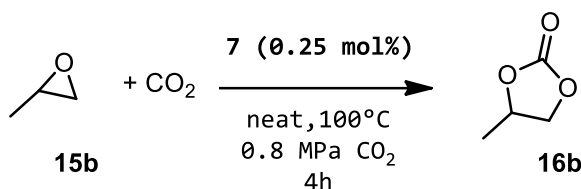
Entry	t (h)	Conversion 15a ^[b] %	Selectivity 16a ^[b] %	TOF (h ⁻¹) ^[c]
11	1	21	71	84
9	3	76	87	101
2	4	85	83	85
12	6	99	86	66

Reaction conditions: styrene oxide (SO) 2.19 mmol; catalyst loading 0.25 mol%; P = 0.8 MPa; T= 100°C. [b] Conversion and selectivity determined by ¹H NMR using mesitylene as internal standard. [c] Turnover frequency (mol_{15a(converted)} · mol_{cat}⁻¹ · reaction time⁻¹).

Reaction time (h)



6.10.6 Scale up reaction:



A 250 mL stainless steel autoclave reactor was equipped with a 50 mL glass vial, containing the catalyst/propylene oxide (PO, **15b**) mixture (0.25 mol% in 2.5 mL PO) and a magnetic bar. The autoclave was then charged with 0.5 MPa CO₂ and vented-off. This operation was performed twice and then the autoclave was charged with 0.8 MPa CO₂ and placed in the heating bath set at 100 °C for 4 hours. The reactor was then cooled and the CO₂ released. To the vial the appropriate amount of internal standard (mesitylene) and 10.0 mL of chloroform were added. 300 μL of the solution were taken and diluted with 350 μL of CDCl₃ to perform quantitative ¹H NMR analysis. The mixture was then passed through a silica plug and eluted with *n*-hexane/EtOAc 5:1 and the filtrate was evaporated to dryness in vacuum yielding to pure propylene carbonate **16b** (3.03 g, 83%).

6.10.7 Recycling experiment:

An autoclave was charged with **15b** and the same procedure of the scale up reaction was followed. The reactor was then cooled and the CO₂ released. At this point, 2.5 mL of PO were added in the vial and the autoclave was again charged with CO₂ (0.8 MPa) and placed in the heating bath set at 100 °C for additional 4 hours. This operation repeated a third time, for a total of 7.5 mL of PO. To the vial the appropriate amount of internal standard (mesitylene) and 10.0 mL of chloroform were added. 300 μL of the solution was taken and diluted with 350 μL of CDCl₃ to perform quantitative ¹H NMR analysis (**85% conversion, TON = 1020**). The mixture was then passed through a silica plug and eluted with *n*-hexane/EtOAc 5:1 and the filtrate was evaporated in vacuum to eliminate residual PO and obtaining pure propylene carbonate.

Yield: 62%, 6,76g

6.10.8 Catalyst recovery and recycle:

A 250 mL stainless steel autoclave reactor was equipped with a 2.5 mL glass vial, containing the catalyst/PO mixture (0.25 mol% in 2.5 mL PO) and a magnetic bar. The autoclave was then charged with 0.5 MPa CO₂ and vented-off. This operation was performed twice and then the autoclave was charged with 0.8 MPa CO₂ and placed in the heating bath set at 100 °C for 4 hours. The reactor was then cooled and the CO₂ released. To each vial the appropriate amount of internal standard (mesitylene) and 1.0 mL of chloroform were added. 300 µL of the solution were taken and diluted with 350 µL of CDCl₃ to perform quantitative ¹H NMR analysis. After that, the product PC and the remaining PO were distilled in vacuum directly from the vial and collected in a Schlenk tube, while the catalyst was recovered and analysed by ESI-MS spectroscopy and reused for a second reaction run to test its robustness.

ESI-MS analysis proved the presence of the ferrate anion (relative abundance 100%) in the recovered catalyst and the reaction results show a good reproducibility.

Yield: 1st run 83%, selectivity 99%,

2nd run 81%, selectivity 99%.

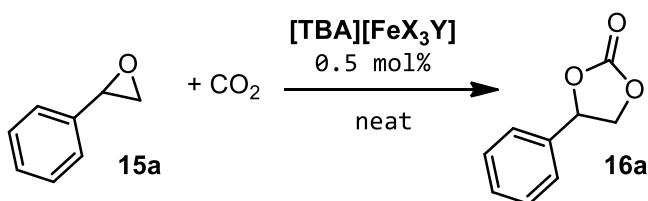
6.11 AMMONIUM FERRATES:

The synthesis and characterization of the ammonium tetrahalogenoferrate salts is described in the previous chapters (see experimental section).

6.11.1 General catalytic procedure:

A 250 mL stainless steel autoclave reactor was equipped with three 2.5 mL glass vials, containing the catalyst/epoxide mixture (0.5 %mol in 250 μ L of substrate) and, when needed, 125 μ L of PC as co-solvent. The vials were equipped with magnetic stirring bars and sealed with specific caps. The autoclave was then treated with the same procedure previously described. After the reaction, to each vial the appropriate amount of the internal standard (mesitylene) and 1 mL of CDCl_3 were added. 50 μ L of the solution was taken and further diluted with CDCl_3 to perform quantitative ^1H NMR analysis.

6.11.2 Reaction optimization:



Entry	Cat. 0.5 mol%	Con. 15a % ^[b]	Sel. 16a % ^[b]	TOF ^[c] (h^{-1})
1	$[\text{TBA}][\text{FeCl}_4]$	73	88	36
2	$[\text{TBA}][\text{FeCl}_3\text{Br}]$	83	95	42
3	$[\text{TBA}][\text{FeBr}_3\text{Cl}]$	99	70	49
4	$[\text{TBA}][\text{FeBr}_4]$	73	88	36
5	TBACl	41	95	21
6	TBABr	33	>99	17

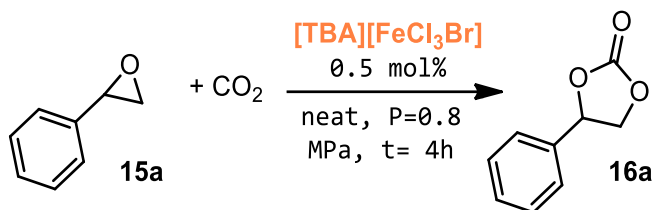
Reaction conditions: styrene oxide (SO) 2.19 mmol; $T = 100$ $^\circ\text{C}$; $P = 0.8$ MPa; $t = 4$ h.
 [b] Conversion and selectivity determined by ^1H NMR using mesitylene as the internal standard. [c] Turnover frequency ($\text{mol}_{1\text{a}(\text{converted})} \cdot \text{mol}_{\text{cat}}^{-1} \cdot \text{reaction time}^{-1}$).

6.11.3 Temperature influence/catalyst screening:

Entry	Cat. 0.1mol%	T (°C)	Con. 1a % ^[b]	Sel. 2a % ^[b]	TOF ^[c] (h ⁻¹)
7	[TBA][FeCl ₄]	100	32	60	80
8	[TBA][FeCl ₃ Br]	100	35	74	87
9	[TBA][FeBr ₄]	100	38	76	95
10	[TBA][FeCl ₄]	125	53	91	132
11	[TBA][FeCl ₃ Br]	125	66	94	164
12	[TBA][FeBr ₄]	125	74	81	184
13	TBABr	125	50	84	125
14	[TBA][FeCl ₄]	150	94	83	234
15	[TBA][FeCl ₃ Br]	150	95	83	237
16	[TBA][FeBr ₄]	150	91	81	227
17 ^[d]	[TBA][FeCl ₄]	150	75	87	374
18 ^[d]	[TBA][FeCl ₃ Br]	150	67	96	319
19 ^[d]	[TBA][FeBr ₄]	150	86	84	428
20 ^[d]	TBACl	150	56	86	279
21 ^[d]	TBABr	150	39	>99	194

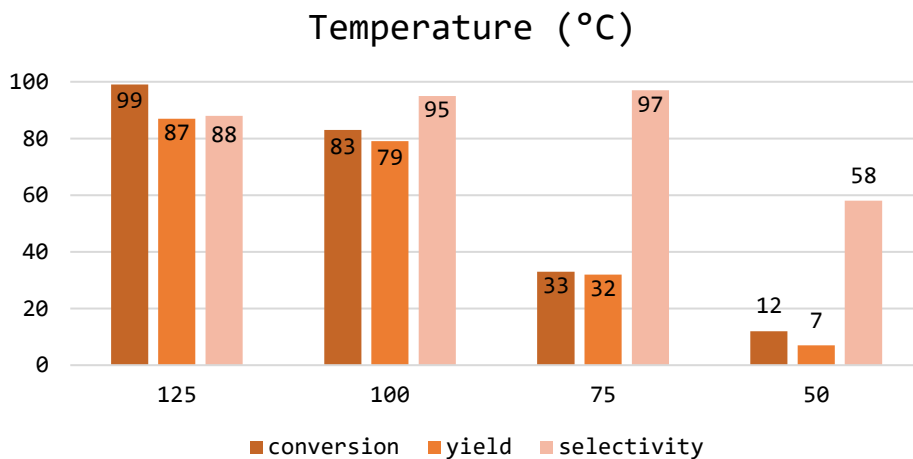
Reaction conditions: styrene oxide (SO) 2.19 mmol; P= 0.8 MPa; t= 4 h. [b] Conversion and selectivity determined by ¹H NMR using mesitylene as the internal standard. [c] Turnover frequency (mol_{1a(converted)}·mol_{cat}⁻¹·reaction time⁻¹). [d] t= 2h.

6.11.4 Temperature influence:



Entry	T (°C)	Con. 15a % ^[b]	Sel. 16a % ^[b]	TOF ^[c] (h ⁻¹)
22	50	12	58	36
23	75	33	97	42
24	100	83	95	49
25	125	99	88	36

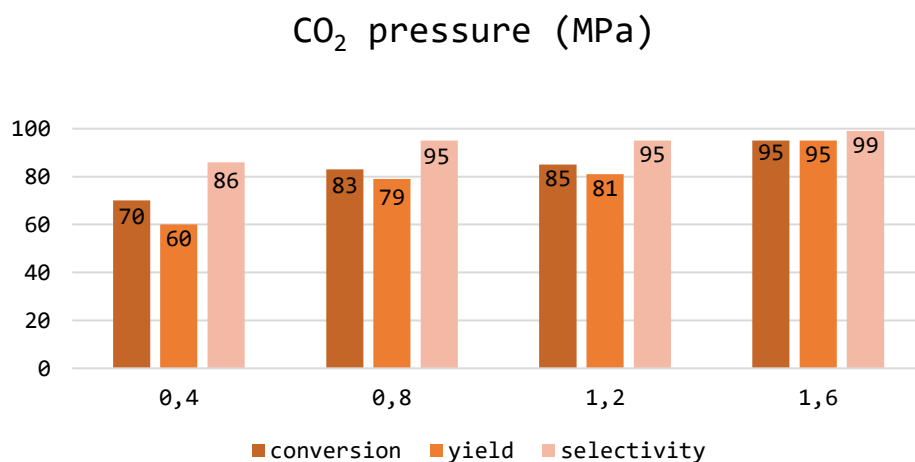
Reaction conditions: styrene oxide (SO) 2.19 mmol; P= 0.8 MPa; t= 4 h. [b] Conversion and selectivity determined by ¹H NMR using mesitylene as the internal standard. [c] Turnover frequency (mol_{1a(converted)}}·mol_{cat}⁻¹·reaction time⁻¹).



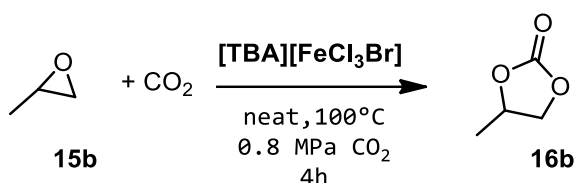
6.11.5 CO₂ pressure influence:

Entry	pCO ₂ (MPa)	Con. 15a % ^[b]	Sel. 16a % ^[b]	TOF ^[c] (h ⁻¹)
26	0.4	70	86	35
23	0.8	83	95	42
27	1.2	85	95	43
28	1.6	95	99	48

Reaction conditions: styrene oxide (SO) 2.19 mmol; T= 100°C; t= 4 h. [b] Conversion and selectivity determined by ¹H NMR using mesitylene as the internal standard. [c] Turnover frequency (mol_{1a(converted)}}·mol_{cat}⁻¹·reaction time⁻¹).



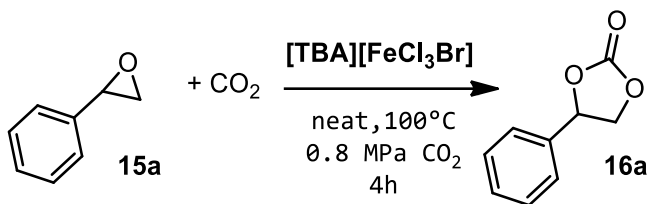
6.11.6 Catalyst recycle experiment:



A 250 mL stainless steel autoclave reactor was equipped with three 2.5 mL glass vials, containing the catalyst/propylene oxide mixture (0.5 mol% in 250 μL of substrate). The vials were equipped with magnetic stirring bars and sealed with specific caps. The autoclave was then charged with 0.5 MPa CO₂ and vented-off. This operation was performed twice and then the autoclave was charged with 0.8 MPa CO₂ and placed in the heating bath for 4 hours. The reactor was then cooled with ice and the CO₂ released. At this point, in one of the three vials, the appropriate amount of internal standard (mesitylene) and 1 mL of CDCl₃ were added. 50 μL of the solution was taken and further diluted with CDCl₃ to perform quantitative ¹H NMR analysis. The other vials were selected for the catalyst recovery put in vacuum at 100 °C for several hours to evaporate completely the products. Once all the volatiles were evaporated, the vials containing the catalyst were filled with fresh propylene oxide and reacted for further 4 hours in the same conditions. The evaporation of the products was then performed on one of the vials, where the other was used to calculate the yield. A final reaction cycle was performed on the last vial and the final yield was then calculated. Data are reported in table; for clarity, the conversion, the selectivity and the TON are considered on the total of the cycles. TON was defined as number of moles_{15b} converted per moles of catalyst.

Entry	Cat (0.5 mol%)	Con. 15b % ^[b]	Sel. 16b % ^[b]	TON (h ⁻¹)
29, first cycle	[TBA][FeCl ₃ Br]	99	99	198
30, second cycle	[TBA][FeCl ₃ Br]	99	98	396
31, third cycle	[TBA][FeCl ₃ Br]	99	97	594

6.11.7 Reaction scale-up:



A 250 mL stainless steel autoclave reactor was equipped with a 100 mL glass vials, containing the catalyst/**15a** mixture (0.5 mol%, 106 mg [TBA][FeCl₃Br] in 5 mL of substrate). The vial was equipped with a magnetic stirring bar and sealed with a specific cap. The autoclave was then charged with 0.5 MPa CO₂ and vented-off. This operation was performed twice and then the autoclave was charged with 0.8 MPa CO₂ and placed in the heating bath for 4 hours. The reactor was then cooled with ice and the CO₂ released. 674 μ L of mesitylene was added as ISTD. Then, 1 mL of CDCl₃ was added to recover the product on the vial walls and 50 μ L of the mixture was taken and further diluted with CDCl₃ to perform quantitative ¹H NMR analysis.

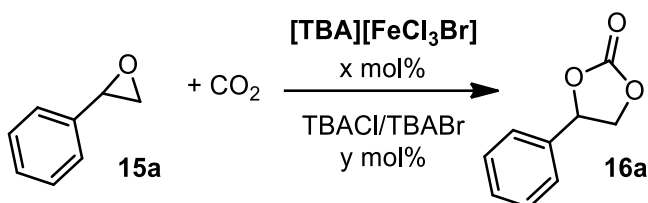
50 mL of hexane were added to the reaction vial and stirred overnight. The vial was then placed at -20° C for several hours and the product styrene carbonate, **16a**, was recovered by filtration as white crystals (traces of iron impurities can be present).

Yield: 70%, **Selectivity:** 95%

Isolated yield: 58%, 4.19g

6.11.8 Effect of external nucleophiles:

Since the scramble of the halides in solution when using $\text{TBAFeCl}_3\text{Br}$ as catalyst, to form $[\text{TBA}][\text{FeCl}_4]$ and $[\text{TBA}][\text{FeCl}_2\text{Br}_2]$, is not negligible and must be taken into account, we performed some reactions to investigate the influence of external nucleophiles to $[\text{TBA}][\text{FeCl}_4]$ by adding catalytic quantities of TBABr or TBACl .



Catalyst	Cat.	Conversion 15a % ^[b]	Selectivity 16a % ^[b]	Added nucleophile
$[\text{TBA}][\text{FeCl}_4]$	0.5 mol%	60	99	none
$[\text{TBA}][\text{FeCl}_4]$	0.375 mol%	72	99	0.125 mol% TBABr
$[\text{TBA}][\text{FeCl}_4]$	0.375 mol%	61	99	0.125 mol% TBACl

Reaction conditions: styrene oxide (SO) 2.19 mmol; $T = 100^\circ\text{C}$; $P_{\text{CO}_2} = 0.8 \text{ MPa}$; $t = 4 \text{ h}$. [b] Conversion and selectivity determined by $^1\text{H NMR}$ using mesitylene as the internal standard.

The addition of external nucleophiles was also investigated on the best catalyst $[\text{TBA}][\text{FeCl}_3\text{Br}]$, at ambient pressure of CO_2 (0.1 MPa).

Catalyst	Cat.	Conversion 15a % ^[b]	Selectivity 16a % ^[b]	Added nucleophile
$\text{TBAFeCl}_3\text{Br}$	0.5 mol%	56	66	none
$\text{TBAFeCl}_3\text{Br}$	0.5 mol%	54	89	0.125 mol% TBACl
$\text{TBAFeCl}_3\text{Br}$	0.5 mol%	60	83	0.125 mol% TBABr

Reaction conditions: styrene oxide (SO) 2.19 mmol; $T = 100^\circ\text{C}$; $P_{\text{CO}_2} = 0.1 \text{ MPa}$; $t = 4 \text{ h}$. [b] Conversion and selectivity determined by $^1\text{H NMR}$ using mesitylene as the internal standard.

6.11.9 Determination of enantiopurity of the product with (R)-Styrene oxide:

The product of the reaction of (R)-styrene oxide was analyzed by HPLC, using a chiral column (Chiralpak-AD).

Styrene carbonate racemic mixture - 0.8 ml/min hex:i-PrOH : 95-5
Chiralpak AD column

Peak #	RT [min]	Type	Width [min]	Area [mAU*s]	Height [mAU]	Area %
1	27.907	MF	0.621	138.837	3.724	49.957
2	28.734	FM	0.644	139.072	3.600	50.043

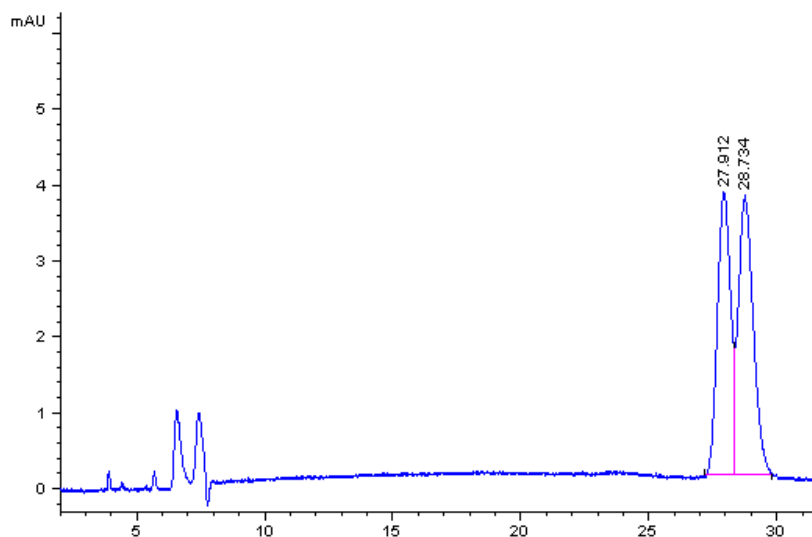


Figure E7. HPLC chromatogram spectra of racemic styrene carbonate.

Styrene carbonate (from enantiomeric pure R-Styrene oxide) - 0.8 ml/min hex:i-PrOH : 95-5 Chiralpak AD column

Peak #	RT [min]	Type	Width [min]	Area [mAU*s]	Height [mAU]	Area %
1	28.851	BB	0.735	2683.324	53.829	100.000

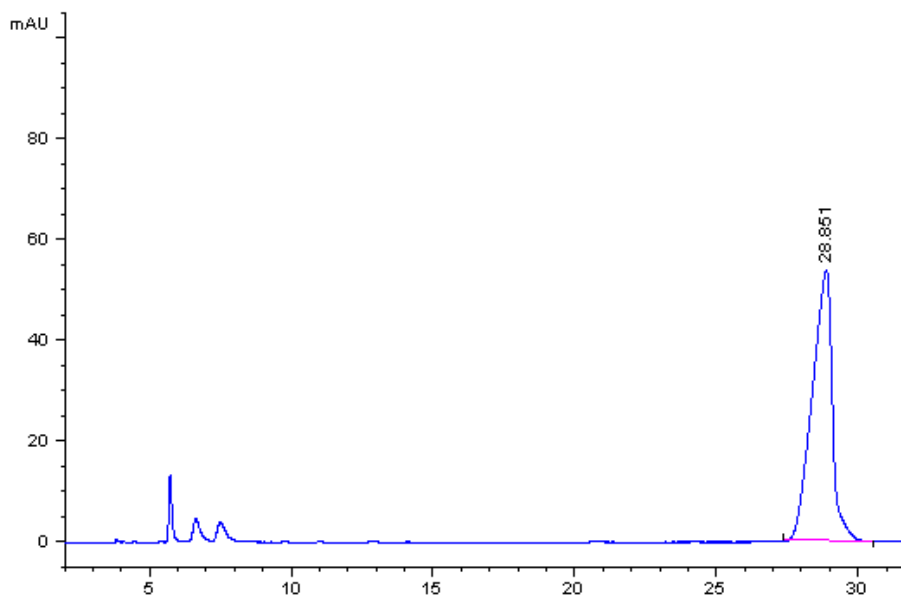


Figure E8. HPLC chromatogram spectra of enantiomeric pure styrene carbonate, coming from (R)-styrene oxide.

6.11.10 DFT calculations:

Theoretical calculations aimed at a better understanding of the reaction mechanism have been performed at two different theory levels.

First, a semiempirical tight-binding based quantum chemistry (QC) method GFNn-xTB^[243] in the framework of meta-dynamics (MTD) was employed, in order to explore the wide variety of possible reaction mechanisms. Within this approach, the total energy E_{tot} of the system is the sum of the total (electronic) tight-binding QC energy $E_{\text{tot}}^{\text{el}}$, the biasing root-mean-square deviation (RMSD) $E_{\text{bias}}^{\text{RMSD}}$, and an optional reactor wall cavitation potential $E_{\text{bias}}^{\text{wall}}$

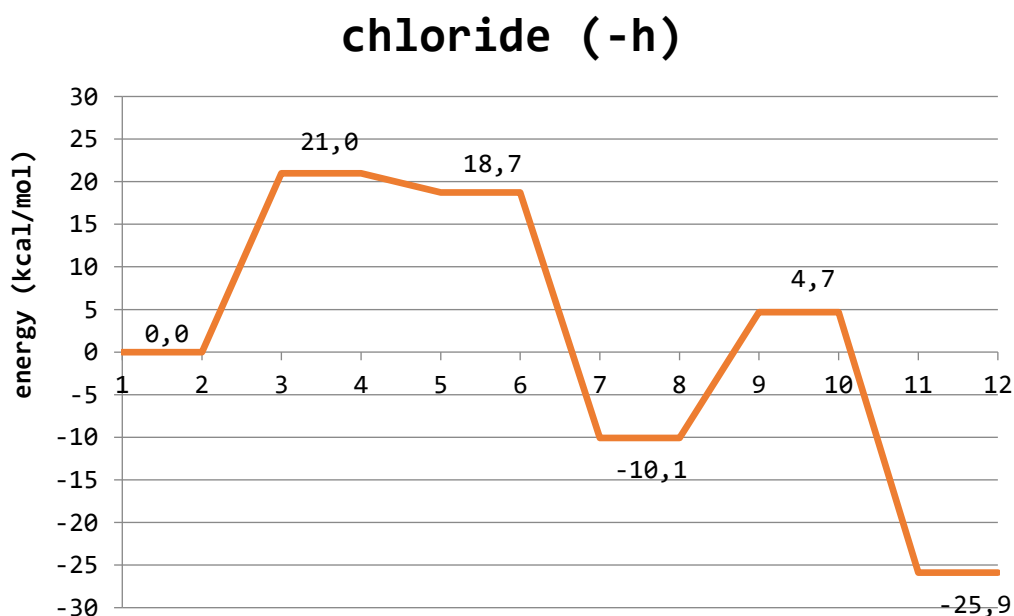
$$E_{\text{tot}} = E_{\text{tot}}^{\text{el}} + E_{\text{bias}}^{\text{RMSD}} + E_{\text{bias}}^{\text{wall}}$$

A standard thermostat bath temperature of 27 °C has been mainly adopted in the molecular dynamics (MD) and MTD simulations, but during the chemical reaction space exploration it has been varied among -73 °C and 327 °C, to guess if unexpected reaction paths could be feasible by slightly heating the system. A MTD simulation, indeed, allows atom-selective heating and thereby efficient crossing of small/large chemical barriers depending on the strength of the bias. As stated by the author,^[243] due to the approximate character of this method, “the resulting structure ensembles require further refinement with more sophisticated approaches”. For this reason, the preliminary GFNn-xTB screening of the reaction paths has been followed by more rigorous first principles all electron simulations, based on DFT adopting the B3LYP hybrid functional^[244,245] as implemented in the Gaussian 09 code.^[246] As for the set of basis functions, we selected the 6-31++g(d,p) basis set, which ensures a reliable description of the valence shell electrons. This same DFT scheme proved successful in a recent investigation focused on the reactivity of organic compounds on an inorganic substrate.^[247] The geometries of reactants, intermediates, TSs and products were fully optimized. The TS structures were searched through the Berny algorithm,^[248] computing the force constants at every point. The presence of solvent in the reaction environment has been taken into account through the Solvation Model based on Density (SMD) approach, which adopts an implicit solvation model.^[249] The solvent considered in our calculations is toluene, whose dielectric constant amounts to 2.38 and is estimated to be close to that of SO.

Dispersion forces of the Grimme type^[250] were included between the molecules involved in the reaction in order to account for van der Waals interactions. The D3 version of Grimme's dispersion with the original D3 damping function has been selected. The calculated reaction barriers (Figure 5 and Table 4) are reported in kcal/mol as total energy differences between adjacent compounds along the reaction coordinate. From the computational point of view the role of the tetrabutylammonium cation in the CO₂ fixation process resulted to be trivial, the only effect of its presence being a rigid downshift of the energy reaction graph. Therefore, it has been neglected in the final calculations.

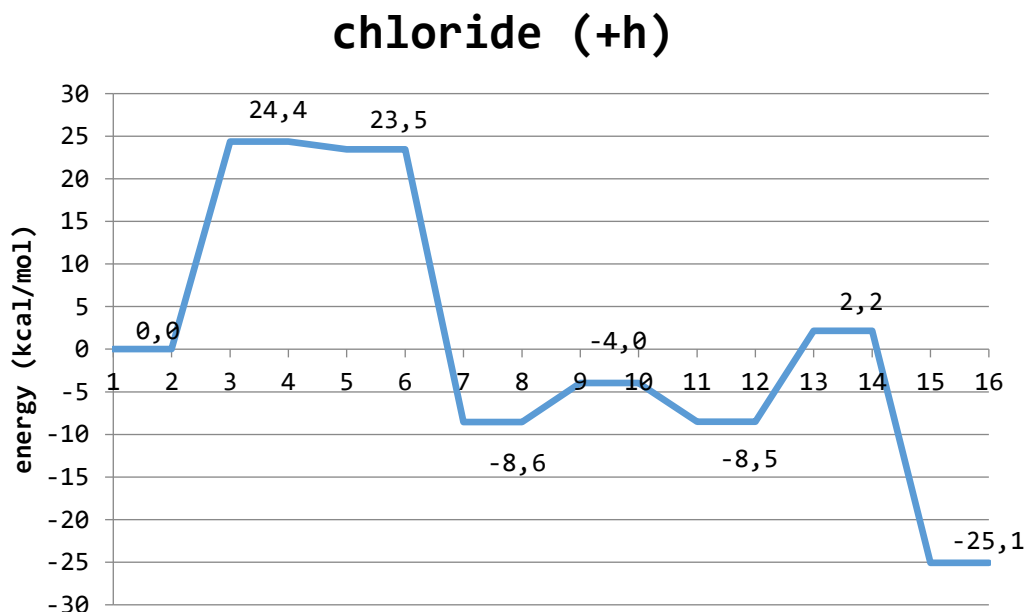
6.11.11 Complete reaction paths from DFT computations:

Figure E9. Energy profile of the reaction with styrene oxide as substrate, no Lewis acid and chloride acting as the nucleophile, attacking the less hindered carbon (-h).



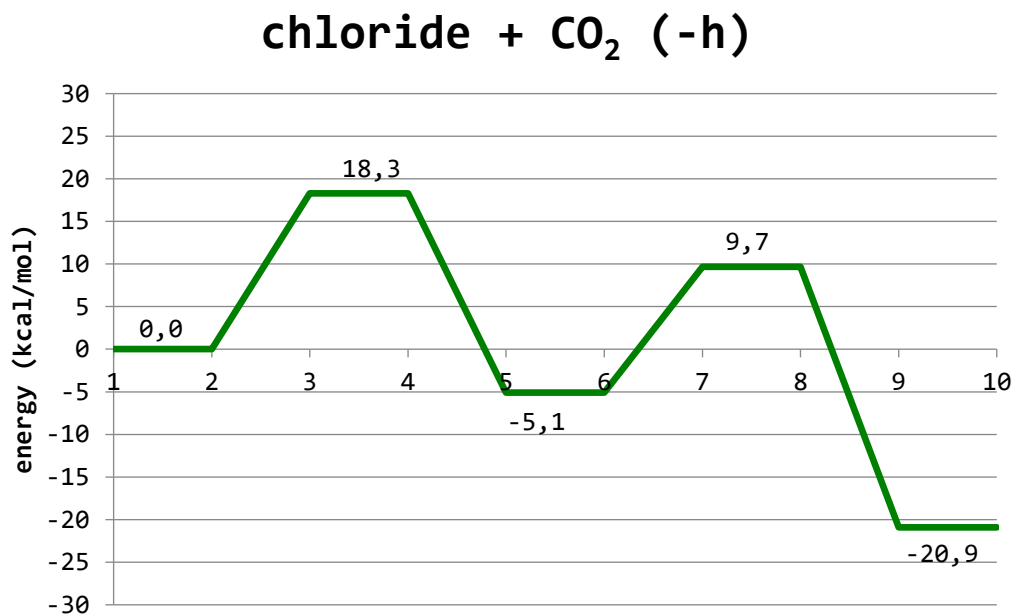
1-2: complex between chloride and the epoxide; 3-4: transition state for epoxide ring opening; 5-6: open epoxide ring, intermediate; 7-8: open carbonate after CO₂ incorporation, intermediate; 9-10: transition state for carbonate ring closure; 11-12: complex between the cyclic carbonate and chloride.

Figure E10. Energy profile of the reaction with styrene oxide as substrate, no Lewis acid and chloride acting as the nucleophile, attacking the most hindered carbon (+h).



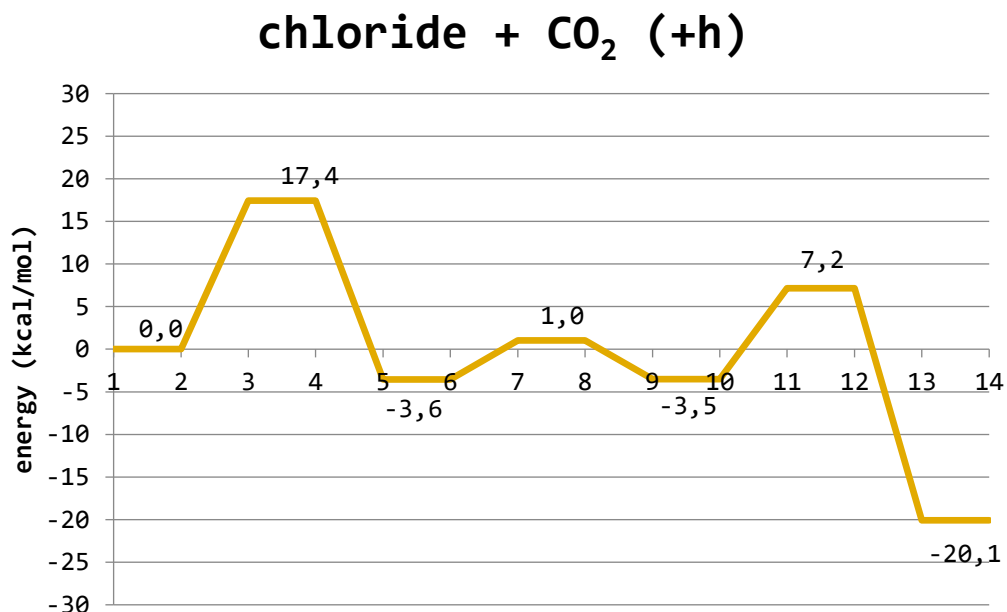
1-2: complex between chloride and the epoxide; 3-4: transition state for epoxide ring opening; 5-6: open epoxide ring, intermediate; 7-8: open carbonate after CO₂ incorporation, intermediate; 9-10: transition state for the conformational rearrangement of the open carbonate; 11-12: open carbonate, second intermediate; 13-14: transition state for carbonate ring closure; 15-16: complex between the cyclic carbonate and chloride.

Figure E11. Energy profile of the reaction with styrene oxide as substrate, CO₂ as Lewis acid and substrate, and chloride acting as the nucleophile, attacking the less hindered carbon (-h).



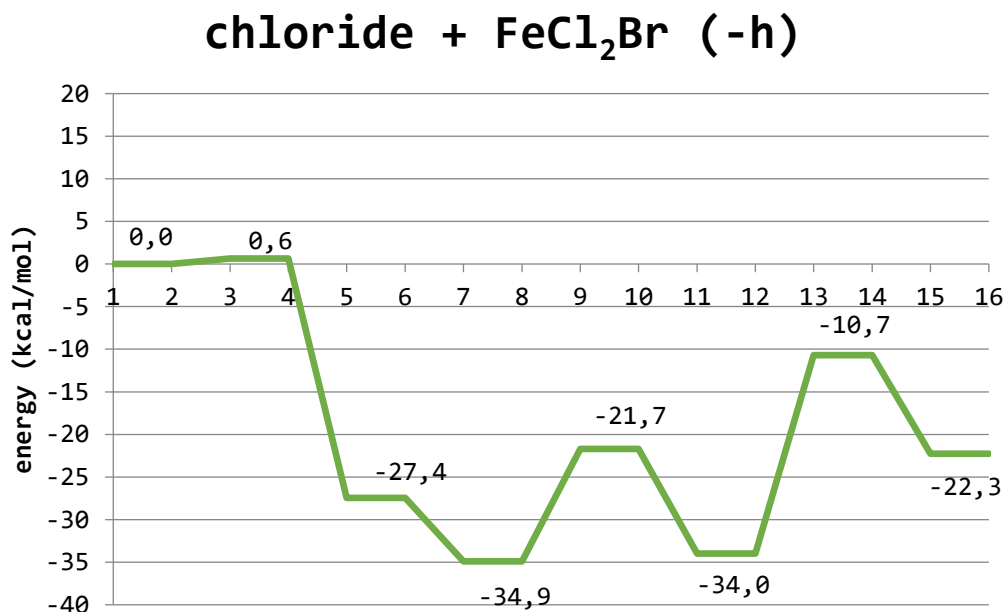
1-2: complex between chloride, carbon dioxide and the epoxide; 3-4: transition state for epoxide ring opening and formation of the open carbonate species; 5-6: open carbonate, intermediate; 7-8: transition state for carbonate ring closure; 9-10: complex between the cyclic carbonate and chloride.

Figure E12. Energy profile of the reaction with styrene oxide as substrate, CO₂ as Lewis acid and substrate, and chloride acting as the nucleophile, attacking the most hindered carbon (+h).



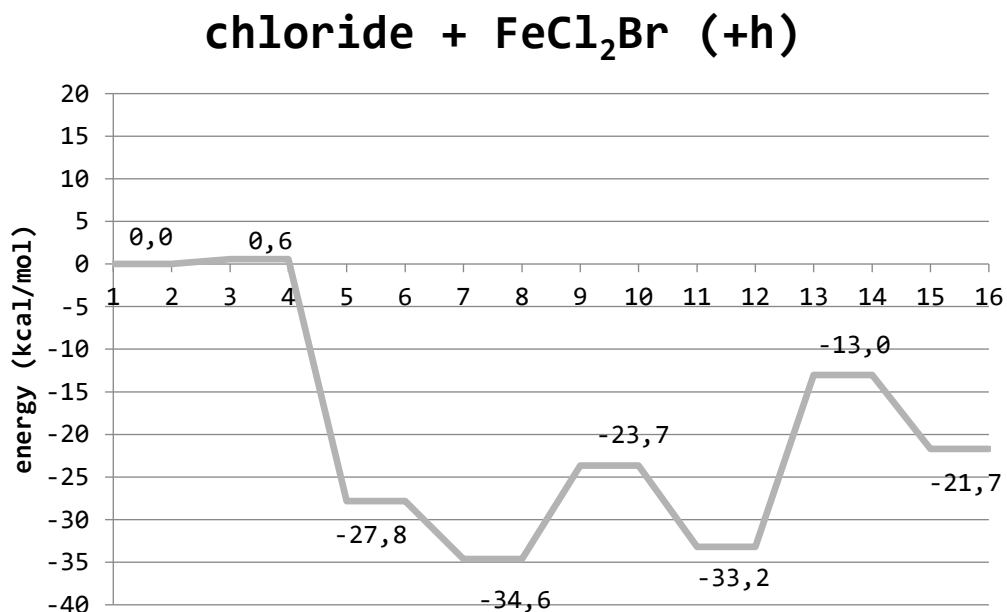
1-2: complex between chloride, carbon dioxide and the epoxide; 3-4: transition state for epoxide ring opening and formation of the open carbonate species; 5-6: open carbonate, intermediate; 7-8: transition state for the conformational rearrangement of the open carbonate; 9-10: open carbonate, second intermediate; 11-12: transition state for carbonate ring closure; 13-14: complex between the cyclic carbonate and chloride.

Figure E13. Energy profile of the reaction with styrene oxide as substrate, FeCl_2Br as Lewis acid, and chloride acting as the nucleophile, attacking the less hindered carbon (-h).



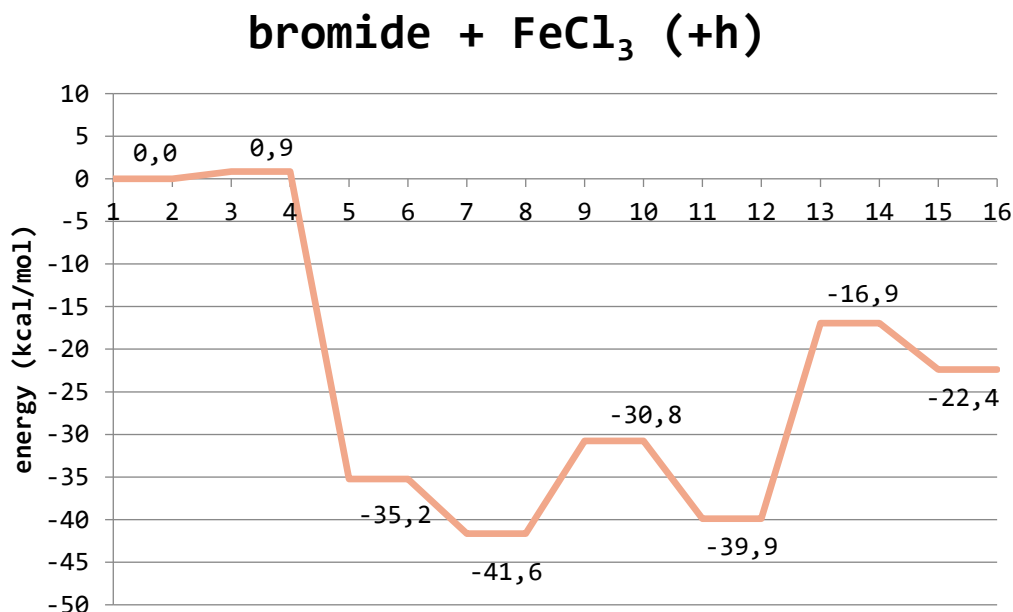
1-2: complex between chloride, the Lewis Acid and the epoxide; 3-4: transition state for epoxide ring opening; 5-6: complex among the open epoxide, the Lewis Acid and chloride, intermediate; 7-8: complex among the open epoxide, the Lewis Acid, chloride and carbon dioxide; 9-10: transition state for the formation of the open carbonate; 11-12: open carbonate, second intermediate; 13-14: transition state for carbonate ring closure; 15-16: complex between the cyclic carbonate, the Lewis Acid and chloride.

Figure E14. Energy profile of the reaction with styrene oxide as substrate, FeCl_2Br as Lewis acid, and chloride acting as the nucleophile, attacking the most hindered carbon (+h).



1-2: complex between chloride, the Lewis Acid and the epoxide; 3-4: transition state for epoxide ring opening; 5-6: complex among the open epoxide, the Lewis Acid and chloride, intermediate; 7-8: complex among the open epoxide, the Lewis Acid, chloride and carbon dioxide; 9-10: transition state for the formation of the open carbonate; 11-12: open carbonate, second intermediate; 13-14: transition state for carbonate ring closure; 15-16: complex between the cyclic carbonate, the Lewis Acid and chloride.

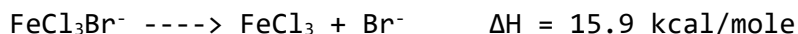
Figure E15. Energy profile of the reaction with styrene oxide as substrate, FeCl_3 as Lewis acid, and bromide acting as the nucleophile, attacking the most hindered carbon (+h).



1-2: complex between bromide, the Lewis Acid and the epoxide; 3-4: transition state for epoxide ring opening; 5-6: complex among the open epoxide, the Lewis Acid and bromide, intermediate; 7-8: complex among the open epoxide, the Lewis Acid, bromide and carbon dioxide; 9-10: transition state for the formation of the open carbonate; 11-12: open carbonate, second intermediate; 13-14: transition state for carbonate ring closure; 15-16: complex between the cyclic carbonate, the Lewis Acid and bromide.

6.11.12 Theoretical estimation of the dissociation of FeCl_3Br^- in styrene oxide:

From ab initio computations:



Assumptions:

1) The contribution of entropy is negligible.

$$\Delta G = \Delta H - T\Delta S \cong \Delta H$$

2) The fraction of dissociated ferrate anion is small with respect to the undissociated fraction, and the concentration of Br^- is much smaller than Cl^- .

$$[\text{Br}^-]_{\text{solution}} \ll [\text{Cl}^-]_{\text{solution}} \ll [\text{FeCl}_3\text{Br}^-]_{\text{solution}} \cong [\text{ammonium salt}]$$

From the basic equation of chemical equilibrium it can be derived the following:

$$[X^-] = \sqrt{[\text{FeCl}_3\text{Br}^-] \cdot e^{-\Delta H/RT}}$$

T (K)	$[\text{FeCl}_3\text{Br}^-]$ (mol/l)		$[\text{FeCl}_3\text{Br}^-]$ (mol/l)	
	$8.7 \cdot 10^{-3}$		$4.4 \cdot 10^{-2}$	
	$[\text{Cl}^-]$	χ (%)	$[\text{Cl}^-]$	χ (%)
373.15	$1.8 \cdot 10^{-4}$	2.0	$4.0 \cdot 10^{-4}$	0.9
398.15	$2.6 \cdot 10^{-4}$	3.0	$5.9 \cdot 10^{-4}$	1.3
423.15	$3.7 \cdot 10^{-4}$	4.2	$8.3 \cdot 10^{-4}$	1.9

χ is the percentage of dissociated ferrate anion. All concentrations are given in mol/l.

T (K)	[FeCl ₃ Br ⁻] (mol/l)		[FeCl ₃ Br ⁻] (mol/l)	
	8.7 · 10 ⁻³		4.4 · 10 ⁻²	
	[Br ⁻]	χ (%)	[Br ⁻]	χ (%)
373.15	1.6 · 10 ⁻⁶	0.019	3.6 · 10 ⁻⁶	0.008
398.15	3.2 · 10 ⁻⁶	0.037	7.3 · 10 ⁻⁶	0.017
423.15	5.9 · 10 ⁻⁶	0.068	1.3 · 10 ⁻⁵	0.030

χ is the percentage of dissociated ferrate anion. All concentrations are given in mol/l.

6.11.13 Theoretical estimate of the activation energy from experimental data:

Reaction of first order in respect of the epoxide concentration, with no inverse reaction occurring:

$$[A] = [A]_0 \cdot e^{-kt} \quad (1)$$

according to the Eyring-Polanyi equation, the coefficient k (i.e. the reaction rate) can be expressed as follows:

$$k = \frac{\kappa k_B T}{h} \cdot e^{-\Delta G/RT} \quad (2)$$

where κ , the transmission coefficient, is set equal to 1. The equation contains the Boltzmann constant k_B , the Plank constant h , the absolute temperature T , the “gas” constant R and the free energy variation from the reactant to the activated complex.

The conversion factor c is defined as:

$$c = ([A]_0 - [A])/[A]_0 \quad (3)$$

combining (1) and (3) leads to:

$$\ln \frac{1}{1-c} = kt \quad (4)$$

combining (4) and (2) leads to:

$$t = \ln \frac{1}{1-c} \frac{h}{k_B T} e^{\Delta G/RT} \quad (5)$$

inversion of (5) reads as:

$$\Delta G = RT \ln \left[\frac{tk_B T}{h} \cdot \frac{1}{\ln \frac{1}{1-c}} \right] \quad (6)$$

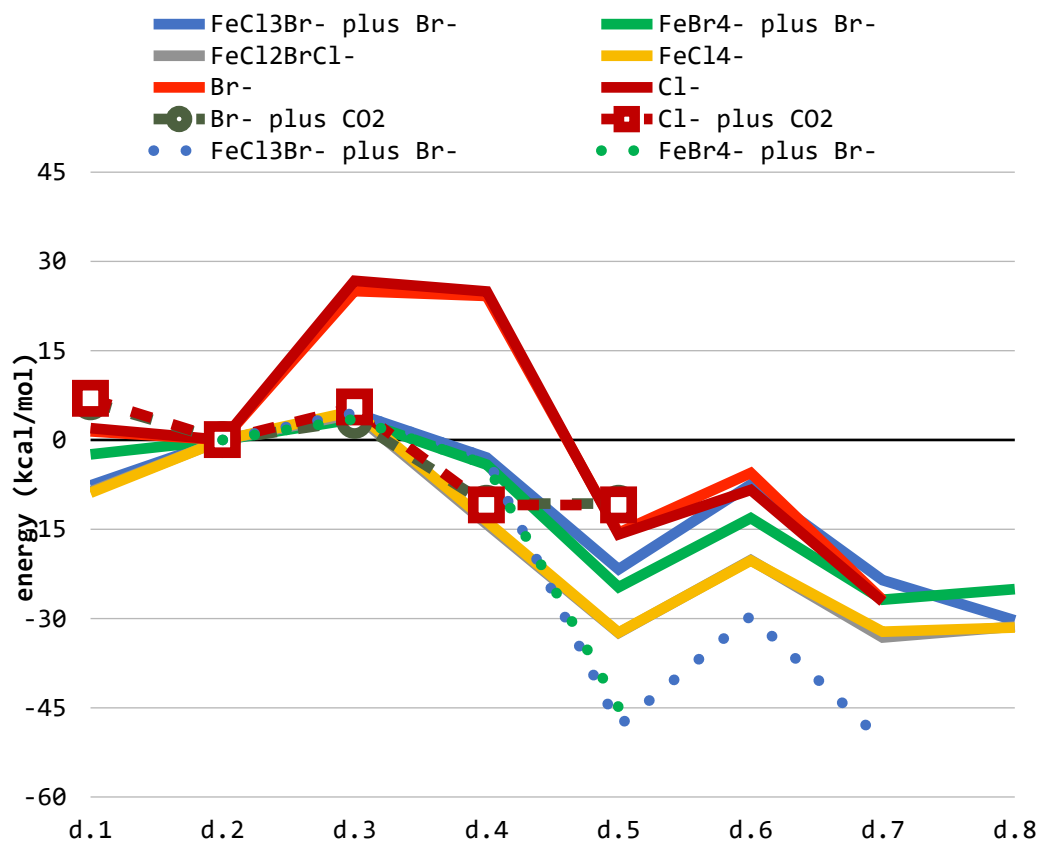
Equation (6) allows an estimate of the activation barrier for the rate determining step of the reaction, reported in the following table:

T (°C)	50	75	100	125
T (K)	323.15	348.15	373.15	398.15
	ΔG (kcal/mol)	ΔG (kcal/mol)	ΔG (kcal/mol)	ΔG (kcal/mol)
Br⁻ / no Lewis acid	23.4	24.0	24.8	25.5
Cl⁻ / no Lewis acid	23.8	24.2	24.6	25.1
Cl⁻ + Lewis acid	22.2	23.2	23.8	24.6

Table E3. Estimate of the activation barrier ΔG (kcal/mol) for the rate determining step from experimental data.

6.11.14 Complete reaction paths from semiempirical tight binding calculations evaluated through the XTB code:

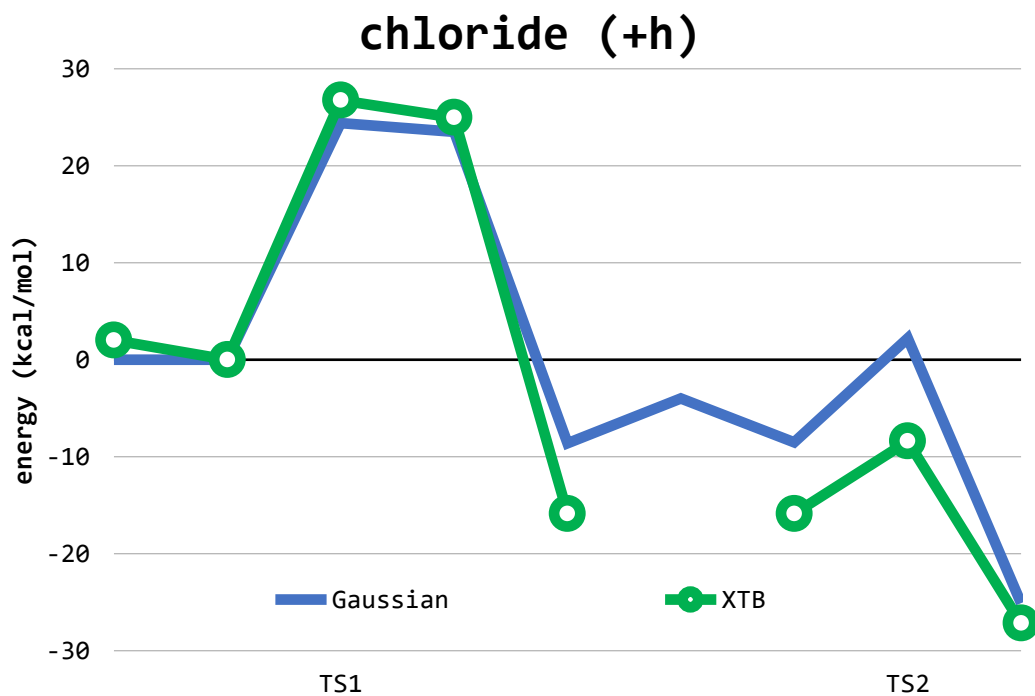
Figure E16. Comparison between reaction paths obtained in presence/absence of the Lewis Acid, with or without CO₂ acting as a Lewis Acid and varying the halogen responsible for the nucleophilic attack on the most hindered carbon (+h). The energies are evaluated with respect to the point labeled as d.2.



d.1: isolated epoxide + isolate nucleophile (FeX_4^- or X^- or $\text{CO}_2 + \text{X}^-$). d.2: epoxide interacting with other components (FeX_4^- or X^- or $\text{CO}_2 + \text{X}^-$) taken as reference energy. d.3: transition states for epoxide ring opening (first step of reaction). d.4: open epoxide ring, first reaction intermediate. d.5: open carbonate species. d.6 transition state for ring closure (second step of reaction). d.7 closed cyclic carbonate interacting with other components (FeX_4^- or X^- or $\text{CO}_2 + \text{X}^-$). d.8: same as d.7, with all the components desorbed and reassociated (if LA is present).

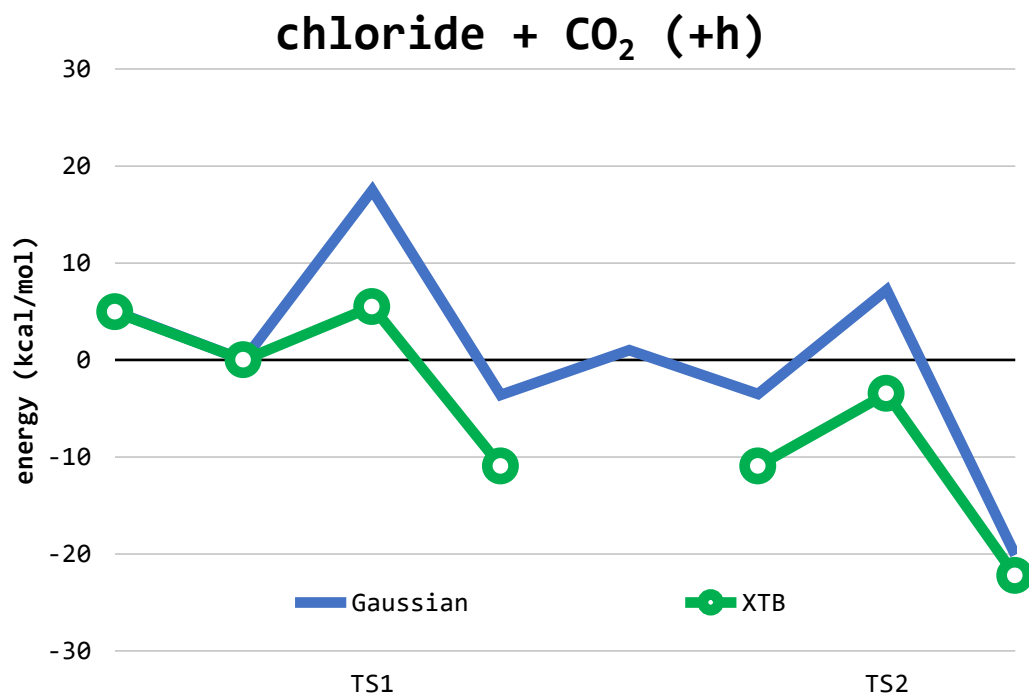
6.11.15 Comparison between semiempirical-XTB and DFT-Gaussian results:

Figure E17. case of chloride nucleophilic attack on the more hindered carbon (+h) in absence of LA, with CO₂ coming into play after epoxide ring opening.



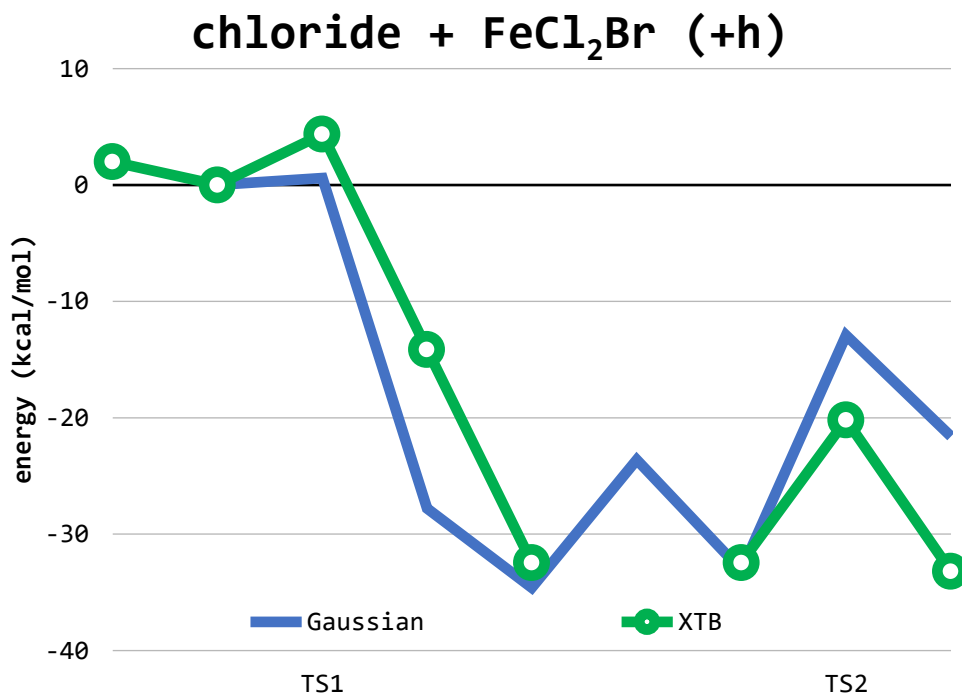
TS1: epoxide ring opening. TS2: closure of the open carbonate species to give the product

Figure E18. case of chloride nucleophilic attack on the more hindered carbon (+h) with CO₂ acting as weak Lewis acid.



TS1: epoxide ring opening. TS2: closure of the open carbonate species to give the product

Figure E19. case of chloride nucleophilic attack on the more hindered carbon (+h) in presence of FeCl_2Br as Lewis acid, with CO_2 coming into play after epoxide ring opening.



TS1: epoxide ring opening. TS2: closure of the open carbonate species to give the product.

6.12 AMMONIUM ZINCATES:

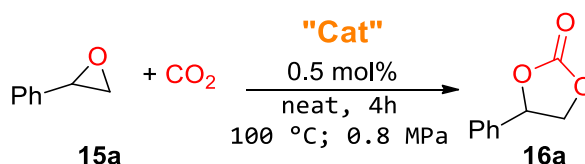
6.12.1 General catalytic procedure:

A 250 mL stainless steel autoclave reactor was equipped with three 2.5 mL glass vials, containing the catalyst/epoxide mixture (250 μ L of substrate). The vials were equipped with magnetic stirring bars and sealed with specific caps. The autoclave was then charged with a specific amount of CO₂ and placed in a thermostated heating bath for a specific amount of time. The reactor was then cooled to room temperature (when needed) and the CO₂ released. To each vial the appropriate amount of the internal standard (mesitylene) and 0.5 mL of CDCl₃ were added to perform quantitative ¹H NMR analysis.

Reactions performed at ambient pressure of CO₂ were placed in glass vials containing the epoxide, the catalyst and a magnetic stirring bar, sealed with a silicon septum and aluminium cap. A CO₂ balloon, sealed to a plastic syringe, was inserted in the vial using a needle to ensure the pressure of CO₂. At the end of the reaction, the appropriate amount of the internal standard (mesitylene) and 0.5 mL of CDCl₃ were added to perform quantitative ¹H NMR analysis.

Optimization of the reaction:

6.12.2 Catalyst screening:



Entry	Cat. 0.5 mol%	Conv. 15a % ^[b]	Sel. 16a % ^[b]
1	[TBA] ₂ [ZnCl ₄]	97	86
2	[TBA] ₂ [ZnBr ₄]	>99	94
3	[TBA] ₂ [ZnI ₄]	>99	95

Reactions performed in an autoclave. Reaction conditions: styrene oxide (SO) 2.19 mmol; cat. 0.5 mol%; P(CO₂) = 0.8 MPa; T = 100 °C; t = 4h. [b] Conversion and selectivity determined by ¹H NMR using mesitylene as the internal standard.

6.12.3 Blank experiments:

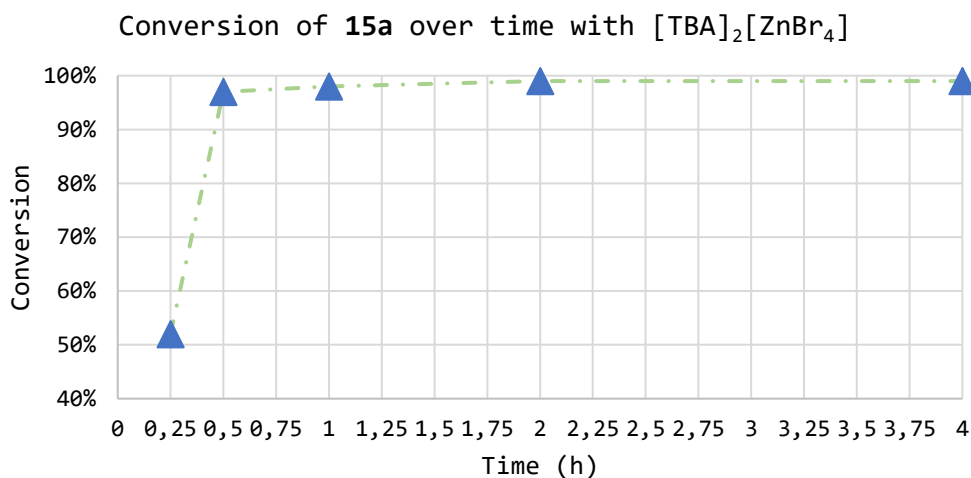
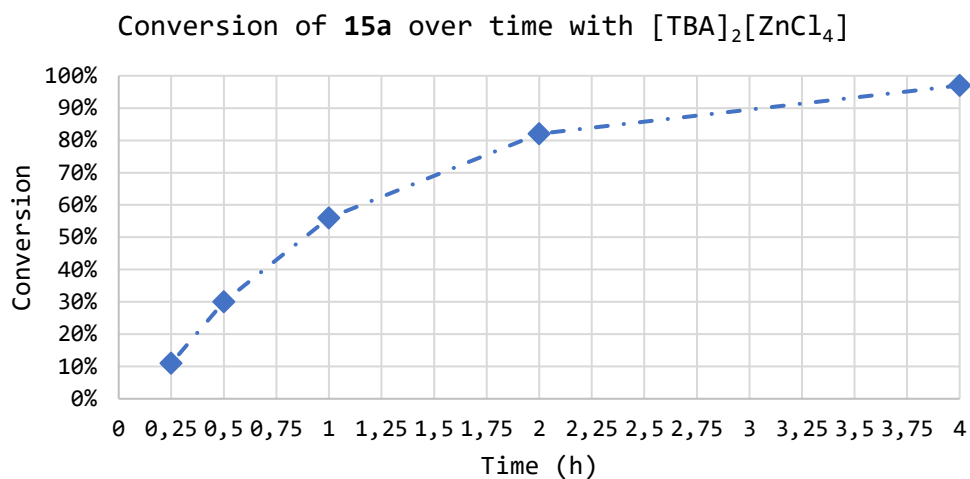
Entry	Cat. 0.5 mol%	Conv. 15a % ^[b]	Sel. 16a % ^[b]
4	TBACl	41	99
5	TBABr	33	99
6	TBAI	42	95
7	None	3	0

Reactions performed in an autoclave. Reaction conditions: styrene oxide (SO) 2.19 mmol; cat. 0.5 mol%; P(CO₂) = 0.8 MPa; T = 100 °C; t = 4h. [b] Conversion and selectivity determined by ¹H NMR using mesitylene as the internal standard.

6.12.4 Reaction time optimization:

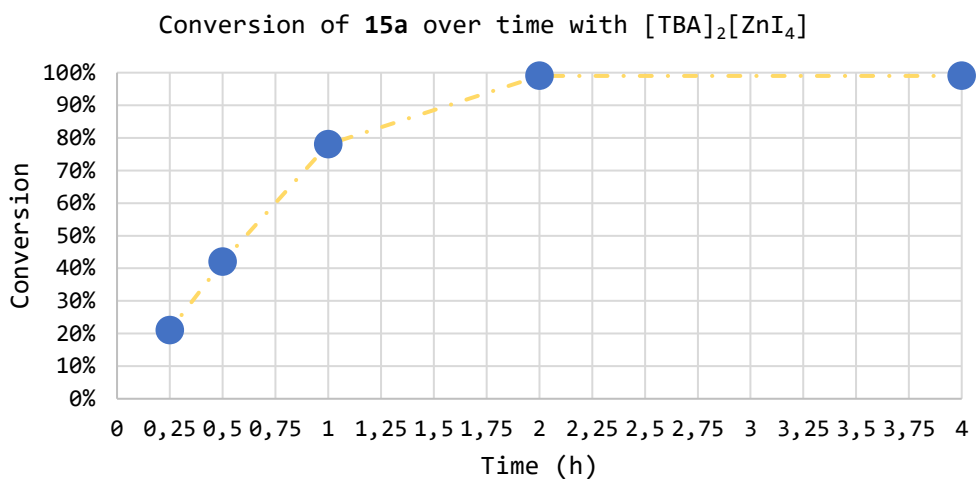
Entry	Cat. 0.5 mol%	t (h)	Conv. 15a % ^[b]	Sel. 16a % ^[b]
8		4	97	86
9		2	82	98
10	[TBA] ₂ [ZnCl ₄]	1	56	95
11		0.5	30	93
12		0.25	11	>99
13		4	>99	94
14		2	>99	95
15	[TBA] ₂ [ZnBr ₄]	1	98	96
16		0.5	87	99
17		0.25	52	92

Reactions performed in an autoclave. Reaction conditions: styrene oxide (SO) 2.19 mmol; cat. 0.5 mol%; P(CO₂) = 0.8 MPa; T = 100 °C. [b] Conversion and selectivity determined by ¹H NMR using mesitylene as the internal standard.

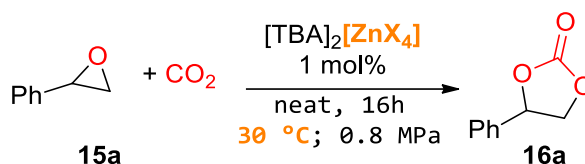


Entry	Cat. 0.5 mol%	t (h)	Conv. 15a % ^[b]	Sel. 16a % ^[b]
18		4	>99	95
19		2	>99	91
20	$[\text{TBA}]_2[\text{ZnI}_4]$	1	78	85
21		0.5	42	99
22		0.25	21	86

Reactions performed in an autoclave. Reaction conditions: styrene oxide (SO) 2.19 mmol; cat. 0.5 mol%; $P(\text{CO}_2) = 0.8 \text{ MPa}$; $T = 100 \text{ }^\circ\text{C}$. [b] Conversion and selectivity determined by ^1H NMR using mesitylene as the internal standard.

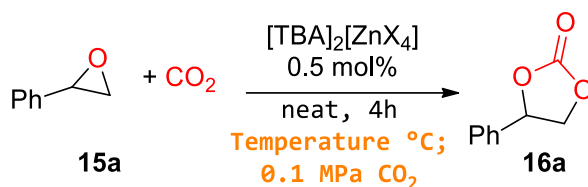


6.12.5 Reactions at room temperature:



Entry	Cat. 0.5 mol%	Conv. 15a % ^[b]	Sel. 16a % ^[b]
23	$[\text{TBA}]_2[\text{ZnCl}_4]$	11	73
24	$[\text{TBA}]_2[\text{ZnBr}_4]$	95	>99
25	$[\text{TBA}]_2[\text{ZnI}_4]$	>99	>99

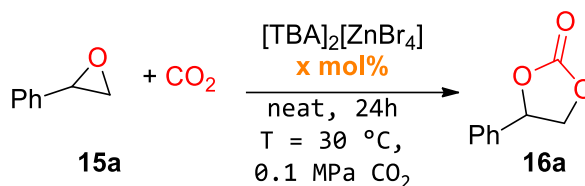
Reactions performed in an autoclave. Reaction conditions: styrene oxide (SO) 2.19 mmol; cat. 1 mol%; $P(\text{CO}_2) = 0.8 \text{ MPa}$; $T = 30 \text{ }^\circ\text{C}$; $t = 16\text{h}$. [b] Conversion and selectivity determined by ^1H NMR using mesitylene as the internal standard.

6.12.6 Reactions at ambient pressure of CO₂:

Entry	Cat. 0.5 mol%	Temperature (°C)	Conv. 15a % ^[b]	Sel. 16a % ^[b]
26	[TBA] ₂ [ZnCl ₄]	100	63	89
27		50	11	91
28	[TBA] ₂ [ZnBr ₄]	100	87	63
29		50	47	96
30	[TBA] ₂ [ZnI ₄]	100	80	83
31		50	22	82

Reactions performed in an autoclave. Reaction conditions: styrene oxide (SO) 2.19 mmol; cat. 0.5 mol%; P(CO₂) = 0.1 MPa; t = 4h. [b] Conversion and selectivity determined by ¹H NMR using mesitylene as the internal standard.

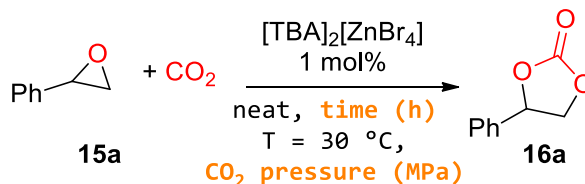
6.12.7 Influence of catalyst loading at room temperature and ambient pressure:



Entry	Cat. loading (mol%)	Conv. 15a % ^[b]	Sel. 16a % ^[b]
32	0.5	34	97
33	1	47	>99
34	5	47	>99

Reaction performed under a CO_2 balloon (0.1 MPa). Reaction conditions: styrene oxide (SO) 2.19 mmol; $T = 30\text{ }^\circ\text{C}$. [b] Conversion and selectivity determined by ^1H NMR using mesitylene as the internal standard.

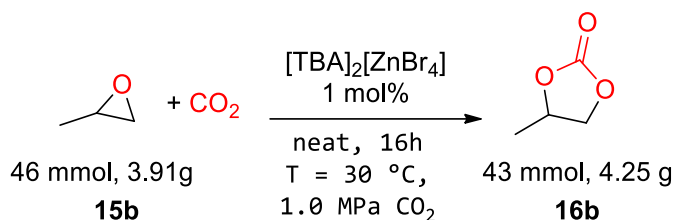
6.12.8 Final optimization of the reaction conditions:



Entry	CO_2 pressure (MPa)	t (h)	Conv. 15a % ^[b]	Sel. 16a % ^[b]
1	0.1	24	47	>99
2	0.1	16	42	98
3 ^[c]	0.1	16	69	>99
4 ^[d]	0.2	16	88	>99
5 ^[d]	0.8	16	87	98

Reaction performed under a CO_2 balloon (0.1 MPa). Reaction conditions: styrene oxide (SO) 2.19 mmol; $T = 30\text{ }^\circ\text{C}$. [b] Conversion and selectivity determined by ^1H NMR using mesitylene as the internal standard. [c] Reaction under CO_2 bubbling. [d] Reaction performed in autoclave.

6.12.9 Multigram scale-up reaction:



A 250 mL stainless steel autoclave reactor was equipped with a 100 mL glass vials, containing the catalyst/propylene oxide mixture (1 mol% (400 mg) of $[\text{TBA}]_2[\text{ZnBr}_4]$ in 3.24 mL (46.3 mmol) of **15b**). The vial was equipped with a magnetic stirring bar and sealed with a specific cap. The autoclave was then charged with 0.5 MPa CO_2 and vented-off. This operation was performed twice and then the autoclave was charged with 1.0 MPa CO_2 and stirred at 30 °C for 16 hours. The stirring was then stopped, and the CO_2 released. The product mixture was weighted and analyzed by ^1H NMR analysis. At the end of the reaction only propylene carbonate and the catalyst were present, while the possible remaining propylene oxide was evaporated during the venting of the autoclave and no other side products were found by NMR analysis (selectivity for **16b** >99%).

Isolated yield: 94%, 4.250 g

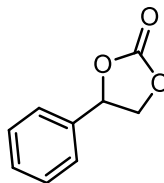
6.12.10 Catalyst recycling experiments:

The product of the scale up reaction was distilled in vacuum to obtain pure propylene carbonate and pure $[\text{TBA}]_2[\text{ZnBr}_4]$. To the latter, 46 mmol of **15b** were added and the mixture was subjected to the same procedure of the scale-up reaction. The reaction was performed at 30°C for 16h under 1.0 MPa CO_2 pressure. The product was obtained and analyzed as previously described, obtaining propylene carbonate as the sole product (selectivity for **16b** >99%). At this point, the product was distilled in vacuum and the reaction was repeated once more, to evaluate the robustness of the catalyst for a total of 3 cycles, after which a total of **12.65 g** of pure **16b** were obtained. The results are summarized in the following table, where also TON and TOF values are reported.

Entry	Cat. 1 mol%	Conv. 15b % ^[a]	Yield 16b % ^[a]	TON ^[b]	TOF ^[b]
1- first cycle	[TBA] ₂ [ZnBr ₄]	94	94	94	5.9
2- second cycle	[TBA] ₂ [ZnBr ₄]	93	93	187	5.8
3- third cycle	[TBA] ₂ [ZnBr ₄]	92	92	279	5.8

[a] Conversion and selectivity determined by ¹H NMR using mesitylene as the internal standard. [b] Turnover number (mol_{1a(converted)}}·mol_{cat}⁻¹) and Turnover frequency (mol_{1a(converted)}}·mol_{cat}⁻¹·reaction time⁻¹).

6.12.11 Product characterization:

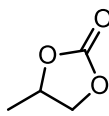


4-Phenyl-1,3-dioxolan-2-one (16a):

¹H NMR (300 MHz, CDCl₃) isolated by precipitation with hexane.

δ 7.54 – 7.46 (m, 3H), 7.42 – 7.38 (m, 2H), 5.70 (t, *J* = 8.2 Hz, 1H), 4.82 (t, *J* = 8.2 Hz, 1H), 4.37 (t, *J* = 8.2 Hz, 1H).

Data are in agreement with literature.^[251]

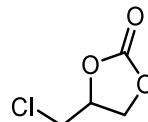


4-Methyl-1,3-dioxolan-2-one (16b):

¹H NMR (300 MHz, CDCl₃)

δ 4.91 – 4.82 (m, 1H), 4.56 (pst, *J* = 8.0 Hz, 1H), 4.03 (pst, *J* = 7.8 Hz, 1H), 1.49 (d, *J* = 6.3 Hz, 3H).

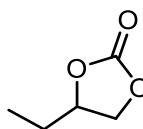
Data are in agreement with literature.^[251]

4-(Chloromethyl)-1,3-dioxolan-2-one (16c):

$^1\text{H NMR}$ (300 MHz, CDCl_3) isolated via column chromatography on silica gel, eluent: hexane ethyl acetate 7:3.

δ 5.02 - 4.96 (m, 1H), 4.60 (pst, $J = 8.6$ Hz, 1H), 4.43 (dd, $J = 8.9, 5.8$ Hz, 1H), 3.80 (dd, $J = 12.1, 4.6$ Hz, 1H), 3.74 (dd, $J = 12.1, 4.6$ Hz, 1H).

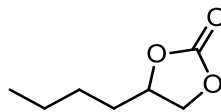
Data are in agreement with the literature.^[251]

4-Ethyl-1,3-dioxolan-2-one (16d):

$^1\text{H NMR}$ (400 MHz, CDCl_3)

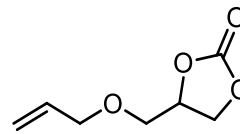
δ 4.69 - 4.61 (m, 1H), 4.52 (dd, $J = 8.0, 7.0$ Hz, 1H), 4.07 (dd, $J = 8.4, 7.0$ Hz, 1H), 1.83 - 1.70 (m, 2H), 1.00 (t, $J = 7.4$ Hz, 3H).

Data are in agreement with the literature.^[251]

4-ⁿButyl-1,3-dioxolan-2-one (16e):

$^1\text{H NMR}$ (300 MHz, CDCl_3)

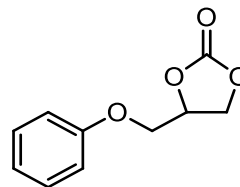
δ 4.74 - 4.67 (m, 1H), 4.54 (dd, 1H, $J = 8.4, 7.0$ Hz), 4.08 (dd, 1H, $J = 8.4, 7.0$ Hz), 1.81 - 1.71 (m, 2H), 1.40 - 1.34 (m, 4H), 0.90 (t, 3H, $J = 7.4$ Hz).

4-((Allyloxy)methyl)-1,3-dioxolan-2-one (16f):

¹H NMR (400 MHz, CDCl₃)

δ 5.93 – 5.83 (m, 1H, H₆), 5.30 (dd, *J* = 17.2, 1.5 Hz, 1H, H₇), 5.23 (dd, *J* = 10.4, 1.2 Hz, 1H, H_{7'}), 4.85 – 4.75 (m, 1H, H₂), 4.51 (pst, *J* = 8.4 Hz, 1H, H₁), 4.41 (dd, *J* = 8.3, 6.1 Hz, 1H, H_{1'}), 4.11 – 4.02 (m, 2H, H₅), 3.70 (dd, *J* = 11.0, 3.9 Hz, 1H, H₃), 3.62 (dd, *J* = 11.0, 3.8 Hz, 1H, H_{3'}).

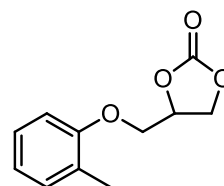
Data are in agreement with the literature.^[251]

4-(Phenoxymethyl)-1,3-dioxolan-2-one (16g):

¹H NMR (400 MHz, CDCl₃)

δ 7.33 (m, 2H), 6.94 (m, 3H), 5.05 (m, 1H), 4.64 (pst, 1H, *J* = 8.8 MHz), 4.58 (m, 1H), 4.25-4.19 (m, 2H).

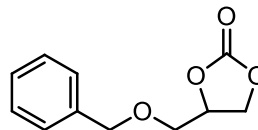
Data are in agreement with the literature.^[155]

4-((o-tolyloxy) methyl)-1,3-dioxolan-2-one (16h):

¹H NMR (400 MHz, CDCl₃)

δ 7.21 (m, 2H), 6.98-6.82 (m, 2H), 5.02 (m, 1H), 4.58 (m, 2H), 4.19-4.08 (m, 2H), 2.28 (s, 3H).

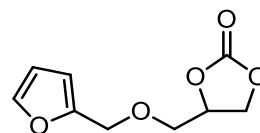
Data are in agreement with the literature.^[252]

4-(benzyloxymethyl)-1,3-dioxolan-2-one (16i):

$^1\text{H NMR}$ (400 MHz, CDCl_3)

δ 7.32 (m, 5H), 4.78 (m, 1H), 4.54 (m, 2H), 4.41 (pst, 1H, $J = 8.4$ MHz), 4.32 (m, 1H), 3.67 (dd, 1H, $J = 11.2$ MHz, $J = 3.2$ MHz), 3.55 (dd, 1H, $J = 11.2$ MHz, $J = 3.6$ MHz).

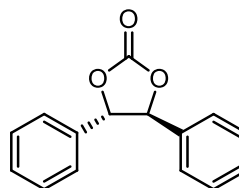
Data are in agreement with the literature.^[252]

4-((Furan-2-ylmethoxy)methyl)-1,3-dioxolan-2-one (16j):

$^1\text{H NMR}$ (400 MHz, CDCl_3)

δ 7.35 (s, 1H), 6.29 (bs, 2H), 4.74 (m, 1H), 4.42 (m, 3H), 4.21 (m, 1H), 3.62-3.52 (m, 2H).

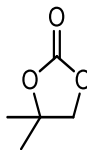
Data are in agreement with the literature.^[251]

***trans*-4,5-Diphenyl-1,3-dioxolan-2-one (16k):**

$^1\text{H NMR}$ (400 MHz, CDCl_3)

δ 7.45 (m, 10H), 5.50 (s, 2H).

Data are in agreement with the literature.^[251]

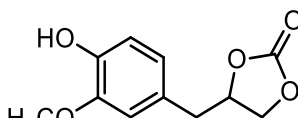


4,4-Dimethyl-1,3-dioxolan-2-one (16l):

$^1\text{H NMR}$ (400 MHz, CDCl_3)

δ 4.12 (s, 2H), 1.45 (s, 6H).

Data are in agreement with the literature.^[251]

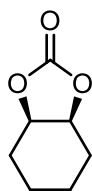


Eugenol carbonate (16m):

$^1\text{H NMR}$ (400 MHz, CDCl_3)

δ 6.88 (d, $J = 8.0$ Hz, 1H), 6.74 (d, $J = 1.6$ Hz, 1H), 6.69 (dd, $J = 8.0, 1.6$ Hz, 1H), 5.69 (bs, 1H), 4.96 – 4.89 (m, 1H), 4.44 (t, $J = 8.2$ Hz, 1H), 4.17 (dd, $J = 8.5, 6.8$ Hz, 1H), 3.90 (s, 3H), 3.05 (dd, $J = 12.4, 6.1$ Hz, 2H), 2.97 (dd, $J = 12.4, 6.0$ Hz, 1H).

Data are in agreement with the literature.^[135]

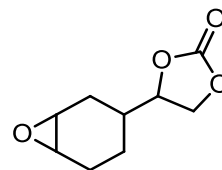


cis-Cyclohexene carbonate (16n):

$^1\text{H NMR}$ (400 MHz, CDCl_3)

δ 4.55 (s, 2H), 1.89 (m, 4H), 1.61 (m, 2H), 1.43 (m, 2H).

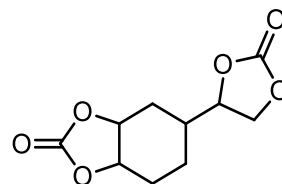
Data are in agreement with the literature.^[251]

4-(7-Oxabicyclo[4.1.0]heptan-3-yl)-1,3-dioxolan-2-one (16p):

¹H NMR (400 MHz, CDCl₃)

δ 4.31 (m, 2H), 3.95 (m, 1H), 3.01-2.95 (m, 3H), 2.00 - 0.80 (m, 6H).

Data are in agreement with the literature.^[251]

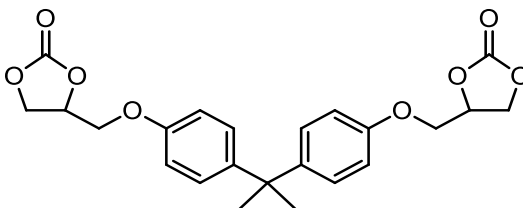
cis-5-(2-Oxo-1,3-dioxolan-4-yl)hexahydrobenzo[d][1,3]dioxol-2-one (16q):

¹H NMR (400 MHz, CDCl₃)

δ 4.71 (m, 1H), 4.62 (m, 2H), 4.42-4.38 (m, 2H), 3.01-2.95 (m, 3H), 2.00 - 0.80 (m, 6H).

Data are in agreement with the literature.^[251]

4,4'-(((propane-2,2-diylbis(4,1-phenylene))bis(oxy))bis(methylene))bis(1,3-dioxolan-2-one) (16r):

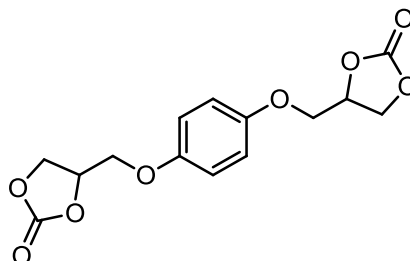


$^1\text{H NMR}$ (400 MHz, CDCl_3)

δ 7.04 (d, 4H, $J = 8.8$ MHz), 6.74 (d, 4H, $J = 8.8$ MHz), 4.92 (m, 2H), 4.46 (pst, 1H, $J = 8.4$ MHz), 4.34 (m, 2H), 4.12 – 4.00 (m, 4H), 1.63 (s, 6H).

Data are in agreement with the literature.^[155]

4,4'-((1,4-phenylenebis(oxy))bis(methylene))bis(1,3-dioxolan-2-one) (16s):

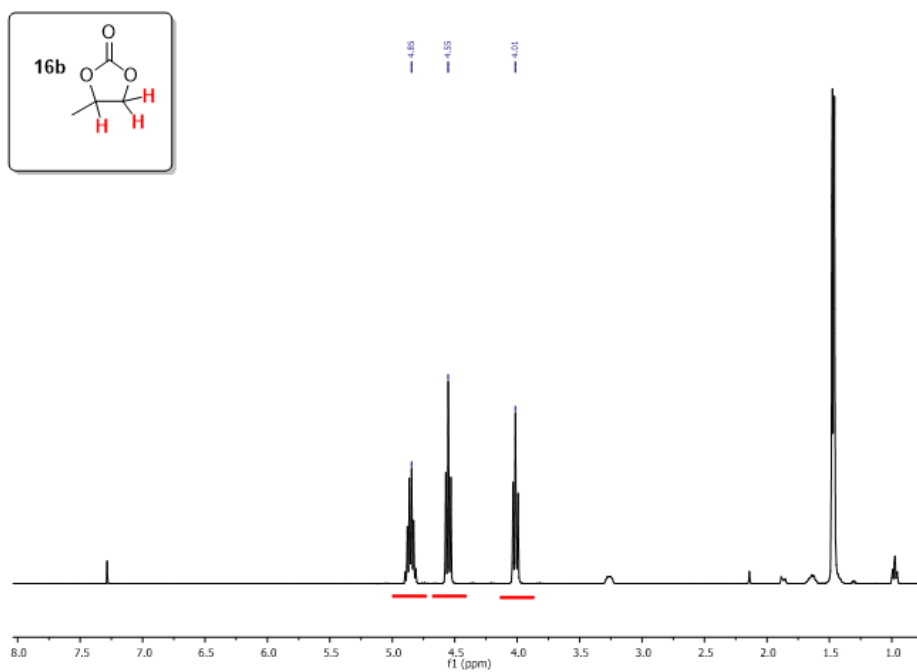
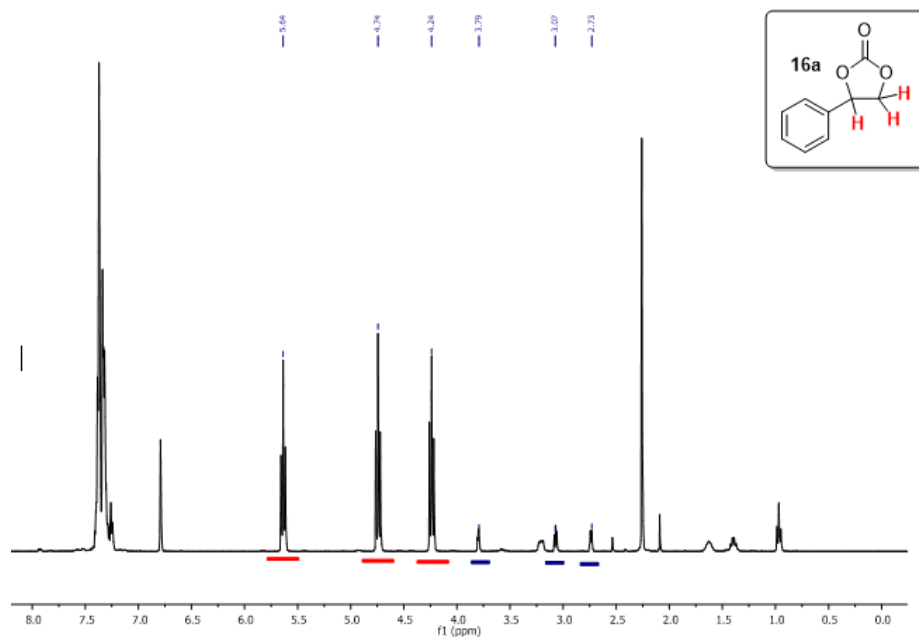


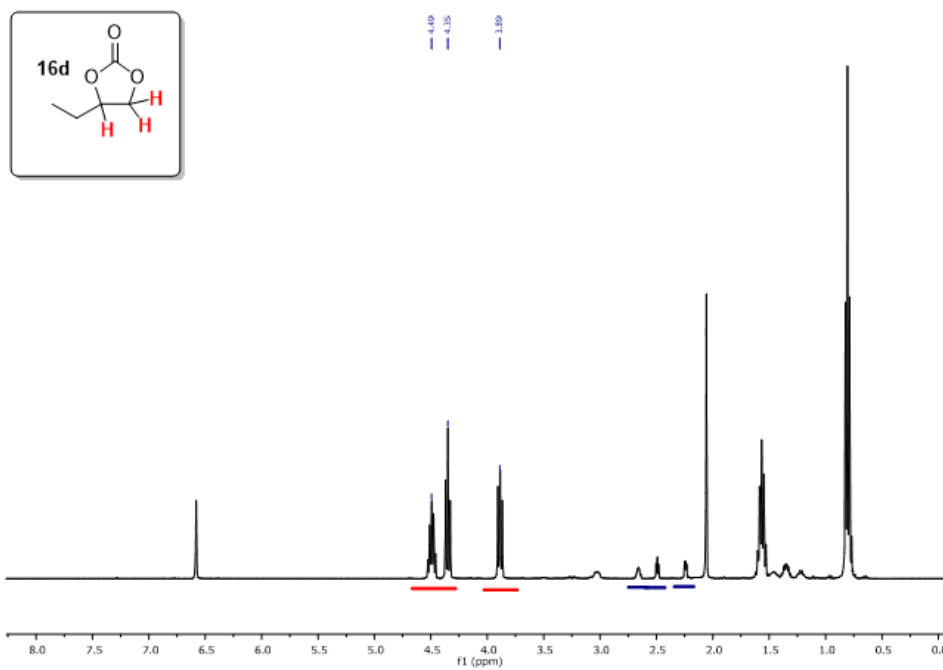
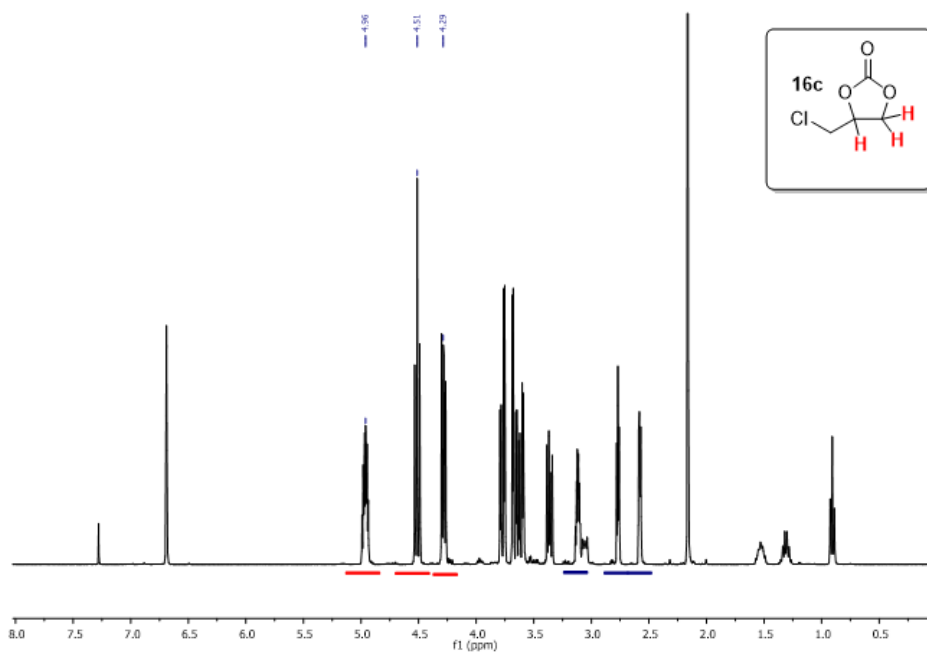
$^1\text{H NMR}$ (400 MHz, CDCl_3)

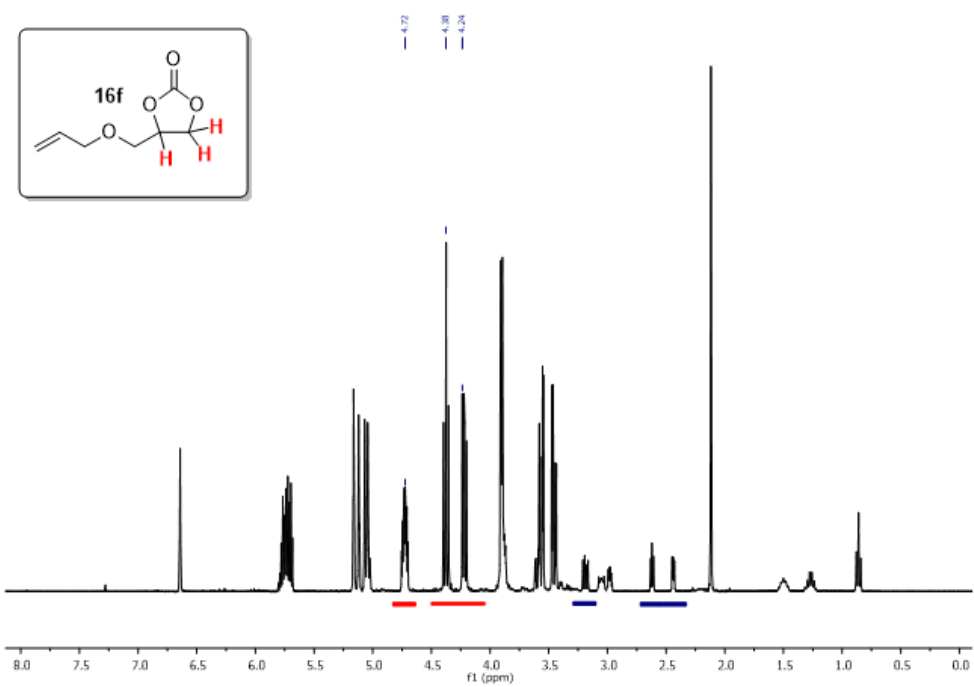
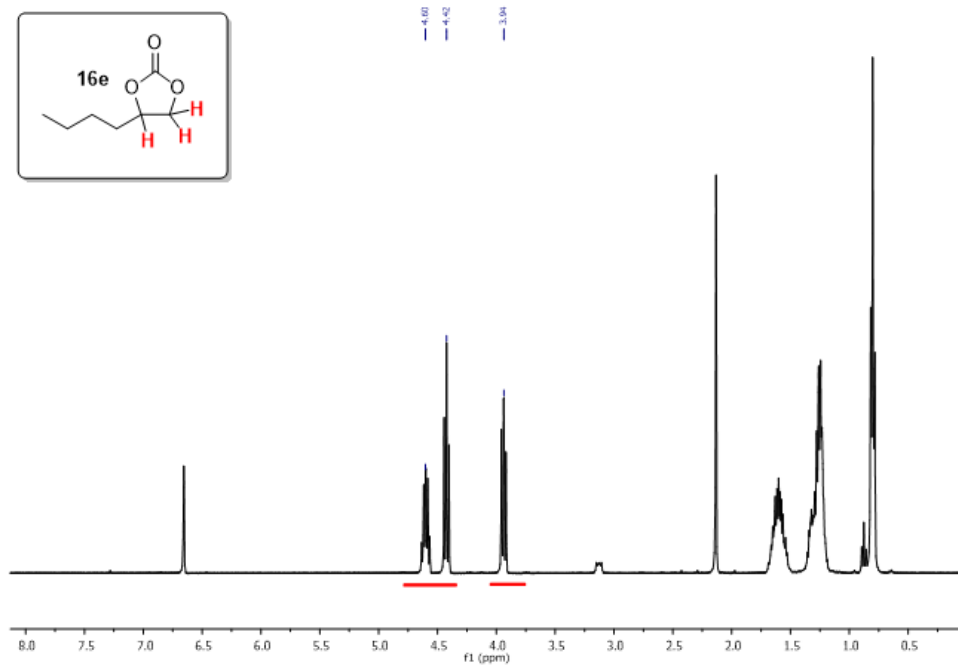
δ 6.92 (m, 4H), 5.13 (m, 2H), 4.62 (pst, 1H, $J = 7.2$ MHz), 4.38 (pst, 1H, $J = 6.8$ MHz), 4.38 – 4.21 (m, 4H).

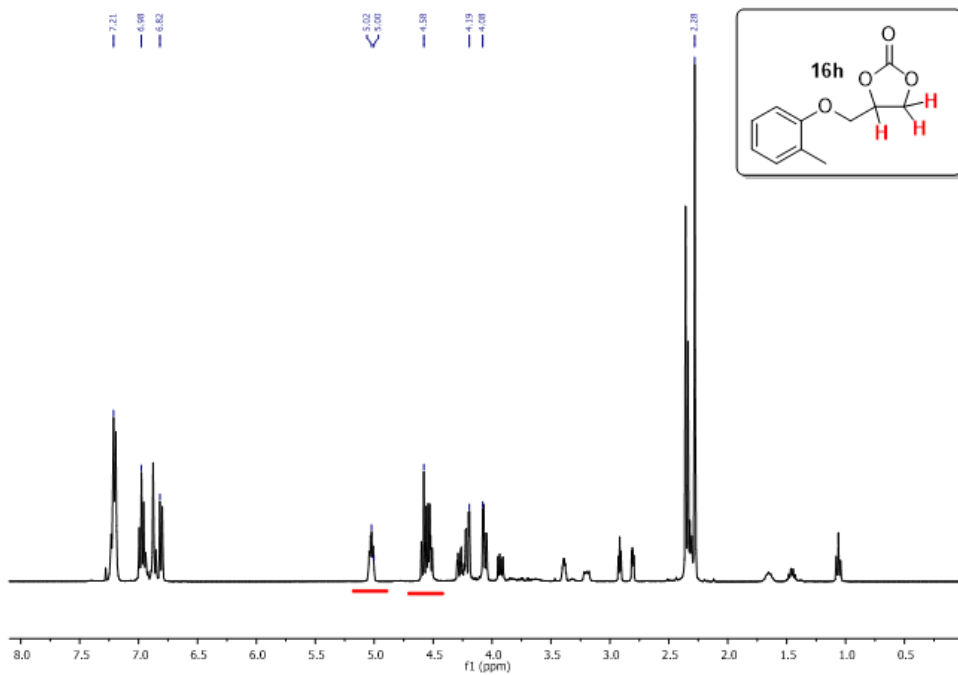
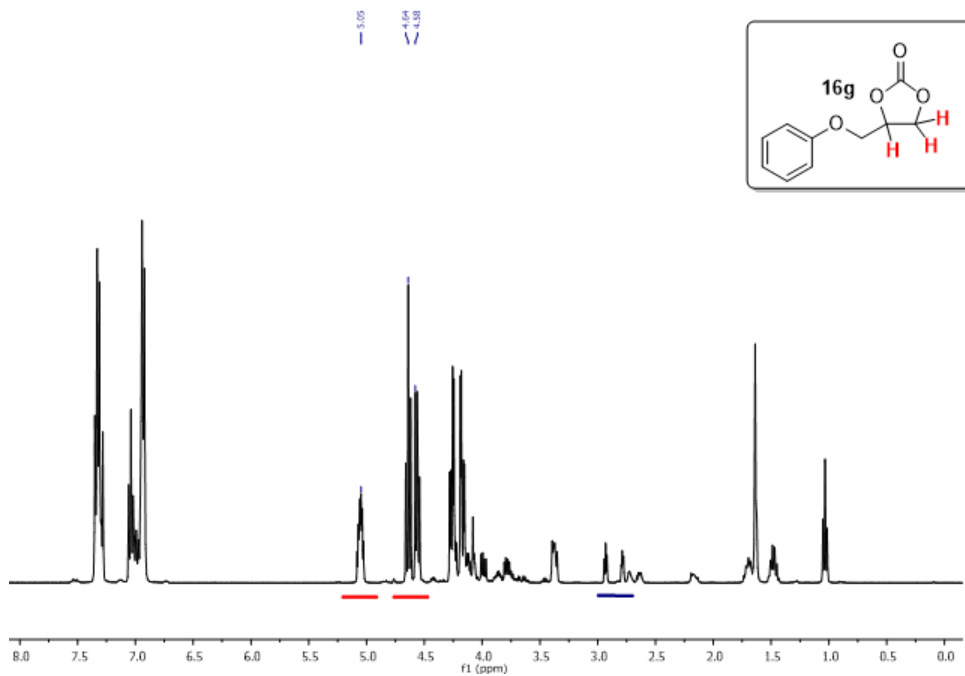
Data are in agreement with the literature.^[155]

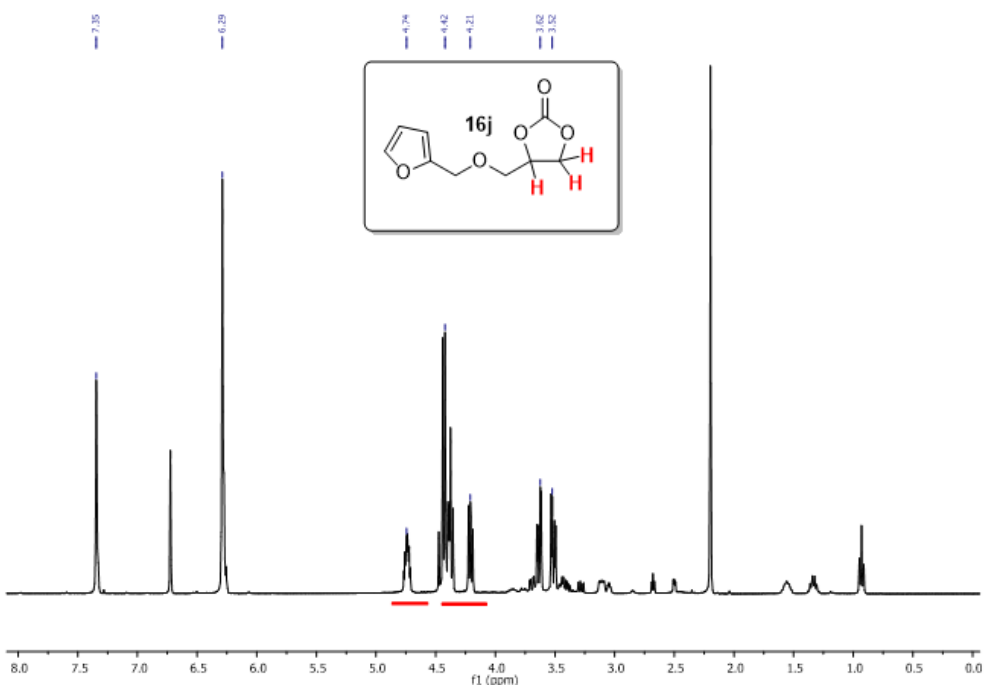
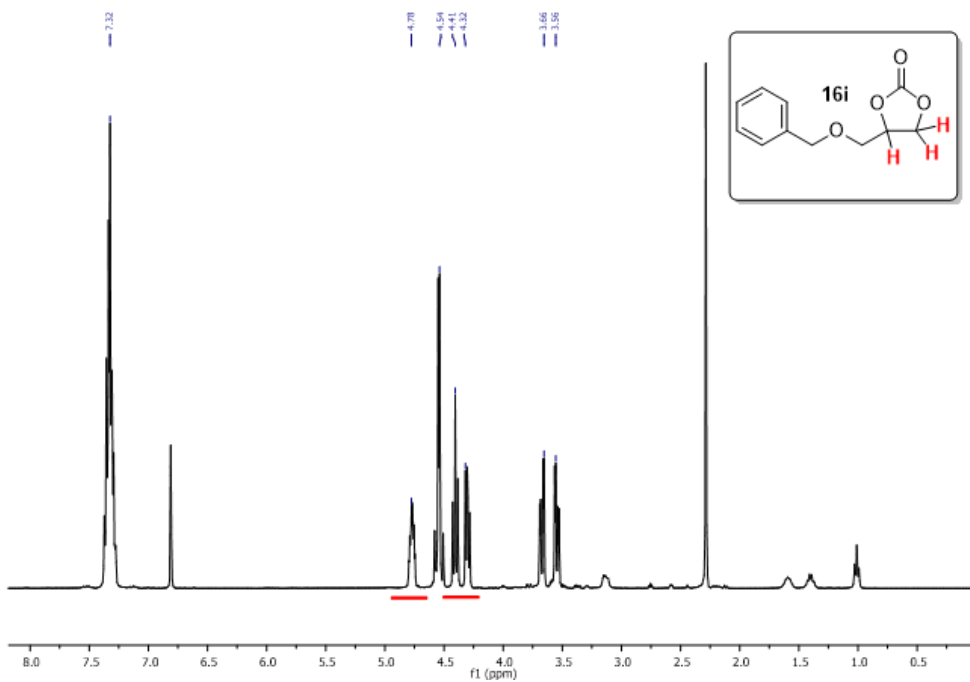
6.12.12 Selected NMR spectra of cyclic carbonates: (blue residues of the starting epoxide)

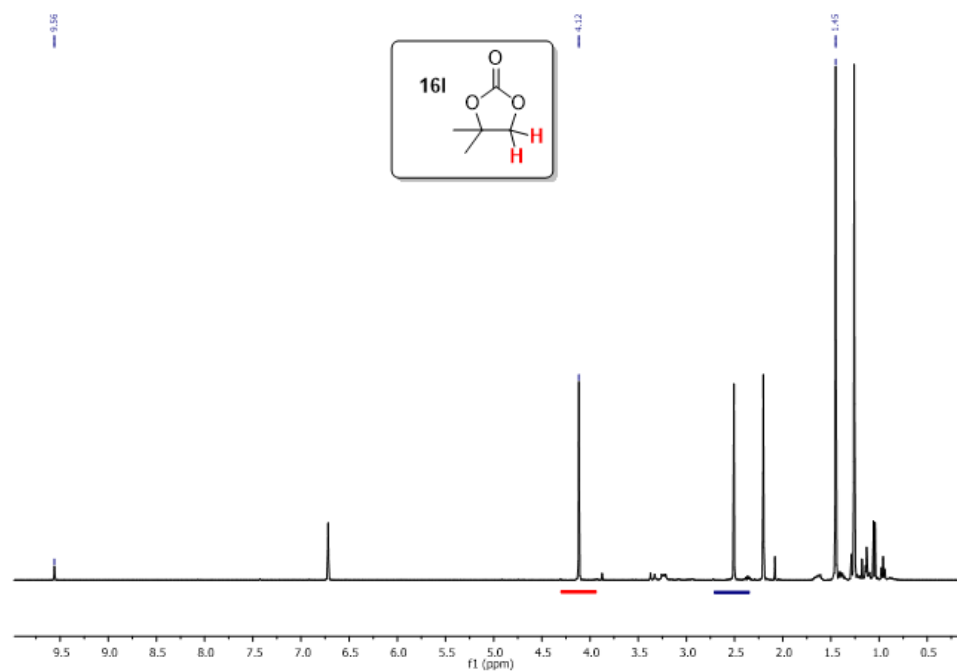
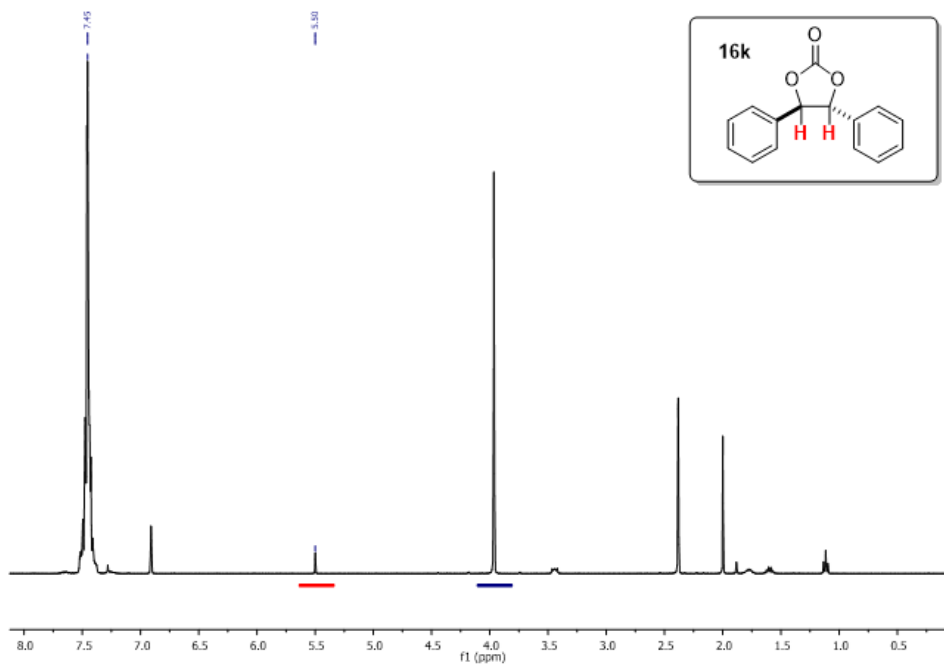


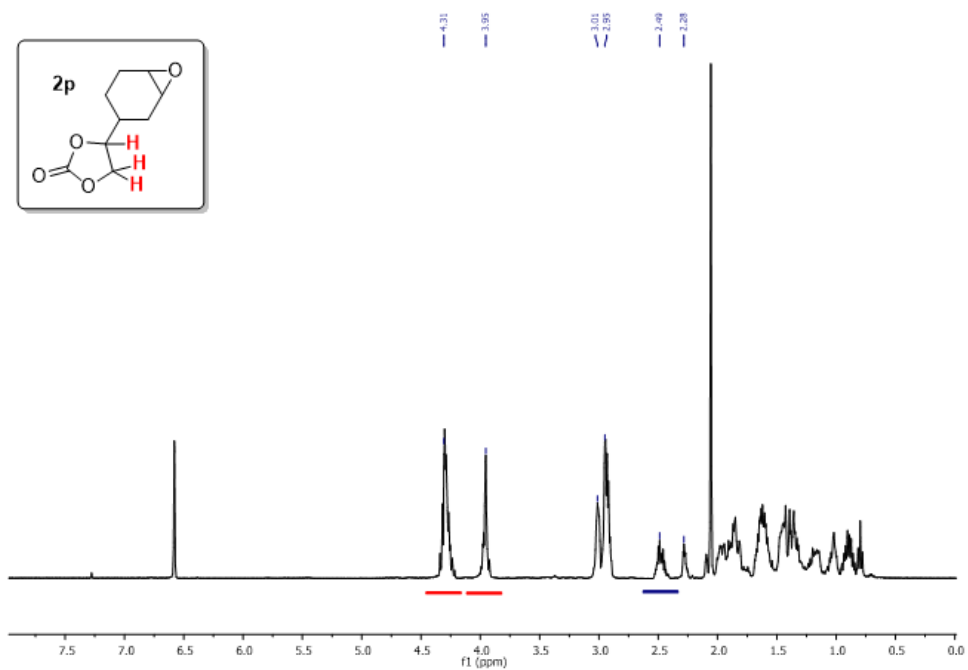
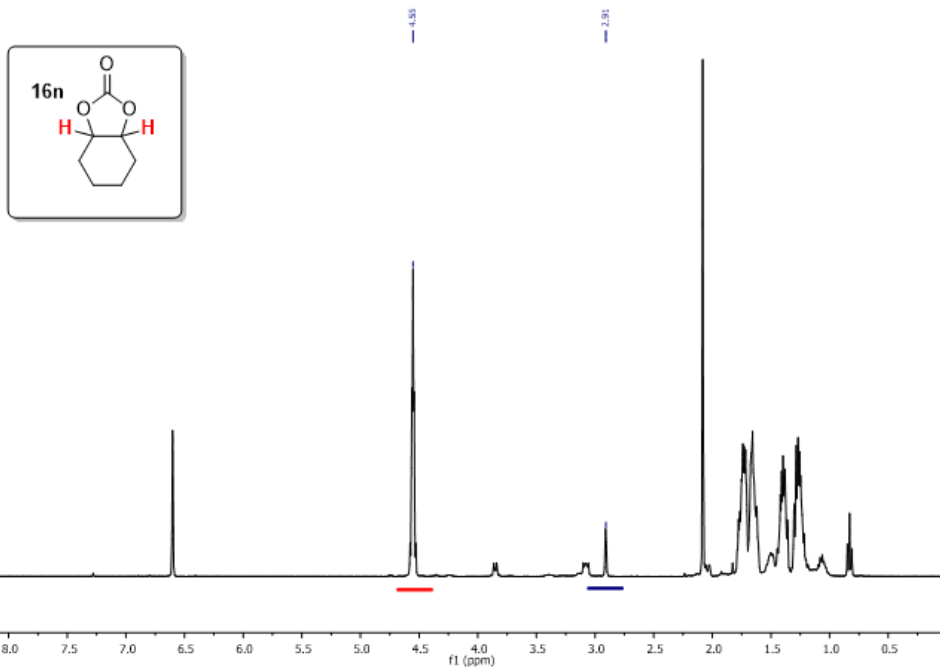


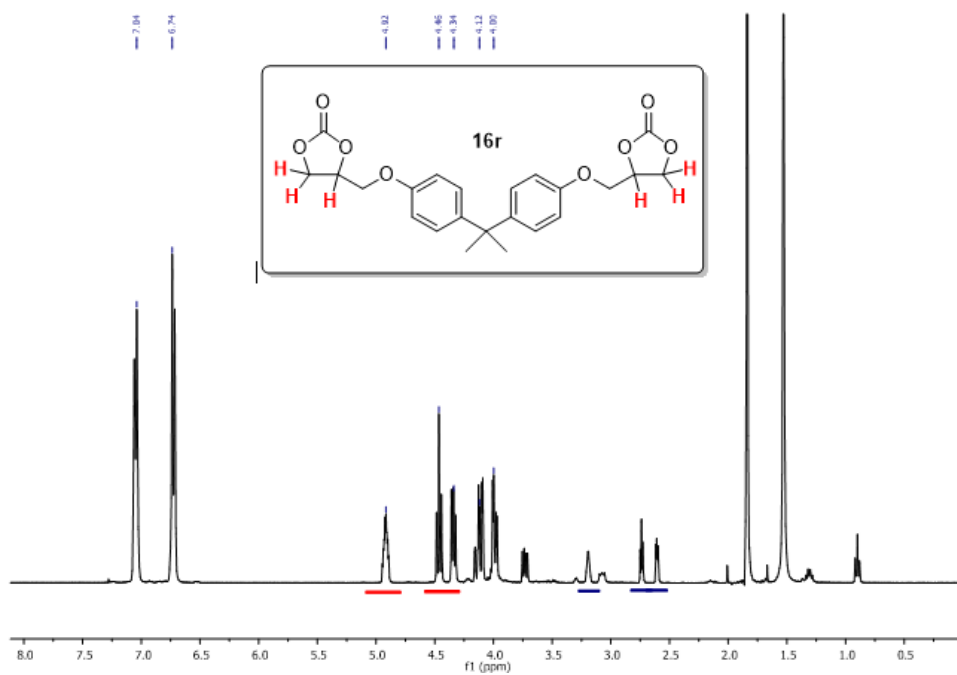
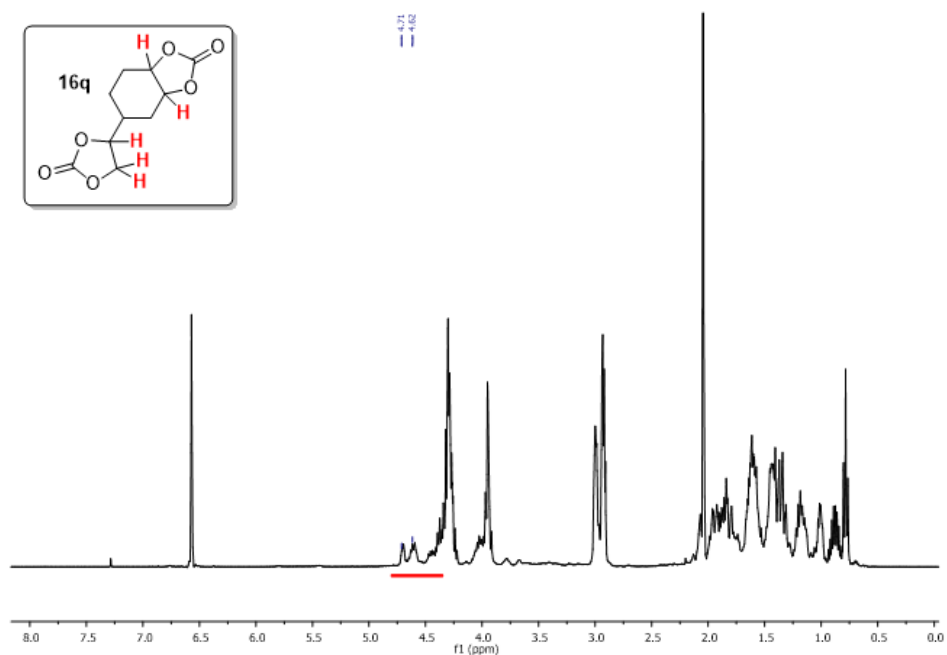


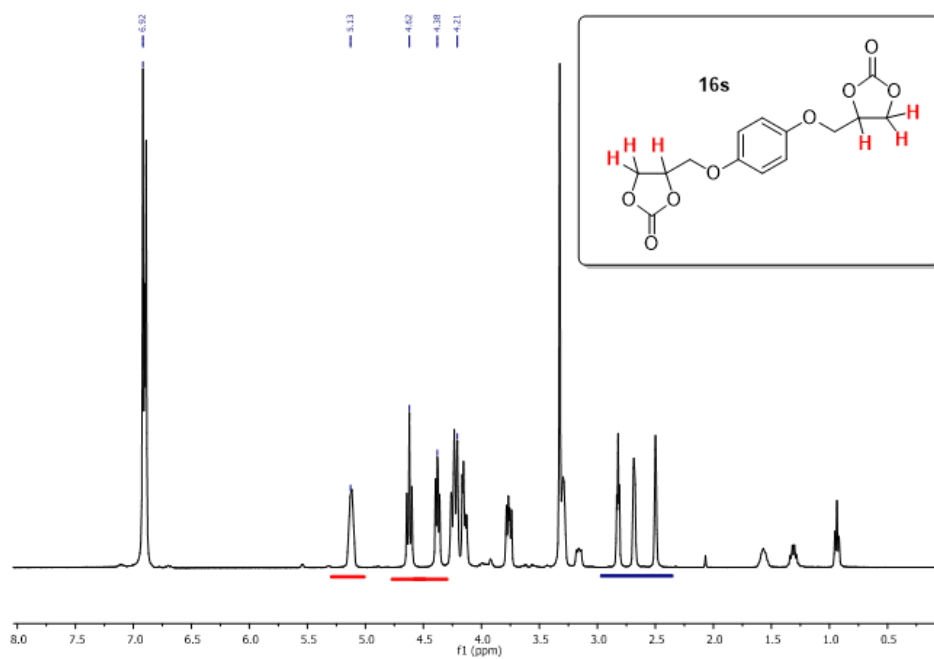






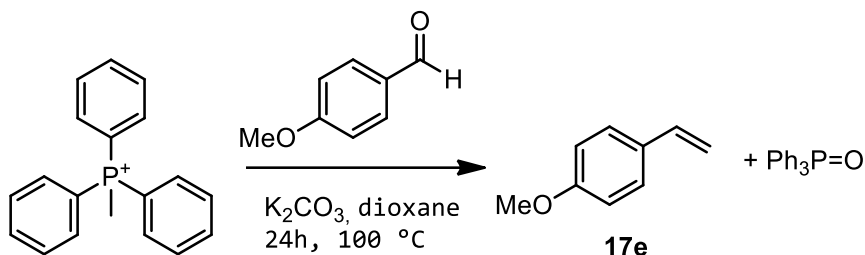






6.13 CYCLOADDITION OF AZIRIDINES AND CO₂, CATALYZED BY AMMONIUM FERRATES:

6.13.1 Synthesis of 4-Methoxystyrene (17e):



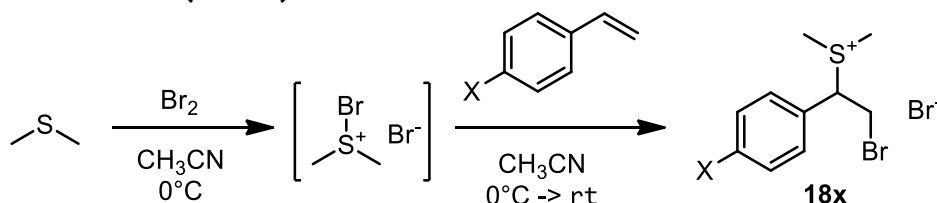
18.435 g of triphenylmethyl phosphonium bromide (300 mmol) and 10.890 g (80 mmol) of potassium carbonate were stirred at room temperature in 150 mL of dioxane for 1 hour under a nitrogen atmosphere. 6 mL of *p*-anisaldehyde (50 mmol) were then dissolved in 14 mL of dioxane and added dropwise to the mixture. The reaction was heated to 100 °C and proceeded for 24 h.

At the end of the reaction, the excess triphenylphosphine oxide was precipitated with the addition of hexane. The mixture was then filtered, and dioxane was distilled off.

Yield: 2.15 g (32%).

¹H NMR (400 MHz, CDCl₃)

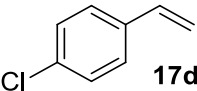
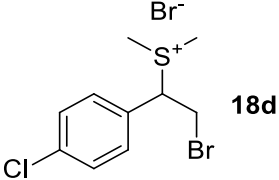
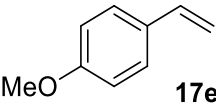
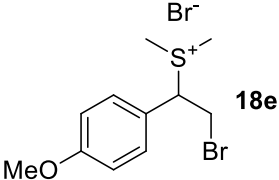
6.13.2 Synthesis of dimethyl-(1-aryl-2-bromo)-ethyl sulfonium bromides (18a-e):



A solution of bromine (1 eq) in acetonitrile was added dropwise to an ice-cold solution of dimethyl sulfide (3.7 eq in acetonitrile). Immediately a yellow precipitate (an adduct between bromide and dimethyl sulfide) was formed. The styrene substrate (17x, 1.27 eq) was added to the mixture, stirred for 30 minutes at 0°C and further 30 minutes at room temperature. Dimethyl-(1-aryl-2-bromo)-ethyl sulfonium bromide precipitated as a white solid, it was filtered and washed with ether. The products were used without further purification.

Table E4. Synthesis of aziridine precursors. General procedure described above, yields reported in the table.

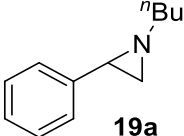
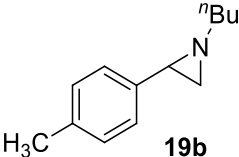
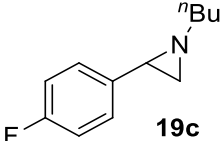
Entry	Substrate (17)	Product (18)	Yield (% product)
1			63
2			45
3			65

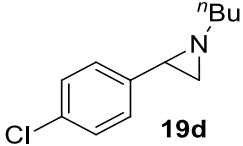
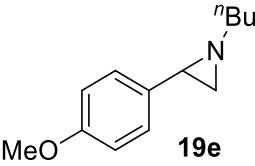
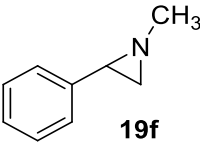
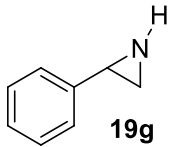
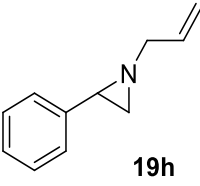
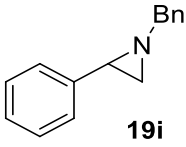
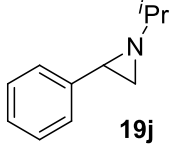
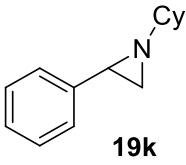
Entry	Substrate (17)	Product (18)	Yield (% product)
4			45
5			17

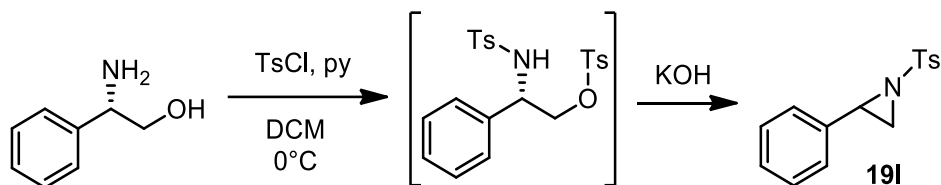
6.13.3 General synthesis of 1-alkyl-2-arylaziridines:

1 eq of dimethyl-(1-aryl-2-bromo)ethyl sulfonium bromide was dissolved in water. To this, an aqueous solution of the necessary amine, 5 fold-excess, was added dropwise. An oily phase separated from the resulting aqueous solution. The mixture was stirred over night at room temperature. The desired aziridine was then extracted with ethyl acetate and washed with brine. The product was purified with a silica plug, using a solution of hexane and ethyl acetate as an eluent, varying their ratio according to the needs of the specific aziridine (from 9:1 to 8:2).

Yield of the reactions are reported in the following table:

Amine	Product	Yield (% product)
Butylamine		86
Butylamine		85
Butylamine		85

Butylamine	 19d	88
Butylamine	 19e	78
Methylamine (EtOH solution)	 19f	78
Ammonia solution (28%)	 19g	26
Allylamine	 19h	87
Benzylamine	 19i	90
^t propylamine	 19j	93
Cyclohexylamine	 19k	89

6.13.4 Synthesis of 1-Tosyl-2-phenylaziridine (191):^[253]

0.864 g of (S)-phenylglycinol (6.3 mmol) were dissolved in 6.5 mL of DCM and added dropwise to an ice-cold solution containing 2.650 g of tosyl chloride (13.9 mmol) and 3.6 mL of pyridine (44.4 mmol) in 7 mL of DCM. The solution was stirred at room temperature overnight. The next day, the solution was washed with 60 mL of HCl 1M and 25 mL of DCM. The product was extracted with DCM and washed with a 10% solution of copper sulfide, and then with two brine washings. The resulting organic phase was dried with sodium sulfate and the solvent was evaporated under vacuum. Crude tosyl-protected phenylglycinol was then purified by column flash chromatography (silica gel, 60 μ m), using a mixture of hexane and ethyl acetate as eluent (2:1).

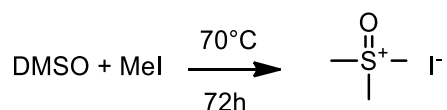
The purified product (2.132 g) is then dissolved in 12 mL of toluene, and an aqueous solution of KOH (0.860 g in 4.5 mL) is added dropwise. The obtained mixture is stirred overnight and then extracted with toluene. The solution is dried with sodium sulfate and the solvent is evaporated with reduced pressure. 1-tosyl-2-phenylaziridine crystallizes under high vacuum

Yield: 69 mg, 4%.

¹H NMR (300 MHz, CDCl₃)

δ 7.88 (d, 2H), 7.38-7.25 (m, 7H), 3.8 (dd, 1H), 2.99 (d, 1H), 2.44 (s, 3H), 2.38 (d, 1H).

6.13.5 Synthesis of trimethylsulfoxonium iodide:

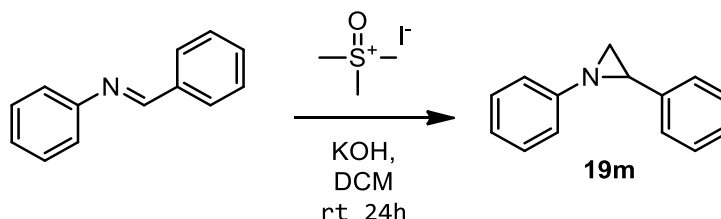


Distilled DMSO (2.5 mL, 35 mmol) and methyl iodide (1.75 mL, 28 mmol) were added in a pressure tube. The reaction mixture was stirred at 70°C for 72 hours. Crude product was filtered and washed with CHCl₃. Pure product was obtained by hot-cold crystallization in water

Yield: 3.512 g, 57%.

The product was immediately used for the next reaction.

6.13.6 Synthesis of 1,2-diphenylaziridine (19m):



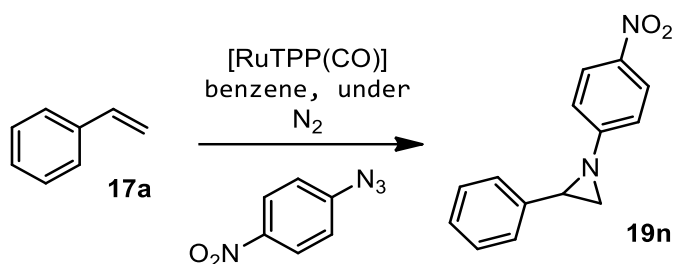
Benzylideneaniline (2 g, 11 mmol) was dissolved in DCM (50 mL). Trimethylsulfoxonium iodide (3.37 g, 16.5 mmol) and finely grounded KOH (2.7 g, 49 mmol) were added to the reactor. The reaction mixture was stirred for 24 hours at room temperature. The mixture was extracted with water and DCM. The organic phase was dried with NaSO₄ and evaporated in vacuum. The product was obtained as a pale-yellow solid after crystallization at -20°C.

Yield: 1.439 g, 67%.

¹H NMR (300 MHz, CDCl₃)

δ 7.45-7.35 (m, 4H), 7.32-7.25 (m, 3H), 7.12-6.98 (m, 3H), 3.13 (dd, 1H), 2.50 (dd, 1H), 2.43 (dd, 1H) ppm.

6.13.7 Synthesis of 1-(4-nitro)-phenyl-2-phenylaziridine (19n):



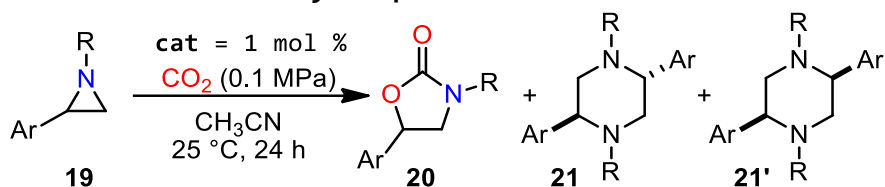
Styrene (0.87 mL, 7.5 mmol) was added in a Schlenk flask with [Ru(TPP)CO] (22 mg, 0.03 mmol) in distilled benzene (30 mL) under nitrogen. 4-nitro-phenylazide (245 mg, 1.5 mmol) was added at 100°C and the reaction mixture was stirred at reflux for 2 hours. Crude product was purified by flash column chromatography (Hexane:AcOEt:TEA 9:1:0.1). Product was obtained as a red oil.

Yield: 180 mg, 50%.

¹H NMR (300 MHz, CDCl₃)

δ 8.15 (d, 2H), 7.45-7.34 (m, 5H), 7.11 (d, 2H), 3.26 (dd, 1H), 2.55 (d, 1H), 2.56 (d, 1H).

6.13.8 General catalytic procedure:



Method A: The catalyst (0.01 mmol or 0.025 mmol), CH_3CN (1 mL) and the substrate (1 mmol) were added in a round bottom Schlenk tube that was previously dried in an oven at 120°C overnight. The reaction mixture was stirred for 16 hours under CO_2 (1 atm) at 25°C . At the end of the reaction, the solvent was evaporated with reduced pressure, dibromomethane (0.35 mL, 0.5 mmol) was added as the internal standard (ISTD) and the mixture was diluted in CDCl_3 for $^1\text{H-NMR}$ analysis. Before acquiring NMR spectra, the CDCl_3 solutions were filtered on celite pad to remove the insoluble catalysts. Isolated products were purified by flash chromatographic column (silica gel, $60 \mu\text{m}$, n -hexane/ $\text{AcOEt} = 8:2 + \text{TEA}$ (triethylamine) 10%).

Method B: A 250 mL stainless steel autoclave reactor was equipped with three 2.5 mL glass vials, containing the catalyst (0.25 mol%), the aziridine (1 mmol) in 1 mL of CH_3CN . The vials were equipped with magnetic stirring bars and sealed with specific caps. The autoclave was then charged with 0.5 MPa CO_2 and vented-off. This operation was performed twice and then the autoclave was charged with 1.6 MPa of CO_2 and placed in the heating bath at 100°C for 16h. The reactor was then cooled to RT and the CO_2 pressure released. The solvent was evaporated with reduced pressure, dibromomethane (0.35 mL, 0.5 mmol) was added as the internal standard (ISTD) and the solute was dissolved in CDCl_3 for $^1\text{H-NMR}$ analysis. Before acquiring NMR spectra, the CDCl_3 solutions were filtered on celite pad to remove the insoluble catalysts. Isolated products were purified by flash chromatographic column (silica gel, $60 \mu\text{m}$, n -hexane/ $\text{AcOEt} = 8:2 + \text{TEA}$ 10%).

6.13.9 GC methods:

Gas-chromatographic analyses were performed with GC-FAST technique using a Shimadzu GC-2010 equipped with a Supelco SLB™-5ms capillary column. Decane was used as the internal standard. The samples were prepared with a concentration of 0.1-0.3 mg/mL in DCM.

PTV parameters:

Temperature = 280 °C

Injection mode: SPLIT

Pressure = 2.74 bar

Total flow = 11.2 mL/min

Column flow = 0.33 mL/min

Linear velocity = 33.7 cm/sec

Purge flow = 1 mL/min

Split Ratio = 30.0

FID parameters:

Temperature = 290 °C

Make-up gas: N₂/air

H₂ flow = 40mL/min

Make-up flow = 30 mL/min

Air flow = 400 mL/min

Column parameters:

RATE	Temperature	Holding Time
-	100 °C	1 min
45 °C/min	290 °C	3 min

6.13.10 Catalyst screening:

Entry	Catalyst	Conversion 19a % ^[b]	Selectivity 20a % ^[b]	TOF ^[c] (h ⁻¹)
1	[TBA][FeCl ₄]	58	96 ^[d]	2.4
2	[TBA][FeCl ₃ Br]	90	97 ^[d]	3.8
3	[TBA][FeBr ₃ Cl]	94	97	3.9
4	[TBA][FeBr ₄]	>99	97	4.1
6	FeBr ₃	88	84	3.7
7	FeCl ₃	23	35	1.0
8	TBACl	10	>99	0.4
9	TBABr	12	>99	0.5
10	TBAI	7	>99	0.3
11	none	5	40	0.2
11	FeBr ₃ + TBABr	>99	99	4.1
12	FeCl ₃ + TBACl	33	67	1.4

Reaction conditions: 1-butyl-2-phenyl aziridine (1 mmol) and catalyst (1 mol%) in CH₃CN (1 mL) under CO₂ atmosphere (P = 0.1 MPa) at T = 25 °C; t = 24 h. [b] Conversion and selectivity determined by ¹H NMR using dibromomethane as the internal standard. [c] Turnover frequency (mol_{1a(converted)}·mol_{cat}⁻¹·reaction time⁻¹). [d] Traces of the 3-butyl-4-phenyl-1,3-oxazolidin-2-one isomer were detected (d.r. = 96:4)

6.13.11 Kinetic study:

Following the general catalytic method A, the reaction's kinetics were studied by taking 15 μL samples over a 24 h period and diluting them with ethyl acetate in a 10 mL volumetric flask. Decane was used as ISTD, in a concentration of 0.1 mg/mL. The timestamps were chosen as it follows: 0 seconds, 10 minutes, 30 minutes, 1 hour, 2 hours. A further control was run after 24 hours. The data was collected for 1-butyl-2-phenylaziridine, **19a**, and for 1-butyl-2-(4-methylphenyl)aziridine, **19b**.

Conversion values of **19a**:

Entry	Time (min)	[19a] (mol/dm ³)
1	3.62	0.73
2	10.15	0.66
3	30.1	0.52
4	60.42	0.48
5	121.4	0.30
6	1440	0.01

At short times the consumption of the reactant is strongly influenced by the formation of piperazines **21a** and **21a'**, which likely follows a second order kinetic with respect to aziridine **19a**. Later on, the reaction is governed by a first order kinetic with respect to the aziridine **19a**, due to the formation of oxazolidin2-one **20a** under an approximately constant concentration of carbon dioxide. To fit experimental data, a mixed kinetic rate expression was solved, as described in the following.

The time-dependent concentration of the reactant is the solution of the Bernoulli problem:

$$\begin{cases} -A'(t) = k_1A(t) + k_2A(t)^2 \\ A(0) = A_0 \end{cases}$$

Where A is the concentration of aziridine, A_0 the initial concentration of aziridine, k_1 is the rate constant for the formation of oxazolidin-2-one, **20a**, k_2 is the rate constant for the formation of piperazines, **21a** and **21a'**. This equation can be solved by introducing a function $z(t)$:

$$z(t) = \frac{1}{A(t)}$$

$$z'(t) = -\frac{1}{A(t)^2} A'(t)$$

Accordingly:

$$\begin{cases} z'(t) = k_1 z(t) + k_2 \\ z(0) = \frac{1}{A_0} \end{cases}$$

The solution of this linear differential equation can be expressed as:

$$z(t) = e^{k_1 t} \cdot \left(\frac{1}{A_0} + \int_0^t k_2 \cdot e^{-k_1 t} dt \right)$$

$$z(t) = e^{k_1 t} \cdot \left(\frac{1}{A_0} + k_2 \left(\frac{-e^{k_1 t} + 1}{k_1} \right) \right)$$

Hence the concentration of A as a function of time reads as (1):

$$A(t) = e^{-k_1 t} \cdot \left(\frac{A_0 k_1}{k_1 + A_0 k_2 - A_0 k_2 \cdot e^{-k_1 t}} \right)$$

This function has been fitted against the experimental results, obtaining the following parameters:

Parameter	1-butyl-2-phenyl-aziridine, 19a	1-butyl-2-(4-methylphenyl)aziridine, 19b
A_0 (M)	0.74	0.74
k_1 (s^{-1})	$2.38 \cdot 10^{-5}$	$1.67 \cdot 10^{-5}$
k_2 ($s^{-1}M^{-1}$)	$2.33 \cdot 10^{-4}$	$4.17 \cdot 10^{-4}$

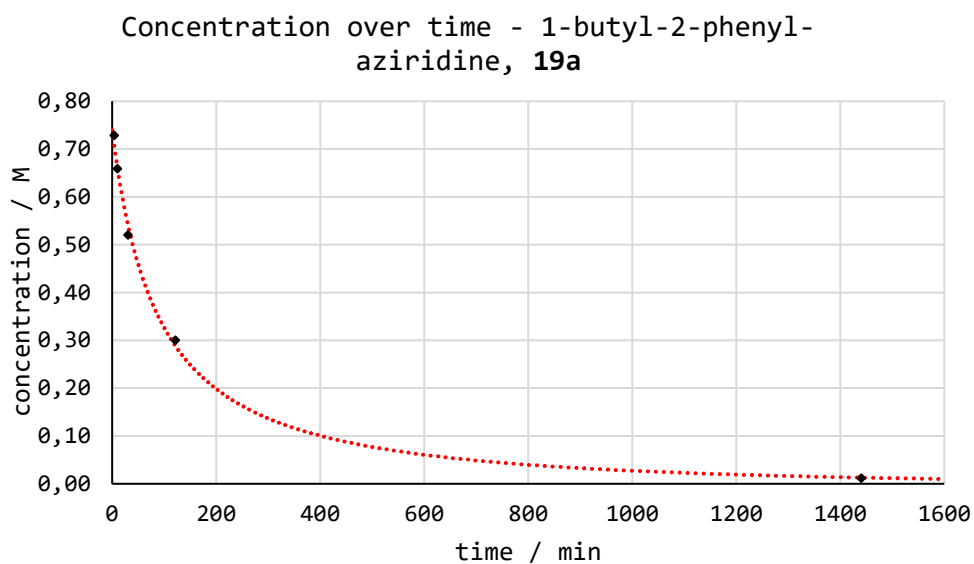


Figure E20. Best fit solution for the kinetic reaction of aziridine **19a**, using equation (1). Data point 4 is not displayed, as it was considered an outlier.

The early data points were also fitted by assuming a first order dependance of the reaction rate with respect to the starting aziridine. Of the two concurring processes (piperazines, **21a** and **21a'** and oxazolidin-2-one, **20a**, formation), it is reasonable to assume that during early reaction times piperazine formation prevails, if a second order kinetic in aziridine **19a** is followed, while later on, the formation of oxazolidin-2-one is likely to become the faster process, as also confirmed by the selectivity of the reaction. In any case, a neat first order with respect of the starting aziridine **19a** was not observed.

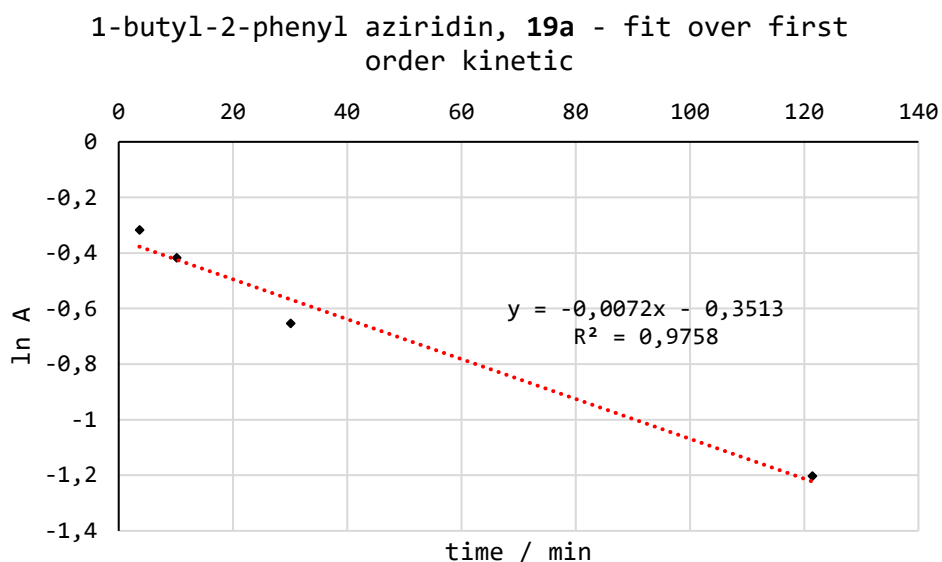


Figure E21. Best fit solution for the first order kinetic reaction of aziridine **19a**. A = aziridine concentration

The observed rate constant can be deduced from the expression (2):

$$\ln A(t) = \ln A_0 - k_1 \cdot t \quad (\text{first order kinetic})$$

The fitted first order constant results in $k_1 = 1.2 \cdot 10^{-4} \text{ s}^{-1}$.

Conversion values of **19b**:

Entry	Time (min)	[19b] (mol/dm ³)
1	4.02	0.72
2	12.27	0.68
3	31.82	0.48
4	62.68	0.37
5	123.75	0.22
6	1440	0.01

The results of the best fit with these data using equation (1) and (2) are graphically reported for aziridine **19b**. A clean first order with respect of the starting aziridine **19b** was not observed.

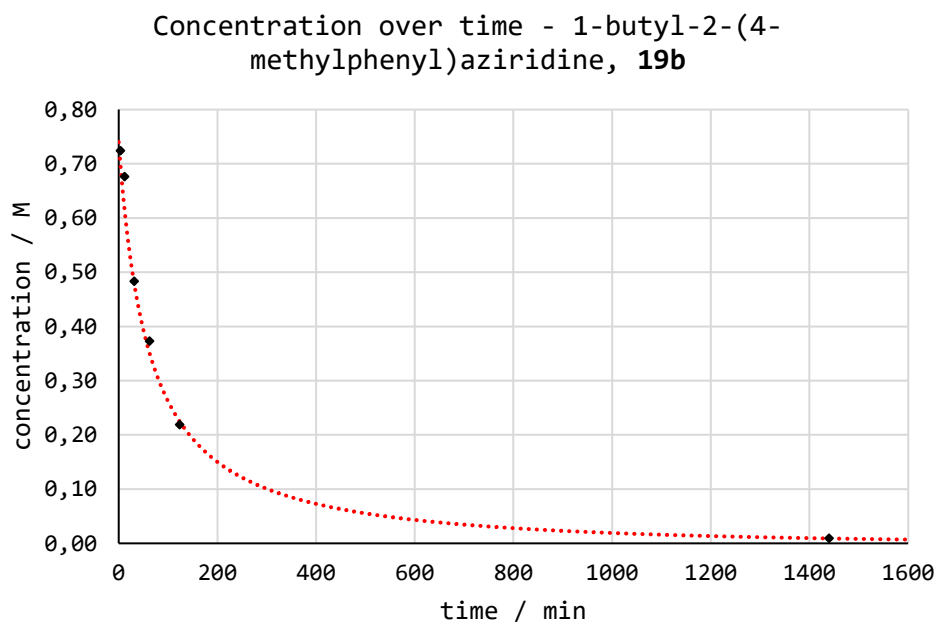


Figure E22. Best fit solution for the kinetic reaction of aziridine **19b**, using equation (1).

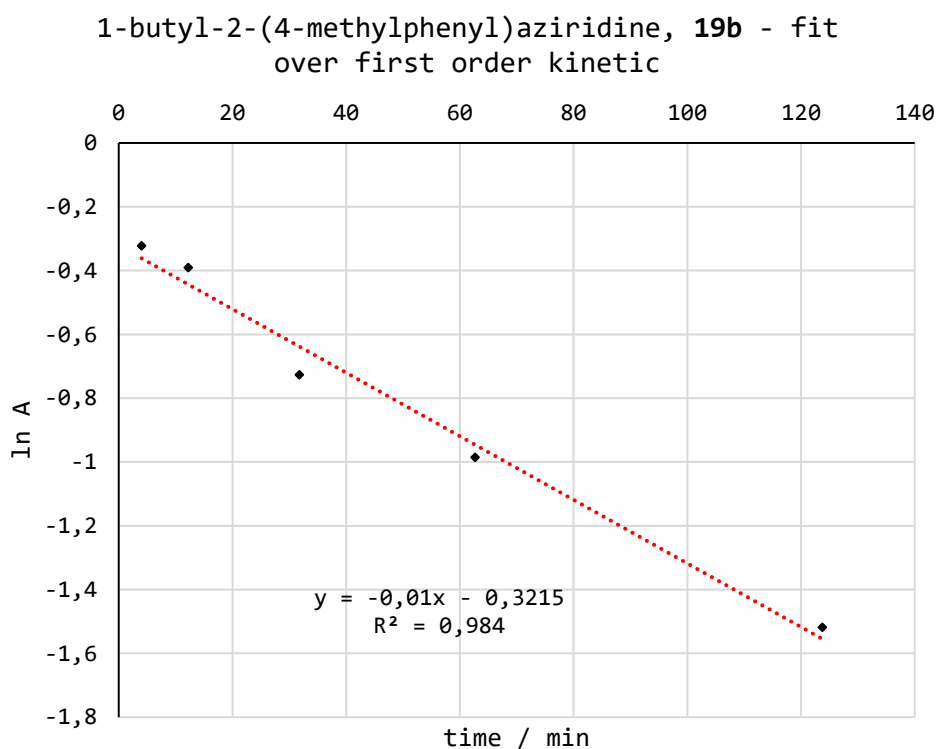


Figure E23. Best fit solution for the first order kinetic reaction of aziridine **19b**. A = aziridine concentration.

First order rate constant for **19b**: $k_1 = 1.67 \cdot 10^{-4} \text{ s}^{-1}$

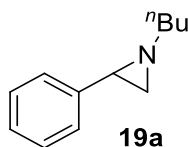
This data proves that the reaction rate for aziridine **19b** consumption is faster than for **19a**.

6.13.12 Scale-up of the reaction (gram scale):

A 200 mL stainless steel autoclave reactor was equipped with a 100 mL glass vials, containing the catalyst (1 mol%, 35 mg [TBA][FeBr₄]) and 1-butyl-2-phenylaziridine **19a** (1.02 g, 5.7 mmol) in 5.7 mL of acetonitrile. The vial was equipped with a magnetic stirring bar and sealed with a specific cap. The autoclave was then charged with 0.5 MPa CO₂ and vented-off. This operation was performed twice and then the autoclave was charged with 0.5 MPa CO₂ and stirred for 24 hours. A sample was withdrawn for GC analysis showing a complete conversion with almost full selectivity in desired **20a**; traces of piperazines **21a** and **21a'** were also detected)

Workup: 3-butyl-5-phenyloxazolidin-2-one, **20a**, was purified by diluting the reaction solution with 50 mL of ethyl acetate and extracting the catalyst with 50 mL of brine for three times. The resulting organic phase was dried with sodium sulfate and the solvent was evaporated with reduced pressure

Isolated yield: 1.02 g, 81%.

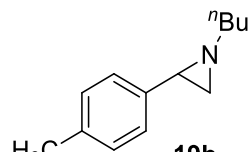
6.13.13 Products characterization:

1-butyl-2-phenylaziridine (19a):

Pale yellow oil.

¹H NMR (300 MHz; CDCl₃; T= 300K)

δ 7.29 - 7.12 (5H, m, H_{Ar}), 2.45 (dt, 1H), 2.28 (dt, 1H), 2.23 (dd, 1H), 1.83 (d, 1H), 1.59 (d, 1H), 1.67 - 1.55 (m, 2H), 1.44 - 1.34 (m, 2H), 0.91 (t, 3H).

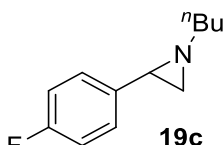


1-butyl-2-(4-methyl)-phenylaziridine (19b):

Deep yellow oil.

$^1\text{H NMR}$ (300 MHz; CDCl_3 ; T = 300K)

δ 7.18-7.09 (dt, 4H), 2.58-2.47 (m, 1H), 2.33 (s, 3H), 2.31-2.25 (m, 2H), 1.87 (d, 1H), 1.72-1.55 (m, 1H), 1.46-1.35 (m, 2H), 0.94 (t, 3H).

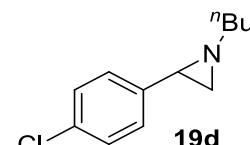


1-butyl-2-(4-fluoro)-phenylaziridine (19c):

Pale yellow oil.

$^1\text{H NMR}$ (300 MHz; CDCl_3 ; T = 300K)

δ 7.21 (dd, 2H), 7 (t, 2H), 2.55-2.45 (m, 1H), 2.38-2.25 (m, 2H), 1.85 (d, 1H), 1.67-1.56 (m, 4H), 1.47-1.36 (m, 2H), 0.94 (t, 3H).

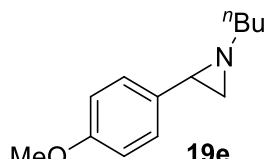


1-butyl-2-(4-chloro)-phenylaziridine (19d):

Brown oil.

$^1\text{H NMR}$ (300 MHz; CDCl_3 ; T = 300K)

δ 7.27 (d, 2H), 7.16 (d, 2H), 2.55-2.46 (m, 1H), 2.38-2.25 (m, 2H), 1.84 (d, 1H), 1.69-1.54 (m, 3H), 1.46-1.33 (m, 2H), 0.92 (t, 3H).

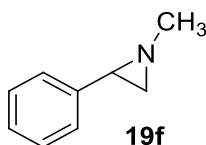


1-butyl-2-(4-methoxy)-phenylaziridine (19e):

Pale yellow oil.

$^1\text{H NMR}$ (300 MHz; CDCl_3 ; T = 300 K)

δ 7.18 (d, 2H), 6.85 (d, 2H), 3.80 (s, 3H), 2.55-2.45 (m, 1H), 2.35-2.22 (m, 2H), 1.87 (d, 1H), 1.68-1.58 (m, 3H), 1.48-1.35 (m, 2H), 0.94 (t, 3H).

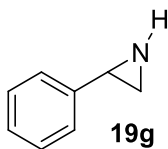


1-methyl-2-phenylaziridine (19f):

Colorless oil.

$^1\text{H NMR}$ (300 MHz; CDCl_3 ; T = 300K)

δ 7.35-7.20 (m, 5H), 2.51 (s, 3H), 2.28 (m, 1H), 1.92 (d, 1H), 1.64 (d, 1H).

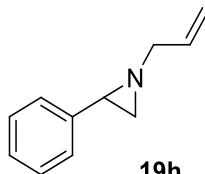


2-phenylaziridine (19g):

Pale yellow oil.

$^1\text{H NMR}$ (300 MHz; CDCl_3 ; T = 300K)

δ 7.37-7.23 (m, 5H); 3.05 (m, 1H); 2.29 (d, 1H); 1.77 (d, 1H).

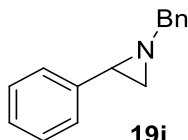


1-allyl-2-phenylaziridine (19h):

Colorless oil.

$^1\text{H NMR}$ (300 MHz; CDCl_3 ; T = 300K)

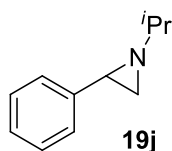
δ 7.40-7.20 (m, 5H, ArH), 6.0 (m, 1H), 5.28 (dd, 1H), 5.15 (dd, 1H), 3.20-3.12 (dd, 1H), 3.06-3.98 (dd, 1H), 2.37 (dd, 1H), 1.94 (d, 1H), 1.73 (d, 1H).

**1-benzyl-2-phenylaziridine (19i):**

Colorless oil.

$^1\text{H NMR}$ (300 MHz; CDCl_3 ; T = 300K)

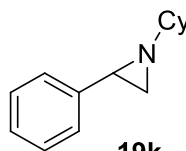
δ 7.47 - 7.28 (m, 10H), 3.74 (q, 2H), 2.59 (dd, 1H), 2.07 (d, 1H), 1.93 (d, 1H).

**1-isopropyl-2-phenylaziridine (19j):**

Pale yellow oil.

$^1\text{H NMR}$ (400 MHz; CDCl_3 ; T = 300K)

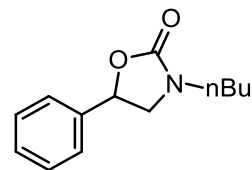
δ 7.51-7.13 (m, 5H), 2.34 (dd, 1H), 1.89 (d, 1H), 1.75-1.55 (m, 2H), 1.31-1.06 (m, 6H).

**1-cyclohexyl-2-phenylaziridine (19k):**

Pale yellow oil.

$^1\text{H NMR}$ (300 MHz; CDCl_3 ; T = 300K)

δ 7.24 - 7.20 (m, 4H), 7.19 - 7.12 (m, 1H), 2.30 (dd, 1H), 1.85 - 1.80 (m, 1H), 1.83 (d, 1H), 1.82 - 1.70 (m, 2H), 1.61 (d, 1H), 1.47 - 1.37 (m, 2H), 1.28 - 1.15 (m, 6H).

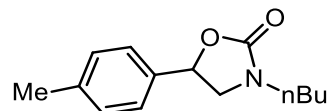
3-butyl-5-phenyloxazolidin-2-one (20a):

¹H NMR (400 MHz, CDCl₃)

δ 7.40-7.34 (m, 5H), 5.48 (pst, 1H, *J* = 8.0 Hz), 3.89 (pst, 1H, *J* = 8.8 Hz), 3.42 (pst, 1H, *J* = 8.0 Hz), 3.37-3.24 (m, 2H), 1.58-1.49 (m, 2H), 1.40-1.31 (m, 2H), 0.94 (t, 3H, *J* = 6.8 Hz).

¹³C NMR (100 MHz, CDCl₃)

δ 157.9, 138.9, 128.9, 128.8, 125.5, 74.3, 52.2, 43.9, 29.4, 19.8, 13.7.

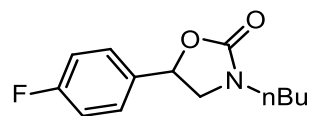
3-butyl-5-(4-methylphenyl)oxazolidin-2-one (20b):

¹H NMR (400 MHz, CDCl₃)

δ 7.25 (d, 2H, *J* = 8.4 Hz), 7.21 (d, 2H, *J* = 8.4 Hz), 5.45 (pst, 1H, *J* = 8.0 Hz), 3.89 (pst, 1H, *J* = 8.8 Hz), 3.42 (dd, 1H, *J* = 8.8, 8.0 Hz), 3.38-3.24 (m, 2H), 2.36 (s, 3H), 1.59-1.51 (m, 2H), 1.44-1.32 (m, 2H), 0.95 (t, 3H, *J* = 7.4 Hz).

¹³C NMR (100 MHz, CDCl₃)

δ 158.0, 138.6, 135.9, 129.5, 125.6, 74.3, 52.2, 43.9, 29.4, 21.1, 19.8, 13.7.

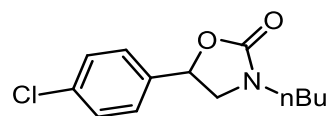
3-butyl-5-(4-fluorophenyl)oxazolidin-2-one (20c):

¹H NMR (400 MHz, CDCl₃)

δ 7.30 (dd, 2H, *J* = 8.4 Hz, *J*^{H-F} = 5.2 Hz), 7.04 (pst, 2H, *J* = 8.4 Hz), 5.42 (pst, 1H, *J* = 8.4 Hz), 3.87 (pst, 1H, *J* = 8.8 Hz), 3.36 (pst, 1H, *J* = 8.4 Hz), 3.33-3.19 (m, 2H), 1.50 (m, 2H), 1.31 (m, 2H), 0.90 (t, 3H, *J* = 7.2 Hz).

¹³C NMR (100 MHz, CDCl₃)

δ 162.9 (d, *J*_{C-F} = 248.0 Hz), 157.9, 134.8, 127.6, 116.7, 73.8, 52.2, 44.1, 29.6, 20.0, 13.7.

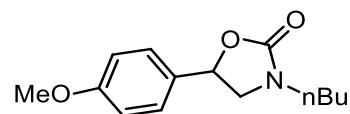
3-butyl-5-(4-chlorophenyl)oxazolidin-2-one (20d):

¹H NMR (400 MHz, CDCl₃)

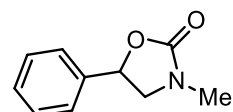
δ 7.32 (d, 2H, *J* = 8.3 Hz), 7.27 (d, 2H, *J* = 8.3 Hz), 5.43 (pst, 1H, *J* = 8.0 Hz), 3.90 (pst, 1H, *J* = 8.8 Hz), 3.35 (pst, 1H, *J* = 8.0 Hz), 3.33-3.21 (m, 2H), 1.50 (m, 2H), 1.32 (m, 2H), 0.90 (t, 3H, *J* = 7.2 Hz).

¹³C NMR (100 MHz, CDCl₃)

δ 157.6, 137.5, 134.5, 129.0, 127.0, 73.5, 51.9, 43.8, 29.3, 19.8, 13.6.

3-butyl-5-(4-methoxyphenyl)oxazolidin-2-one (20e):**¹H NMR** (400 MHz, CDCl₃)

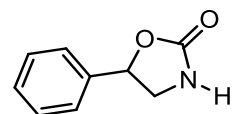
δ 7.28 (d, 2H, *J* = 8.8 Hz), 6.91 (d, 2H, *J* = 8.8 Hz), 5.42 (pst, 1H, *J* = 8.4 Hz), 3.85 (m, 1H), 3.81 (s, 3H), 3.42 (pst, 1H, *J* = 8.4 Hz), 3.38-3.22 (m, 2H), 1.58-1.48 (m, 2H), 1.44-1.28 (m, 2H), 0.94 (t, 3H, *J* = 7.4 Hz).

3-methyl-5-phenyloxazolidin-2-one (20f):**¹H NMR** (300 MHz, CDCl₃)

δ 7.40-7.30 (m, 5H), 5.45 (pst, 1H, *J* = 8.6 Hz), 3.90 (pst, 1H, *J* = 8.6 Hz), 3.42 (pst, 1H, *J* = 8.6 Hz), 2.89 (s, 3H).

¹³C NMR (100 MHz, CDCl₃)

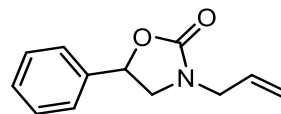
δ 158.2, 138.8, 128.9, 128.8, 125.6, 74.2, 54.4, 31.1.

5-phenyloxazolidin-2-one (20g):**¹H NMR** (300 MHz, CDCl₃)

δ 7.39 (m, 5H), 6.77 (bs, 1H, NH), 5.61 (pst, 1H, *J* = 8.5 Hz), 3.98 (pst, 1H, *J* = 8.5 Hz), 3.54 (pst, 1H, *J* = 8.5 Hz).

¹³C NMR (100 MHz, CDCl₃)

δ 160.4, 138.6, 128.9 (2C overlapping), 125.8, 78.0, 48.4.

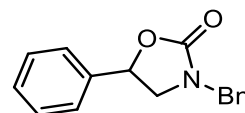
3-allyl-5-phenyloxazolidin-2-one (20h):

¹H NMR (300 MHz, CDCl₃)

δ 7.43-7.35 (m, 5H), 5.85-5.73 (m, 1H), 5.49 (pst, 1H, *J* = 8.0 Hz), 5.26-5.22 (m, 2H), 3.99-3.82 (m, 3H), 3.40 (pst, 1H, *J* = 8.0 Hz).

¹³C NMR (100 MHz, CDCl₃)

δ 157.7, 138.7, 131.9, 128.9, 128.8, 125.5, 118.8, 74.5, 51.8, 46.9.

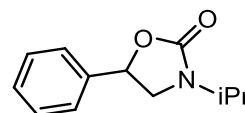
3-benzyl-5-phenyloxazolidin-2-one (20i):

¹H NMR (300 MHz, CDCl₃)

δ 7.43-7.26 (m, 10H), 5.44 (pst, 1H, *J* = 8.5 Hz), 4.53 (d, 1H, *J* = 15.0 Hz), 4.42 (d, 1H, *J* = 15.0 Hz), 3.77 (pst, 1H, *J* = 8.5 Hz), 3.30 (pst, 1H, *J* = 8.5 Hz).

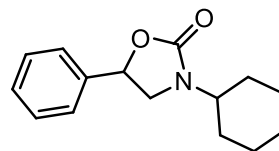
¹³C NMR (100 MHz, CDCl₃)

δ 158.0, 138.7, 135.7, 128.9 (2C overlapping), 128.8, 128.2, 128.0, 125.6, 74.5, 51.5, 48.4.

3-isopropyl-5-phenyloxazolidin-2-one (20j):

¹H NMR (400 MHz, CDCl₃)

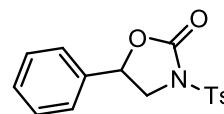
δ 7.32-7.29 (m, 5H), 5.46 (pst, 1H, *J* = 8.1 Hz), 4.16 (m, 1H), 3.80 (pst, 1H, *J* = 8.5 Hz), 3.67 (pst, 1H, *J* = 8.5 Hz), 1.23 (d, 3H, *J* = 6.7 Hz), 1.18 (d, 3H, *J* = 6.7 Hz).

3-cyclohexyl-5-phenyloxazolidin-2-one (20k):**¹H NMR** (300 MHz, CDCl₃)

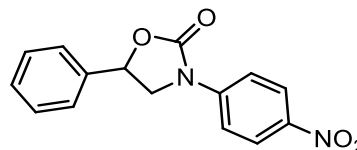
δ 7.38-7.27 (m, 5H), 5.47 (pst, 1H, *J* = 8.1 Hz), 3.88 (pst, 1H, *J* = 8.6 Hz), 3.64 (m, 1H), 3.39 (pst, 1H, *J* = 8.1 Hz), 1.92-1.07 (m, 10H).

¹³C NMR (100 MHz, CDCl₃)

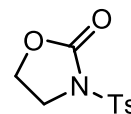
δ 129.3, 129.1, 125.9, 75.0, 48.7, 31.0, 30.5, 25.7.

3-tosyl-5-phenyloxazolidin-2-one (20l):**¹H NMR** (400 MHz, CDCl₃)

δ 7.95 (m, 2H), 7.40-7.22 (m, 7H), 5.52 (pst, 1H, *J* = 8.0 Hz), 4.42 (pst, 1H, *J* = 8.0 Hz), 4.87 (pst, 1H, *J* = 8.0 Hz), 2.43 (s, 3H).

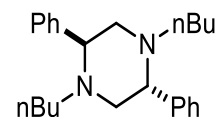
3-(4-nitrophenyl)-5-phenyloxazolidin-2-one (20n):**¹H NMR** (400 MHz, CDCl₃)

δ 8.23 (d, 2H, *J* = 9.3 Hz), 7.80 (d, 2H, *J* = 9.3 Hz), 7.50-7.40 (m, 5H), 5.73 (pst, 1H, *J* = 7.9 Hz), 4.50 (pst, 1H, *J* = 8.8 Hz), 4.10 (dd, 1H, *J* = 8.8 Hz, 7.9 Hz).

3-tosyl-oxazolidin-2-one (20o):

¹H NMR (400 MHz, CDCl₃)

δ 7.92 (m, 2H), 7.34 (m, 2H), 4.34 (m, 2H), 4.03 (m, 2H), 2.44 (s, 3H).

1,4-dibutyl-2,5-diphenylpiperazine (21a) (meso):

¹H NMR (400 MHz, CDCl₃)

δ 7.47-7.42 (m, 4H), 7.40-7.34 (m, 4H), 7.32-7.28 (m, 2H), 3.42 (dd, 2H, *J* = 10.6, 2.6 Hz), 3.09 (dd, 2H, *J* = 11.6, 2.8 Hz), 2.48 (pst, 2H, *J* = 11.0 Hz), 2.27 (m, 2H), 1.92 (m, 2H), 1.41-1.29 (m, 4H), 1.25-1.02 (m, 4H), 0.95 (t, 6H, *J* = 7.2 Hz).

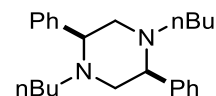
¹³C NMR (100 MHz, CDCl₃)

δ 142.2 (C), 128.4 (CH), 128.1 (CH), 127.3 (CH), 67.8 (CH), 60.9 (CH₂), 54.4 (CH₂), 28.3 (CH₂), 20.5 (CH₂), 14.0 (CH₃).

MS-ESI(+): calculated for C₂₄H₃₄N₂ 350.27; found: 351.36 (100%, M+1); 176.26 (40%, M/2 + 1).

Elem. An. calculated for C₂₄H₃₄N₂ C, 82.23; H, 9.78; N, 7.99; found: C, 82.44; H, 10.01; N, 7.78.

m.p. = 103-105 °C

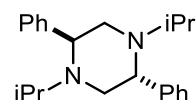
1,4-dibutyl-2,5-diphenylpiperazine (21a') (±):**¹H NMR** (400 MHz, CDCl₃)

δ 7.70 (d, 4H, *J* = 7.3 Hz), 7.44-7.19 (m, 6H), 3.70 (m, 2H), 3.02 (dd, 2H, *J* = 11.8, 6.2 Hz), 2.64 (dd, 2H, *J* = 11.8, 3.4 Hz), 2.34 (m, 2H), 2.17 (m, 2H), 1.52-1.36 (m, 4H), 1.36-1.12 (m, 4H), 0.85 (t, 6H, *J* = 7.4 Hz).

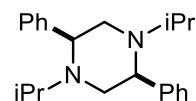
¹³C NMR (100 MHz, CDCl₃)

δ 141.2 (C), 129.3 (CH), 128.0 (CH), 127.1 (CH), 64.5 (CH), 61.6 (CH₂), 54.9 (CH₂), 29.3 (CH₂), 20.6 (CH₂), 14.1 (CH₃).

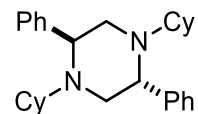
MS-ESI(+): calculated for C₂₄H₃₄N₂ 350.27; found: 351.26 (100%, *M* + 1); 176.24 (40%, *M*/2 + 1).

1,4-diisopropyl-2,5-diphenylpiperazine (21j) (meso):^[254]**¹H NMR** (400 MHz, CDCl₃)

δ 7.43 (m, 4H), 7.35 (pst, 4H, *J* = 7.2 Hz), 7.31-7.28 (m, 2H), 3.66 (dd, 2H, *J* = 10.2, 2.6 Hz), 2.88-2.81 (m, 4H), 2.44 (pst, 2H, *J* = 10.8 Hz), 0.97 (d, 6H, *J* = 6.8 Hz), 0.76 (d, 6H, *J* = 6.5 Hz).

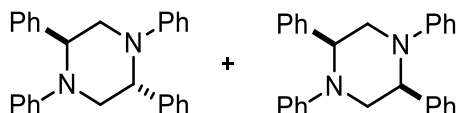
1,4-diisopropyl-2,5-diphenylpiperazine (21j') (±):**¹H NMR** (400 MHz, CDCl₃)

δ 7.67 (d, 4H, *J* = 8.0 Hz), 7.36-7.32 (m, 4H), 7.28-7.25 (m, 2H), 3.90 (m, 2H), 2.91 (dd, 2H, *J* = 11.8, 6.4 Hz), 2.84-2.78 (m, 4H), 0.91 (d, 6H, *J* = 6.4 Hz), 0.83 (d, 6H, *J* = 6.6 Hz).

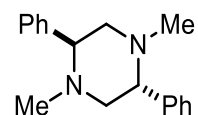
1,4-dicyclohexyl-2,5-diphenylpiperazine (21k) (meso):**¹H NMR** (400 MHz, CDCl₃)

δ 7.39 (m, 4H), 7.34 (pst, 4H, *J* = 7.2 Hz), 7.30-7.26 (m, 2H), 3.76 (d, 2H, *J* = 9.8 Hz), 2.88 (d, 2H, *J* = 10.4 Hz), 2.53 (pst, 2H, *J* = 10.4 Hz), 2.34 (m, 2H), 1.76-1.32 (m, 12H), 1.07-0.80 (m, 8H).

MS-ESI(+): calculated for C₂₈H₃₈N₂ 402.30; found: 403.45 (100%, M+1).

1,2,4,5-tetraphenylpiperazine (21m) + (21m'):^[255]**¹H NMR** (300 MHz, CDCl₃)

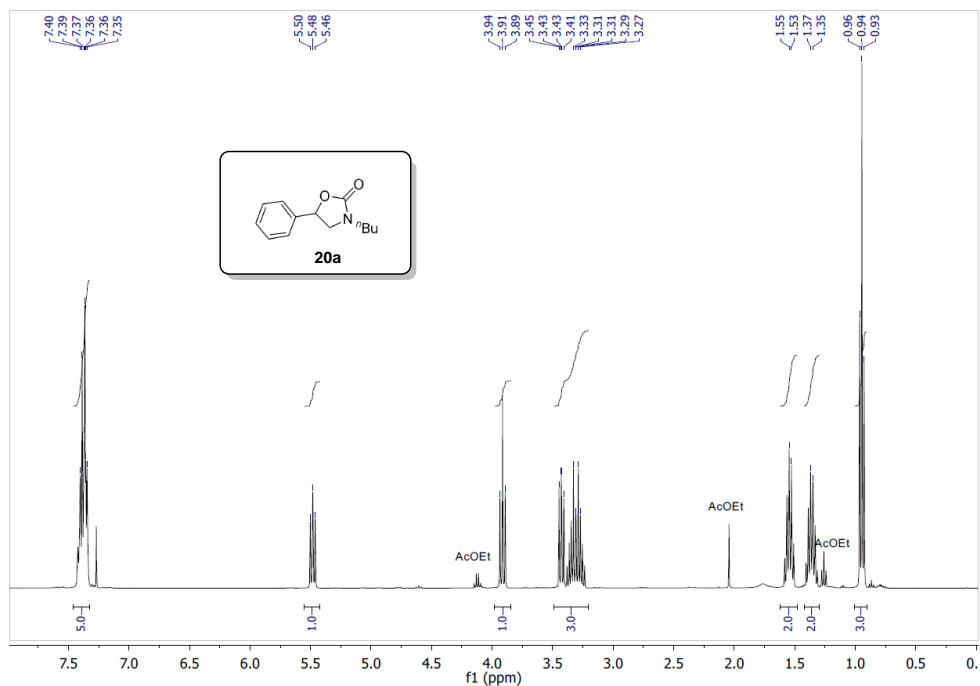
δ 7.42-7.04 (m, 32H), 7.78-6.64 (m, 8H), 4.87 (m, 2H), 4.76 (m, 2H), 4.20 (m, 2H), 4.02 (m, 2H), 3.80 (m, 2H), 3.67 (m, 2H).

1,4-dimethyl-2,5-diphenylpiperazine (21f) (meso):**¹H NMR** (400 MHz, CDCl₃)

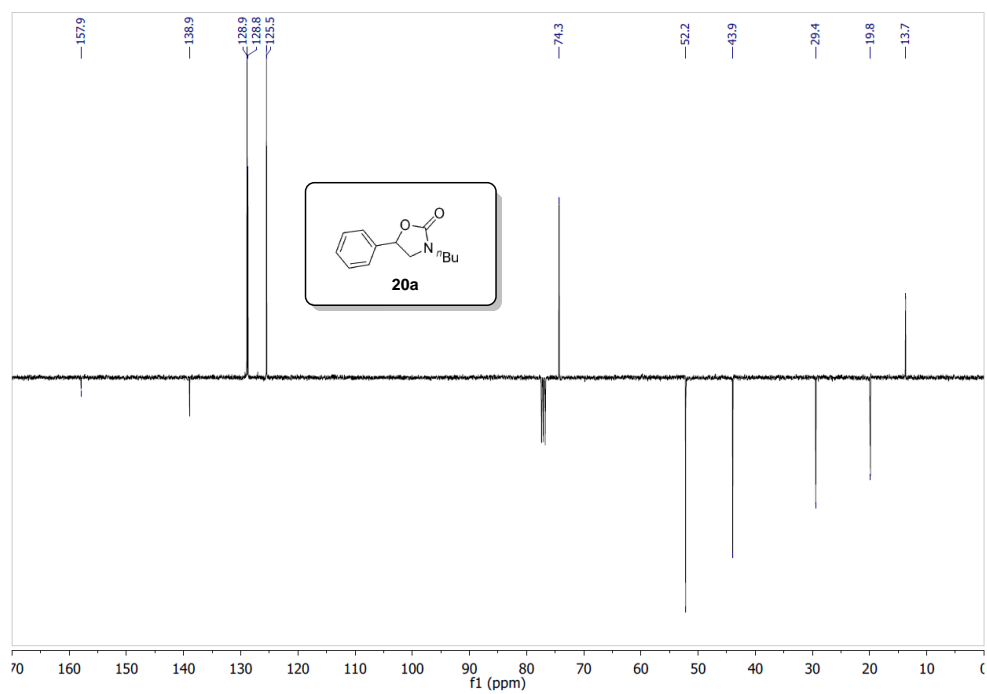
δ 7.44 (d, 4H, *J* = 7.6 Hz), 7.37 (t, 4H, *J* = 7.4 Hz), 7.30 (d, 2H, *J* = 7.3 Hz), 3.29 (dd, 2H, *J* = 10.7, 2.9 Hz), 2.99 (dd, 2H, *J* = 11.7, 3.0 Hz), 2.40 (t, 2H, *J* = 11.2 Hz), 2.08 (s, 6H).

¹³C NMR (100 MHz, CDCl₃)

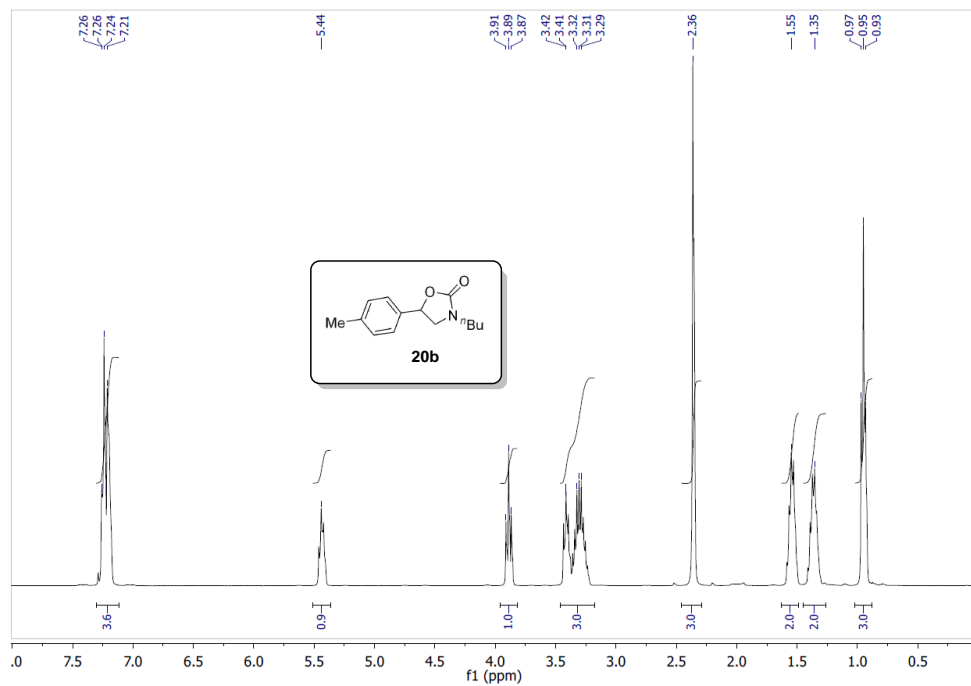
δ 141.3 (C), 128.5 (CH), 127.92 (CH₃), 127.6 (CH), 69.4 (CH₃), 64.2 (CH₂), 43.3 (CH₃)



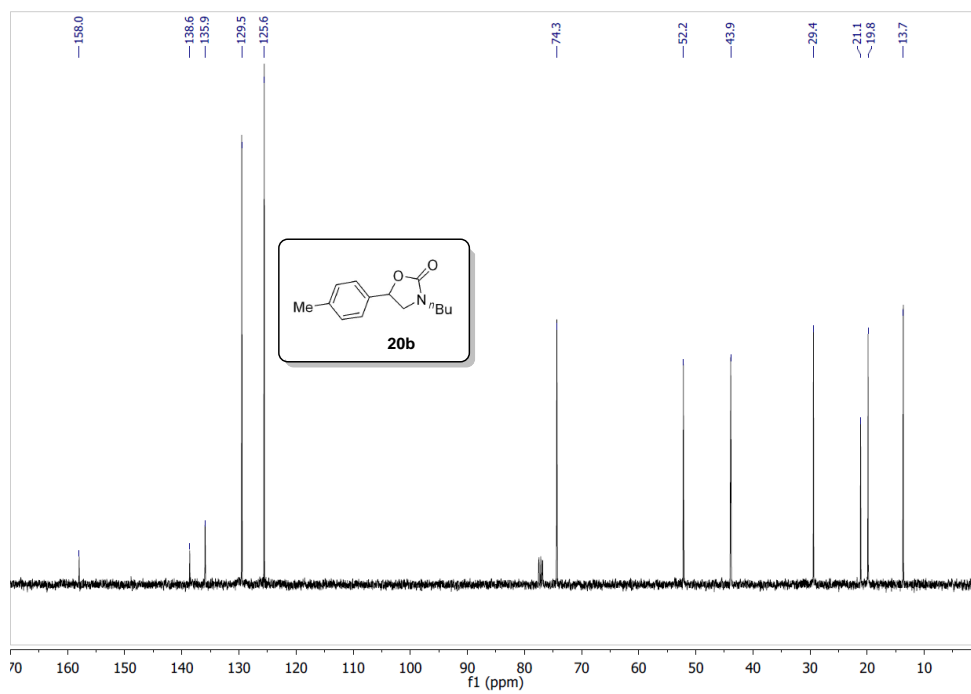
¹H NMR of **20a** in CDCl₃



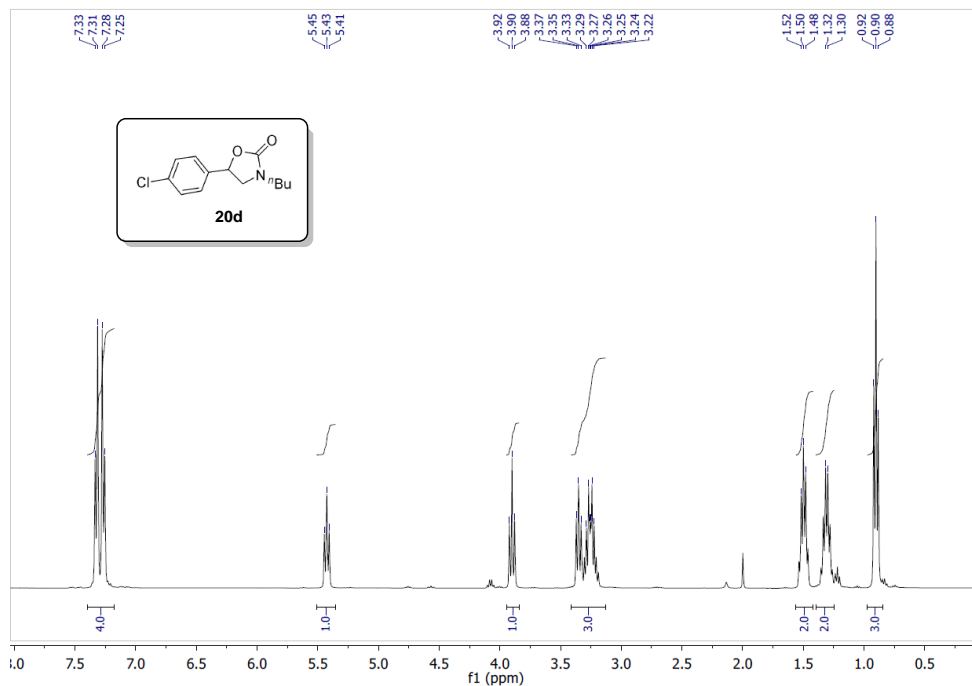
¹³C NMR of **20a** in CDCl₃



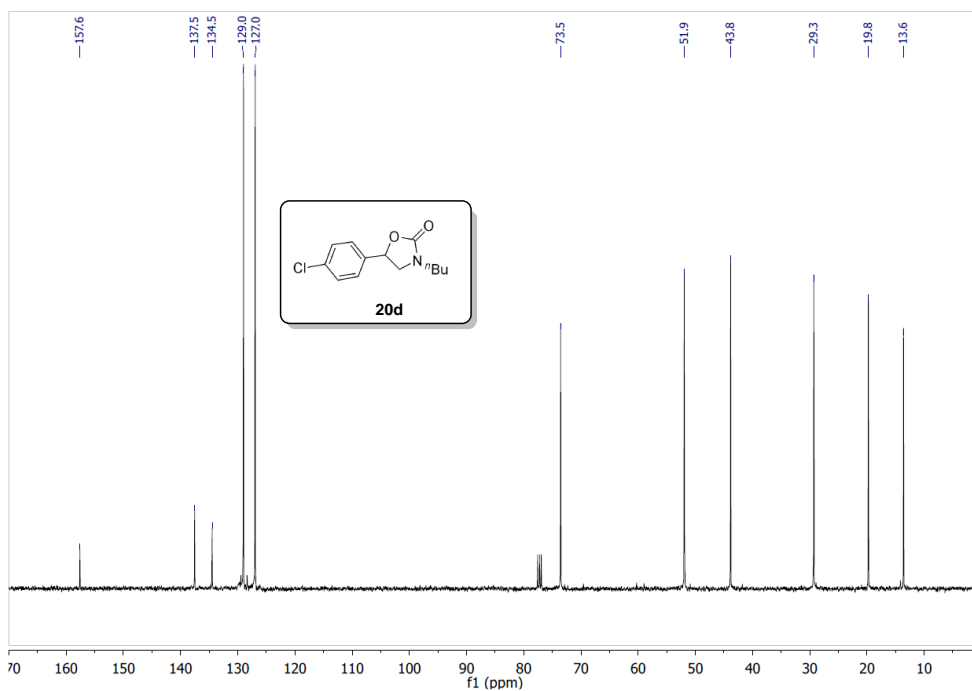
1H NMR of 20b in CDCl₃



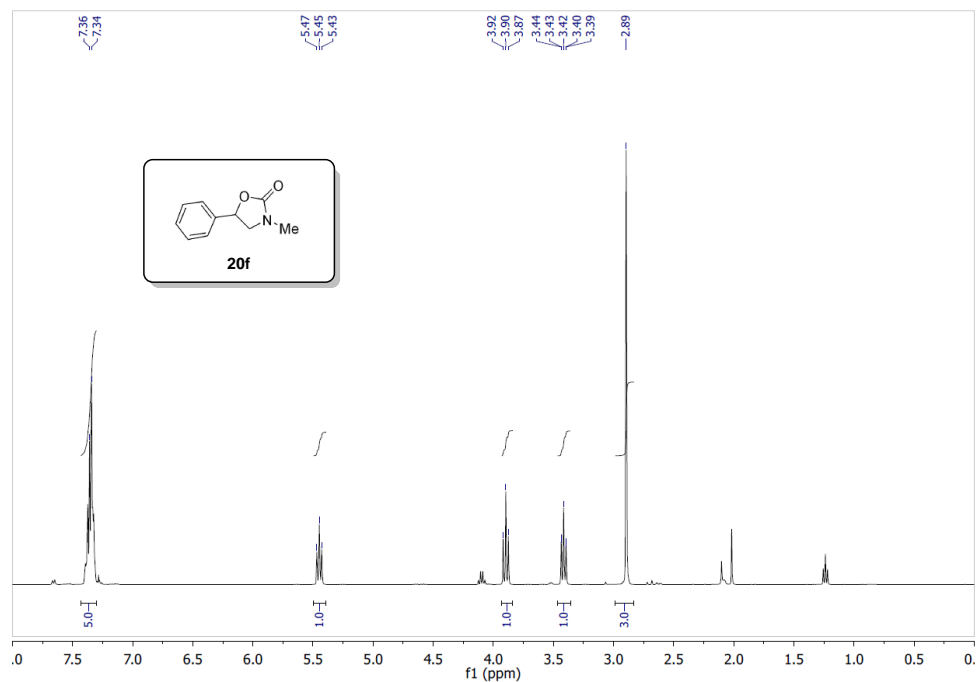
13C NMR of 20b in CDCl₃



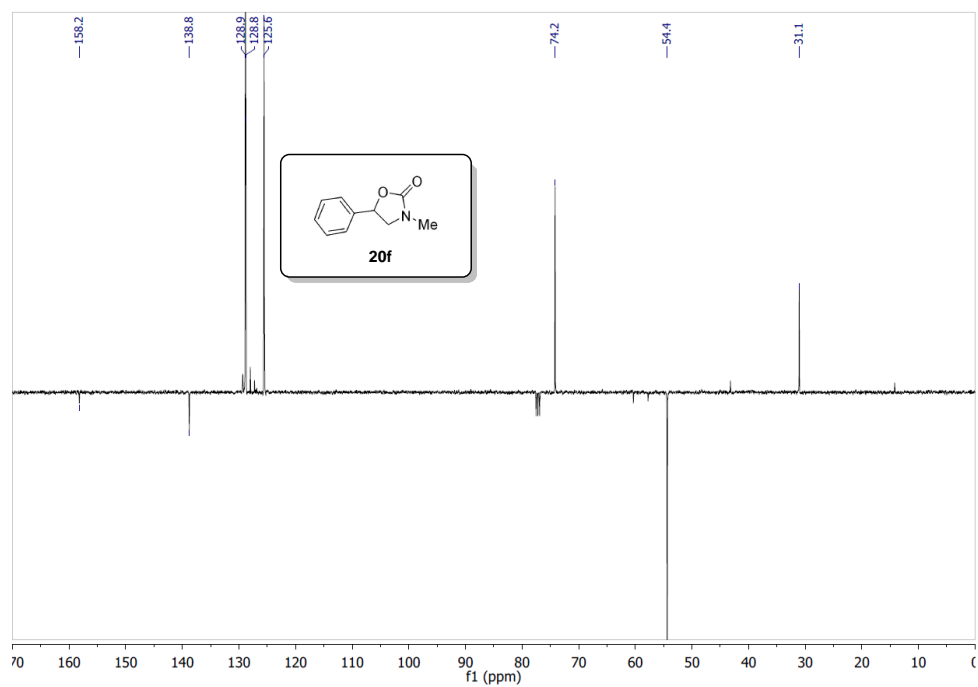
^1H NMR of **20d** in CDCl_3



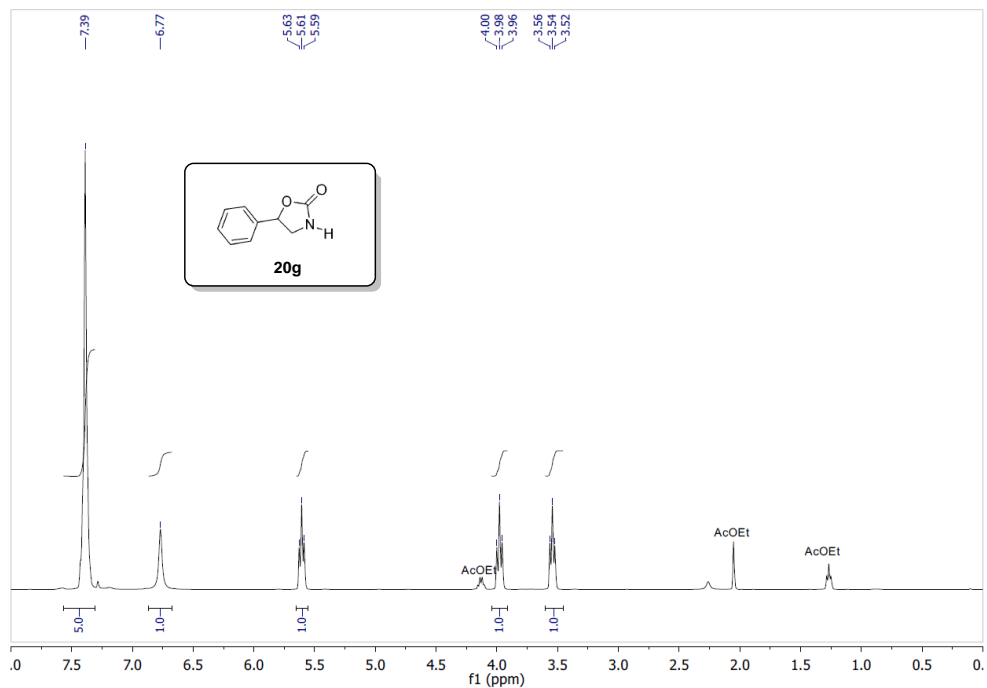
^{13}C NMR of **20d** in CDCl_3



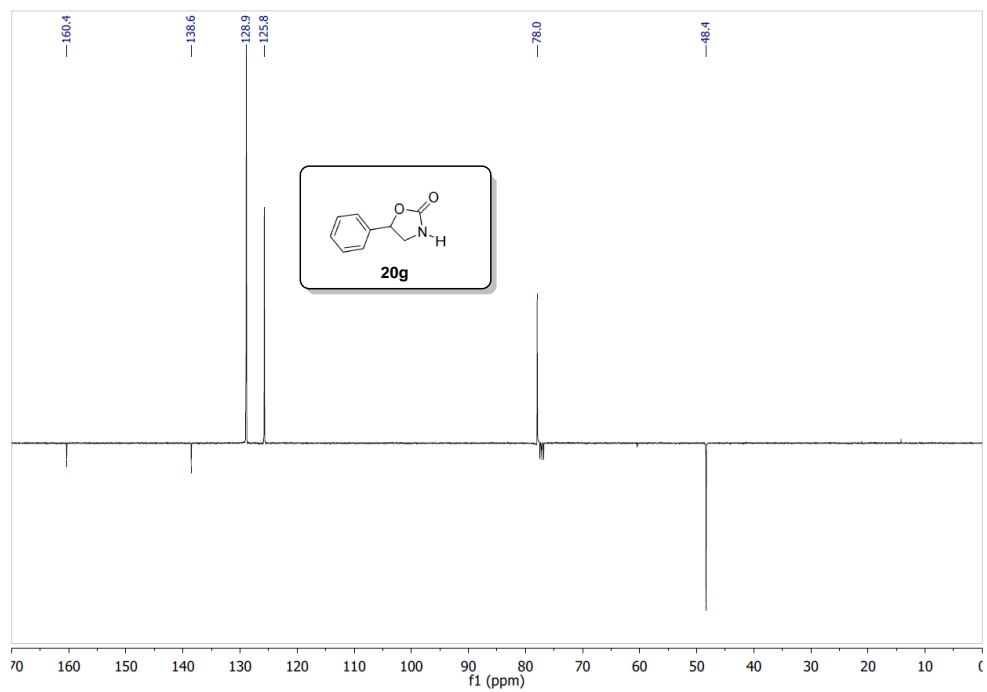
^1H NMR of **20f** in CDCl_3



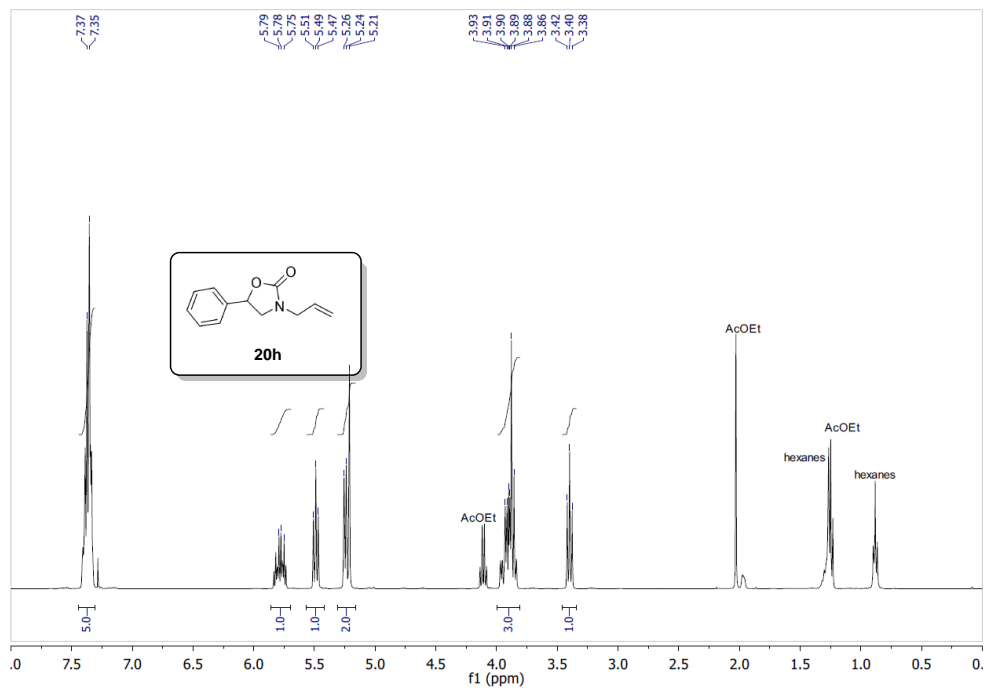
^{13}C NMR of **20f** in CDCl_3



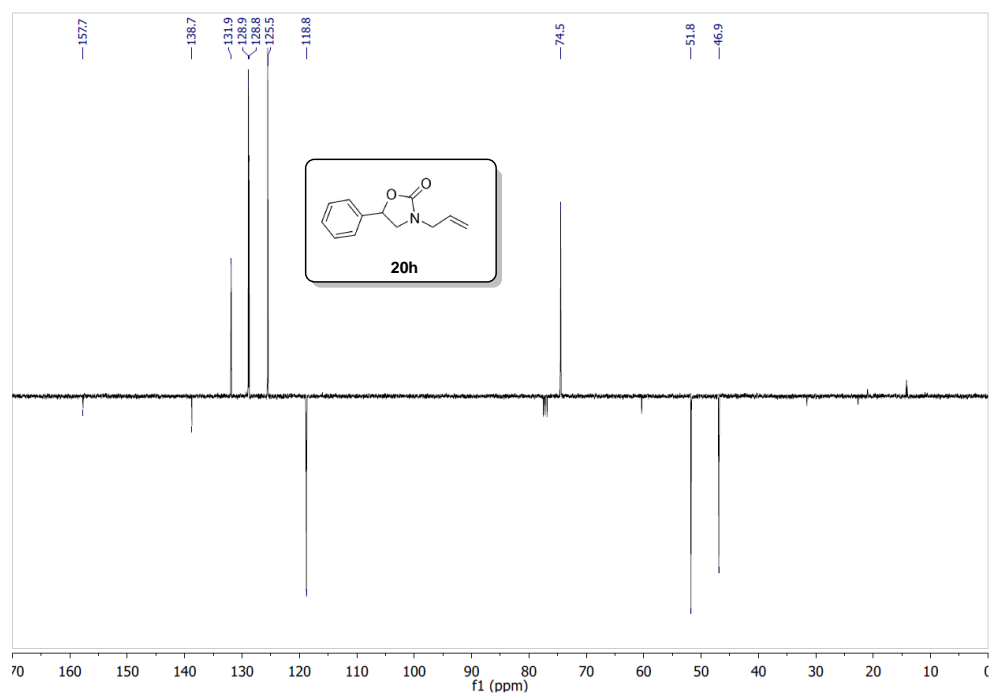
¹H NMR of 20g in CDCl₃



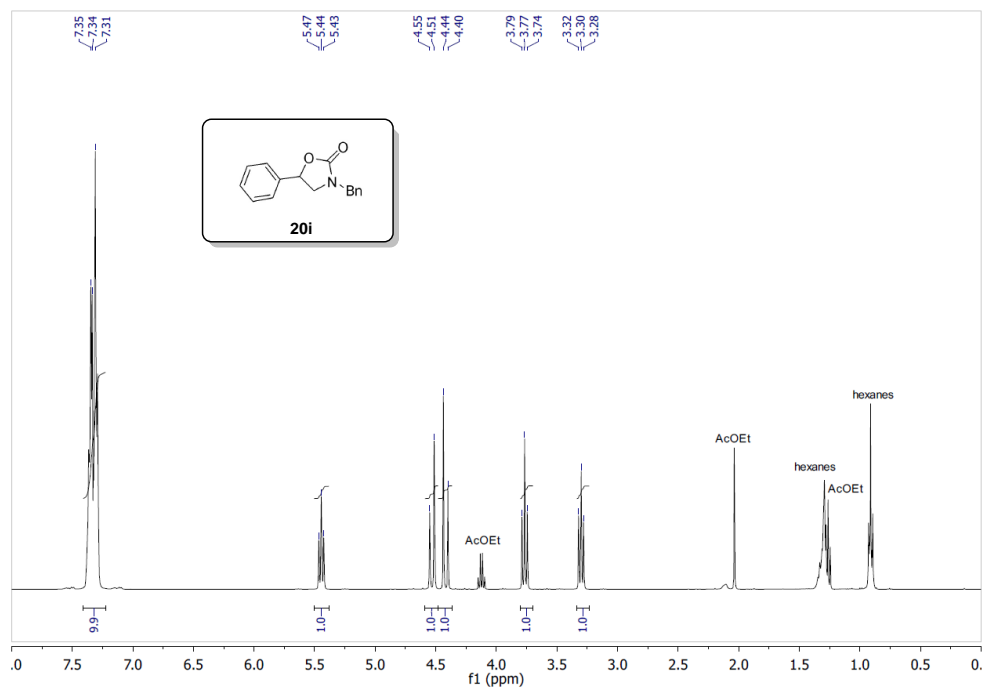
¹³C NMR of 20g in CDCl₃



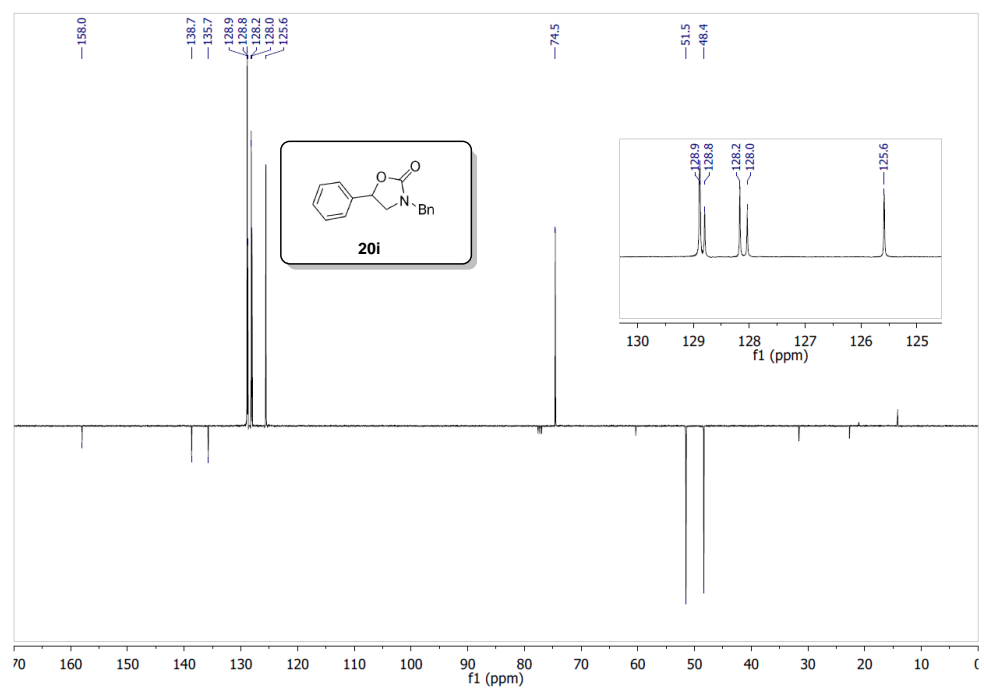
^1H NMR of **20h** in CDCl_3



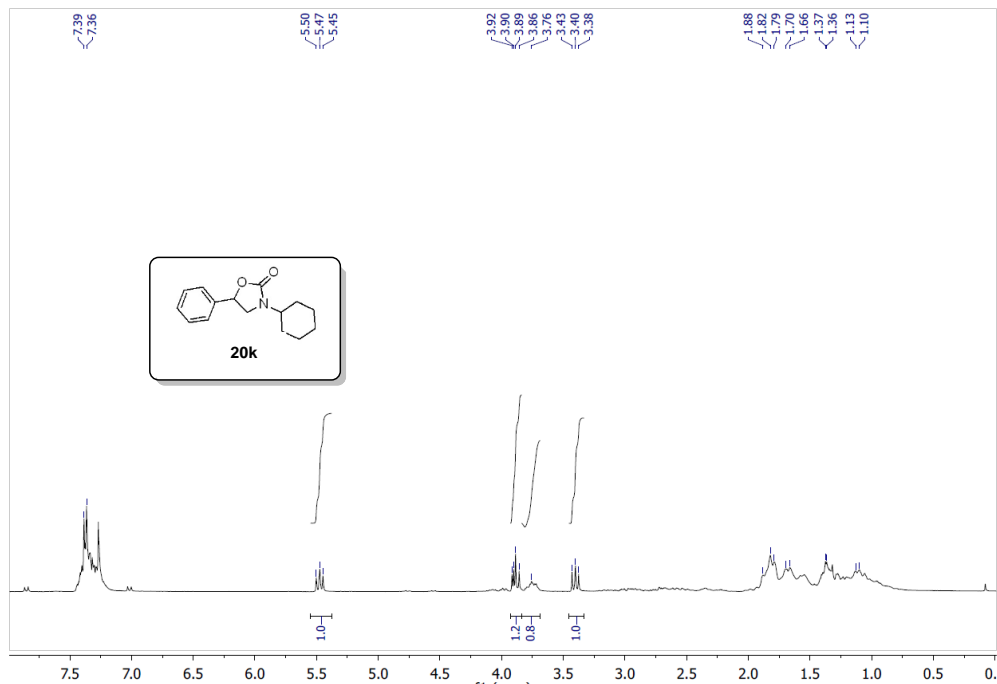
^{13}C NMR of **20h** in CDCl_3



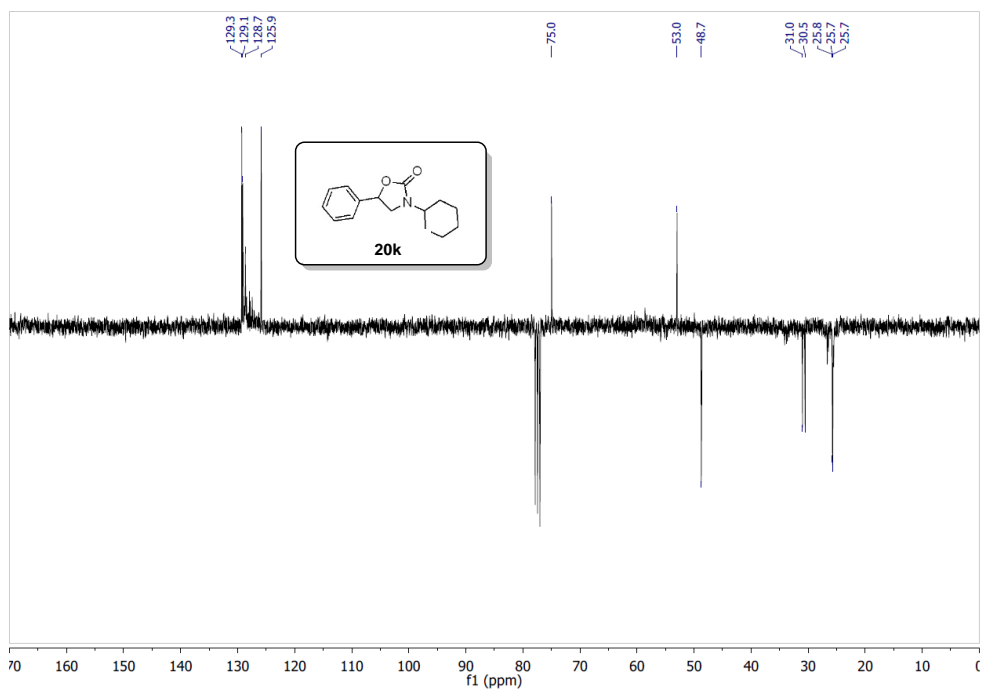
1H NMR of 20i in CDCl₃



13C NMR of 20i in CDCl₃



^1H NMR of **2k** in CDCl_3



^{13}C NMR of **2i** in CDCl_3

6.13.14 DFT studies:

General details are described in the previous chapters (see experimental section).

Chemical processes are driven by free energy, still in this study we presented and discussed enthalpies. Indeed, the variations of entropy along the reaction path (at the temperature of 25 °C) have been estimated assuming gas phase conditions. In steps where the molecularity of the system decreases, the variation of entropy induces a significant and positive contribution to the change in free energy (larger than 5 kcal/mol), and *vice versa*. Indeed, when the molecularity of a step does not change, the contribution of entropy to the variation of free energy results almost negligible (below 1 kcal/mol). In this reaction, no transition state implies a change in molecularity, suggesting that our evaluation of energy barriers is almost unaffected by entropy. Furthermore, we simulated a condensed phase environment and not a gas phase system, using an implicit model for the solvent. As extensively discussed by Alejandro Garza in a recent article,^[256] to estimate the variations of entropy derived from gas phase systems in the description of solutions leads to relevant and unavoidable errors. We therefore opted for presenting properly defined minimum enthalpy reaction paths. We are confident that our discussion, as well as the general conclusions, represent a valid option for the specific systems investigated in this study.

6.13.15 Complete energy profiles as obtained by DFT computations. No zero-point correction is considered:

The following graphs represents the energetic profile of the reaction in two different cases, described in detail.

.

Figure E24. Complete energy profiles for the reaction under investigation: conversion of aziridine to 5-methyl-1,3-oxazolidin-2-one, **20f**, in presence of a Lewis acid, FeBr₃, and bromide

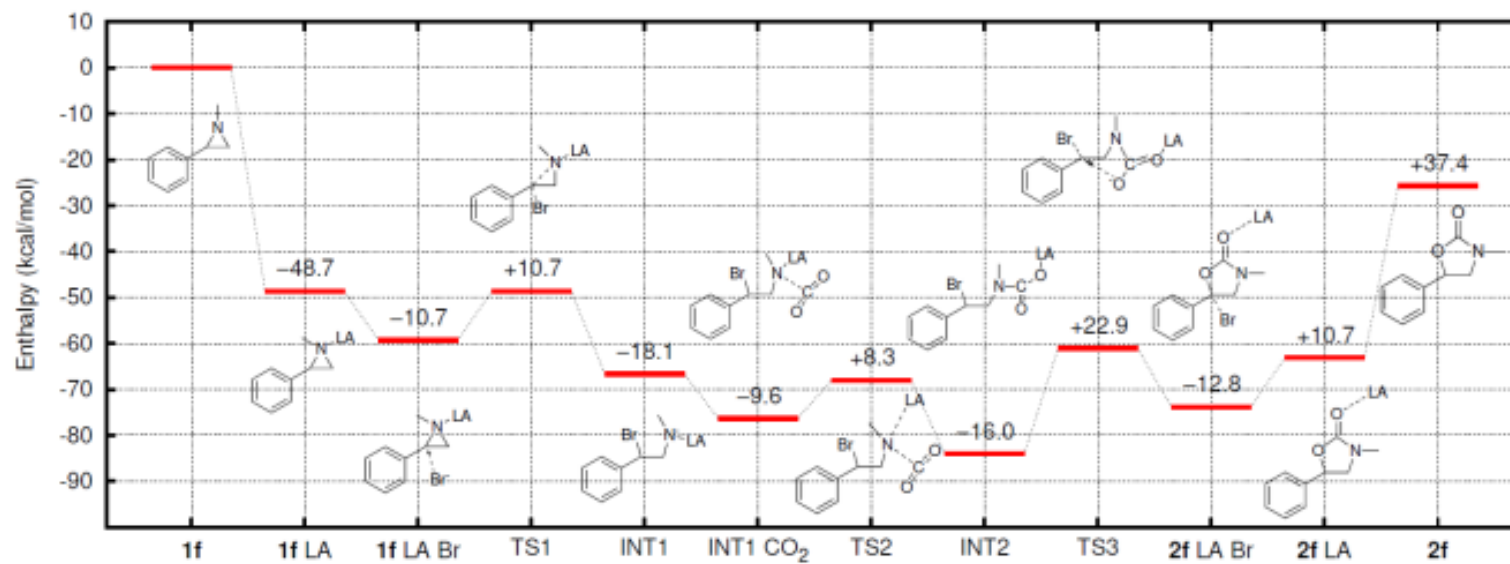
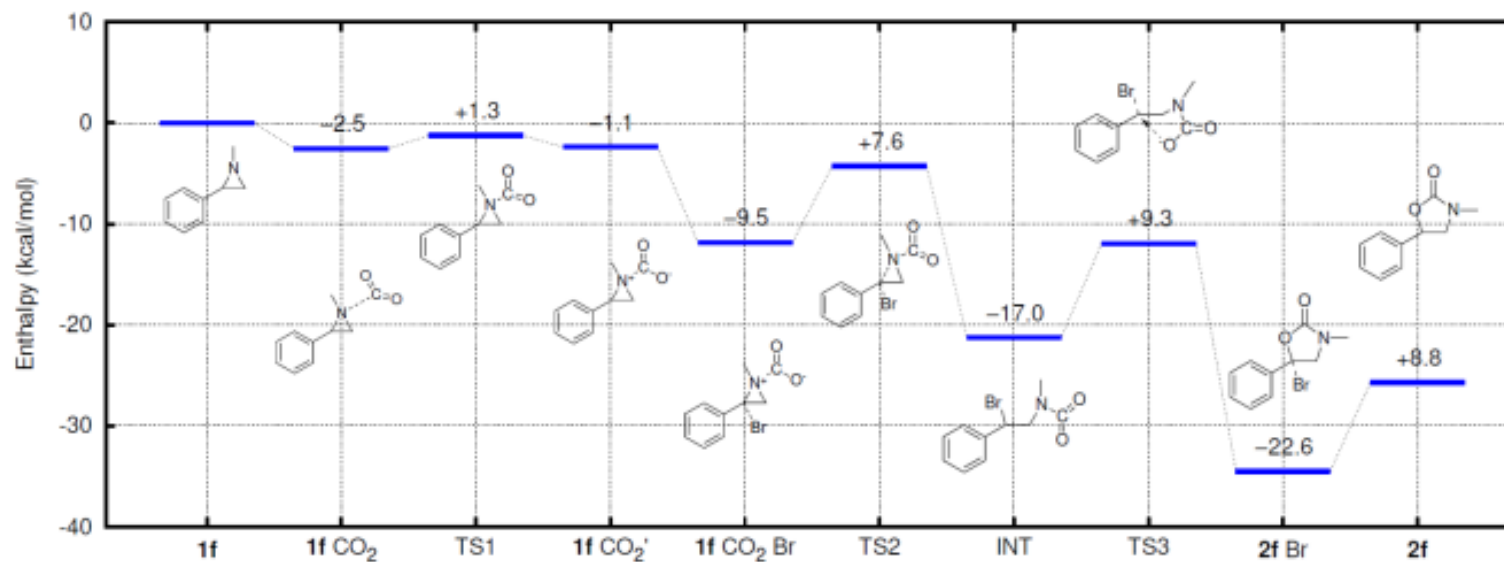


Figure X: Values reported on each plateau are the energy difference with respect to the previous step. Energies do not include zero-point vibrational correction. The chemical structure of each species is depicted in the proximity of its energy level. From left to right: (**19f**) aziridine molecule; (**19f LA**) **19f** interacts with the Lewis acid, FeBr_3 ; (**19f LA Br**) a bromide anion is added to the **19f LA** complex; (**TS1**) transition state: bromide attacks the aziridine ring to form a Br-C bond; (**INT1**) stable intermediate, Br-C is formed and the aziridine ring is open; (**INT1 CO₂**) **INT1** interacts with carbon dioxide; (**TS2**) transition state: the carbon atom of CO_2 approaches nitrogen; (**INT2**) stable intermediate: one carbon atom from CO_2 is chemically bound to nitrogen; (**TS3**) transition state: the second carbon of CO_2 attacks the more hindered carbon of the former aziridine; (**20f LA Br**) the product **20f** is formed, still interacting with the Lewis acid and bromide; (**20f LA**) bromide is removed, the product interacts just with the Lewis acid; (**20f**) product moiety.

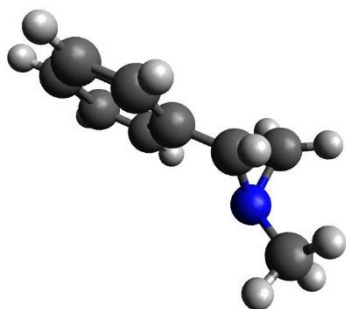
Figure X: Values reported on each plateau are the difference with respect to the previous step. Energies do not include zero-point vibrational correction. The chemical structure of every species is depicted in the proximity of its energy level. From left to right: (**19f**) an aziridine molecule; (**19f CO₂**) **19f** interacts with carbon dioxide; (**TS1**) transition state for internal rearrangement; (**19f CO₂'**) stable intermediate: a complex with different conformation with respect to **19f CO₂** is formed; (**19f CO₂ Br**) bromide is allowed to interact with **19f CO₂'**; (**TS2**) transition state: bromide attacks the aziridine ring to form a Br-C bond; (**INT**) stable intermediate, Br-C is formed and the aziridine ring is open; (**TS3**) transition state: the free carbon atom of CO_2 attacks the more hindered carbon of the former aziridine; (**20f Br**) the product **20f** is formed, still interacting with bromide; (**20f**) bromide is removed: isolated product moiety.

Figure E25. Complete energy profiles for the conversion of aziridine to 5-methyl-1,3-oxazolidin-2-one, **20f**. The Lewis acid FeBr_3 is not included in the reaction environment. The presence of bromide and of CO_2 are instead contemplated.

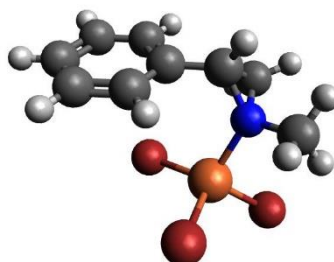


6.13.16 Visual representation of the intermediates:

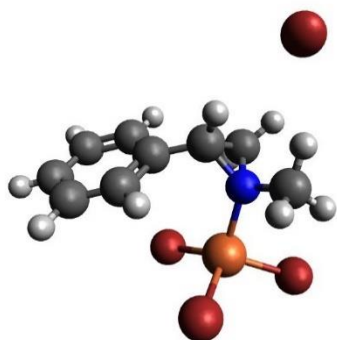
19f
Aziridine **19f**



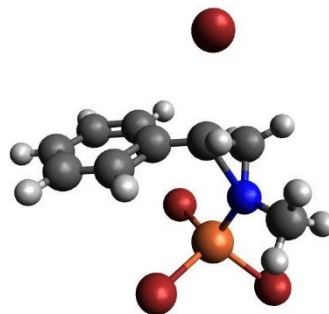
19f_LA
complex between aziridine and the Lewis Acid



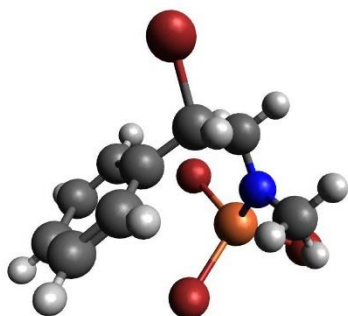
19f_LA_Br
complex between aziridine, the Lewis Acid,
and bromide



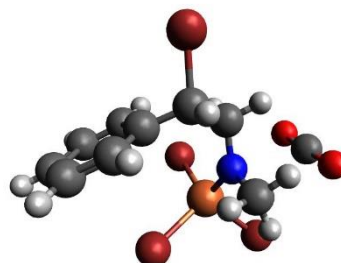
TS1
transition state for aziridine ring opening



INT1
first reaction intermediate: open aziridine ring



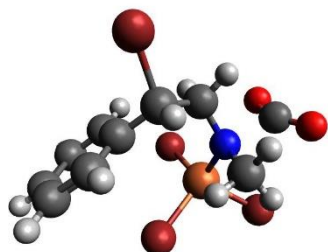
INT1_CO2
complex between the first intermediate and
carbon dioxide



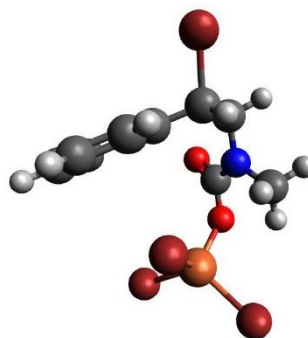
TS2

INT2

transition state for the bonding of CO₂ to
nitrogen

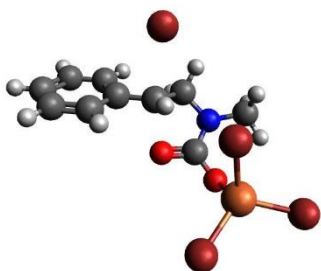


second reaction intermediate



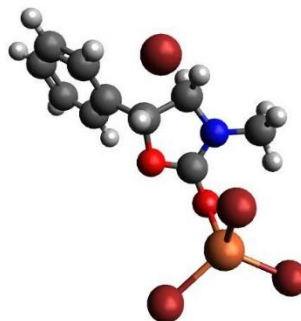
TS3

transition state for ring closure



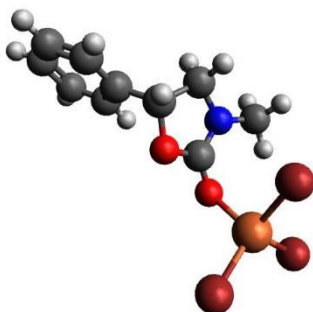
20f_LA_Br

complex between the product, LA and bromide



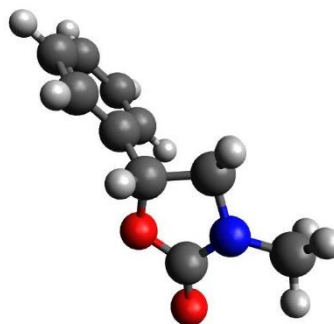
20f_LA

complex between the product **20f** and LA



2f

Product **20f**



6.14 DIMERIZATION OF AZIRIDINES: SYNTHESIS OF PIPERAZINES

6.14.1 General catalytic procedure:

Method A, conventional heating

The catalyst (0.025 mmol), acetonitrile (1 mL) and the substrate (1 mmol) were added in this order in a round bottom pressure tube. Each piece of glassware was previously dried in an oven at 120 °C. The reaction mixture was stirred for 16 hours at 75°C in aluminum heating block.

Method B, microwave heating:

The catalyst (0.025 mmol), acetonitrile (1 mL) and the substrate (1 mmol) were added in this order in a microwave vial. The reaction was stirred for 20–80 minutes at 100–140 °C.

6.14.2 Work-up procedures:

¹H NMR analysis:

At the end of the reaction, the solvent is evaporated under reduced pressure. To the residue, 35 µL (0.5 mmol) of dibromomethane are added as internal standard (ISTD), and 300 µL of CDCl₃ are added for ¹H-NMR analysis.

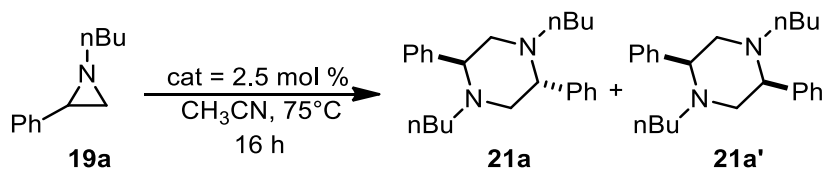
Separation of *meso* form (21x):

Products **21x** precipitate in the reaction mixture, upon cooling. This allows the separation of the product by simple filtration. The filtrate can be then analyzed by ¹H NMR.

GC analysis:

The reaction mixture was diluted with ethyl acetate in a 10 mL volumetric flask, with the addition of dimethylterephthalate (DMT) as ISTD. 5 mL of the resulting solution were used to calculate product yields by quantitative ¹H NMR, while 0.5 mL were further diluted in a volumetric flask to obtain a concentration of analytes in the range of 0.1–0.3 mg/mL. The final solution was injected in the GC and conversion of the substrate was calculated comparing the integration of the area of aziridine peak and the integration of the ISTD peak, with the previously prepared calibration curves.

6.14.3 Catalyst screening:



Entry	Catalyst	Conversion 19a % ^[b]	Selectivity 21a + 21a' % ^[b]	TOF (h ⁻¹) ^[c]
1	[TBA] ₂ [ZnCl ₄]	62	63	1.6
2	[TBA] ₂ [ZnBr ₄]	84	69	2.1
3	[TBA] ₂ [ZnI ₄]	>99	68	2.5

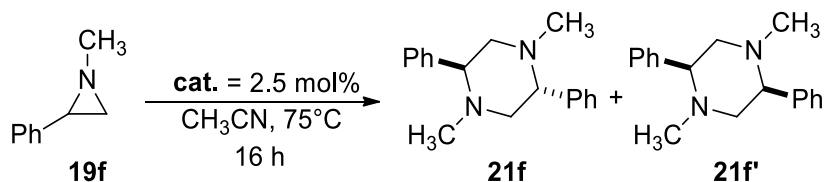
Reaction conditions: 1-butyl-2-phenyl aziridine, **19a**, (1 mmol) and catalyst (2.5 mol%) in CH₃CN (1 mL) at T = 75 °C, t = 16 h. [b] Conversion and selectivity determined by ¹H NMR using dibromomethane as the internal standard. [c] Turnover frequency (mol_{19a(converted)}} · mol_{cat}⁻¹ · reaction time⁻¹).

6.14.4 Lower aziridine concentration experiments:

Entry	Catalyst	Loading (mol%)	Conv. 19a % ^[b]	Sel. 21a + 21a' % ^[b]	TOF (h ⁻¹) ^[c]
4	[TBA] ₂ [ZnCl ₄]	2.5	13	0	0.3
5	[TBA] ₂ [ZnBr ₄]	2.5	23	78	0.6
6	[TBA] ₂ [ZnI ₄]	2.5	70	94	1.8
7	[TBA] ₂ [ZnCl ₄]	5.0	17	6	0.2
8	[TBA] ₂ [ZnBr ₄]	5.0	35	63	0.4
9	[TBA] ₂ [ZnI ₄]	5.0	>99	80	1.2

Reaction conditions: 1-butyl-2-phenyl aziridine, **19a**, (0.5 mmol) and catalyst (2.5 mol% and 5 mol%) in CH₃CN (5 mL) at T = 75 °C, t = 16 h. [b] Conversion and selectivity determined by ¹H NMR using dibromomethane as the internal standard. [c] Turnover frequency (mol_{19a(converted)}} · mol_{cat}⁻¹ · reaction time⁻¹).

6.14.5 Other metallates:



Entry	Catalyst	Conversion 19f % ^[b]	Selectivity 21f + 21f' % ^[b]	TOF (h^{-1}) ^[c]
10	[TBA] ₂ [ZnCl ₄]	11	91	0.3
11	[TBA] ₂ [ZnBr ₄]	38	97	1.0
12	[TBA] ₂ [ZnI ₄]	75	96	1.9
13	[TBA][FeBr ₄]	>99	27	2.5
14	[TMA] ₂ [ZnCl ₄]	0	0	0.0
15	[TMA] ₂ [CuCl ₄]	>99	20	2.5
16	[TMA] ₂ [MnCl ₄]	73	18	1.8
17	[TMA] ₂ [CoCl ₄]	63	29	1.6

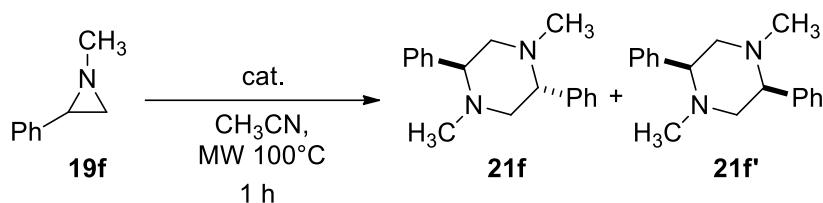
Reaction conditions: 1-methyl-2-phenyl aziridine, **19f**, (1 mmol) and catalyst (2.5 mol%) in CH_3CN (1 mL) at $T = 75^\circ\text{C}$, $t = 16$ h. [b] Conversion and selectivity determined by ^1H NMR using dibromomethane as the internal standard. [c] Turnover frequency ($\text{mol}_{19\text{f}(\text{converted})} \cdot \text{mol}_{\text{cat}}^{-1} \cdot \text{reaction time}^{-1}$).

6.14.6 Control experiments:

Entry	Catalyst	Loading (mol%)	Conv. 19f % ^[b]	Sel. 21f + 21f' % ^[b]	TOF (h^{-1}) ^[c]
18	TBACl	5	0	0	0.0
19	TBAB	5	42	88	0.3
20	TBAI	5	95	54	0.6
21	ZnI ₂	2.5	>99	44	0.7

Reaction conditions: 1-methyl-2-phenyl aziridine, **19f**, (1 mmol) and catalyst in CH_3CN (1 mL) at $T = 75^\circ\text{C}$, $t = 30$ h. [b] Conversion and selectivity determined by ^1H NMR using dibromomethane as the internal standard. [c] Turnover frequency ($\text{mol}_{19\text{f}(\text{converted})} \cdot \text{mol}_{\text{cat}}^{-1} \cdot \text{reaction time}^{-1}$).

6.14.7 Microwave heating optimization:



Entry	Catalyst	Loading (mol%)	Conv. 19f % ^[b]	Sel. 21f + 21f' % ^[b]	TOF (h ⁻¹) ^[c]
1	[TBA] ₂ [ZnCl ₄]	2.5	7	>99	2.8
2	[TBA] ₂ [ZnBr ₄]	2.5	75	97	30.0
3	[TBA] ₂ [ZnI ₄]	2.5	96	73	38.4
4	[TBA] ₂ [ZnI ₄]	0.25	50	80	200.0

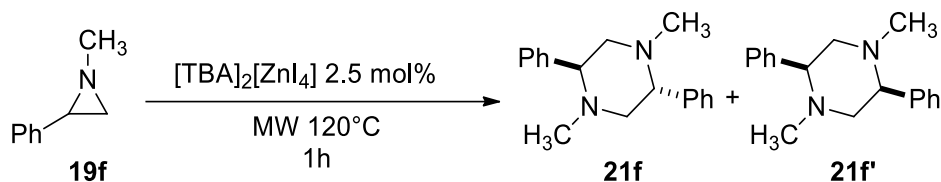
Reaction conditions: 1-methyl-2-phenyl aziridine, **19f**, (1 mmol) and catalyst in CH₃CN (1 mL) at T = 100 °C, MW heating, t = 1 h. [b] Conversion and selectivity determined by ¹H NMR using dibromomethane as the internal standard. [c] Turnover frequency (mol_{19f(converted)}} · mol_{cat}⁻¹ · reaction time⁻¹).

6.14.8 Temperature optimization:

Entry	Catalyst	T (°C)	Time (min)	Conv. 19f % ^[b]	Sel. 21f + 21f' % ^[b]	TOF (h ⁻¹) ^[c]
3	[TBA] ₂ [ZnI ₄]	100	60	96	73	38.4
5	[TBA] ₂ [ZnI ₄]	140	60	95	48	38.0
6	[TBA] ₂ [ZnI ₄]	120	20	80	95	96.0
7	[TBA] ₂ [ZnBr ₄]	120	20	70	76	74.0

Reaction conditions: 1-methyl-2-phenyl aziridine, **19f**, (1 mmol) and catalyst (2.5 mol%) in CH₃CN (1 mL), MW heating. [b] Conversion and selectivity determined by ¹H NMR using dibromomethane as the internal standard. [c] Turnover frequency (mol_{19f(converted)}} · mol_{cat}⁻¹ · reaction time⁻¹).

6.14.9 Solvent screening:



Entry	Solvent	Conv. 19f % ^[b]	Sel. 21f + 21f' % ^[b]	TOF (h ⁻¹) ^[c]	ϵ (F M ⁻¹) ^[d]
1	Acetone	77	90	31.0	20.7
2	Dioxane	25	56	10.0	2.21
3	TBME	33	40	13.1	2.6
4	Ethyl acetate	50	56	19.9	6
5	Toluene	41	24	16.4	2.4
6	THF	91	59	36.4	7.58
7	MEK	97	62	38.8	18.51
8	PC	87	57	34.8	64
9	CD ₃ CN ^[e]	90	84	36.0	37.5
10	DMSO	87	33	34.8	46.7
11 ^[f]	CH ₃ CN + H ₂ O	99	82	120.3	-

Reaction conditions: 1-methyl-2-phenyl aziridine, **19f**, (1 mmol) and catalyst ($[\text{TBA}]_2[\text{ZnI}_4]$, 2.5 mol%) in 1 mL of solvent, MW heating set to 120°C for 1 hour. [b] Conversion determined by GC using decane as the internal standard and selectivity determined by ¹H NMR using dibromomethane as the internal standard. [c] Turnover frequency ($\text{mol}_{19\text{f}(\text{converted})} \cdot \text{mol}_{\text{cat}}^{-1} \cdot \text{reaction time}^{-1}$). [d] Dielectric constant of the solvent. TBME= Terbutyl-methylether, MEK= Methyl-ethyl ketone, PC= Propylene carbonate. [e] Conversion and yield determined by ¹H-NMR, using dibromomethane as the internal standard. [f] 2 equivalents (relative to **19f**) of water were added to the solvent.

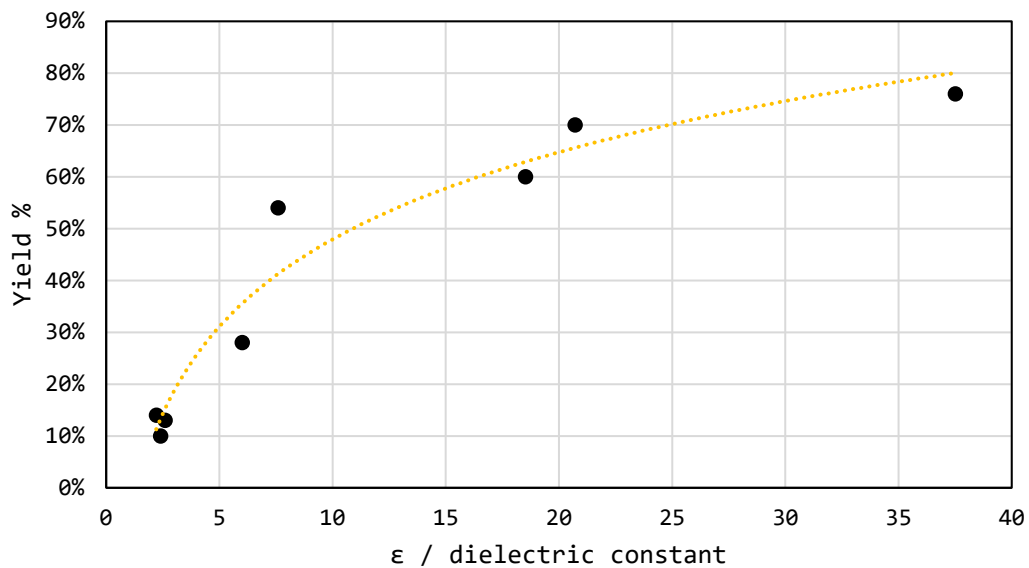


Figure E26 Correlation between dielectric constant of solvent and yield of 1-methyl-2-phenylaziridine **19f** dimerization product (**21f** + **21f'**).

6.15 POLYETHYLENE TEREPHTHALATE (PET) DEPOLYMERIZATION:

All the reactions were performed using commercial quality rPET as substrate. Reactions performed directly using a waste bottle of water are specified. The results are typically expressed in terms of monomeric species yield.

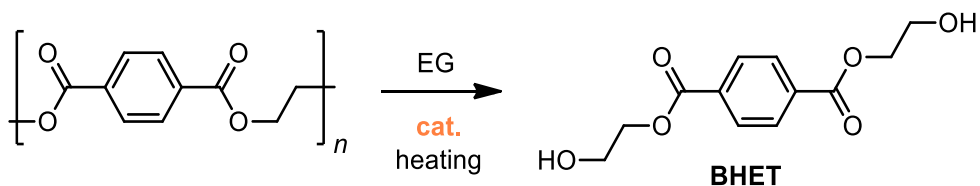
6.16 PET GLYCOLYSIS:

6.16.1 General catalytic procedure:

Conventional heating: Catalytic glycolysis of PET was performed by conventional heating in sealed screw cap glass vials, using an aluminum heating block. rPET (125 mg) and ethylene glycol (EG, 0.8 mL) were placed in the glass vials equipped with a magnetic stirrer. The vial was placed in the aluminum block and heated at 170 °C for 16 hours. At the end of the reaction, the mixture was added to hot water and filtered to eliminate residual unreacted PET and insoluble oligomers. Conversion of PET was calculated by weighting these eventual residues, after drying in vacuum, compared to the starting PET. The filtrate was concentrated in vacuum to 1/10 of the volume and cooled at 4 °C overnight. The product *bis*-(2-hydroxyethyl)-terephthalate (BHET) is formed as white needle-like crystals. The crystals are filtered, dried in vacuum and weighted to calculate the yield of the reaction.

Microwave heating: Catalytic glycolysis of PET was performed by microwave heating in specific glass vials. rPET (125 mg) and ethylene glycol (EG, 2 mL) were placed in a glass vial equipped with a magnetic stirrer, which was then sealed with an aluminum cap. The reaction was heated by microwave irradiation at specific temperature for a specific amount of time. At the end of the reaction, the vial was opened, the mixture was added to hot water and filtered to eliminate residual unreacted PET and insoluble oligomers. Conversion of PET was calculated by weighting these eventual residues, after drying in vacuum, compared to the starting PET. The filtrate was concentrated in vacuum to 1/10 of the volume and cooled at 4 °C overnight. The product *bis*-(2-hydroxyethyl)-terephthalate (BHET) is formed as white needle-like crystals. The crystals are filtered, dried in vacuum and weighted to calculate the yield of the reaction.

6.16.2 Blank experiments, conventional heating:



Entry	Catalyst	Conversion %	Yield BHET %
1	-	0	0
2	TMACl	0	0
3	MnCl ₂ ·4H ₂ O	76.3	51.7
4	CoCl ₂ ·6H ₂ O	72.4	48.9
5	ZnCl ₂	94.4	74.2
6	FeCl ₃ ·6H ₂ O	56.1	9.0

Reaction performed in screw cap glass tubes, temperature= 170 °C, catalyst loading= 5 mol%, reaction time= 16h.

6.16.3 Catalyst screening:

Entry	Catalyst	Conversion %	Yield BHET %
7	[TMA][CuCl ₃]	2.0	0
8	[TMA] ₂ [CuCl ₄]	6.6	0
9	[TBA][FeCl ₄]	86.6	51.1
10	[PPh ₄][FeCl ₄]	91.9	47.3
11	[TMA][FeCl ₄]	89.0	33.8
12	[TMA] ₂ [CoCl ₄]	95.2	48.8
13	[TMA][CoCl ₃]	95.3	22.7
14	[TMA] ₂ [ZnCl ₄]	89.6	38.1

15	[TMA][MnCl ₃]	73.7	45.2
16	[TMA] ₂ [MnCl ₄]	78.5	59.6

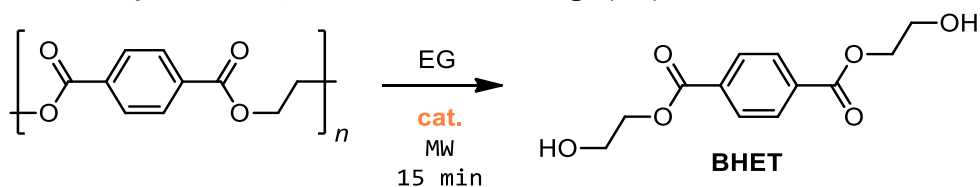
Reaction performed in screw cap glass tubes, temperature= 170 °C, catalyst loading= 5 mol%.

6.16.4 Influence of reaction time:

Entry	Catalyst	Time (h)	Conversion %	Yield BHET %
17	[TMA][FeCl ₄]	3	45.0	5.4
11	[TMA][FeCl ₄]	16	89.0	33.8
18	[TMA][FeCl ₄]	24	93.7	29.6
19	[TMA] ₂ [MnCl ₄]	3	11.1	0
16	[TMA] ₂ [MnCl ₄]	16	78.5	59.6
20	[TMA] ₂ [MnCl ₄]	24	94.3	57.1
21	[TMA] ₂ [CoCl ₄]	3	16.1	0
12	[TMA] ₂ [CoCl ₄]	16	95.2	48.8
22	[TMA] ₂ [CoCl ₄]	24	93.0	50.1

Reaction performed in screw cap glass tubes, temperature= 170 °C, catalyst loading= 5 mol%.

Blank experiments, microwave heating (MW):



Entry	Catalyst	Conversion %	Yield BHET %
1	-	0	0
2	TMACl	0	0
3	$\text{FeCl}_3 \cdot 6\text{H}_2\text{O}$	100	65.3
4	$\text{MnCl}_2 \cdot 4\text{H}_2\text{O}$	100	80.6
5	$\text{CoCl}_2 \cdot 6\text{H}_2\text{O}$	100	74.4
6	ZnCl_2	100	69.9

Reaction performed in MW glass tubes, temperature= 170 °C, catalyst loading= 5 mol%, reaction time= 15min.

6.16.5 Catalyst screening, microwave heating:

Entry	Catalyst	Conversion %	Yield BHET %
7	[TMA][FeCl_4]	100	54.1
8	[TBA][FeCl_4]	100	27.8
9	[PPh ₄][FeCl_4]	100	47.2
10	[TMA][MnCl_3]	100	77.9
11	[TMA] ₂ [MnCl_4]	100	55.2
12	[TMA][CoCl_3]	100	72.8
13	[TMA] ₂ [CoCl_4]	98.2	54.3
14	[TMA] ₂ [ZnCl_4]	100	64.4
15	[TMA][CuCl_3]	0	0
16	[TMA] ₂ [CuCl_4]	16.7	0

Reaction performed in MW glass tubes, temperature= 170 °C, catalyst loading= 5 mol%, reaction time= 15min.

6.16.6 Reaction time influence, microwave heating:

Entry	Catalyst	Time (min)	Conversion %	Yield BHET %
17		5	100	45.3
7		15	100	54.1
18	[TMA][FeCl ₄]	30	100	66.3
19		60	100	62.6
20		120	100	47.8

Reaction performed in MW glass tubes, temperature= 170 °C, catalyst loading= 5 mol%.

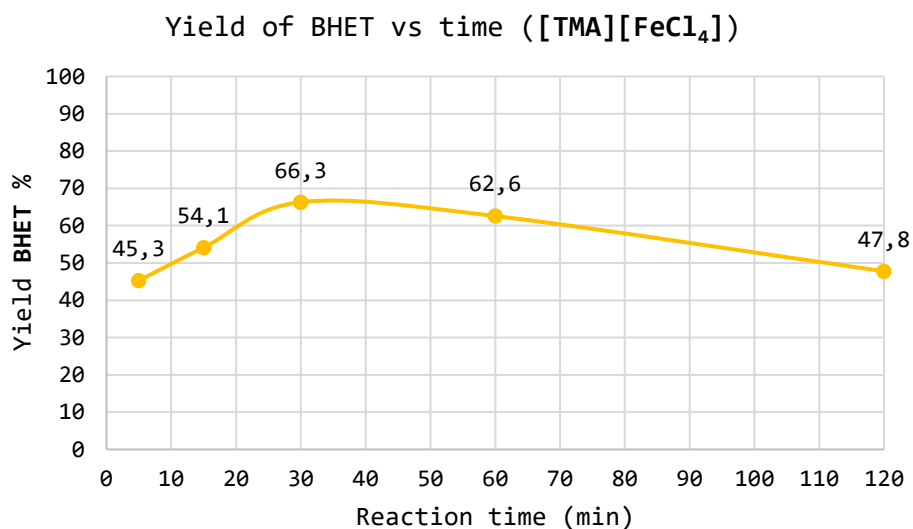


Figure E27. Correlation between reaction time and yield of BHET using [TMA][FeCl₄] as catalyst, with microwave heating.

Entry	Catalyst	Time (min)	Conversion %	Yield %
21	[TMA] ₂ [MnCl ₄]	5	100	64.9
11		15	100	55.2
22		30	100	47.7
23		60	100	39.5

Reaction performed in MW glass tubes, temperature= 170 °C, catalyst loading= 5 mol%.

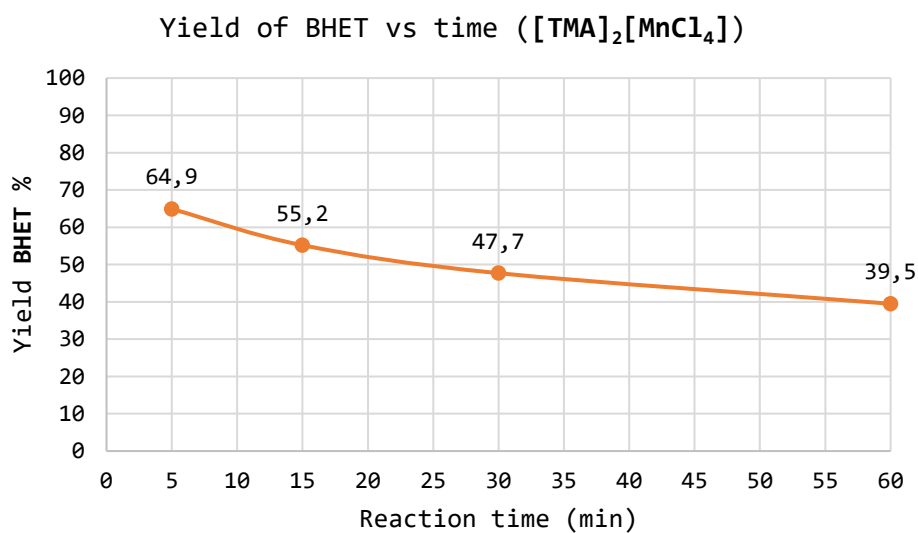


Figure E28. Correlation between reaction time and yield of BHET using [TMA]₂[MnCl₄] as catalyst, with microwave heating.

Entry	Catalyst	Time (min)	Conversion %	Yield %
24		5	100	56.5
14	$[\text{TMA}]_2[\text{ZnCl}_4]$	15	100	64.4
25		30	100	72.6

Reaction performed in MW glass tubes, temperature= 170 °C, catalyst loading= 5 mol%.

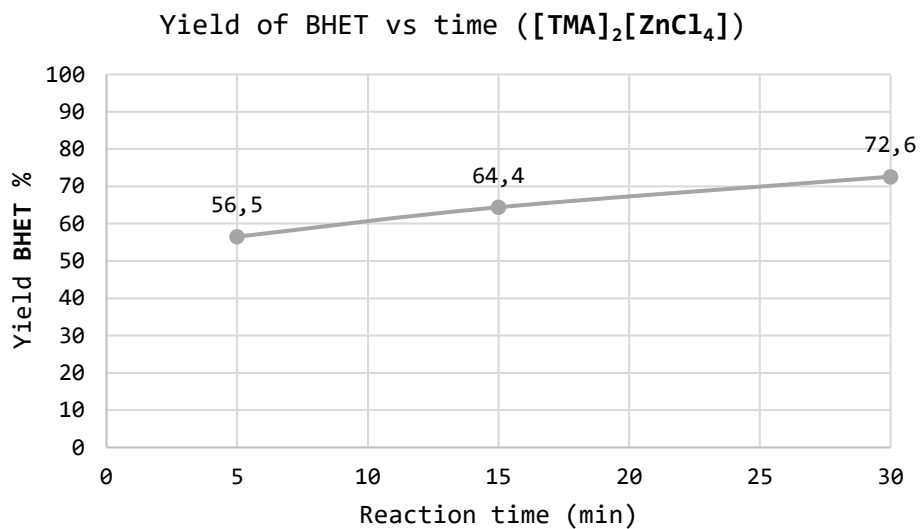


Figure E29. Correlation between reaction time and yield of BHET using $[\text{TMA}]_2[\text{ZnCl}_4]$ as catalyst, with microwave heating.

Entry	Catalyst	Time (min)	Conversion %	Yield %
26		5	100	56.5
12	[TMA][CoCl ₃]	15	100	64.4
27		30	100	72.6

Reaction performed in MW glass tubes, temperature= 170 °C, catalyst loading= 5 mol%.

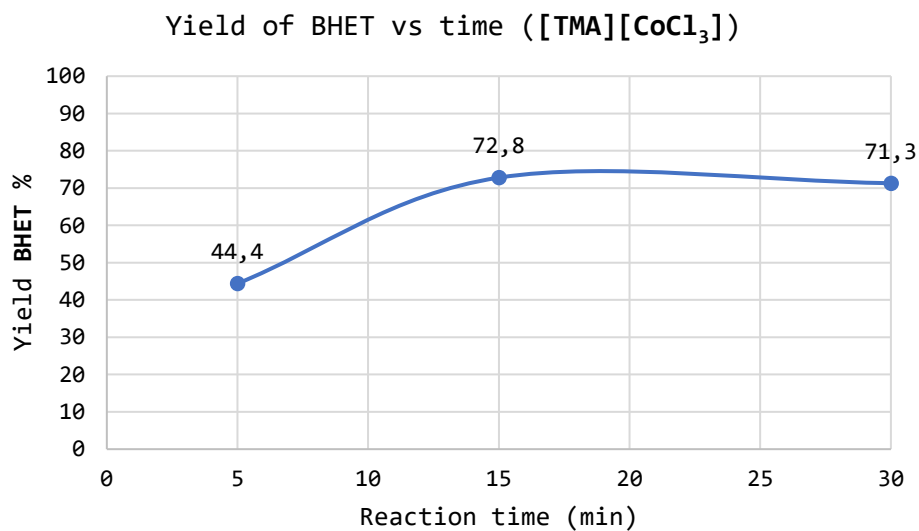


Figure E30. Correlation between reaction time and yield of BHET using [TMA][CoCl₃] as catalyst, with microwave heating.

6.16.7 Influence of temperature, microwave heating:

Entry	Catalyst	T (°C)	Conversion %	Yield %
7	[TMA][FeCl ₄]	170	100	54.1
28		180	100	64.2
29		190	100	70.4
11	[TMA] ₂ [MnCl ₄]	170	100	55.2
30		180	100	68.1
31		190	100	77.0
12	[TMA][CoCl ₃]	170	100	64.4
32		180	100	61.5
33		190	100	66.5

Reaction performed in MW glass tubes, reaction time= 15min, catalyst loading= 5 mol%.

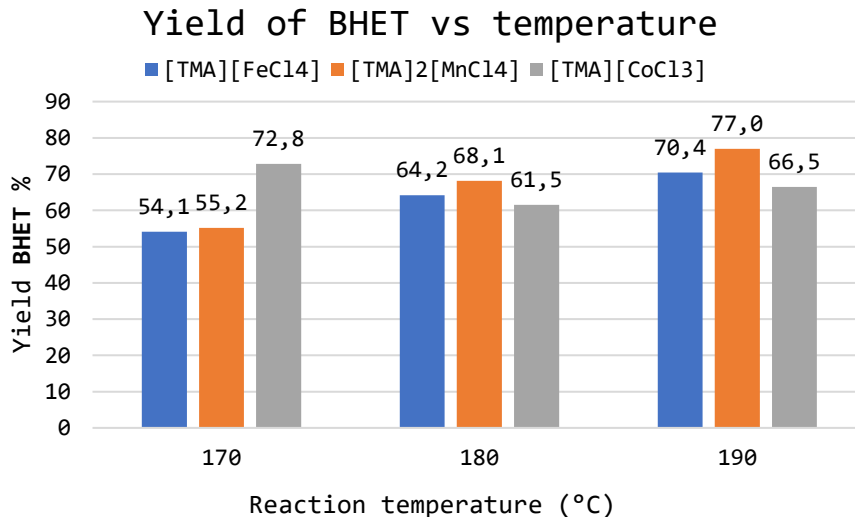
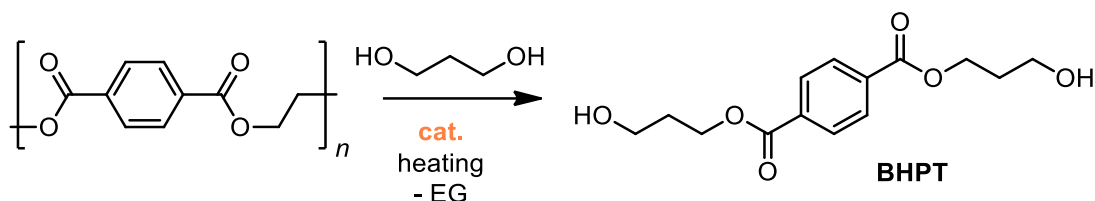


Figure E40. Correlation between reaction temperature and yield of BHET using different catalysts, with microwave heating for 15 minutes.

6.16.8 Glycolysis with 1,3-propandiol, microwave heating:



Entry	Catalyst	T (°C)	Conversion %	Yield of BHPT %
34	[TMA][FeCl ₄]	170	100	57.5
35	[TMA] ₂ [MnCl ₄]	170	0	0
36	[TMA] ₂ [CoCl ₄]	170	100	14.2
37	[TMA] ₂ [ZnCl ₄]	170	0	0
38	[TMA][FeCl ₄]	180	100	45.3
39	[TMA][FeCl ₄]	190	100	31.5

Reaction performed in MW glass tubes, catalyst loading= 5 mol%.

6.16.9 Comparison of BHET yield between commercial rPET and untreated water bottle:

Entry	Catalyst	Type of PET	Conversion %	Yield of BHPT %
40 ^[a]	[TMA][FeCl ₄]	rPET	89.0	33.8
41 ^[a]	[TMA][FeCl ₄]	bottle	n.d.	22.2
19 ^[b]	[TMA][FeCl ₄]	rPET	100	62.6
42 ^[b]	[TMA][FeCl ₄]	bottle	100	57.5
43 ^[a]	[TMA] ₂ [MnCl ₄]	rPET	78.5	59.6
44 ^[a]	[TMA] ₂ [MnCl ₄]	bottle	n.d.	49.5
23 ^[b]	[TMA] ₂ [MnCl ₄]	rPET	100	39.6
45 ^[b]	[TMA] ₂ [MnCl ₄]	bottle	100	60.9

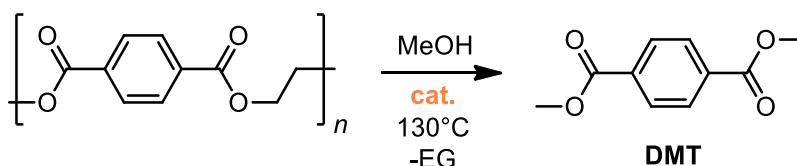
[a] Reaction performed in screw cap glass vials, catalyst loading= 5 mol%, T= 170°C, t=16h, conventional heating. [b] Reaction performed in MW glass tubes, catalyst loading= 5 mol%, T= 170°C, t=60 min, MW heating.

6.17 PET METHANOLYSIS :

6.17.1 General catalytic methods:

Catalytic methanolysis of PET was performed by conventional heating in sealed glass pressure tubes or stainless-steel autoclaves, using an aluminum heating block. rPET (250 mg, 1-5-10 g) and methanol (4-16-80 mL) were placed in the selected reactor vessel with a magnetic stirrer. The reaction was placed in the aluminum block and heated at 170 °C for 16 hours. At the end of the reaction, the monomeric product dimethyl terephthalate (DMT) can be recovered as crystals by cooling the mixture. The so obtained product can be further re-crystallized by hot ethyl acetate. Conversion of PET was calculated by weighting these eventual residues, after drying in vacuum, compared to the starting PET. The crystals are filtered, dried in vacuum and weighted to calculate the yield of the reaction.

6.17.2 PET methanolysis in pressure tubes, catalyst screening:



Entry	Catalyst	Conversion %	Yield DMT %
1	[TMA][FeCl ₄]	100	64.1
2	[TMA] ₂ [CoCl ₄]	100	72.4
3	[TMA][CoCl ₃]	55.0	17.5
4	[TMA] ₂ [MnCl ₄]	4.6	0
5	[TMA][MnCl ₃]	36.9	22.2
6	[TMA][ZnCl ₄]	9.7	0
7 ^[b]	[TMA][FeCl ₄]	72.4	56.6
8 ^[b]	[TMA] ₂ [CoCl ₄]	28.3	18.1

Reaction performed in glass pressure tubes, 250 mg rPET, 4 mL MeOH, catalyst loading= 5 mol%, reaction time= 16h, T= 130°C. [b] reaction time= 8h.

6.17.3 PET methanolysis in autoclave, catalyst screening:

Entry	Catalyst	Conversion %	Yield DMT %
9	[TMA][FeCl ₄]	100	70.4
10	[TMA] ₂ [CoCl ₄]	100	69.8
11	[TMA][CoCl ₃]	74.3	64.5
12	[TMA] ₂ [MnCl ₄]	74.3	49.8
13	[TMA][MnCl ₃]	58.5	49.9
14	[TMA][ZnCl ₄]	12.5	0
15 ^[b]	[TMA][FeCl ₄]	99	44.7
16 ^[b]	[TMA] ₂ [CoCl ₄]	35.8	30.6

Reaction performed in autoclave, 1 g rPET, 16 mL MeOH, catalyst loading= 5 mol%, reaction time= 3h, T= 170°C. [b] reaction time= 1.5h

6.17.4 PET methanolysis, control experiments in autoclave:

Entry	Catalyst	Conversion %	Yield DMT %
17	-	0	0
18	FeCl ₃ ·6H ₂ O	100	62.4
19	CoCl ₂ ·6H ₂ O	100	52.6
20	MnCl ₂ ·4H ₂ O	26.5	2.3
21	ZnCl ₂	34.8	9

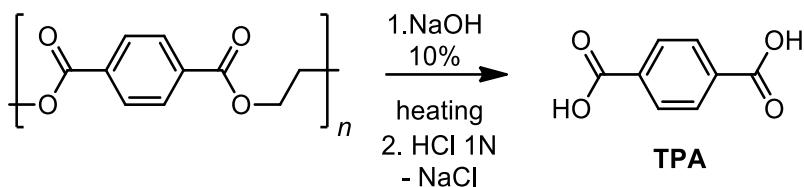
Reaction performed in autoclave, 1 g rPET, 16 mL MeOH, catalyst loading= 5 mol%, reaction time= 3h, T= 170°C.

6.18 PET HYDROLYSIS:

6.18.1 General catalytic methods:

Catalytic hydrolysis of PET was performed by microwave heating in specific MW vials or by conventional heating in a stainless-steel autoclave, using an aluminum heating block. rPET (125 mg) and water or NaOH (10%) (2 mL) were placed in the reaction vessel with a magnetic stirrer. The reaction was heated by MW at the desired temperature for a certain amount of time. At the end of the reaction, the monomeric product terephthalic acid (TPA) can be recovered as white powder by precipitation with diluted HCl. Conversion of PET was calculated by weighting eventual residues in the reaction mixture, after drying in vacuum, compared to the starting PET. The product is then filtered, dried in vacuum and weighted to calculate the yield of the reaction. A scale up of the reaction was made on a single, entire empty bottle of water, using a stainless-steel autoclave as reactor at 170 °C in an aluminum heating block.

6.18.2 Optimization of the reaction:



Entry	Catalyst	Solvent	Temperature (°C)	Time (min)	Yield TPA %
1 ^[a]	-	NaOH 10%	110-170	15	97.2
2 ^[a]	-	H ₂ O	110-170	15	0.0
3 ^[a]	[TMA][FeCl ₄]	H ₂ O	110-170	15	0.0
4 ^[a]	[TMA][FeCl ₄]	NaOH 10%	110-170	15	70.4
5 ^[b]	-	NaOH 10%	150	5	66.9
6 ^[c]	-	NaOH 10%	170	16h	44.7

[a] Reaction conditions: 125 mg rPET, 2 mL solvent, MW heating, 15 min at 110 °C followed by 20 seconds at 170 °C. [b] Reaction conditions: 125 mg rPET, 2 mL solvent, MW heating, 5 min at 150 °C. [c] scale up reaction on empty water bottle (5.9g), in autoclave at 170 °C for 16h.

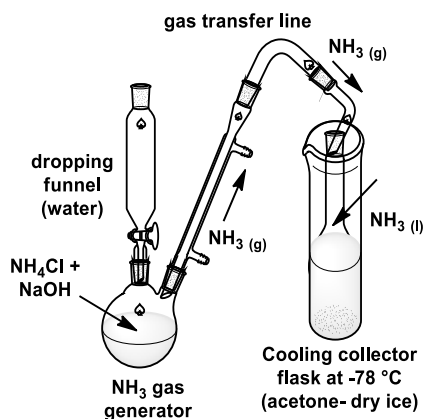
6.19 PET AMMONOLYSIS :

6.19.1 General catalytic procedure:

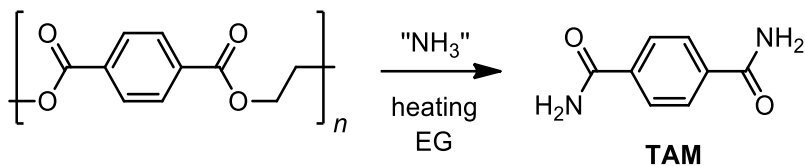
Catalytic ammonolysis of PET was performed by conventional heating in glass pressure tubes or stainless-steel autoclave, using an aluminum heating block. rPET (125 mg) and ethylene glycol (EG) as solvent (4 mL) were placed in the reaction vessel with a magnetic stirrer. The ammonia surrogate was added and the reaction was heated at the desired temperature for a certain amount of time. The monomeric product terephthalamide (TAM) can be recovered as white powder directly at the end of the reaction. Conversion of PET was calculated by weighting eventual residues in the reaction mixture, after drying in vacuum, compared to the starting PET.

6.19.2 Synthesis of ammonium carbamate:

The laboratory scale production of ammonium carbamate was performed by a modified tailored procedure. The apparatus needed for the reaction consists in a gaseous ammonia generation two neck round bottom flask, equipped with a dropping funnel and a vertical condenser, a gas transfer line, and a cooling apparatus where liquid ammonia is accumulated. The generation of gaseous ammonia is started upon mixing solid ammonium chloride and powdered sodium hydroxide in the round bottom flask, which is gently heated. The reaction is limited by the poor contact of the two reagents at the solid state, therefore water can be added at small portions by the dropping funnel. The condenser is needed to avoid the condensation of water vapor in the cooled liquid ammonia collector. Ammonium carbamate is directly produced by careful addition of excess solid carbon dioxide (dry ice) to liquid ammonia. The product is formed as a white solid, recovered by the container and stored at 4 °C (ammonium carbamate decomposes at moderately low temperatures ≈ 40 °C).



6.19.3 Preliminary results:

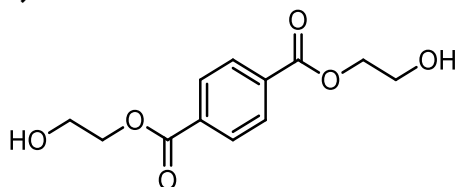


Entry	catalyst	Ammonia surrogate	Time (h)	Yield TAM %
1 ^[b]	-	Ammonium carbamate 30 mol%	16	62.4
2	-	Ammonium carbamate 10 mol%	24	43.3
3	-	Ammonium bicarbonate 10 mol%	24	17.5
4	[TMA][FeCl ₄] 5 mol%	Ammonium carbamate 10 mol%	24	43.3
5	-	Ammonium carbamate 10 mol%	16	71.2

Reaction conditions: 125 mg rPET, 4 mL solvent, at 120 °C in pressure tubes [b] reaction performed in autoclave.

6.19.4 Products characterization:

Bis-(2-hydroxyethyl)terephthalate (BHET):



¹H NMR (400 MHz, DMSO-d₆)

δ 8.14 (s, 4H), 4.96 (t, J= 5.7 Hz, 2H), 4.48-4.19(m, 4H,), 3.72 (dd, 4H, J = 10.0, 5.4 Hz).

¹H NMR (400 MHz, CDCl₃)

δ 8.13 (s, 4H), 4.53-4.50 (m, 4H), 4.02-3.99 (m, 4H,), 2.13 (bs, 2H).

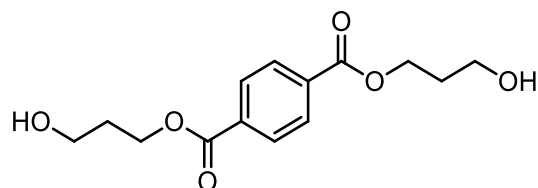
¹³C NMR (100 MHz, CDCl₃):

δ 166.06, 133.87, 129.71, 67.04, 61.26.

MS-ESI(+): m/z (%) calculated for $C_{12}H_{14}O_6$ 254.08; found: 277.26 (100%, M + Na); 255.12 (20%, M + 1). In certain cases, MS analysis show the presence of dimers, trimers and tetramers of BHET (as a proof of a sequential depolymerization to form oligomers and monomers) with signal at 469.18 (dimer), 661.18 (trimer), 853.18 (tetramer).

Elem. An. calculated for $C_{12}H_{14}O_6$ C: 56.69, H: 5.55; found: C: 56.68, H: 5.63.

Bis-(3-hydroxypropyl)terephthalate (BHPT):



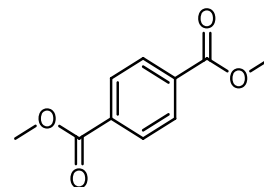
1H NMR (400 MHz, $CDCl_3$)

δ 8.12 (s, 4H), 4.54 (t, $J = 6.0$ Hz, 4H), 3.82 (t, $J = 6.0$ Hz, 4H), 2.06 (p, $J = 6.0$ Hz, 4H), 2.03 (bs, 2H).

^{13}C NMR (100 MHz, $CDCl_3$):

δ 166.09, 134.01, 129.59, 62.27, 59.15, 31.81.

MS-ESI(+): m/z (%) calculated for $C_{14}H_{18}O_6$ 282.11; found: 282.87 (100%, M + 1);

Dimethylterephthalate (DMT):

¹H NMR (400 MHz, CDCl₃)

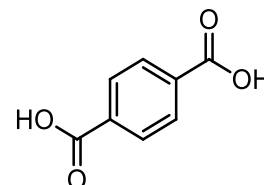
δ 8.12 (s, 4H), 3.97 (s, 6H).

¹³C NMR (100 MHz, CDCl₃):

δ 166.29, 133.93, 129.56, 52.42.

Elem. An. (pre-crystallization): calculated for C₁₀H₁₀O₄ C: 61.85; H: 5.19; found: C: 61.58; H: 5.32; N: 0.04;

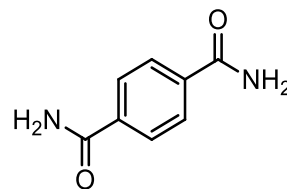
Elem. An. (pre-crystallization): calculated for C₁₀H₁₀O₄ C: 61.85; H: 5.19; found: C: 61.77; H: 5.25.

Terephthalic acid (TPA):

¹H NMR (400 MHz, DMSO-d₆)

δ 8.05 (s, 4H).

Terephthalamide (TAM):

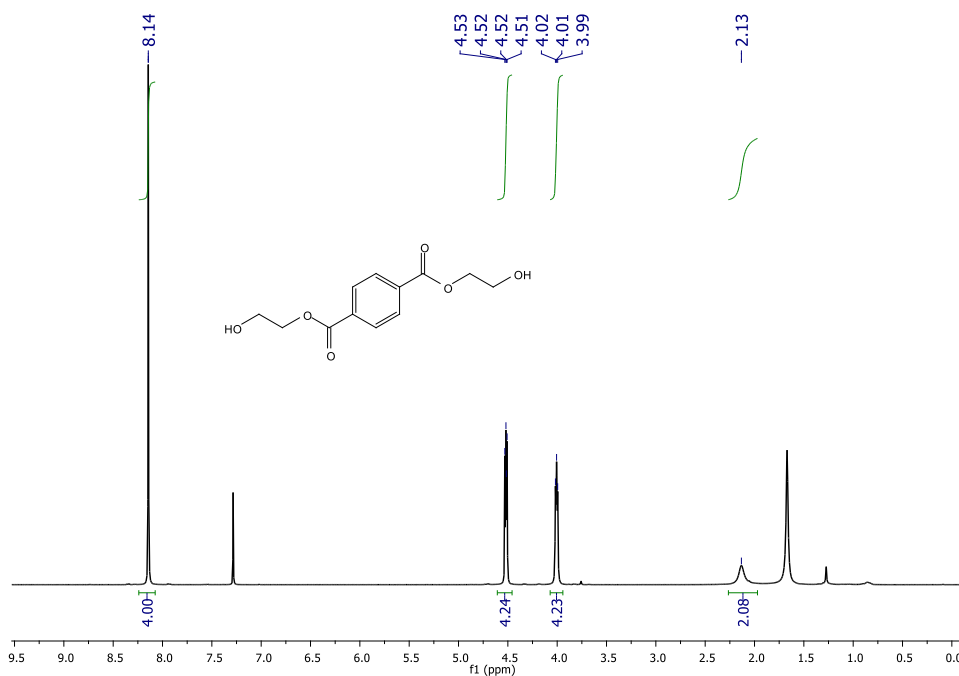


$^1\text{H NMR}$ (400 MHz, DMSO-d^6)

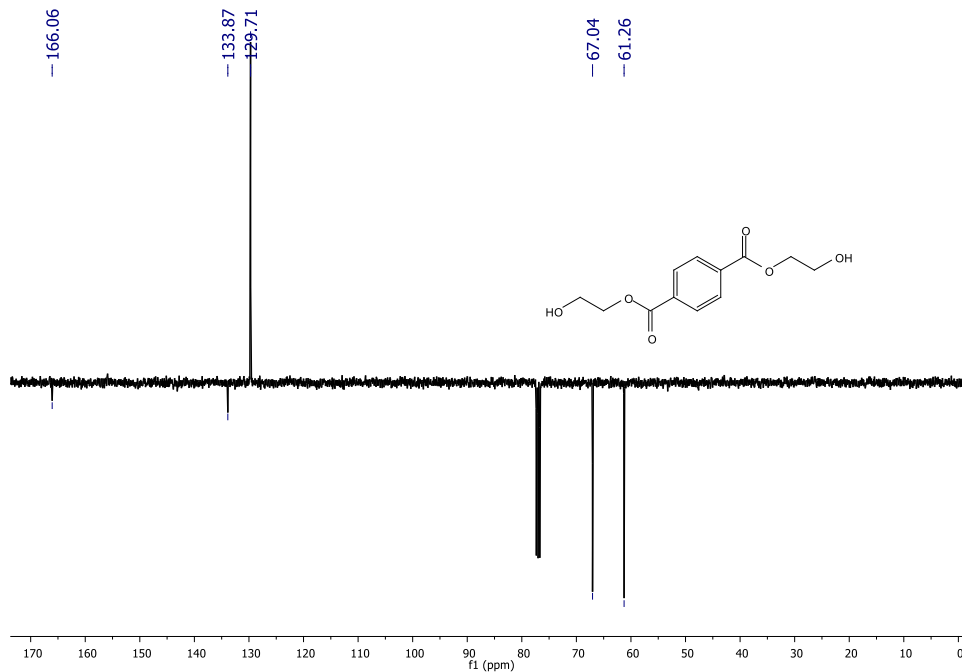
δ 8.06 (s, 2H), 7.92 (s, 4H), 7.47 (s, 2H).

MS-ESI(+): m/z (%) calculated for $\text{C}_8\text{H}_8\text{N}_2\text{O}_6$ 164.06; found: 190.86 (100%, M + Na), 355.24 (dimer + Na).

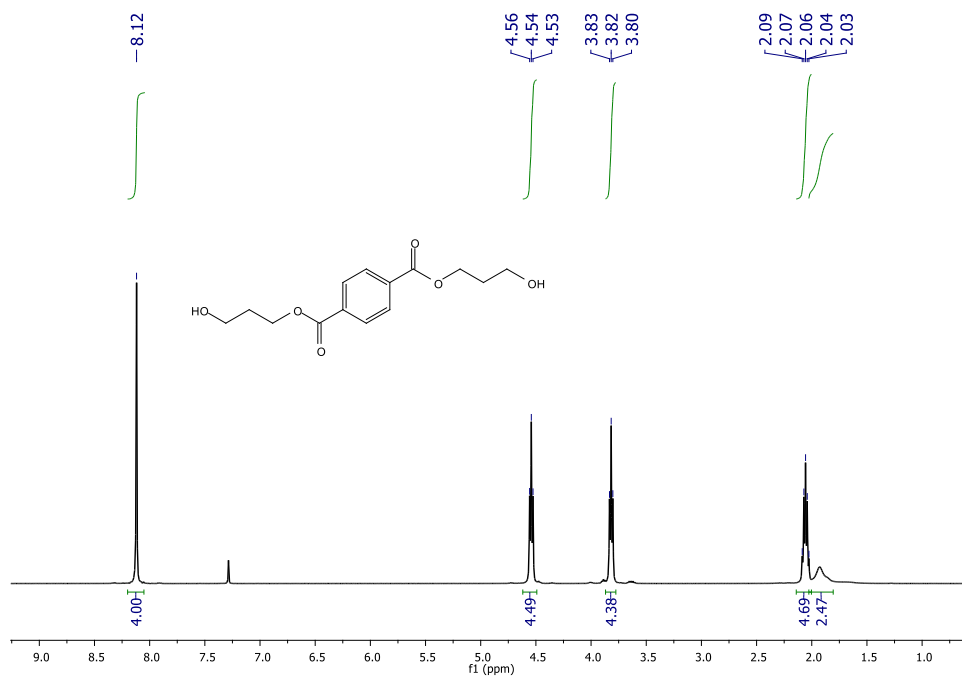
Elem. An. calculated for $\text{C}_8\text{H}_8\text{N}_2\text{O}_6$ C: 58.53; H: 4.91; N: 17.06; found: C: 58.69; H: 4.88; N: 16.73;



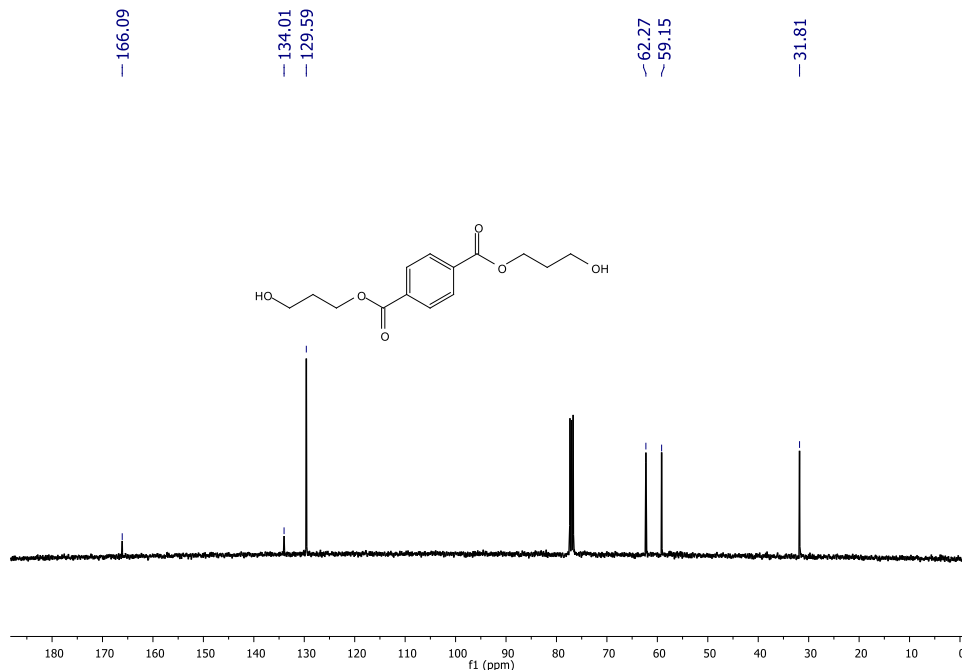
$^1\text{H NMR}$ of BHET in CDCl_3



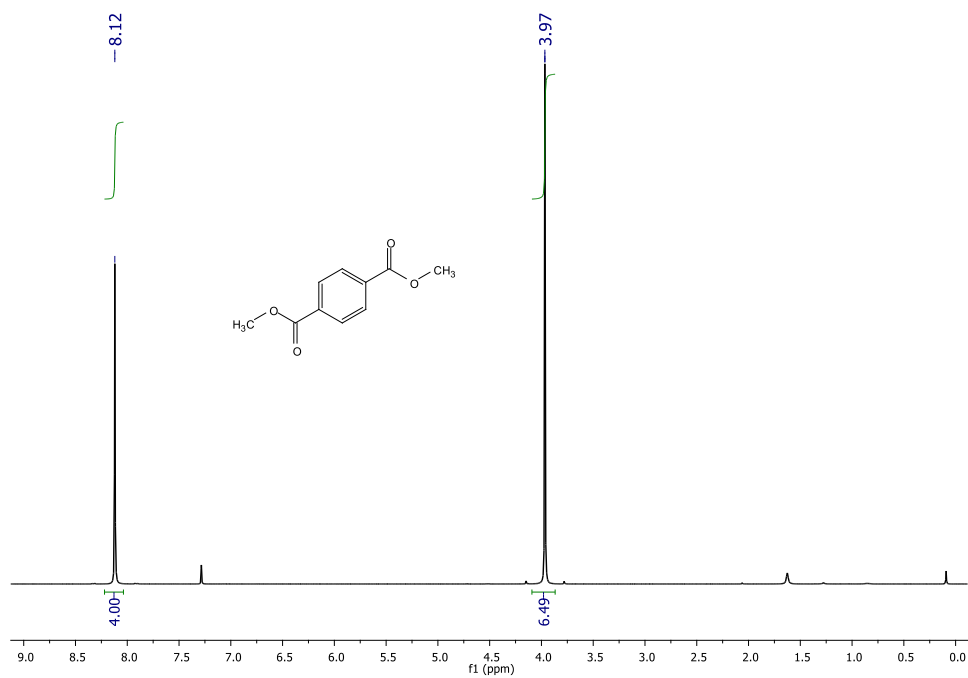
¹³C NMR of BHET in CDCl₃



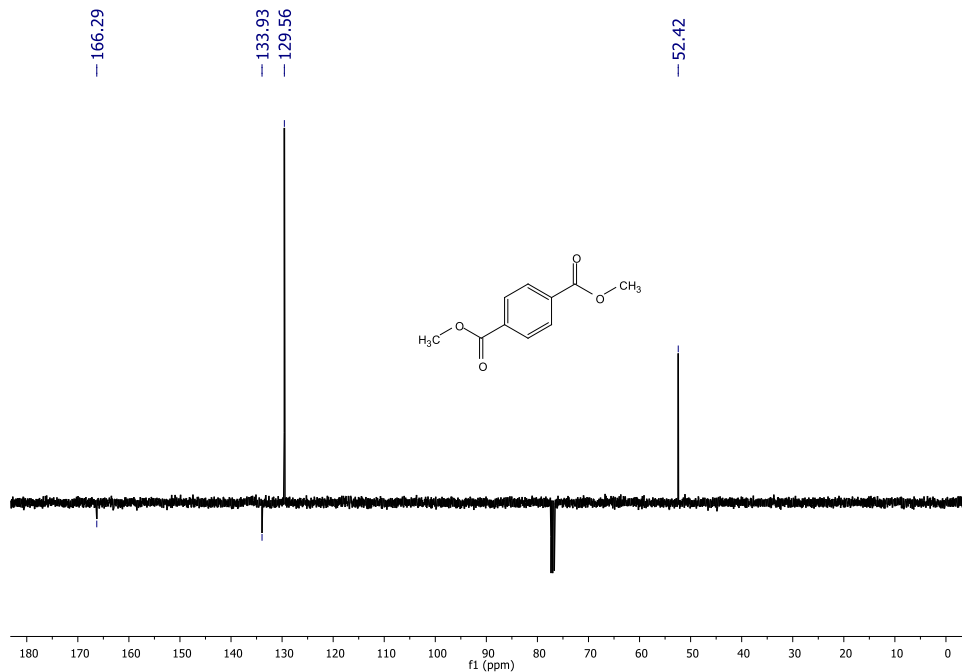
¹H NMR of BHPT in CDCl₃



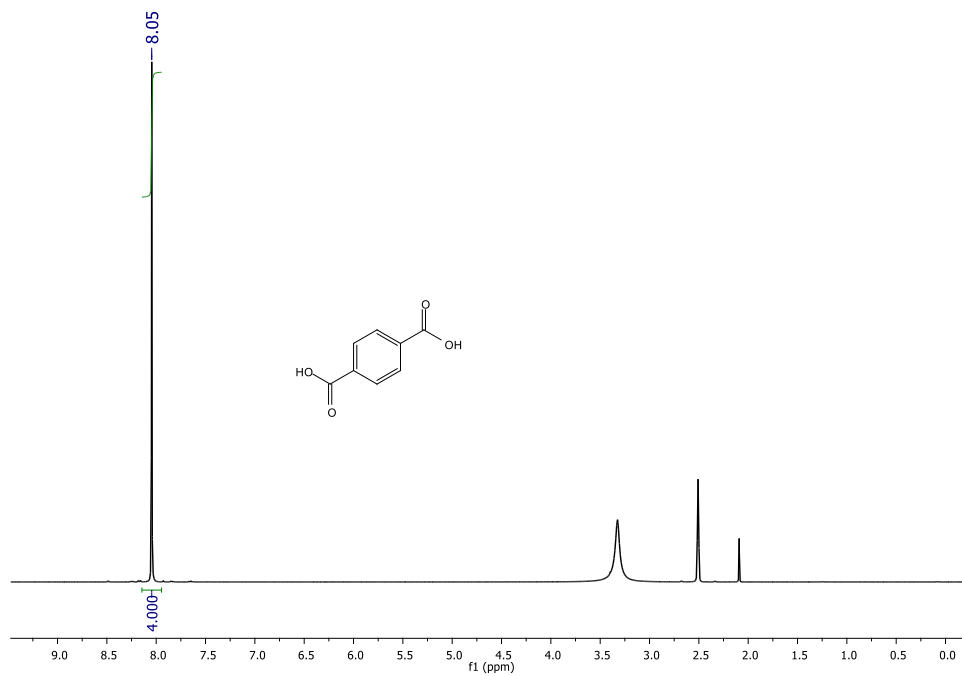
¹³C NMR of BHPT in CDCl₃



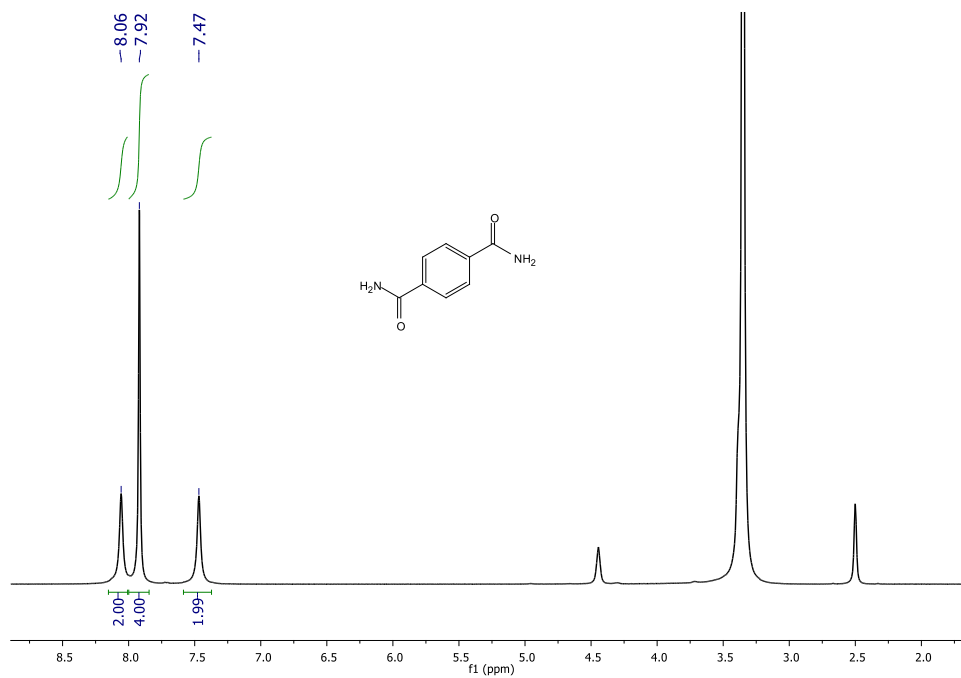
¹H NMR of DMT in CDCl₃



¹³C NMR of DMT in CDCl₃



¹H NMR of TPA in CDCl₃

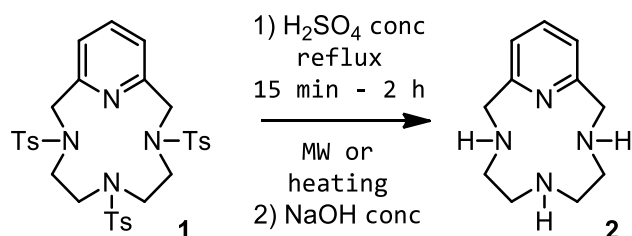


^1H NMR of TAM in CDCl_3

7 THESIS OVERVIEW:

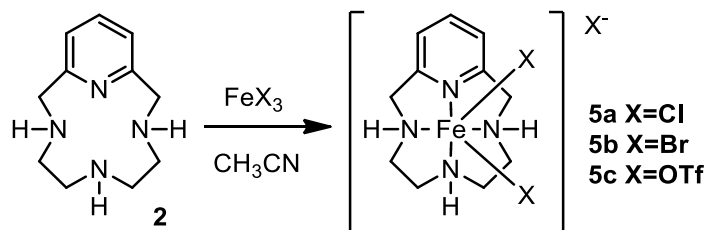
CATALYTIC OXIDATION OF ALCOHOLS WITH PYCLEN IRON(III) COMPLEXES:

We modified a procedure for the deprotection of pycLEN ligand **1**,^[49] which allows the completion of the reaction in shorter times at lower temperatures (20 minutes at 120 °C) using microwaves (Scheme 01).



Scheme 01. Syntheric pathway for ligand **2**, by acid hydrolysis with concentrated sulfuric acid, under traditional or MW heating.

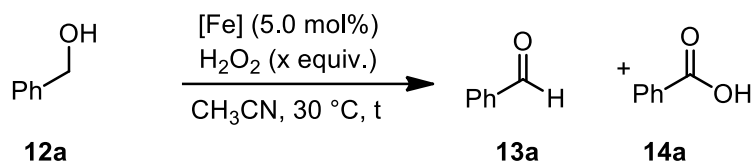
Metal complexes **5a-c** were prepared in acetonitrile,^[47] by slow addition of the metal precursor to a solution of the ligand in acetonitrile at room temperature (Scheme 02). The mixture is stirred for a few hours, even if the precipitation of the complexes is almost immediate. In certain cases, if the precipitation does not occur, the solvent is evaporated, and the residue treated several times with diethyl ether and/or hexane and separated by filtration.



Scheme 02. Synthesis of complex **5a-c** using different metal precursors.

Oxidation of benzyl alcohol **12a** was chosen as benchmark reaction for the optimization of the catalytic conditions. In terms of homogeneous catalysts, few examples are reported of being capable

of yielding selectively benzaldehyde in this transformation, leaving the room for a further optimization of the reaction.



Scheme 03. General reaction scheme for the oxidation of benzyl alcohol

When the oxidant was added in small portions, the catalytic system based on complex **5b** was highly selective and, for instance, if 1 equivalent of hydrogen peroxide was added every 15 minutes to the reaction mixture, a reasonable selectivity for benzaldehyde with good conversion (78% conversion, 76% selectivity, table 4, entry 1) in just 3h was observed (in total 12 equivalents of hydrogen peroxide). A huge boost in selectivity was obtained by slowly adding 2 equivalents of the oxidant by syringe pump in 2 h and allowing the reaction mixture to stir at 30 °C for further 22 h (Table 4, entry 2), and the best compromise between conversion and selectivity in terms of the overall process was obtained by the slow addition of 4 equivalents of oxidant and allowing the reaction to stir at 30 °C for 24 h (Table 4, entry 3).

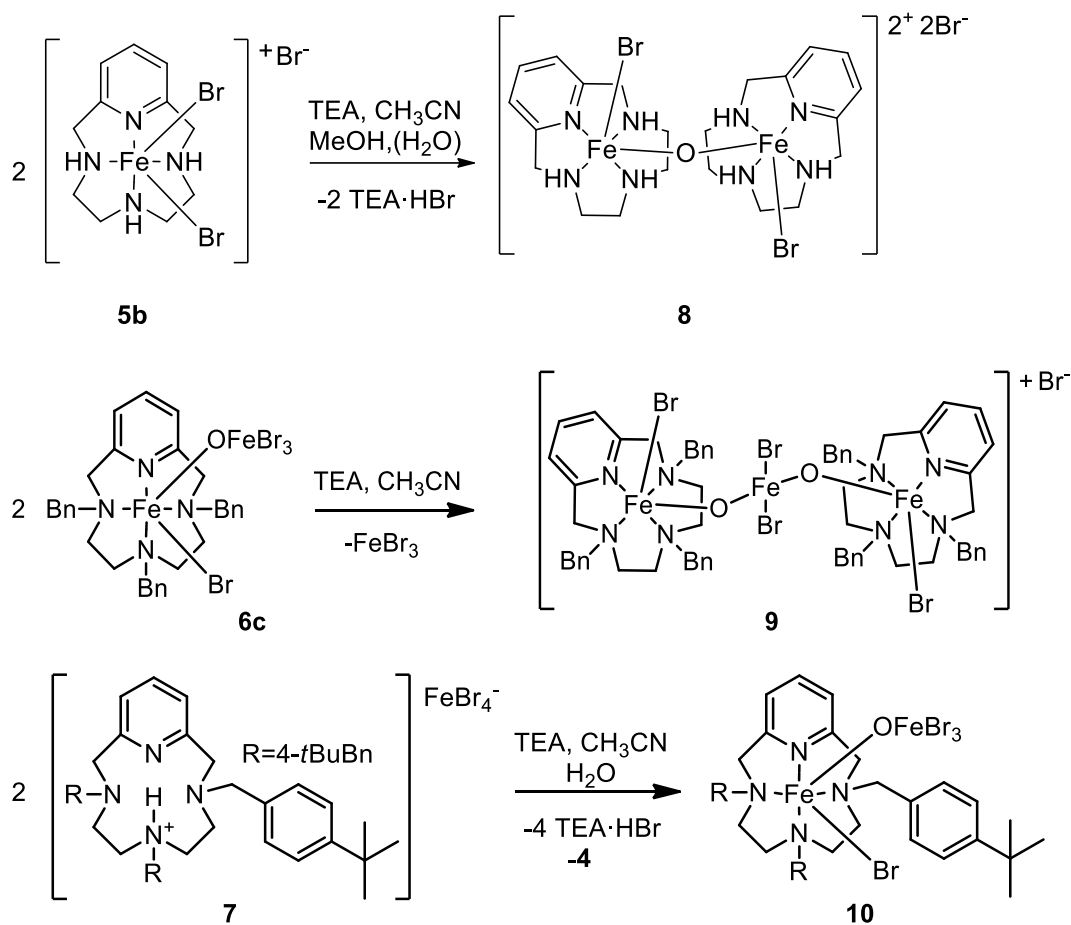
Table 01. Optimization of the reaction with complex **5b** as catalyst.

Entry	Catalyst	eq H ₂ O ₂	Conv (%)	12a	Select (%)	13a	Select (%)	14a
1	5b	12	78		76		3	
2	5b	2	50		98		2	
3	5b	4	96		90		10	

A large scope of reaction was performed, which confirmed the activity of the system based on complex **5b** on most of the substrates, with high conversion and selectivity for benzylic ones. Aliphatic substrates were converted in lower rates and a fall in selectivity was noticed when unsaturated alcohols were used as substrates.

The mechanism was investigated by means of different experiments (Hammett plot, KIE value, oxidation of cyclobutanol) which prompted us to the possible coexistence of different reaction pathways, mainly in terms of hydrogen atom abstraction and radical formation.

The formation of dimeric oxo-bridged form of complex **5b** was studied by means of structural and spectroscopical features. Different bridged species were prepared by reaction of precursors and a base in acetonitrile (Scheme 04).



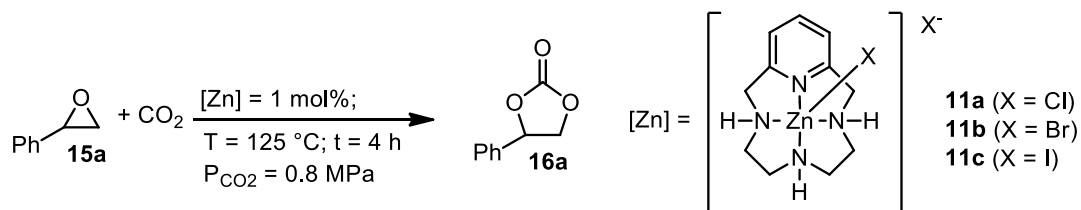
Scheme 04. Synthesis of dimeric complexes **8,9,10**.

Those species were crystallized, and the structure obtained by single crystal XRD. Their vibrational features were observed using Raman spectroscopy, which proved to be a useful tool to discriminate

the existence and the symmetric/asymmetric nature of the Fe-O-Fe moiety in different coordination environment (See chapter 1).

CYCLOADDITION OF CO₂ TO EPOXIDES WITH PYCLEN METAL COMPLEXES AS CATALYSTS:

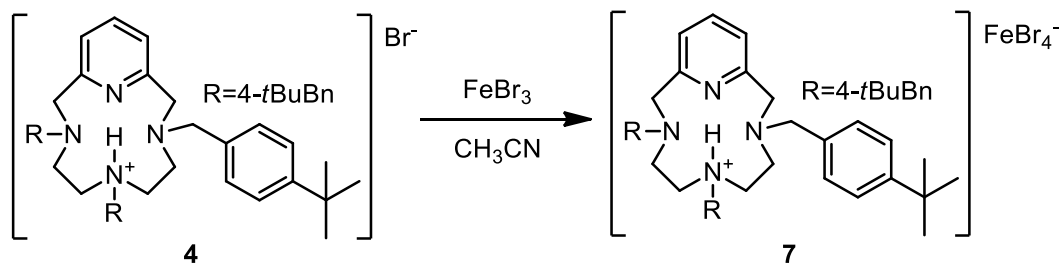
We compared the catalytic activity of different zinc complexes (**11a-c**) in the model reaction between CO₂ and styrene oxide **15a** (Scheme 05) with simple quaternary ammonium halides, which are known to exhibit good activities in carbon dioxide fixation with epoxide.^[139] Efficient binary catalytic systems composed by zinc and ammonium salts have already been reported, and the presence of both Lewis acid and nucleophile in the binary catalytic system facilitate the ring-opening step, which is often considered as rate-defining, making it less energetically demanding. In our vision, due to the specific coordination geometry, metal-complexes **11a-c** were themselves perfectly suited to act as bifunctional systems, without the addition of nucleophilic co-catalyst.



Scheme 05. Model reaction of styrene oxide **15a** and CO₂ with zinc catalysts **11a-c**, to yield styrene carbonate **16a**.

Indeed the zinc complexes proved to be active without addition of any external nucleophile, especially in the case of the zinc bromide complex **11b**. This catalyst was exploited in a large reaction scope with satisfactory yields of a large number of cyclic carbonates.

Due to its abundance, low toxicity and ecocompatibility we decided to move towards the use of iron as metal. We designed a functionalized pyclen ligand **4** to enhance the solubility of the complex in the epoxides. While doing so, we unexpectedly obtained a salt in which iron is present as tetrabromoferrate anion, with the macrocycle bearing a proton (Scheme 06).



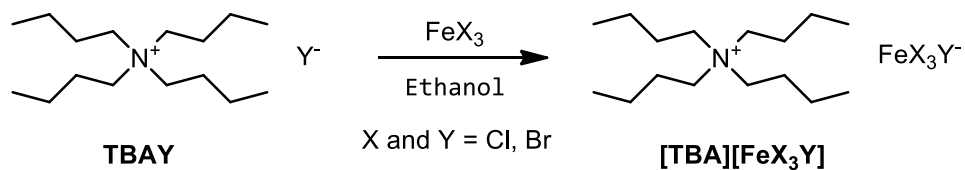
Scheme 06. Synthesis of complex **7**, starting from protonated ligand **4**.

This species proved to be even more active than the zinc complexes previously described, and much more soluble in the epoxides tested as substrates. The activity of this species in absence of any external nucleophile was addressed to the particular nature of the ferrate anion, bearing in a single unit both the Lewis acid (FeBr_3) and the nucleophile (Br^-) needed for the reaction to occur.

AMMONIUM METALLATES FOR CYCLIC CARBONATES SYNTHESIS FROM EPOXIDES AND CO_2 :

After the aforementioned results with the unexpected ferrate species **7** we decided to synthesize, and test in the same reaction, very simple ammonium ferrates. The synthesis of a series of tetrabutylammonium (TBA) tetrahalogenoferrate (Table 02) was performed by a reported procedure.^[154] The products are obtained by mixing an ethanolic solution of a TBA halide and an iron(III) halide precursor. All the species were obtained as solids and characterized by means of HRMS and elemental analysis.

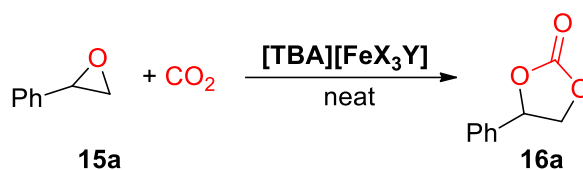
Table 02. The four synthesized homo and mixed tetrahalogenoferrate salts and their experimental melting point.



FeX ₃	TBAY	[TBA][FeX ₃ Y]	m. p.
FeCl ₃	TBACl	[TBA][FeCl ₄]	113 °C
FeCl ₃	TBABr	[TBA][FeCl ₃ Br]	132 °C
FeBr ₃	TBACl	[TBA][FeBr ₃ Cl]	129 °C
FeBr ₃	TBABr	[TBA][FeBr ₄]	135 °C

The activity of the different TBA ferrates was evaluated in the model reaction of styrene oxide and carbon dioxide, in the condition used for the previous work (Table 03).

Table 03. Preliminary results with TBA ferrates in the cycloaddition of carbon dioxide and styrene oxide.



Entry	Cat. mol%	Con. 15a %	Sel. 16a %	TOF ^[b] (h ⁻¹)
1	[TBA][FeCl ₄] 0.5%	73	88	36
2	[TBA][FeCl ₃ Br] 0.5%	83	95	42
4	[TBA][FeBr ₃ Cl] 0.5%	99	70	49
5	[TBA][FeBr ₄] 0.5%	73	88	36
7	TBACl 0.5%	41	95	21
8	TBABr 0.5%	33	>99	17

Reaction conditions: styrene oxide (SO) 2.19 mmol; T = 100 °C; P = 0.8 MPa; t = 4h. Conversion and selectivity determined by ¹H NMR using mesitylene as internal standard. [b] TON = mol_{15a(converted)} · mol_{cat}⁻¹; TOF = TON · reaction time⁻¹

With the best catalyst (Trichlorobromo ferrate) we evaluated the influence of different parameters such as temperature, pressure of carbon dioxide, catalyst loading. In the optimized conditions we performed a satisfactory reaction scope in which such simple catalytic system proved to be active on a very large number of substrates in mild conditions.

The system was deeply investigated by means of DFT calculations, to evaluate the real nature of the catalyst and the energetics of the process. A combined approach between a preliminar screening and a final ab-initio calculations on the most probable reaction path shed light on the reaction mechanism. The energetics of the process are summarized in Figure 01, where it is clear how the presence of the Lewis acid completely annihilates the barrier for the ring-opening step. Therefore, the rate determining step results in the ring-closing of the product.

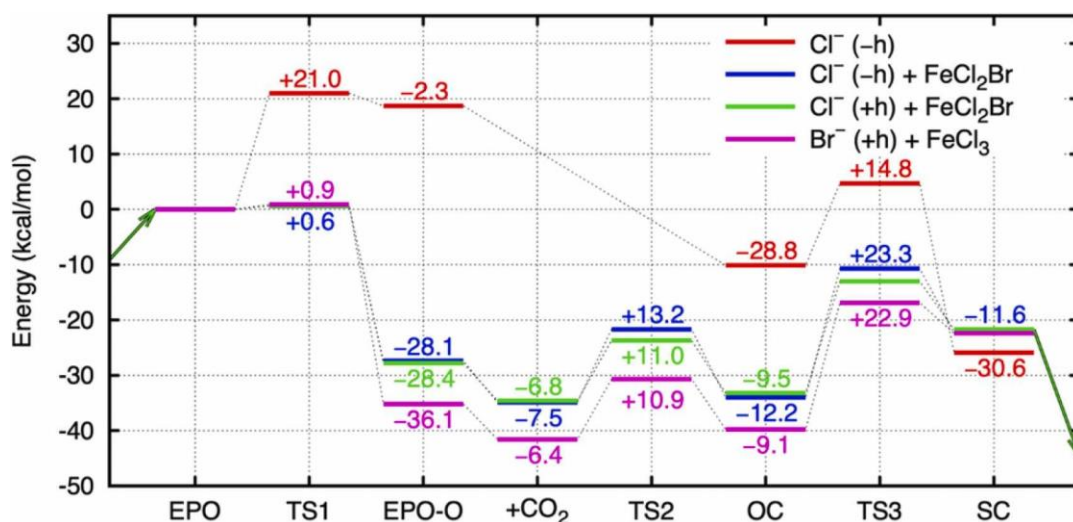
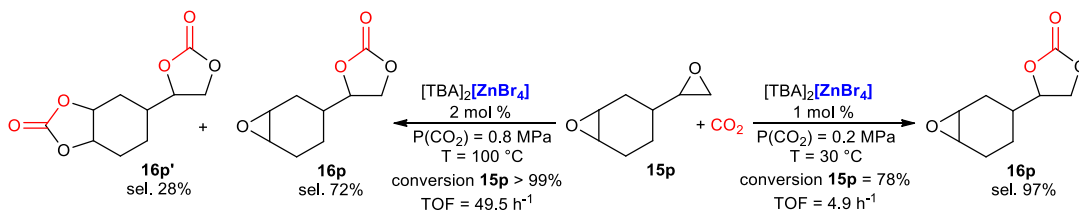


Figure 01 Schematic energy profiles for the relevant step in the reaction studied (see experimental for further details).

The zinc analogues of the ammonium ferrates showed very high activity at extremely mild reaction conditions (room temperature and ambient pressure of carbon dioxide, in the case of the bromo zincate salt). Even in this case, a large reaction scope was performed successfully and we were able in certain cases to discriminate the

selectivity of the reaction by tailoring the reaction conditions as shown in Scheme 07.

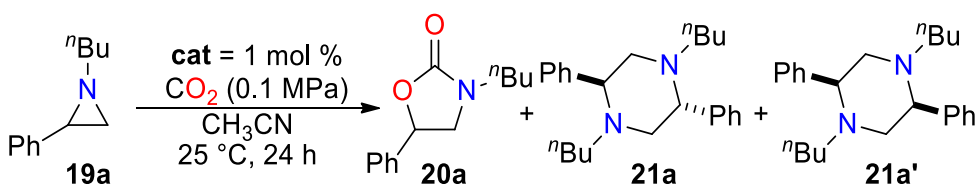


Scheme 07. Different reaction outcome with changing the experimental conditions with substrate **15p**.

SYNTHESIS OF OXAZOLIDINONES FROM AZIRIDINES AND CO_2 CATALYZED BY AMMONIUM FERRATES:

The activity of the previously reported ammonium ferrates were exploited also in the reaction between aziridines and carbon dioxide to yield cyclic carbamates, a chemical moiety largely present in pharmaceuticals. The preliminary investigation proved the activity of the ferrate compounds, especially in the case of the tetrabromo one. Interestingly, even if the formation of two isomers is possible, the reaction proved to be highly selective for the formation of a single isomer, deriving from a selective attack of the bromide anion at the benzylic position of the substrate (Table 04 summarizes the results).

Table 04. Preliminary investigation in the formation of oxazolidinones catalyzed by ferrate salts.



Entry	Catalyst	Conversion 19a % ^[b]	Selectivity 20a % ^[b]	TOF ^[c] (h ⁻¹)
1	[TBA][FeCl ₄]	58	96 ^[d]	2.4
2	[TBA][FeCl ₃ Br]	90	98 ^[d]	3.8
3	[TBA][FeBr ₃ Cl]	94	97	3.9
4	[TBA][FeBr ₄]	>99	97	4.1
5	FeBr ₃	88	84	3.7
6	TBABr	12	>99	0.5
7	FeBr ₃ + TBABr	>99	99	4.1

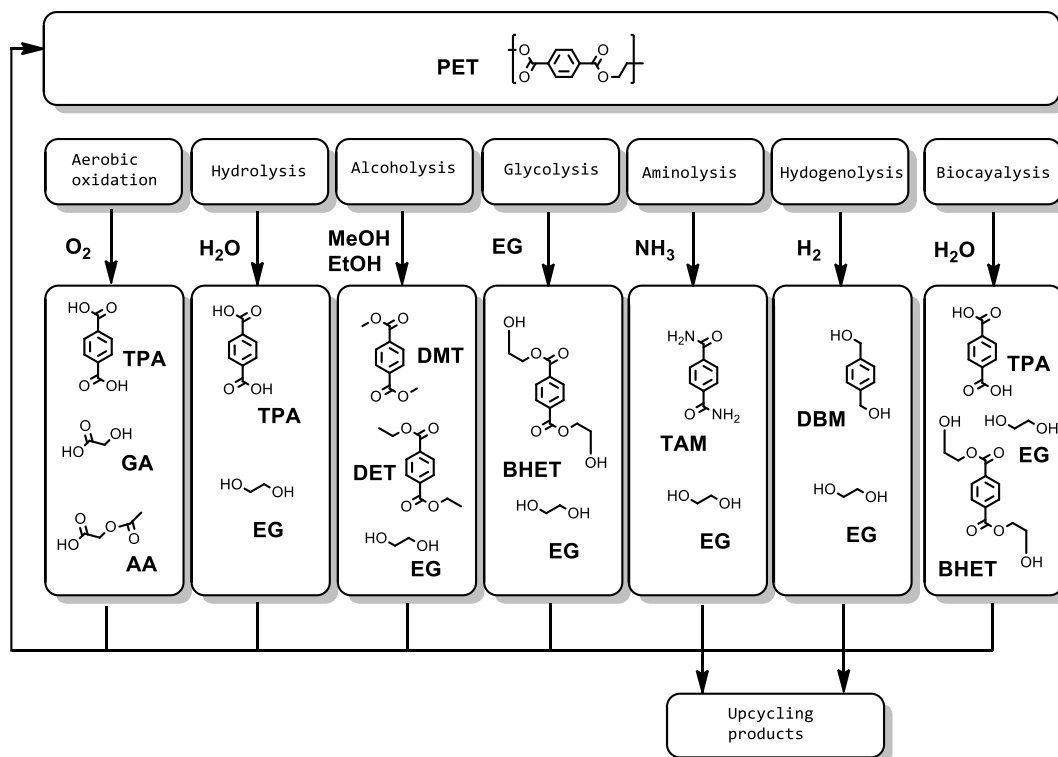
Reaction conditions: 1-butyl-2-phenyl aziridine, **19a**, (1 mmol) and catalyst (1 mol%) in CH₃CN (1 mL) under CO₂ atmosphere (P = 0.1 MPa) at T = 25 °C; t = 24 h. [b] Conversion and selectivity determined by ¹H NMR using dibromomethane as the internal standard and confirmed by GC (decane as ISTD) [c] Turnover frequency (mol_{19a}(converted)·mol_{cat}⁻¹·reaction time⁻¹). [d] Traces of the 3-butyl-4-phenyl-1,3-oxazolidin-2-one isomer were detected (d.r. = 97:3).

A kinetic study highlighted the initial rapid formation of the aziridine dimerization product at the start of the reaction (when aziridine concentration is high) and the progressive switch to the formation of the oxazolidinone as major product. Even in this case, a detailed DFT study confirmed the experimental findings.

The system was active at really mild reaction conditions, but unfortunately the scope was limited to N-alkyl substrates

CHEMICAL RECYCLING OF POLYETHYLENE TEREPHTHALATE (PET):

Different ammonium metallates were successfully employed as catalysts in the chemical depolymerization of PET waste. Different strategies were used, using both traditional and microwave heating to achieve good results in very short times. The chemical depolymerization products of PET can be tailored by changing the solvent of the reaction (Scheme 08). We obtained very good results in the glycolysis of PET to obtain BHET monomer and in the methanolysis (using methanol as solvent and iron/cobalt-based catalysts). Different reactions were also tested and are currently under study.



Scheme 08. Schematic representation of the possible chemical depolymerization of PET and respective products.

8 REFERENCES:

- [1] S. Sahu, D. P. Goldberg, *J Am Chem Soc* **2016**, *138*, 11410–11428.
- [2] W. Nam, *Acc Chem Res* **2015**, *48*, 2415–2423.
- [3] S. M. Barry, G. L. Challis, *ACS Catal* **2013**, *3*, 2362–2370.
- [4] N. Panza, G. Tseberlidis, A. Caselli, R. Vicente, *Dalton Transactions* **2022**, *51*, 10635–10657.
- [5] J. Serrano-Plana, W. N. Oloo, L. Acosta-Rueda, K. K. Meier, B. Verdejo, E. García-España, M. G. Basallote, E. Münck, L. Que, A. Company, M. Costas, *J Am Chem Soc* **2015**, *137*, 15833–15842.
- [6] W. N. Oloo, R. Banerjee, J. D. Lipscomb, L. Que, *J Am Chem Soc* **2017**, *139*, 17313–17326.
- [7] R. Fan, J. Serrano-Plana, W. N. Oloo, A. Draksharapu, E. Delgado-Pinar, A. Company, V. Martin-Diaconescu, M. Borrell, J. Lloret-Fillol, E. García-España, Y. Guo, E. L. Bominaar, L. Que, M. Costas, E. Münck, *J Am Chem Soc* **2018**, *140*, 3916–3928.
- [8] T. J. Collins, A. D. Ryabov, *Chem Rev* **2017**, *117*, 9140–9162.
- [9] V. Dantignana, J. Serrano-Plana, A. Draksharapu, C. Magallón, S. Banerjee, R. Fan, I. Gamba, Y. Guo, L. Que, M. Costas, A. Company, *J Am Chem Soc* **2019**, *141*, 15078–15091.
- [10] G. Tseberlidis, L. Demonti, V. Pirovano, M. Scavini, S. Cappelli, S. Rizzato, R. Vicente, A. Caselli, *ChemCatChem* **2019**, *11*, 4907–4915.
- [11] R. Latifi, T. D. Palluccio, W. Ye, J. L. Minnick, K. S. Glinton, E. v. Rybak-Akimova, S. P. de Visser, L. Tahsini, *Inorg Chem* **2021**, *60*, 13821–13832.
- [12] G. Tseberlidis, D. Intrieri, A. Caselli, *Eur J Inorg Chem* **2017**, *2017*, 3589–3603.
- [13] M. H. S. A. Hamid, P. A. Slatford, J. M. J. Williams, *Adv Synth Catal* **2007**, *349*, 1555–1575.
- [14] *Organic Syntheses by Oxidation with Metal Compounds* **1986**, DOI 10.1007/978-1-4613-2109-5.
- [15] Jan-Erling Bäckvall, *Modern Oxidation Methods*, John Wiley & Sons, **2011**.

- [16] F. Minisci, F. Recupero, M. Rodinò, M. Sala, A. Schneider, **2003**, DOI 10.1021/op034063o.
- [17] E. Farnetti, C. Crotti, E. Zangrando, *Inorganica Chim Acta* **2020**, *502*, 119318.
- [18] A. Guðmundsson, K. E. Schlipköter, J. Bäckvall, *Angewandte Chemie* **2020**, *132*, 5441–5444.
- [19] J. E. Chàvez, C. Crotti, E. Zangrando, E. Farnetti, *J Mol Catal A Chem* **2016**, *421*, 189–195.
- [20] A. F. Vailati, R. D. Huelsmann, E. Martendal, A. J. Bortoluzzi, F. R. Xavier, R. A. Peralta, *New Journal of Chemistry* **2020**, *44*, 2514–2526.
- [21] Y. Zhao, C. Yu, S. Wu, W. Zhang, W. Xue, Z. Zeng, *Catal Letters* **2018**, *148*, 3082–3092.
- [22] Q. Yan, Y. C. Fang, Y. X. Jia, X. H. Duan, *New Journal of Chemistry* **2017**, *41*, 2372–2377.
- [23] I. Guerrero, Z. Kelemen, C. Viñas, I. Romero, F. Teixidor, *Chemistry - A European Journal* **2020**, *26*, 5027–5036.
- [24] E. Prathibha, R. Rangasamy, A. Sridhar, K. Lakshmi, *ChemistrySelect* **2020**, *5*, 988–993.
- [25] C. W. Ding, W. Luo, J. Y. Zhou, X. J. Ma, G. H. Chen, X. P. Zhou, D. Li, *ACS Appl Mater Interfaces* **2019**, *11*, 45621–45628.
- [26] J. Lee, J. C. Lee, *Lett Org Chem* **2018**, *15*, 895–898.
- [27] S. Enthaler, K. Junge, M. Beller, S. Enthaler, K. Junge, M. Beller, *Angewandte Chemie International Edition* **2008**, *47*, 3317–3321.
- [28] K. Gopalaiah, *Chem Rev* **2013**, *113*, 3248–3296.
- [29] S. M. Hölzl, P. J. Altmann, J. W. Kück, F. E. Kühn, *Coord Chem Rev* **2017**, *352*, 517–536.
- [30] M. Guo, T. Corona, K. Ray, W. Nam, *ACS Cent Sci* **2019**, *5*, 13–28.
- [31] M. L. Neidig, E. I. Solomon, *Chemical Communications* **2005**, 5843–5863.
- [32] L. Vicens, M. Costas, *Dalton Transactions* **2018**, *47*, 1755–1763.
- [33] O. Pestovsky, A. Bakac, *J Am Chem Soc* **2004**, *126*, 13757–13764.

- [34] M. C. Esmelindro, E. G. Oestreicher, H. Márquez-Alvarez, C. Dariva, S. M. S. Egues, C. Fernandes, A. J. Bortoluzzi, V. Drago, O. A. C. Antunes, *J Inorg Biochem* **2005**, *99*, 2054–2061.
- [35] A. Kejriwal, A. N. Biswas, A. Choudhury, P. Bandyopadhyay, *Transition Metal Chemistry* **2014**, *39*, 909–915.
- [36] Y. Sakaguchi, A. Call, M. Cibian, K. Yamauchi, K. Sakai, *Chemical Communications* **2019**, *55*, 8552–8555.
- [37] W. Lin, L. Zhang, H. Suo, A. Vignesh, N. Yousuf, X. Hao, W. H. Sun, *New Journal of Chemistry* **2020**, *44*, 8076–8084.
- [38] N. Raffard, V. Baland, J. Simaan, S. Létard, M. Nierlich, K. Miki, F. Banse, E. Anxolabéhère-Mallart, J.-J. Girerd, *Comptes Rendus Chimie* **2002**, *5*, 99–109.
- [39] S. Taktak, S. v. Kryatov, T. E. Haas, E. v. Rybak-Akimova, *J Mol Catal A Chem* **2006**, *259*, 24–34.
- [40] S. M. Brewer, T. M. Schwartz, M. A. Mekhail, L. S. Turan, T. J. Prior, T. J. Hubin, B. G. Janesko, K. N. Green, *Organometallics* **2021**, *40*, 2467–2477.
- [41] C. v. Raman, K. S. Krishnan, *Nature 1928 121:3048* **1928**, *121*, 501–502.
- [42] J. Sanders-Loehr, W. D. Wheeler, A. K. Shiemke, B. A. Averill, T. M. Loehr, *J Am Chem Soc* **1989**, *111*, 8084–8093.
- [43] B. G. Fox, J. Shanklin, A. Jingyuan, T. M. Loehr, J. Sanders-Loehr, *Biochemistry* **1994**, *33*, 12776–12786.
- [44] D. M. Kurtz, *Chem Rev* **1990**, *90*, 585–606.
- [45] C. Brémard, P. Kowalewski, J. C. Merlin, S. Moreau, *Journal of Raman Spectroscopy* **1992**, *23*, 325–333.
- [46] I. M. Wasser, C. F. Martens, C. N. Verani, E. Rentschler, H. W. Huang, P. Moëgne-Loccoz, L. N. Zakharov, A. L. Rheingold, K. D. Karlin, *Inorg Chem* **2004**, *43*, 651–662.
- [47] G. Tseberlidis, L. Demonti, V. Pirovano, M. Scavini, S. Cappelli, S. Rizzato, R. Vicente, A. Caselli, *ChemCatChem* **2019**, *11*, 4907–4915.
- [48] J. Serrano-Plana, A. Aguinaco, R. Belda, E. García-España, M. G. Basallote, A. Company, M. Costas, *Angewandte Chemie - International Edition* **2016**, *55*, 6310–6314.
- [49] T. Csupász, D. Szücs, F. K. Kálmán, O. Hollóczki, A. Fekete, D. Szikra, É. Tóth, I. Tóth, G. Tircsó, *Molecules* **2022**, *27*, DOI 10.3390/MOLECULES27020371.

- [50] F. della Monica, A. Buonerba, V. Paradiso, S. Milione, A. Grassi, C. Capacchione, *Adv Synth Catal* **2019**, *361*, 283–288.
- [51] M. D. Timken, D. N. Hendrickson, E. Sinn, *Inorg Chem* **1985**, *24*, 3947–3955.
- [52] S. M. Brewer, P. M. Palacios, H. M. Johnston, B. S. Pierce, K. N. Green, *Inorganica Chim Acta* **2018**, *478*, 139–147.
- [53] S. M. Brewer, K. R. Wilson, D. G. Jones, E. W. Reinheimer, S. J. Archibald, T. J. Prior, M. A. Ayala, A. L. Foster, T. J. Hubin, K. N. Green, *Inorg Chem* **2018**, *57*, 8890–8902.
- [54] E. Prathibha, R. Rangasamy, A. Sridhar, K. Lakshmi, *ChemistrySelect* **2020**, *5*, 988–993.
- [55] A. Shaabani, R. Mohammadian, H. Farhid, M. Karimi Alavijeh, M. M. Amini, *Catal Letters* **2019**, *149*, 1237–1249.
- [56] T. L. Hwang, A. J. Shaka, *J Magn Reson A* **1995**, *112*, 275–279.
- [57] C. Walling, *Acc Chem Res* **1998**, *31*, 155–157.
- [58] S. E. Martín, A. Garrone, *Tetrahedron Lett* **2003**, *44*, 549–552.
- [59] P. A. Payard, Y. T. Zheng, W. J. Zhou, L. Khrouz, L. Bonneviot, R. Wischert, L. Grimaud, M. Pera-Titus, *European J Org Chem* **2020**, *2020*, 3552–3559.
- [60] W. Ye, R. J. Staples, E. v. Rybak-Akimova, *J Inorg Biochem* **2012**, *115*, 1–12.
- [61] C. He, F. Ma, W. Zhang, R. Tong, *Org Lett* **2022**, *2022*, 3499–3503.
- [62] Y. Wang, P. Prinsen, F. Mangin, A. Yopez, A. Pineda, E. Rodríguez-Castellón, M. R. Hasan Shah Gilani, G. Xu, C. Len, R. Luque, *Molecular Catalysis* **2019**, *474*, 110409.
- [63] N. N. H. M. Eisink, A. J. Minnaard, M. D. Witte, *Synthesis (Stuttg)* **2017**, *49*, 822–829.
- [64] N. Y. Oh, Y. Suh, M. J. Park, M. S. Seo, J. Kim, W. Nam, *Angewandte Chemie* **2005**, *117*, 4307–4311.
- [65] S. Kumar, S. Vaidya, M. Pissas, Y. Sanakis, R. Gupta, *Eur J Inorg Chem* **2012**, 5525–5533.
- [66] G. Roelfes, M. Lubben, R. Hage, L. Que, B. L. Feringa, **n.d.**, DOI 10.1002/1521-3765(20000616)6:12.
- [67] R. M. Solbrig, L. L. Duff, D. F. Shriver, I. M. Klotz, *J Inorg Biochem* **1982**, *17*, 69–74.

- [68] J. E. Plowman, T. M. Loehr, C. K. Schauer, O. P. Anderson, *Inorg Chem* **1984**, *23*, 3553–3559.
- [69] A. K. Shiemke, T. M. Loehr, J. Sanders-Loehr, *J Am Chem Soc* **1984**, *106*, 4951–4956.
- [70] P. Gómez-Romero, G. B. Jameson, E. H. Witten, W. M. Reiff, G. Backes, J. Sanders-Loehr, *J Am Chem Soc* **1989**, *111*, 9039–9047.
- [71] S. K. Dutta, R. Werner, U. Flörke, S. Mohanta, K. K. Nanda, W. Haase, K. Nag, *Inorg Chem* **1996**, *35*, 2292–2300.
- [72] J. B. H. Strautmann, S. Dammers, T. Limpke, J. Parthier, T. P. Zimmermann, S. Walleck, G. Heinze-Brückner, A. Stammler, H. Bögge, T. Glaser, *Dalton Transactions* **2016**, *45*, 3340–3361.
- [73] V. Félix, J. Costa, R. Delgado, M. G. B. Drew, M. T. Duarte, C. Resende, *Journal of the Chemical Society, Dalton Transactions* **2001**, 1462–1471.
- [74] N. Arulsamy, D. J. Hodgson, J. Glerup, *Inorganica Chim Acta* **1993**, *209*, 61–69.
- [75] T. Kojima, R. A. Leising, S. Yan, L. Que, *J Am Chem Soc* **1993**, *115*, 11328–11335.
- [76] R. M. Buchanan, R. J. O'Brien, J. F. Richardson, J. M. Latour, *Inorganica Chim Acta* **1993**, *214*, 33–40.
- [77] M. Pascaly, M. Duda, A. Rompel, B. H. Sift, W. Meyer-Klaucke, B. Krebs, *Inorganica Chim Acta* **1999**, *291*, 289–299.
- [78] B. Kwak, K. Woong Cho, M. Pyo, M. Soo Lah, *Inorganica Chim Acta* **1999**, *290*, 21–27.
- [79] M. Merkel, M. Pascaly, B. Krebs, J. Astner, S. P. Foxon, S. Schindler, *Inorg Chem* **2005**, *44*, 7582–7589.
- [80] E. A. Duban, T. N. Drebuschak, K. P. Bryliakov, E. P. Talsi, *Mendeleev Communications* **2007**, *17*, 291–293.
- [81] H. Sun, M. Wang, F. Li, P. Li, Z. Zhao, L. Sun, *Appl Organomet Chem* **2008**, *22*, 573–576.
- [82] C. Wegeberg, A. de Aguirre, F. Maseras, C. J. McKenzie, *Inorg Chem* **2020**, *59*, 16281–16290.
- [83] N. Panza, A. di Biase, E. Gallo, A. Caselli, *Journal of CO2 Utilization* **2021**, *51*, DOI 10.1016/j.jcou.2021.101635.

- [84] L. Benhamou, H. Jaafar, A. Thibon, M. Lachkar, D. Mandon, *Inorganica Chim Acta* **2011**, *373*, 195–200.
- [85] Y. Yang, C. Lu, H. Wang, X. Liu, *Dalton Transactions* **2016**, *45*, 10289–10296.
- [86] N. K. Thallaj, O. Rotthaus, L. Benhamou, N. Humbert, M. Elhabiri, M. Lachkar, R. Welter, A. M. Albrecht-Gary, D. Mandon, *Chemistry - A European Journal* **2008**, *14*, 6742–6753.
- [87] J. Sanders-Loehr, W. D. Wheeler, A. K. Shiemke, B. A. Averill, T. M. Loehr, *J Am Chem Soc* **1989**, *111*, 8084–8093.
- [88] D. M. Kurtz, *Chem Rev* **1990**, *90*, 585–606.
- [89] C. Brémard, P. Kowalewski, J. C. Merlin, S. Moreau, *Journal of Raman Spectroscopy* **1992**, *23*, 325–333.
- [90] B. G. Fox, J. Shanklin, J. Ai, T. M. Loehr, J. Sanders-Loehr, *Biochemistry* **1994**, *33*, 12776–12786.
- [91] I. M. Wasser, C. F. Martens, C. N. Verani, E. Rentschler, H. W. Huang, P. Moënnelocoz, L. N. Zakharov, A. L. Rheingold, K. D. Karlin, *Inorg Chem* **2004**, *43*, 651–662.
- [92] N. Panza, A. Biase, S. Rizzato, E. Gallo, G. Tseberlidis, A. Caselli, *European J Org Chem* **2020**, *2020*, 6635–6644.
- [93] C. A. Clausen, M. L. Good, *Inorg Chem* **1970**, *9*, 220–223.
- [94] T. Birchall, M. F. Morris, *Can J Chem* **1972**, *50*, 211–216.
- [95] N. T. Madhu, P. K. Radhakrishnan, M. Grunert, P. Weinberger, W. Linert, *Thermochim Acta* **2003**, *407*, 73–84.
- [96] B. Huchinson, M. Hoffbauer, J. Takemoto, *Spectrochim Acta A* **1976**, *32*, 1785–1792.
- [97] W. S. Szulbinski, R. S. Czernuszewicz, *Inorganica Chim Acta* **1996**, *247*, 11–18.
- [98] C. C. Wagner, E. J. Baran, *Spectrochim Acta A Mol Biomol Spectrosc* **2010**, *75*, 807–810.
- [99] P. Gomez-Romero, E. H. Witten, W. M. Reiff, G. Backes, J. Sanders-Loehr, G. B. Jameson, *J Am Chem Soc* **1989**, *111*, 9039–9047.
- [100] R. E. Norman, S. Yan, L. Que, G. Backes, J. Ling, J. Sanders-Loehr, J. H. Zhang, C. J. O'Connor, *J Am Chem Soc* **1990**, *112*, 1554–1562.
- [101] T. Mejean, M. T. Forel, M. T. Bourgeois, M. Jacon, *J Chem Phys* **1980**, *72*, 687–693.

- [102] G. P. Bhavsar, K. Sathianandan, *J Mol Struct* **1973**, *16*, 343–345.
- [103] J. R. Schoonover, J. F. Ni, L. Roecker, P. S. White, T. J. Meyer, *Inorg Chem* **1996**, *35*, 5885–5892.
- [104] G. Haselhorst, K. Wiegardt, S. Keller, B. Schrader, *Inorg Chem* **1993**, *32*, 520–525.
- [105] N. Panza, A. di Biase, S. Rizzato, E. Gallo, G. Tseberlidis, A. Caselli, *European J Org Chem* **2020**, *2020*, 6635–6644.
- [106] N. Panza, A. di Biase, A. Caselli, *Inorganica Chim Acta* **2022**, *541*, 121091.
- [107] P. P. Pescarmona, **2021**, DOI 10.1016/j.cogsc.2021.100457.
- [108] Q. Liu, L. Wu, R. Jackstell, M. Beller, *Nat Commun* **2015**, *6*, DOI 10.1038/ncomms6933.
- [109] *Int J Toxicol* **1987**, *6*, 23–51.
- [110] M. Sathish, K. J. Sreeram, J. Raghava Rao, B. Unni Nair, *ACS Sustain Chem Eng* **2016**, *4*, 1032–1040.
- [111] M. Aresta, A. Dibenedetto, E. Quaranta, *J Catal* **2016**, *343*, 2–45.
- [112] V. Besse, F. Camara, C. Voirin, R. Auvergne, S. Caillol, B. Boutevin, *Polym Chem* **2013**, *4*, 4545–4561.
- [113] B. Schöffner, F. Schöffner, S. P. Verevkin, A. Börner, *Chem Rev* **2010**, *110*, 4554–4581.
- [114] S. Inoue, H. Koinuma, T. Tsuruta, *J Polym Sci B* **1969**, *7*, 287–292.
- [115] G. Rokicki, W. Kuran, B. Pogorzelska-Marciniak, *Monatshefte für Chemie / Chemical Monthly 1984 115:2* **1984**, *115*, 205–214.
- [116] N. Kihara, N. Hara, T. Endo, *Journal of Organic Chemistry* **1993**, *58*, 6198–6202.
- [117] M. Ratzenhofer, H. Kisch, *Angewandte Chemie* **1980**, *92*, 303–303.
- [118] T. Aida, S. Inoue, *Macromolecules* **1982**, *15*, 682–684.
- [119] W. Clegg, R. W. Harrington, M. North, R. Pasquale, *Chemistry – A European Journal* **2010**, *16*, 6828–6843.
- [120] D. J. Darensbourg, M. W. Holtcamp, *Coord Chem Rev* **1996**, *153*, 155–174.
- [121] V. Campisciano, C. Calabrese, F. Giacalone, C. Aprile, P. lo Meo, M. Gruttadauria, *Journal of CO2 Utilization* **2020**, *38*, 132–140.

- [122] C. A. Montoya, A. B. Paninho, P. M. Felix, M. E. Zakrzewska, J. Vital, V. Najdanovic-Visak, A. V. M. Nunes, *Journal of Supercritical Fluids* **2015**, *100*, 155–159.
- [123] J.-Q. Wang, K. Dong, W.-G. Cheng, J. Sun, S.-J. Zhang, *Catal Sci Technol* **2012**, *2*, 1480–1484.
- [124] V. Caló, A. Nacci, A. Monopoli, A. Fanizzi, *Org Lett* **2002**, *4*, 2561–2563.
- [125] W. N. Sit, S. M. Ng, K. Y. Kwong, C. P. Lau, *Journal of Organic Chemistry* **2005**, *70*, 8583–8586.
- [126] J. Sun, S. Fujita, M. Arai, *J Organomet Chem* **2005**, *690*, 3490–3497.
- [127] C. J. Whiteoak, A. Nova, F. Maseras, A. W. Kleij, *ChemSusChem* **2012**, *5*, 2032–2038.
- [128] A. J. Kamphuis, F. Picchioni, P. P. Pescarmona, *Green Chemistry* **2019**, *21*, 406–448.
- [129] K. A. Andrea, F. M. Kerton, *Polym J* **2021**, *53*, 29–46.
- [130] I. Bauer, H.-J. Knölker, *Chem Rev* **2015**, *115*, 3170–3387.
- [131] X. Sheng, L. Qiao, Y. Qin, X. Wang, F. Wang, *Polyhedron* **2014**, *74*, 129–133.
- [132] A. J. Kamphuis, F. Milocco, L. Koiter, P. P. Pescarmona, E. Otten, *ChemSusChem* **2019**, *12*, 3635–3641.
- [133] K. A. Andrea, E. D. Butler, T. R. Brown, T. S. Anderson, D. Jagota, C. Rose, E. M. Lee, S. D. Goulding, J. N. Murphy, F. M. Kerton, C. M. Kozak, *Inorg Chem* **2019**, *58*, 11231–11240.
- [134] O. J. Driscoll, C. H. Hafford-Tear, P. McKeown, J. A. Stewart, G. Kociok-Köhn, M. F. Mahon, M. D. Jones, *Dalton Transactions* **2019**, *48*, 15049–15058.
- [135] M. Cavalleri, N. Panza, A. di Biase, G. Tseberlidis, S. Rizzato, G. Abbiati, A. Caselli, *European J Org Chem* **2021**, *2021*, 2764–2771.
- [136] K. M. Lincoln, M. E. Offutt, T. D. Hayden, R. E. Saunders, K. N. Green, *Inorg Chem* **2014**, *3*, 1–15.
- [137] K. M. Lincoln, P. Gonzalez, T. E. Richardson, D. A. Julovich, R. Saunders, J. W. Simpkins, K. N. Green, *Chemical Communications* **2013**, *49*, 2712–2714.
- [138] A. W. Addison, T. N. Rao, J. Reedijk, J. van Rijn, G. C. Verschoor, *Journal of the Chemical Society, Dalton Transactions* **1984**, 1349–1356.
- [139] J. Q. Wang, K. Dong, W. G. Cheng, J. Sun, S. J. Zhang, *Catal Sci Technol* **2012**, *2*, 1480–1484.

- [140] M. Zhang, Y. Yang, L. Chen, *Cuihua Xuebao/Chinese Journal of Catalysis* **2015**, *36*, 1304–1311.
- [141] M. K. Leu, I. Vicente, J. A. Fernandes, I. de Pedro, J. Dupont, V. Sans, P. Licence, A. Gual, I. Cano, *Appl Catal B* **2019**, *245*, 240–250.
- [142] V. Besse, F. Camara, C. Voirin, R. Auvergne, S. Caillol, B. Boutevin, *Polym Chem* **2013**, *4*, 4545–4561.
- [143] C. Cheng, Y. Li, X. Zhang, J. Li, *Iranian Polymer Journal 2017 26:11* **2017**, *26*, 821–831.
- [144] E. Rix, E. Grau, G. Chollet, H. Cramail, *Eur Polym J* **2016**, *84*, 863–872.
- [145] I. Lovel, Y. Goldberg, M. Shymanska, E. Lukevics, *Appl Organomet Chem* **1987**, *1*, 371–378.
- [146] E. Lukevics, D. I. Barabanov, L. M. Ignatovich, *Appl Organomet Chem* **1991**, *5*, 379–383.
- [147] R. A. Benkeser, J. Kang, *J Organomet Chem* **1980**, *185*, C9–C12.
- [148] A. M. Karateyev, P. P. Kushch, Y. N. Frolov, N. S. Ovanesyan, E. A. Dzhavadyan, B. A. Rozenberg, *Polymer Science U.S.S.R.* **1988**, *30*, 1115–1121.
- [149] M. H. Valkenberg, C. DeCastro, W. F. Hölderich, *Appl Catal A Gen* **2001**, *215*, 185–190.
- [150] K. Bica, P. Gaertner, *Org Lett* **2006**, *8*, 733–735.
- [151] P. E. Maligres, S. W. Krska, P. G. Dormer, *Journal of Organic Chemistry* **2012**, *77*, 7646–7651.
- [152] K. Laxmikeshav, A. P. Sakla, S. E. John, N. Shankaraiah, *Green Chemistry* **2022**, *24*, 1259–1269.
- [153] B. Chatterjee, S. Jena, V. Chugh, T. Weyhermüller, C. Werlé, *ACS Catal* **2021**, *11*, 7176–7185.
- [154] D. Wyrzykowski, R. Kruszyński, U. Kucharska, Z. Warnke, *Z Anorg Allg Chem* **2006**, *632*, 624–628.
- [155] N. Panza, R. Soave, F. Cargnoni, M. I. Trioni, A. Caselli, *Journal of CO2 Utilization* **2022**, *62*, 102062.
- [156] P. Gabrielli, M. Gazzani, M. Mazzotti, *Ind Eng Chem Res* **2020**, *59*, 7033–7045.

- [157] A. Modak, P. Bhanja, S. Dutta, B. Chowdhury, A. Bhaumik, *Green Chemistry* **2020**, *22*, 4002–4033.
- [158] *CO₂ as a Building Block in Organic Synthesis*, Wiley, **2020**.
- [159] R. Dalpozzo, N. della Ca, B. Gabriele, R. Mancuso, *Catalysts* **2019**, *Vol. 9*, Page 511 **2019**, *9*, 511.
- [160] T. Niemi, T. Repo, *European J Org Chem* **2019**, *2019*, 1180–1188.
- [161] K. Michalska, I. Karpiuk, M. Król, S. Tyski, *Bioorg Med Chem* **2013**, *21*, 577–591.
- [162] M. Nasibullah, F. Hassan, N. Ahmad, A. R. Khan, M. Rahman, *Adv Sci Eng Med* **2015**, *7*, 91–111.
- [163] P. Jadhavar, M. Vaja, T. Dhameliya, A. Chakraborti, *Curr Med Chem* **2015**, *22*, 4379–4397.
- [164] A. Bhushan, N. J. Martucci, O. B. Usta, M. L. Yarmush, <http://dx.doi.org/10.1517/17425255.2016.1162292> **2016**, *12*, 475–477.
- [165] C. Roger, J. A. Roberts, L. Muller, *Clinical Pharmacokinetics* **2017**, *57*, 559–575.
- [166] A. Z. Bialvaei, M. Rahbar, M. Yousefi, M. Asgharzadeh, H. S. Kafil, *Journal of Antimicrobial Chemotherapy* **2017**, *72*, 354–364.
- [167] S. D. Burdette, R. Trotman, *Clinical Infectious Diseases* **2015**, *61*, 1315–1321.
- [168] D. McBride, T. Krekel, K. Hsueh, M. J. Durkin, <http://dx.doi.org/10.1080/17425255.2017.1290080> **2017**, *13*, 331–337.
- [169] S. Lemaire, P. M. Tulkens, F. van Bambeke, *Antimicrob Agents Chemother* **2010**, *54*, 2540–2548.
- [170] A. Wookey, P. J. Turner, J. M. Greenhalgh, M. Eastwood, J. Clarke, C. Sefton, *Clinical Microbiology and Infection* **2004**, *10*, 247–254.
- [171] K. C. Murdock, *Journal of Organic Chemistry* **1968**, *33*, 1367–1371.
- [172] B. Wang, E. H. M. Elageed, D. Zhang, S. Yang, S. Wu, G. Zhang, G. Gao, *ChemCatChem* **2014**, *6*, 278–283.
- [173] U. R. Seo, Y. K. Chung, *Green Chemistry* **2017**, *19*, 803–808.
- [174] Y. F. Xie, C. Guo, L. Shi, B. H. Peng, N. Liu, *Org Biomol Chem* **2019**, *17*, 3497–3506.

- [175] C. Mei, Y. Zhao, Q. Chen, C. Cao, G. Pang, Y. Shi, *ChemCatChem* **2018**, *10*, 3057–3068.
- [176] M. Zhou, X. Zheng, Y. Wang, D. Yuan, Y. Yao, *ChemCatChem* **2019**, *11*, 5783–5787.
- [177] T. Niemi, I. Fernández, B. Steadman, J. K. Mannisto, T. Repo, *Chemical Communications* **2018**, *54*, 3166–3169.
- [178] P. Yingcharoen, W. Natongchai, A. Poater, V. D’Elia, *Catal Sci Technol* **2020**, *10*, 5544–5558.
- [179] S. Arshadi, A. Banaei, S. Ebrahimiasl, A. Monfared, E. Vessally, *RSC Adv* **2019**, *9*, 19465–19482.
- [180] S. Pulla, C. M. Felton, P. Ramidi, Y. Gartia, N. Ali, U. B. Nasini, A. Ghosh, *Journal of CO2 Utilization* **2013**, *2*, 49–57.
- [181] X. Y. Dou, L. N. He, Z. Z. Yang, J. L. Wang, *Synlett* **2010**, *2010*, 2159–2163.
- [182] Z. Z. Yang, Y. N. Li, Y. Y. Wei, L. N. He, *Green Chemistry* **2011**, *13*, 2351–2353.
- [183] D. Adhikari, A. W. Miller, M. H. Baik, S. T. Nguyen, *Chem Sci* **2015**, *6*, 1293–1300.
- [184] M. Sengoden, M. North, A. C. Whitwood, *ChemSusChem* **2019**, *12*, 3296–3303.
- [185] D. Intrieri, C. Damiano, P. Sonzini, E. Gallo, <https://doi.org/10.1142/S1088424619300015> **2019**, 1107–1130.
- [186] T. D. Hu, Y. H. Ding, *Organometallics* **2020**, *39*, 505–515.
- [187] X. M. Kang, L. H. Yao, Z. H. Jiao, B. Zhao, *Chem Asian J* **2019**, *14*, 3668–3674.
- [188] J. Liu, A. Wang, H. Jing, *Cuihua Xuebao/Chinese Journal of Catalysis* **2014**, *35*, 1669–1675.
- [189] H. Xu, X. F. Liu, C. S. Cao, B. Zhao, P. Cheng, L. N. He, *Advanced Science* **2016**, *3*, DOI 10.1002/ADVS.201600048.
- [190] Y. Du, Y. Wu, A. H. Liu, L. N. He, *Journal of Organic Chemistry* **2008**, *73*, 4709–4712.
- [191] G. Bresciani, M. Bortoluzzi, G. Pampaloni, F. Marchetti, *Org Biomol Chem* **2021**, *19*, 4152–4161.
- [192] M. Sengoden, M. North, A. C. Whitwood, *ChemSusChem* **2019**, *12*, 3296–3303.
- [193] C. Damiano, P. Sonzini, G. Manca, E. Gallo, *European J Org Chem* **2021**, *2021*, 2807–2814.
- [194] J. D. Eldwards, S. F. Pickering, *Sci. Pap. Bureau Stand.* **1920**, *16*, 327–361.

- [195] N. Panza, M. Alberti, S. Galiè, C. Damiano, F. Cargnoni, M. Italo Trioni, A. Caselli, *European J Org Chem* **2022**, 2022, e202200908.
- [196] R. C. Thompson, S. H. Swan, C. J. Moore, F. S. vom Saal, *Philosophical Transactions of the Royal Society B: Biological Sciences* **2009**, 364, 1973–1976.
- [197] R. Geyer, J. R. Jambeck, K. L. Law, *Sci Adv* **2017**, 3, DOI 10.1126/SCIADV.1700782/SUPPL_FILE/1700782_SM.PDF.
- [198] G. Cecchin, G. Morini, F. Piemontesi, *Kirk-Othmer Encyclopedia of Chemical Technology* **2003**, DOI 10.1002/0471238961.2609050703050303.A01.
- [199] G. Natta, P. Corradini, *Il Nuovo Cimento (1955-1965)* 1960 15:1 **2007**, 15, 40–51.
- [200] S. Mandal, A. Dey, *PET Chemistry*, William Andrew Publishing, **2019**.
- [201] G.N. VanderPlaats, **1999**.
- [202] H. T. B. H. J. H. J. Bjorksen, *Polyesters and Their Applications*, Chapman And Hall, UK, **1956**.
- [203] C.A. Harper, *Modern Plastics Handbook: Handbook*, McGraw-Hill Professional, New York, **2000**.
- [204] S. D. I. G.W. Parshall, *Homogeneous Catalysis: The Application and Chemistry of Catalysis by Soluble Transition Metal Complexes*, Wiley, New York, **1992**.
- [205] “<https://www3.epa.gov/ttnchie1/ap42/ch06/final/c06s06-2.pdf>,” **n.d.**
- [206] A. J. Ragauskas, G. W. Huber, J. Wang, A. Guss, H. M. O’Neill, C. S. K. Lin, Y. Wang, F. R. Wurm, X. Meng, *ChemSusChem* **2021**, 14, 3982–3984.
- [207] J. R. Jambeck, R. Geyer, C. Wilcox, T. R. Siegler, M. Perryman, A. Andrady, R. Narayan, K. L. Law, *Science (1979)* **2015**, 347, 768–771.
- [208] S. Allen, D. Allen, F. Baladima, V. R. Phoenix, J. L. Thomas, G. le Roux, J. E. Sonke, *Nature Communications* 2021 12:1 **2021**, 12, 1–10.
- [209] C. Benson, **2001**, 36, 1–25.
- [210] “<https://archive.ellenmacarthurfoundation.org/explore/plastics-and-the-circular-economy>,” **n.d.**
- [211] K. P. Rajan, A. Gopanna, S. P. Thomas, *Recycling 2019, Vol. 4, Page 10* **2019**, 4, 10.
- [212] F. Awaja, D. Pavel, *Eur Polym J* **2005**, 41, 1453–1477.

- [213] Z. O. G Schyns, M. P. Shaver, Z. O. G Schyns, M. P. Shaver, *Macromol Rapid Commun* **2021**, *42*, 2000415.
- [214] “<https://eu.patagonia.com/it/it/our-footprint/recycled-polyester.html>,” **n.d.**
- [215] “https://www.patagonia.com/on/demandware.static/Sites-patagonia-us-Site/Library-Sites-PatagoniaShared/en_US/PDF-US/common_threads_whitepaper.pdf,” **n.d.**
- [216] “<https://coripet.it/cosa-facciamo/>,” **n.d.**
- [217] “<https://www.efanews.eu/it/item/27508-coca-cola-hbc-nuovo-stabilimento-per-bottiglie-in-pet-riciclato.html#:~:text=Coca%2DCola%20Hbc%20ha%20inaugurato,oltre%2030%20milioni%20di%20euro.>,” **n.d.**
- [218] Partenheimer Walter, *TRANSFORMATION OF POLYMERS TO USEFUL CHEMICALS BY OXIDATION*, **2002**.
- [219] W. Partenheimer, *Catal Today* **1995**, *23*, 69–158.
- [220] S. Ügdüler, K. M. van Geem, R. Denolf, M. Roosen, N. Mys, K. Ragaert, S. de Meester, *Green Chemistry* **2020**, *22*, 5376–5394.
- [221] G. P. Karayannidis, A. P. Chatziavgoustis, D. S. Achilias, *Advances in Polymer Technology* **2002**, *21*, 250–259.
- [222] M. N. Siddiqui, D. S. Achilias, H. H. Redhwi, D. N. Bikiaris, K. A. G. Katsogiannis, G. P. Karayannidis, *Macromol Mater Eng* **2010**, *295*, 575–584.
- [223] F. Liu, X. Cui, S. Yu, Z. Li, X. Ge, *J Appl Polym Sci* **2009**, *114*, 3561–3565.
- [224] L. Zhang, J. Gao, J. Zou, F. Yi, *J Appl Polym Sci* **2013**, *130*, 2790–2795.
- [225] D. Stanica-Ezeanu, D. Matei, *Scientific Reports* **2021**, *11:1* **2021**, *11*, 1–7.
- [226] A. J. Martín, C. Mondelli, S. D. Jaydev, J. Pérez-Ramírez, *Chem* **2021**, *7*, 1487–1533.
- [227] S. L. Fávaro, A. R. Freitas, T. A. Ganzerli, A. G. B. Pereira, A. L. Cardozo, O. Baron, E. C. Muniz, E. M. Giroto, E. Radovanovic, *J Supercrit Fluids* **2013**, *75*, 138–143.
- [228] G. P. Karayannidis, D. S. Achilias, *Macromol Mater Eng* **2007**, *292*, 128–146.
- [229] J. Y. Chen, C. F. Ou, Y. C. Hu, C. C. Lin, *J Appl Polym Sci* **1991**, *42*, 1501–1507.
- [230] C. H. Chen, *J Appl Polym Sci* **2003**, *87*, 2004–2010.
- [231] H. Wang, R. Yan, Z. Li, X. Zhang, S. Zhang, *Catal Commun* **2010**, *11*, 763–767.

- [232] S. H. Mansour, N. E. Ikladios, *Polym Test* **2002**, *21*, 497–505.
- [233] K. Fukushima, J. M. Lecuyer, D. S. Wei, H. W. Horn, G. O. Jones, H. A. Al-Megren, A. M. Alabduhman, F. D. Alsewailam, M. A. McNeil, J. E. Rice, J. L. Hedrick, *Polym Chem* **2013**, *4*, 1610–1616.
- [234] V. Sinha, M. R. Patel, J. v. Patel, *Journal of Polymers and the Environment* **2008** *18:1* **2008**, *18*, 8–25.
- [235] J. Serrano-Plana, A. Aguinaco, R. Belda, E. García-España, M. G. Basallote, A. Company, M. Costas, *Angewandte Chemie International Edition* **2016**, *55*, 6310–6314.
- [236] N. Panza, A. di Biase, E. Gallo, A. Caselli, *Journal of CO2 Utilization* **2021**, *51*, DOI 10.1016/J.JCOU.2021.101635.
- [237] N. Panza, A. di Biase, S. Rizzato, E. Gallo, G. Tseberlidis, A. Caselli, *European J Org Chem* **2020**, *2020*, 6635–6644.
- [238] N. Panza, A. di Biase, A. Caselli, *Inorganica Chim Acta* **2022**, *541*, DOI 10.1016/J.ICA.2022.121091.
- [239] N. Panza, M. Alberti, C. Damiano, A. Caselli, *Frontiers in Catalysis* **2022**, *0*, 19.
- [240] P. S. Hallman, T. A. Stephenson, G. Wilkinson, *Inorganic Syntheses: Volume XII* **2006**, 237–240.
- [241] M. Takahashi, K. Oshima, S. Matsubara, <http://dx.doi.org/10.1246/cl.2005.192> **2005**, *34*, 192–193.
- [242] E. M. Elgendy, S. A. Khayyat, *Russian Journal of Organic Chemistry* **2008** *44:6* **2008**, *44*, 823–829.
- [243] S. Grimme, *J Chem Theory Comput* **2019**, *15*, 2847–2862.
- [244] C. Lee, W. Yang, R. G. Parr, *Phys Rev B* **1988**, *37*, 785.
- [245] A. D. Becke, *J Chem Phys* **1998**, *98*, 5648.
- [246] D. J. F. M.J. Frisch, G.W. Trucks, H.B. Schlegel, G.E. Scuseria, M.A. Robb, J.R. Cheeseman, G. Scalmani, V. Barone, B. Mennucci, G.A. Petersson, H. Nakatsuji, M. Caricato, X. Li, H.P. Hratchian, A.F. Izmaylov, J. Bloino, G. Zheng, J.L. Sonnenberg, M. Hada, M. Ehar, **2013**.
- [247] T. Tabanelli, S. Passeri, S. Guidetti, F. Cavani, C. Lucarelli, F. Cargnoni, M. Mella, *J Catal* **2019**, *370*, 447–460.

- [248] H. B. Schlegel, *J Comput Chem* **1982**, *3*, 214–218.
- [249] A. v. Marenich, C. J. Cramer, D. G. Truhlar, *Journal of Physical Chemistry B* **2009**, *113*, 6378–6396.
- [250] S. Grimme, J. Antony, S. Ehrlich, H. Krieg, *J Chem Phys* **2010**, *132*, 154104.
- [251] J. Steinbauer, A. Spannenberg, T. Werner, *Green Chemistry* **2017**, *19*, 3769–3779.
- [252] W. D. Yu, Y. Zhang, Y. Y. Han, B. Li, S. Shao, L. P. Zhang, H. K. Xie, J. Yan, *Inorg Chem* **2021**, *60*, 3980–3987.
- [253] C. A. M. Cariou, B. M. Kariuki, J. S. Snaith, *Org Biomol Chem* **2008**, *6*, 3337–3348.
- [254] P. Trinchera, B. Musio, L. Degennaro, A. Moliterni, A. Falcicchio, R. Luisi, *Org Biomol Chem* **2012**, *10*, 1962–1965.
- [255] O. Tsuge, S. Mataka, *Bull Chem Soc Jpn* **1971**, *44*, 1896–1900.
- [256] A. J. Garza, *J Chem Theory Comput* **2019**, *15*, 3204–3214.

Acknowledgments:

Writing this thesis was the perfect summary of the last three years of my PhD journey, a complete rollercoaster of emotions that can't be described in few lines. During these years, even if I often felt alone, I had few people around myself that helped me going through all of this. That's the reason I am now writing this, as a celebration of the good and bad memories shared with these people, which constitute who I am now and who I will be in the future. First, I want to thank my boss, *il capo*, Professor Caselli. You gave me this opportunity and I hope I made you proud, in some ways. I know I have been a pain sometimes, but I never forgot that I was lucky to be able to work there and to learn so many things from you. I truly hope we will find a way, sooner or later, to keep making science together. Thanks to all the people that helped me to develop my research with their precious work, like Marco, Mario and Pasquale. Also, thanks to Professor Fumagalli for her help with Raman spectroscopy, Professor Rizzato for the crystal structure determination and Dr. Marco Ortenzi for his patience while working together on our plastic recycling project (he also made me fall in love with polymers, who would have thought). Thanks to our theoretical trio Fausto, Raffaella and Mario for their precious time spent discussing together about chemistry and not only. Thanks to Albe, you are my successor, I am sure you will have an extremely bright experience. Thank you for listening to me when no one else would. Thanks to Giulia, even if things seem to have taken a wrong turn (and I wish they did not), I am grateful to have been able to work with you but also to have made different wonderful experiences, together with the others. Indeed, thanks to Simone, Luca, Andrea, Ema, Gabri and all the other students who worked in our lab; I am sorry for when I did wrong, you always shown your commitment and I am proud of how fast you learned. Thanks to Armando, my lovely flatmate: thanks for your infinite patience at home and also at work; even if we both are of few words, I am enormously grateful to have met you. Another incredible person I met during my journey in the university is Cava: thank you for being a TRUE friend, I don't need to add any other thing. Thanks to Silvio, you are one of the few people that is able to make everything enjoyable; I loved all the things we shared. Thanks to Simo, even if times has been rough, I always knew you were a friend, and I am grateful for every time you put a smile on my face just by saying few words (I will miss it). To the old guard: Giorgio for being an inspiration at the time

and Fabio for being Fabio, thank you so much guys. Thanks to all the other people who made my stay in Milano truly enjoyable and unforgettable, in good times and bad times. Thanks to Valerio, Pippo, Irisi, Ivan, Cristian, Mattia and Bogdan for being my closest friends. Thanks to Paolo, Luca, Ale, Carra and Radici. Also thanks to the ones that kept me company while I was actually alone at home working or relaxing like Paolo, NNarcos, Fragola and many others. Thanks so much especially to Giulia (StudyTme) for keeping me focused while writing this thesis. I want to thank a beautiful human being that I am so grateful to have in my life: thank you Batta for all the help and laugh and cry and everything. I will not forget that you were there to give me a hug when I truly needed it. Thanks to my therapist Laura for her enormous help during last year. Of course, I want to thank my family, especially my parents. You are the ones that probably know me better, but I hope I will keep surprising you and making you proud, as much as I am proud of having you as parents. There would still be room for so many people to thank and I am realizing now that I feel so grateful to everyone who shared with me some of his time. At last, I want to thank myself, as I never do it, for being able to carry on.

Thank you very warmly all, again.

Nicola

December 2022